1-1-2017

Evaluation Of Earth-Abundant Monometallic And Bimetallic Complexes For Catalytic Water Splitting

Kenneth Kwame Kpogo
Wayne State University,

EVALUATION OF EARTH-ABUNDANT MONOMETALLIC AND BIMETALLIC COMPLEXES FOR CATALYTIC WATER SPLITTING

by

KENNETH KWAME KPOGO

DISSERTATION

Submitted to the Graduate School

of Wayne State University,

Detroit, Michigan

in partial fulfillment of the requirements

for the degree of

DOCTOR OF PHILOSOPHY

2017

MAJOR: CHEMISTRY (Inorganic)

Approved By:

_____

Advisor Date

_____

_____

_____

DEDICATION

I dedicate this dissertation to Nicole and my lovely family for encouraging me to pursue my dreams and completing this work. You are the love of my life.

ACKNOWLEDGEMENTS

To say that Dr. Claudio Verani is a great mentor and advisor would be an understatement. He is the best to have. My wonderful encounter with Dr. Verani began in March of 2012 when I was visiting with Wayne State as part of my admission process. Dr. Verani was then the Graduate recruiting committee chairman. I was very skeptical about coming to school in Detroit but he did a great job in allaying all my fears. He personally convinced me that Wayne State was the best choice I could possibly make for my academic career. I found his enthusiasm in talking about Wayne State endearing. I have to say he was to a large extent the reason why I chose to come to Wayne State for my Ph.D. I naturally chose to join his research group when it was time to select mentors and advisors and I have not regretted my decision. Dr. Verani's passion for science is second to none. He exemplifies science in everything he does. He has an ability to answer and explain my scientific questions in depth and yet simplifies them with an interdisciplinary point of view that makes them easier to understand. His unassuming personality makes him approachable. He always has an open office door as well as an open mind for conversation. I have spent many hours discussing a wide variety of subjects with Claudio (he insists everyone calls him by his first name). He is a true friend to all his students He genuinely cares about us as individuals and serves as my life mentor as well as an academic mentor. He helps me find my drive and passion for education and research and I consider him as my role model. It has been a worthwhile experience to have Dr. Verani's guidance these past five years and I am looking forward to more years of having him as a mentor even after my graduation.

My appreciation goes to my dissertation advisory committee, Professors Matthew J. Allen, Jennifer L. Stockdill, and Eranda Nikolla for gracefully accepting to be my academic mentors during my Ph.D. program. I am grateful to you all for time and energy you sacrificed in meeting

with me on numerous occasions. Your tenacity of purpose, patience and special attention you paid to my oral document, pre-defense document, and dissertation is second to none. Thank you.

Scientific breakthroughs mostly occur through collaborative efforts, and the Verani group at WSU is noted for having long-standing collaborations. The first and perhaps the longest one is the one with the Schlegel group at WSU. I was a beneficiary of this collaboration and I thank Professor Schlegel, Drs. Mazumder, and Thapa for their professionalism in helping me with computational calculations. I appreciate your patience during the long discussions and your insightful conversations, points of view and advice. Professor John Endicott is acknowledged for the discussions regarding the photochemistry of ruthenium and other questions and the numerous times I 'invaded' his office with general questions.

External collaborations are a testament to the visibility of research efforts. I want to thank Professor Adam T. Fiedler for recognizing the quality of work the Verani group does and deciding to collaborate with us. I am grateful for the steadfastness and professionalism exhibited by Prof. Fiedler during the collaborative work in general and the preparation of the manuscript. Dr. Denan Wang is acknowledged for synthesizing the compounds for our work. Dr. Oleg Poluektov and Dr. Jens Niklas from Argonne National Laboratory are acknowledged for their help with EPR spectroscopy.

My stay in the Verani group would not have been successful without the camaraderie and professional cohesion that exists in the laboratory. From the moment I joined the lab, I was met with senior students such as Drs. Dakshika Wanniarachchi, Dajena Tomco, Lanka Wickramasinghe and Debashis Basu who exuded scientific confidence and guided me when I was still 'green'. I appreciate all their help in transforming me from a synthetic organic chemist to an expert in physical inorganic chemistry. I learned a lot from my other colleagues with whom I spent

the last five years. To Dr. Sunalee Gonawala, thank you for your calm assertiveness and the knowledge you imparted when we were collaborating on the corrosion project. To Habib Baydoun, buddy thank you for your valuable criticisms, they challenged me in ways you could not imagine. To Pavithra Hettiarachchi, Danushka Ekanayake, Nour El-Harakeh, Krista Kulesa, Jordyn Burdick and Isuri Weeraratne I thank you all for encouraging me, helping me in all our scientific endeavors. I feel I am losing a great team but I know you will be there for me for a long time. I appreciate all the strong bonds of friendship that we held. To Pavithra and Danushka, it was really great collaborating with you on the nickel and copper projects as well because you brought excellent professionalism to our discussions despite us being friends. Thank you. To Fredericka and Samudra, You have already shown that you will be assets to the Verani group. Fredericka, I know you will bring the same dedication and strong work ethic that you are known for to the Verani group, and I am sure Samudra will as well, I appreciate you all.

I want to acknowledge the indefatigable Mrs. Melissa Rochon, for her immense help during my entire stay in the Chemistry department at Wayne State University. You always had time for my questions and helped me with all my problems. I am grateful to Ms. Jacqueline Baldyga and the entire front office staff, I am forever indebted to you. I would like to express appreciation to the business office staff and the professors I taught undergraduate chemistry for. Professors, Barber, Zibuck, Munk and Matti, you imparted excellent teaching skills during my time as a graduate teaching assistant. Thank you.

Thanks to the entire Lumigen Instrument Center staff for helping with data analysis, especially Drs. Judy Westrick, Lew, Phil Martin, Yuri Danylyuk, Mei, Bashar Ksebati, and Johnna Birbeck, Nestor Ocampo, and all the science store staff.

To Nicole Lenca and my family, words cannot express my gratitude for all that you have sacrificed for me during these difficult times. Your patience, care, and affection are greatly treasured. We made it!!

Last but not the least, I am grateful to the Chemistry Department and Graduate School, Wayne State University for offering me teaching assistantships and tuition support at various points during my study. I acknowledge the Department of Energy (DOE) and the National Science Foundation (NSF) for providing the necessary funding for my research and stipend with various grants. I want to thank Dr. Paul Schaap and his wife, the Mary Gorny Wood Foundation, and the Thomas Rumble Foundation for supporting me with Fellowships during my Ph.D. Your financial support made graduate school bearable. Thank you.

TABLE OF CONTENTS

LIST OF FIGURES

LIST OF TABLES

LIST OF SCHEMES

CHAPTER 1:

INTRODUCTION

Water Splitting

$$2H_2O \longrightarrow O_2 + 2H_2$$

CHAPTER 1: INTRODUCTION

1.1. Background to Global Demand for Alternative Energy

Global population increase and pollution of the environment are major concerns.[1] According to the United Nations, about 89% of global energy sources are based on carbon sources. The use of these fuels produces byproducts such as carbon dioxide (CO_2) and other harmful greenhouse gases. It is expected that, at the turn of the century, more than 13.3 gigatonnes of carbon per year (GtC/yr) would be produced and have a harmful effect on our environment.[2] More alarming is the fact that carbon-based energy sources are not renewable and their substantial use will lead to their depletion by 2055 unless new sizable reserves are found.[3] This crisis, therefore, requires the search for an alternative energy source.[4] Hydrogen production from water using the Sun as an energy source is considered the answer to this looming global fuel crisis.[5] Water splitting involves a series of thermodynamically demanding redox reactions in which water is converted into its basic components, namely, dihydrogen and dioxygen, as shown in equations 1 to 3.[6-8]

$$2H_2O \rightarrow 2H_2 + O_2 \qquad (1)$$

$$2H_2O \rightarrow O_2 + 4H^+ + 4e^- \qquad E^0 = 1.23\ V \qquad (2)$$

$$4H^+ + 4e^- \rightarrow 2H_2 \qquad E^0 = 0\ V \qquad (3)$$

However, there is a thermodynamic barrier of 1.23 V for converting water into dihydrogen and dioxygen.[9] In order to overcome this energy barrier, an efficient, robust and affordable catalyst capable of offering a milder mechanistic pathway to obtain the desired products is needed. The development of water-splitting catalysts incorporating transition metals is of immense scientific interest. So far the most efficient water-splitting catalysts are noble metals such as ruthenium[10,11,12] and iridium.[13] Yet, in the past decade, commercial availability and Earth-abundance have become the overriding factors necessary to finding effective alternatives to these noble-metal catalysts. The

development of electrocatalysts based on low-cost materials made of Earth-abundant metals such as cobalt,[14-21] nickel,[22-25] copper,[26-27] and iron,[28-30] is therefore perceived as an indispensable step towards the generation of efficient photocatalysts.

1.1.1 Hydrogen as an Energy Source

It is expected that hydrogen will eventually reduce the Earth's dependence on crude oil for its energy needs due to its high efficiency and low polluting nature.[1, 31,32] It can be easily stored in large quantities and transported with relative ease. Hydrogen can be obtained from the electrolysis of water, or the steam reformation of hydrocarbons such as methane. While steam reformation is currently the cheapest method of producing dihydrogen, it uses fossil fuels and contributes to greenhouse effects. It is therefore not a sustainable alternative to the use of coal.

The electrolysis of water to produce hydrogen, however, involves using electric current to 'split' water into its constituent elements, dihydrogen and oxygen gas. This process is unfortunately extremely expensive because it requires the use of electrical energy as well.

1.1.2 Oxygen as an Energy Source

To produce dihydrogen by electrolysis, water must be oxidized according to Equation 2. This process is energetically unfavorable as it requires 238 $kJmol^{-1}$ of energy to occur. The scientific community has invested effort in solving this 'bottleneck' over the past two decades.[11, 33-42] Nature, however, has perfected the process of oxidizing water to dioxygen through photosynthesis. Plants oxidize water to oxygen by utilizing a series of proton-coupled-electron-transfer (PCET) steps that include the formation of an essential O – O bond in the photosystem II (PS II).[43]

In the (PS) II, a central pair of chlorophylls, P_{680} is excited by energy from the sun and transfers an electron to the acceptor system Q_A, which subsequently reduces CO_2. The oxidized

form, $P_{680}^{\bullet+}$, which is a strong oxidant with an oxidation potential of *ca.* +1.2 V versus the normal hydrogen electrode (vs NHE),[44] then recovers the electron from a Mn_4Ca-cluster in the oxygen-evolving complex (OEC) via a tyrosine bridge.

After four consecutive electron abstractions from the OEC, two molecules of H_2O are oxidized to generate one molecule of O_2 and four protons as shown in equation 3 above. Numerous research efforts have been directed at mimicking this process. However, these efforts have been quite daunting due to the non-trivial multi electronic nature of producing hydrogen through photosynthesis, and the mechanistic intricacies associated with the photosynthetic process. There is, therefore, an urgent need to focus attention on some persisting design and mechanistic questions in order to develop a system optimized to support photocatalysis.

1.2. Methods of Water Splitting Catalysis

The process of converting water into dioxygen and dihydrogen, using a catalyst can be broadly categorized into two main categories.

1.2.1 Water Reduction Catalysis

A) **Electrocatalytic Proton/Water Reduction:** The catalytic reduction of weak organic acids in organic solvents, or of water, with a catalyst is known as electrocatalytic proton/water reduction. Typical acid sources for proton reduction are CH_3COOH and CF_3COOH, while water serves as the proton source for water reduction. An efficient proton/water reduction catalyst undergoes successive electron reductions to attain a monovalent state when an appropriate electrochemical potential is applied. The monovalent species is then nucleophilic enough to attract a proton and form a metallo-hydride and subsequently, produces hydrogen.

B) **Photocatalytic Water Reduction:** Water reduction by a catalyst, and photosensitizer in the presence of a sacrificial electron donor. Here also, the photosensitizer absorbs light radiation

of an appropriate wavelength, is excited, and quenched by the electron donor. The photosensitizer subsequently transfers an electron to reduce the catalyst. Hydrogen is subsequently produced.

1.2.2 Water Oxidation Catalysis

A) **Chemical water oxidation:** This is a method of catalysis where a chemical substance is used as a sacrificial oxidant. In this type of water oxidation, the catalyst of choice, the substrate (water) and the chemical oxidant are reacted and the evolution of gas (oxygen) is observed and quantified after a specified period of time. An efficient chemical oxidant must have a reduction potential sufficient enough to oxidize the water oxidation catalyst.[45] Chemical oxidants such as cerium (IV) ammonium nitrate, Oxone ($KHSO_5$), NaOCl, are the most commonly used in chemical water oxidation The use of these oxidants is advantageous because it enables the study of oxidative intermediates in solution. They also aid in the production of relatively large amounts of oxygen, thereby making the screening of catalytic parameters for potential catalysts rapid and cost effective. The main disadvantage of their use is that they do not perfectly mimic the conditions that will be experienced by a catalyst and hence are considered preliminary at best.

B) **Electrocatalytic Water Oxidation:** In this method, the oxidation of water is achieved at the surface of an electrode when an electrochemical potential is applied to a solution containing an electrocatalyst.

C) **Photocatalytic Water Oxidation:** This process involves the use of a photosensitizer, a catalyst, and a sacrificial electron acceptor. The photosensitizer absorbs radiation of an appropriate wavelength and transitions to an excited state where the transfer of electron/s to the sacrificial acceptor takes place. The catalyst then transfers its electrons unto the photosensitizer by sequential oxidations until a high-valent electrophilic oxidation state is attained. Water then attacks and produces oxygen.

1.3. Important Parameters for Electrocatalytic Water Splitting

A water-splitting catalyst must meet and be benchmarked against certain parameters that are relevant water splitting electrocatalysis.

Those parameters are:

Turnover number (TON): The number of moles of hydrogen generated per mole of catalyst used

TON = number of moles of hydrogen/number of moles of catalyst

Turnover frequency (TOF): The turnover number per unit time. This parameter describes the rate of efficiency of a catalyst.

TOF = TON/time

Faradaic efficiency (FE): The ratio of the number of moles of hydrogen generated (n_{H2}) to half of the moles of the number of electrons passed during the electrocatalytic experiment ($n_e/2$).

FE = $n_{H2}/(n_e/2)$

An efficient molecular electrocatalyst should operate at a Faradaic efficiency of 80 – 100%.

1.4. Mechanistic Pathways for Catalytic Water/Proton Reduction

The production of H_2 from Co^{III}-H follows either heterolytic or homolytic pathways shown in **Figure 1.1**.[46,16,47] The former mechanism relies on a single Co^{III}–H^- reacting with another H^+, while homolytic mechanisms involve two independent Co^{III}–H^-moieties.[48]

The reliance on a particular mechanism is governed by factors such as the concentration of acid used,[49] catalyst design, applied potential,[50] the rate constants for hydride formation,[51] and whether H_2 is evolved by hydride protonation or dimerization.[52] Weak organic acids such as trifluoroacetic acid (TFA),[53-55] acetic acid, and triethyl ammonium chloride, have been used as proton source in electrocatalytic hydrogen production but are susceptible to concentration degradation, and organic waste produced during the production of dihydrogen.[56] The susceptibility

to degradation can limit the wide use of weak acids as suitable proton sources, therefore a more benign source is desirable.

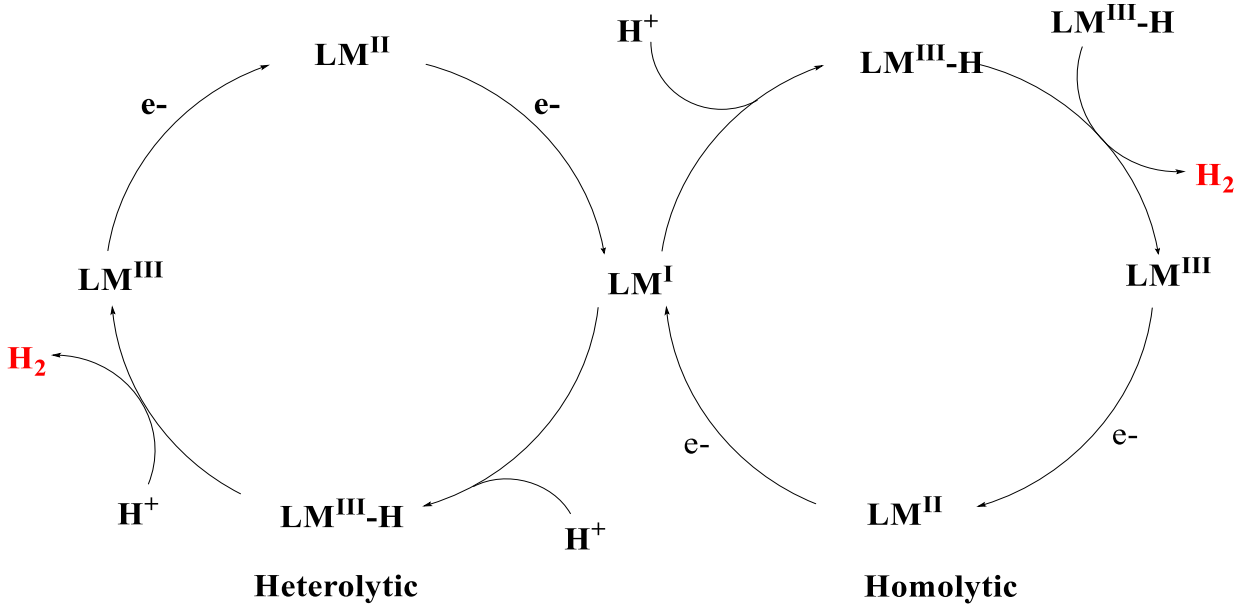

Figure 1.1. Generalized Catalytic mechanisms of H_2 generation.

1.5. Homogeneous Molecular Catalysts for Water/Proton Reduction

The efficient reduction of protons or water to form dihydrogen as shown in Equation 3 above is crucial to the use of hydrogen as the fuel for the future. Therefore Earth-abundant molecular proton/water reduction catalysts have been of immense scientific importance in the past three decades. Ideally, a transition metal-complex should be reduced to its monovalent state and be sufficiently nucleophilic when it accepts an electron. This nucleophilic monovalent species should then attract protons, reduce them to hydrogen and get oxidized to its original oxidation state. The most efficient proton reducing electrocatalysts are based on platinum complexes.[57,58] platinum catalysts are however expensive and rare. First-row transition metals such as manganese, iron,[29-30, 59-60] nickel,[23-25, 61-64] and cobalt[62, 65-67] have been explored as affordable replacements for the platinum catalysts.

1.5.1 Molecular Water/Proton Reduction Catalysts based on Cobalt

1.5.1.1. Molecular Cobalt Oximes

Schrauzer and Holland[68] observed hydrogen evolved hydridocobaloximes when working on model analogs of Vitamin B12 **(Figure 1.2a)**. This discovery led to the exploration of the field of hydrogen generation led by Espenson and Connelly in 1986.[14] During their work on an analog of Schrauzer's cobaloxime **(Figure 1.2b)**, they found out that upon treatment of the complex with Cr^{2+} reductants under acidic conditions, hydrogen gas could be formed.

Peters *et al*,[53] and, Artero *et al*[50, 69] have studied cobalt-based oximes **(Figures 1.2c,d)** extensively and found that they are excellent catalysts for proton reduction in organic media with weak organic acids. These compounds require low overpotentials to generate hydrogen from acids. Verani[54] and coworkers performed an extensive study on cobalt oximes bearing hetero-axial ligands **(Figure 1.3)** to evaluate the effect of coordination preferences on their mechanistic pathways.

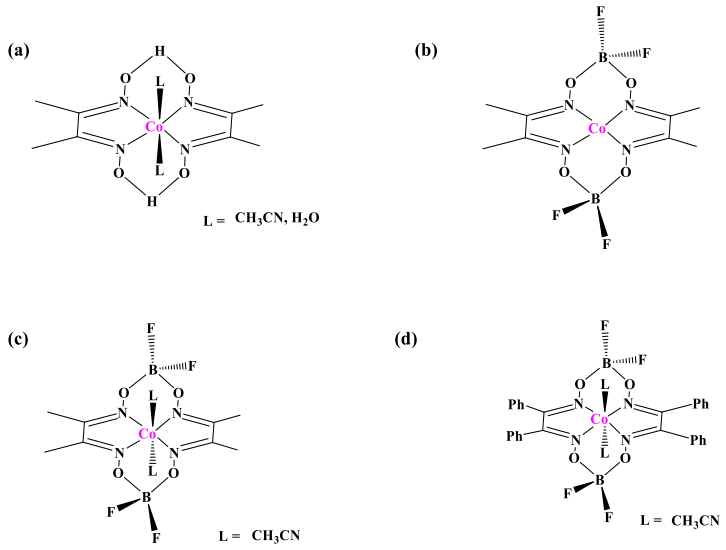

Figure 1.2. Selected cobalt-based oximes for proton reduction.

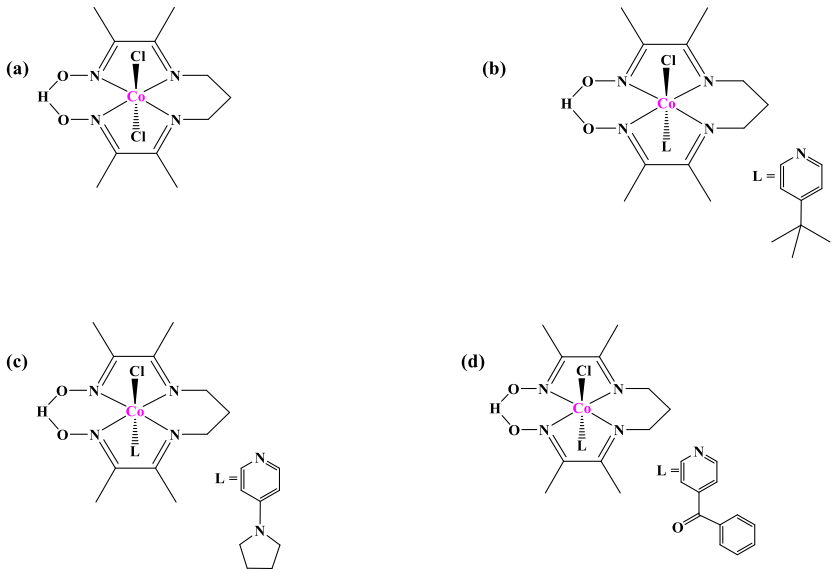

Figure 1.3. Selected heteroaxial cobalt oximes for proton reduction by the Verani *et al*.[54]

The variation of axial ligands has a significant effect on both the overpotential and TONs of the catalysts, except in the case of pyridine substitution where TONs are affected but overpotentials remain unchanged. The study provided experimental evidence for a five-coordinate environment for the catalytically active $3d^8$ Co^I species.

A catalytic pathway was proposed for H_2 production by the complex in **(Figure 1.3b)** in the presence of TFA in CH_3CN, where the catalytically Co^{III}–H^+ intermediate undergoes either a heterolytic or a homolytic pathway, with the latter mechanism more likely under low acidic conditions **(Figure 1.4)**.

The main drawback associated with cobalt oxime catalysts is ligand stability under harsh acidic conditions;[66] therefore, pyridine ligands were introduced to provide some steric bulk and robustness. Pyridines are aromatic and have strong bonds, hence tend to be hydrolysis resistant. They are strong σ-donors and are capable of π back-bonding as well, hence are capable of stabilizing monovalent cobalt species.

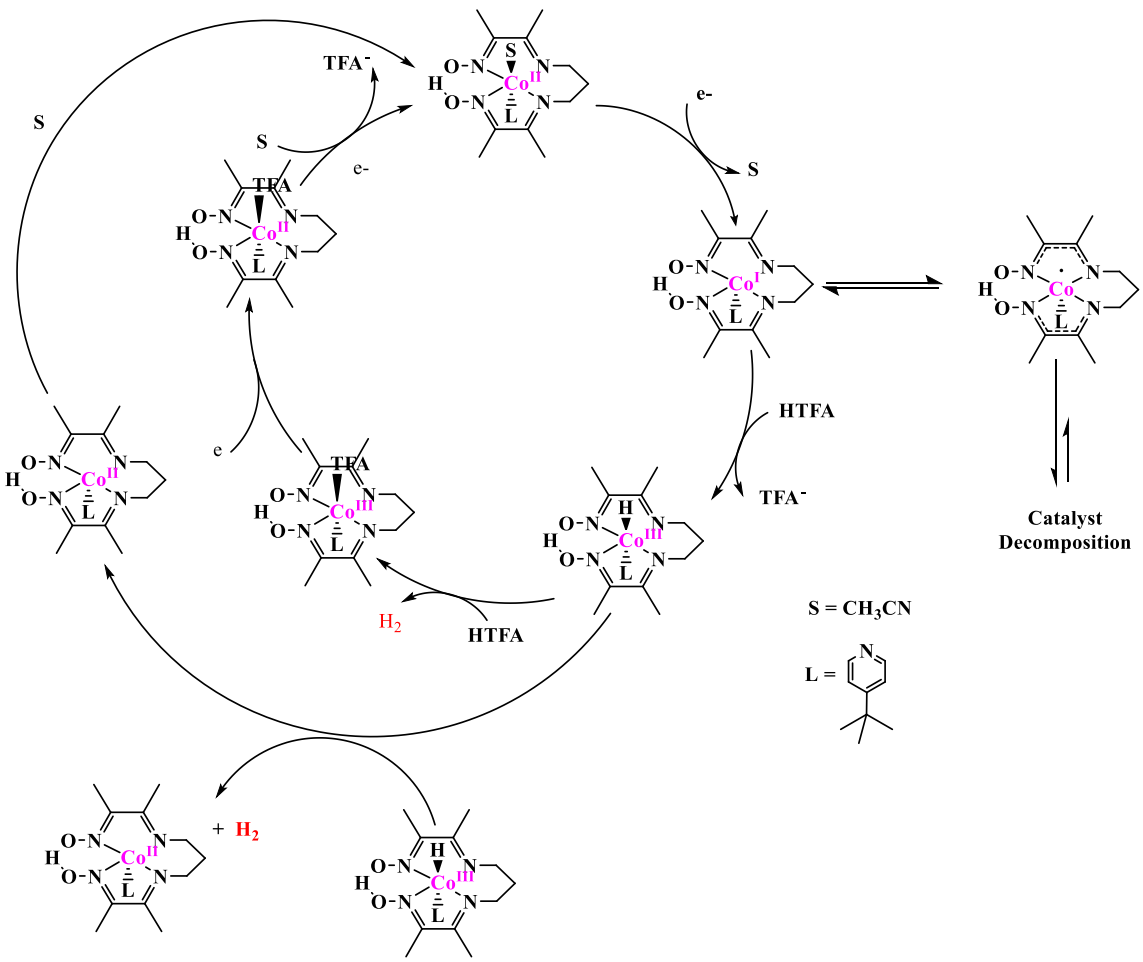

Figure 1.4. Proposed proton reduction catalytic mechanism of H_2 generation by Verani *et. al.*[54]

1.5.1.2. Molecular Cobalt Polypyridyl Systems

Chang[70] and coworkers studied the proton/water reduction catalysis of a $[Co(Py_4)CH_3CN]$ complex **(Figure 1.5a)** (Py_4 = 2-bis(2-pyridyl)(methoxy)methyl-6-pyridylpyridine). The pyridine ligands gave an added advantage of solubility in water which improved the catalytic activity during proton reduction with 99% Faradaic yields in organic solvent, and CH_3CN : water (50 : 50). However, the authors did not report any TONs, choosing instead to do a qualitative study. Zhao *et. al.* [71] studied the electro- and photocatalytic activity of a mononuclear Co complex, [Co(DPA-Bpy)Cl]Cl and its Aqua analog $[Co(DPA\text{-}Bpy)(H_2O)](PF_6)_3$ (**1.5b**), [DPA-Bpy = *N*,*N*-bis(2-pyridinylmethyl)-2,2′-bipyridine-6-methanamine] and observed that the aqua complex catalyzed

H_2 production from H^+ efficiently with an overpotential of 0.6 V in water. Seeking to investigate the electronic effects of replacing the pyridines with a more basic isoquinoline ligand on catalytic efficiency of the catalyst, the authors replaced the ligand moiety to yield [Co(DIQ-Bpy)Cl]Cl and [Co(DIQ-Bpy)(H_2O)](PF_6)$_3$ (**1.5c**), [DIQ-Bpy = *N*,*N*-bis((isoquinolin-1-yl)methyl)(6-(pyridin-2-yl)pyridin-2-yl)methanamine]. When a more basic and conjugated ligand moiety replaces pyridines for their cobalt catalyst, the water reduction catalytic efficiency increased dramatically with lower overpotential, improved TON and TOF, and a more robust and stable catalyst overall.

A detailed mechanistic study was undertaken by Muckerman, Fujita, and Polyansky,[72] using Zhao's 1st generation catalyst **(Figure 1.5b).** They relied on an array of experimental and theoretical techniques such as cyclic voltammetry, bulk electrolysis, mass spectrometry, pulse radiolysis, laser flash photolysis, and density functional theory (DFT), to track, and characterize the relevant intermediates proposed in the catalytic cycle.

The results of their study indicated that the aqua axial ligand is strongly bound to the trivalent cobalt center in an octahedral geometry. Upon one-electron reduction, the Co – O bond weakens making the $3d^7$ $[Co^{II}–OH]^+$ species relatively stable. Upon a second one-electron reduction of the $[Co^{II}–OH]^+$ yields a $3d^8$ Co^I species in which the Co-O bond further weakens and eventually breaks to form a five-coordinate $[Co^I–VS]^+$ species (VS = vacant site). Interestingly, they observed that there was a transient rearranged $[Co^I(\kappa^4\text{-L})(OH_2)]^+$ intermediate species where water is still bound and one pyridine is detached from the Co center instead. The results of this study benchmarked the now widely accepted conclusion that the $3d^8$ Co^I species undergoes some structural reorientation to form a preferred five-coordinate geometry prior to attracting a proton, to form a cobalt hydride. This structural reorganization or transformation is considered the rate-

determining step (RDS). Pentadentate ligand platforms have been designed for cobalt catalysts after the study described to ensure a more efficient catalysis

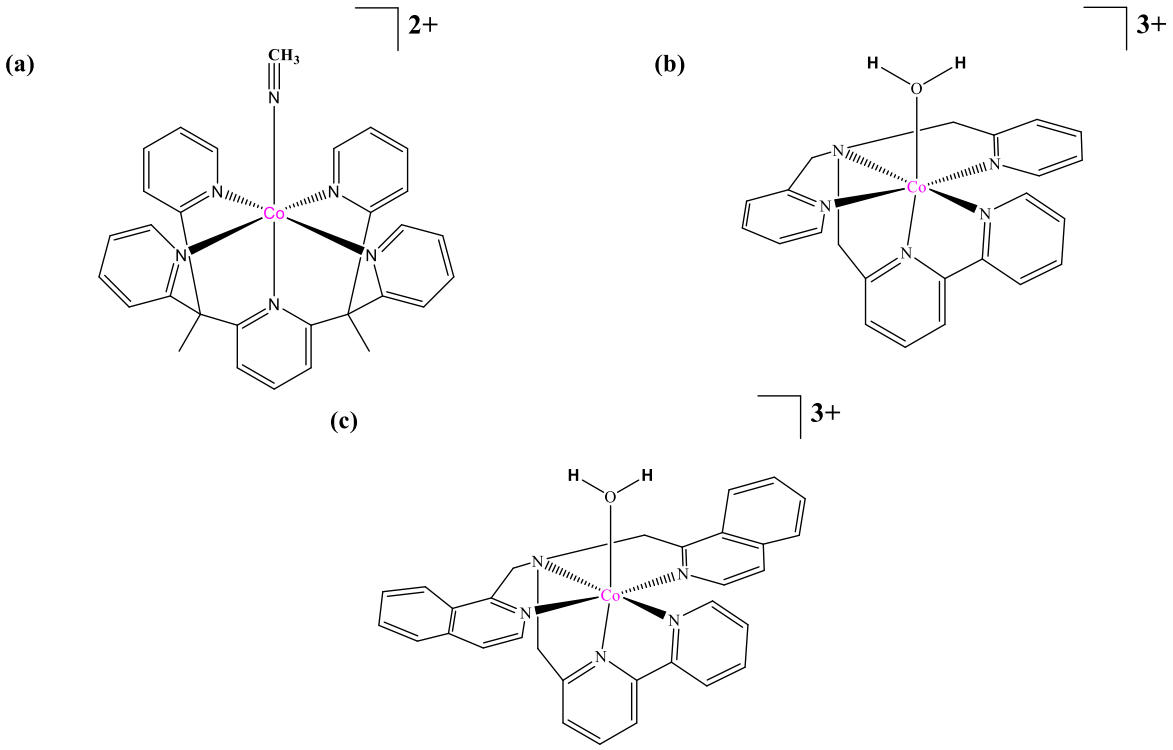

Figure 1.5. Selected cobalt-based polypyridyl catalysts for water reduction.

The Verani group recently published a series of water-reduction catalysts **(Figure 1.6)** based on pentadentate pyridine-rich ligand platforms of iminopyridine **(Figure 1.6a)**, amidopyridine **(Figure 1.6b)**, methoxy-substituted **(Figure 1.6c)**, and *N*-methyl substituted pyridine **(Figure 1.6d)**.[73]

The methoxy and amido catalysts resulted from the transformation of ligand scaffold in imine complex by adventitious methanol and water solvents, respectively. The *N*-methylated ligand analog prevented the transformation but increased the overpotential required for catalytic water reduction because the ligand has lost its redox activity.

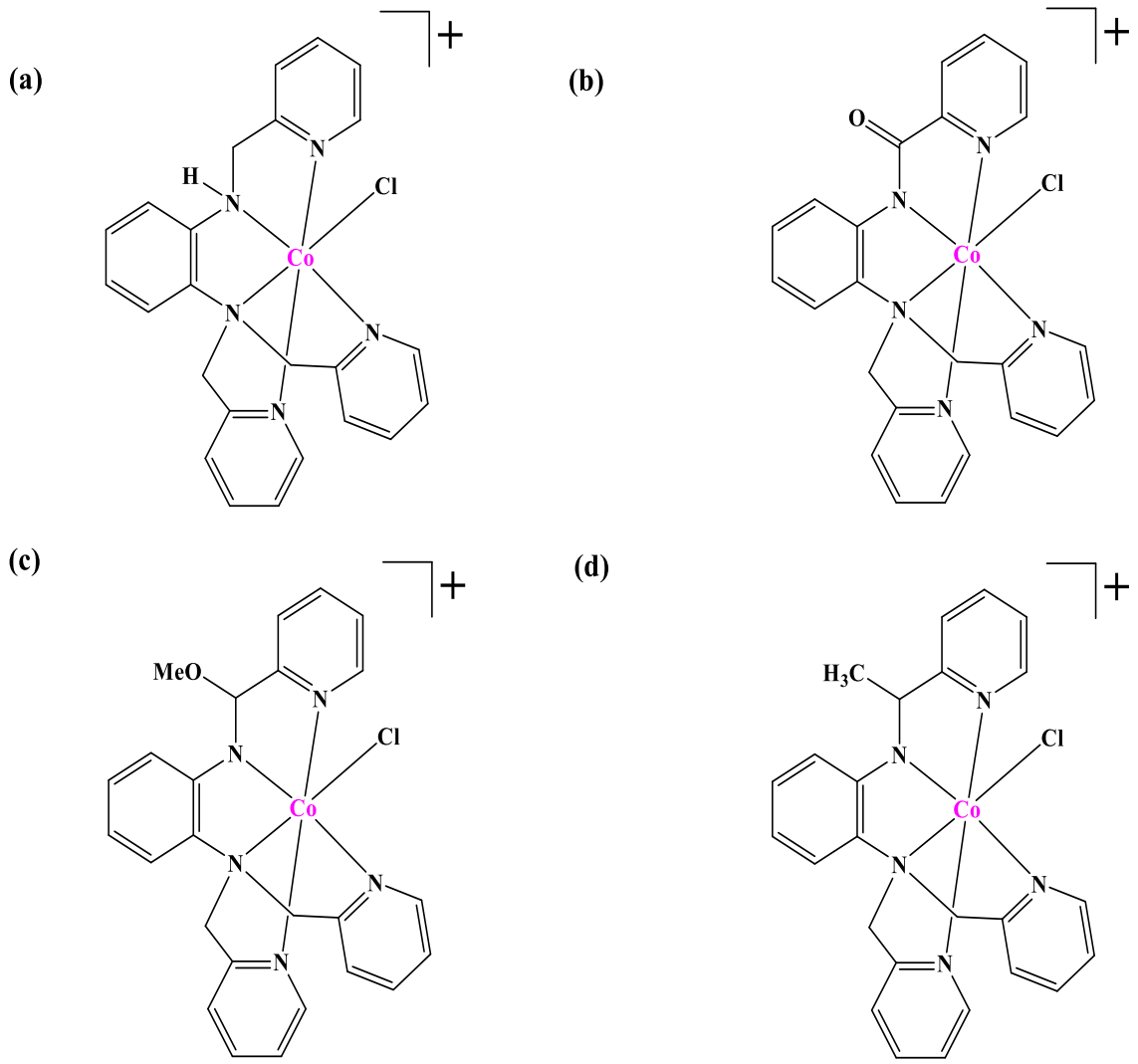

Figure 1.6. Pentadentate cobalt-based polypyridyl catalysts by Verani *et. al.*[73]

The two catalysts, **1.6b and 1.6d**, showed excellent water reduction activity with $TONs_{18h}$ of 7000 and 6000 respectively, placing them among the most efficient molecular cobalt catalysts for hydrogen production. Based on experimental and DFT results, a detailed mechanism was proposed **(Figure 1.7),** in which a nucleophilic five-coordinate $3d^8$ Co^I attracts a proton to form a Co^{III}-H, which undergoes further reduction to a Co^{II}-H state before attracting another proton to give hydrogen.

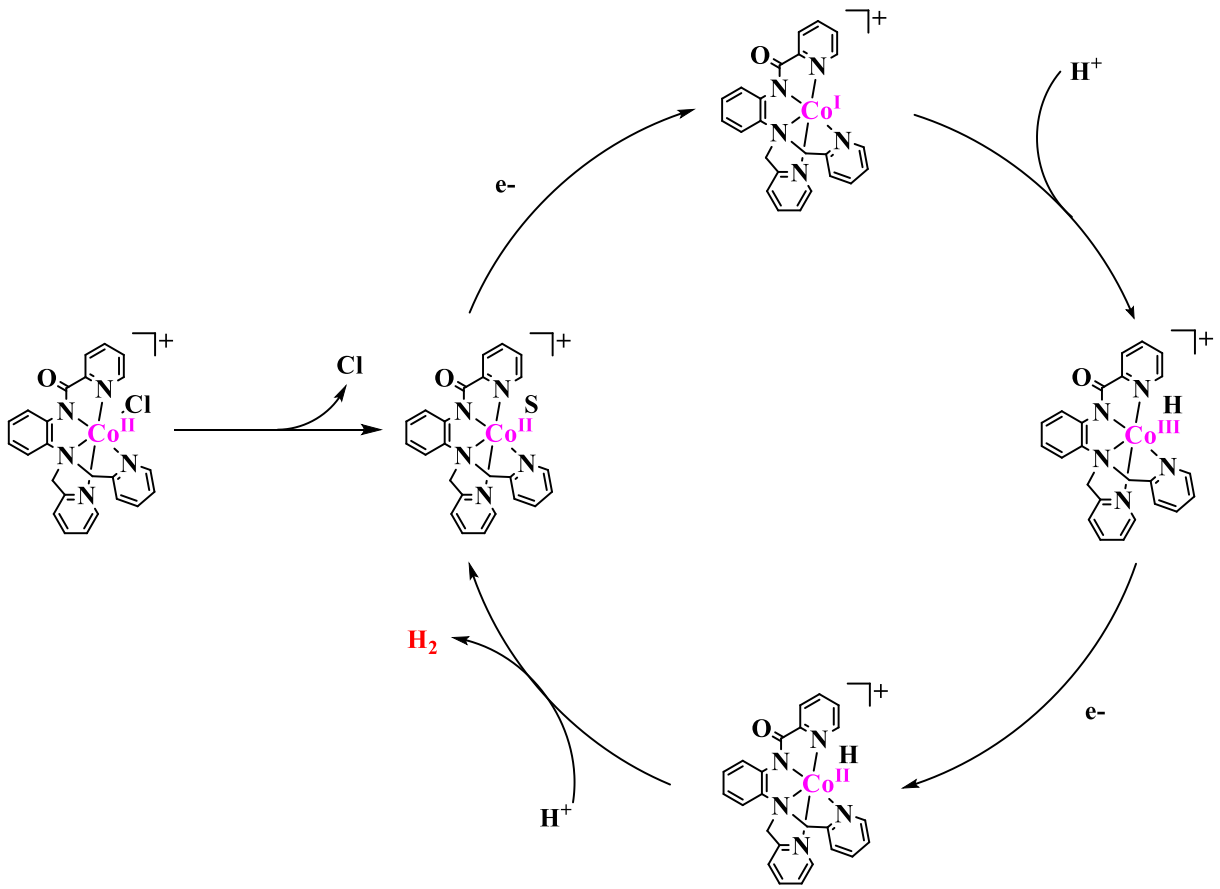

Figure 1.7. Catalytic pathway for H_2O reduction with cobalt amidopyridine by Verani *et al*.[73]

1.5.1.3. Molecular Bimetallic Cobalt Systems

Over the past 5 years, attempts were made to design and study the catalytic activity of bimetallic cobalt proton reduction catalyst with the expectation of enhanced performance. The idea of bimetallic catalysts being twice as efficient as their monometallic counterparts has led to the design of bimetallic cobalt complexes **(Figure 1.8).** Peters[74] and his group synthesized a dinuclear $Co_2(dmgBF_2)_2L_2$ complex based on a bridging pyridazine backbone **(Figure 1.8a).** This complex did not catalyze the production of hydrogen from protons but served to be a model for rich redox chemistry of bimetallic cobalt complexes.

Fukuzumi[48] and coworkers designed a bimetallic Co complex with bis(pyridyl)-pyrazolato (bpp) and terpyridine (terpy) ligand platforms **(Figure 1.8b)** and studied its catalytic activity

towards proton reduction by a combination of chemical and electrochemical techniques designed to track the kinetics of the catalytic process. The parent [$Co^{III}Co^{III}$] undergoes a three- or four-electron reduction by cobaltocene in acetonitrile to produce [$Co^{II}Co^{I}$] or [$Co^{I}Co^{I}$], respectively, which they observed was in the protonation equilibrium with [$Co^{II}Co^{III}$–H] intermediate. The hydride was further protonated by trifluoroacetic acid (TFA) to produce hydrogen. The authors, however, did not see a cooperative mechanism suggested by Gray[75] and coworkers. The catalyst operates at an overpotential of 0.6 V. A heterolytic mechanistic pathway was proposed where either cobalt center forms the hydride and produces hydrogen independent of the other.

Gray[76] and his group investigated the proton reduction catalysis of two bimetallic $Co(dmgBF_2)_2$ type catalysts; one with an eight-carbon (8C) chain bridge **(Figure 1.8c)**, and the other with a boron bridge **(Figure 1.8d)**. When the catalytic activity of the long chain complex was compared with a monometallic model, there was no improvement in catalysis, which suggests that the long chain complex undergoes catalysis through a bimolecular heterolytic pathway. The boron-bridged analog performed less efficiently than its monometallic analog operating at an overpotential of 1 V). Dinolfo[77] and his group studied the proton reduction catalytic activity of two dicobalt tetrakis-Schiff base catalysts, [Co_2LAc^+] and [Co_2L^{2+}] (Figure 1.12e), in CH_3CN using with TFA and CH_3COOH as proton sources, [L = N_6O_2 Schiff base macrocycle; Ac = acetate bridge].

Results of the study indicate that Co_2L^{2+} operates at an average Faradaic efficiency of 90% in the presence of CH_3COOH but requires a relatively high overpotential for catalysis. Hydrogen production may be initiated by a bimetallic catalytic mechanism involving adjacent [Co^{III}–H]$_2$ or a heterolytic attack of an incoming proton on a [$Co^{II}Co^{II}$-H] due to the close proximity of the two

Co ions in both complexes (3.2 Å), but no evidence was provided by the authors to support the proposed mechanism.

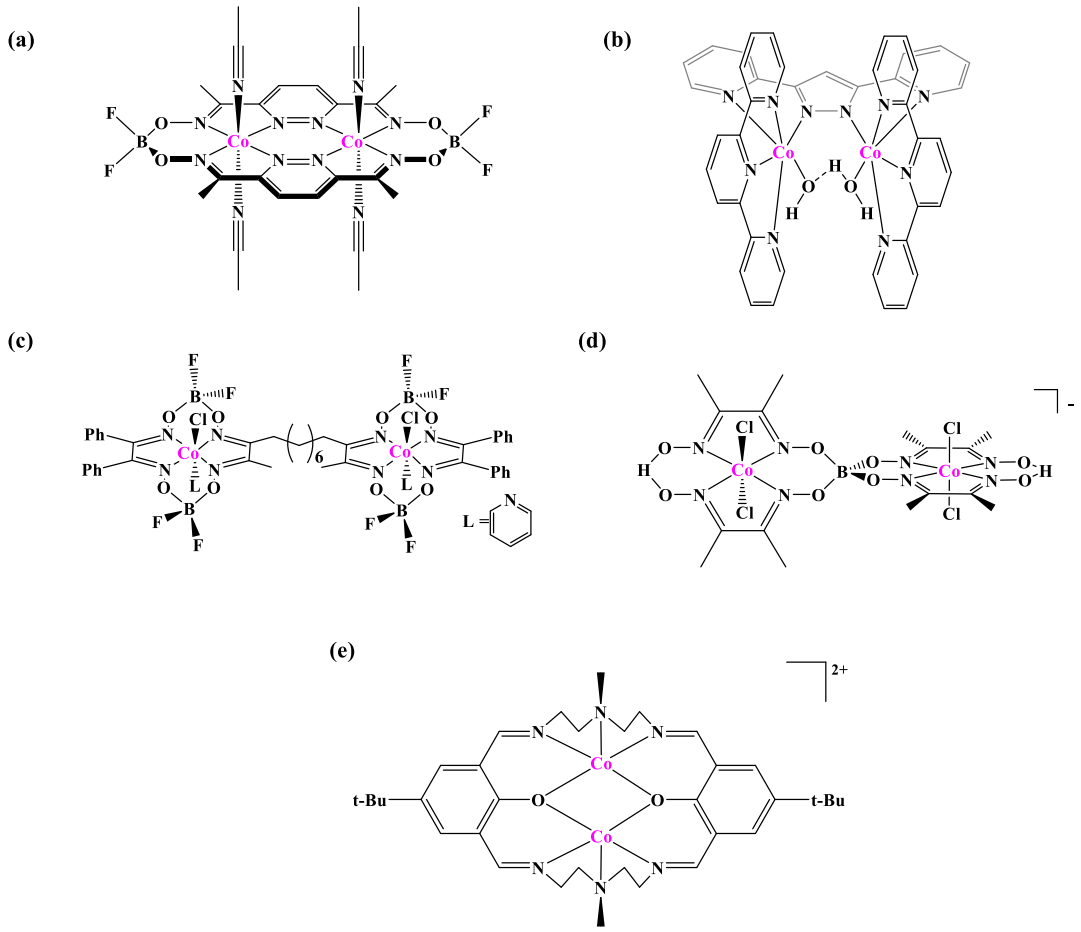

Figure 1.8. Selected bimetallic cobalt-based catalysts for proton reduction.

1.6. Homogeneous Molecular Catalysts for Water Oxidation

Over the decades, scientists have tried to mimic the functions of the oxygen-evolving complex (OEC) in Photosystem II, thereby designing not only functional mimics but also structural mimics for water oxidation. An efficient water oxidation catalyst is expected to allow the transfer of four electrons at potentials greater than the thermodynamic potential of +1.23 V in one-electron oxidation processes. The design of such a catalyst requires identifying and characterizing key intermediates and the understanding of mechanistic pathways. The catalyst will have to stabilize

various intermediates required to oxidize water to oxygen in order to lower the kinetic energy barrier and hence result in quicker turnovers of oxygen from water. Many transition-metal complexes have been developed as catalysts for water oxidation. These include but are not limited to manganese, ruthenium, cobalt, iron, and iridium. Each of these elements has shown catalytic efficiency with ligand platforms such as terpyridines,[7, 78] phenolates,[79, 80] and pyridines.[41, 81] The search for an efficient artificial catalytic water oxidation catalyst was started by Calvin[82] and coworkers in the mid-1970s where, they performed photochemical evaluations on a dinuclear -μ-oxo bridged mixed-valent manganese polypyridine complex. However, their results were inconclusive, as they later observed that the oxygen detected may have percolated through their experimental set up from the atmosphere.

1.6.1 Molecular Water Oxidation Catalysts based on Ruthenium Complexes

Several studies based on ruthenium have been undertaken since that time **(Figure 1.9)** Meyer[83] and coworkers are known to have developed the first 'true' homogeneous water oxidation catalyst $[(bpy)_2Ru^{III}(\mu\text{-}O\text{-})\ Ru^{III}(bpy)_2]^{4+}$, called the "Blue Dimer" **(Figure 1.9a)**, utilizing a bipyridine ligand platform and ruthenium.

The choice of ruthenium afforded the observation of key intermediates due to relatively slower ligand exchange rates in ruthenium complexes. They observed the rapid evolution of oxygen upon addition of four or more equiv of a one-electron chemical oxidant, ceric ammonium nitrate (Ce^{IV}), suggesting that the catalytic-active species is a four-electron oxidized intermediate. The authors, therefore, proposed a mechanism involving an initial four-electron oxidation to give a pentavalent dimeric rutenyl intermediate, which in turn gives O_2 in a concerted four-electron step. Llobet *et. al.* [84] reported on a bimetallic Ru catalyst bearing a Hbpp type bridging ligand **(Figure 1.9b).** This terpy-Ru-bpp dimer $[Ru_2^{II}(bpp)(terpy)_2(H_2O)_2]^{3+}$ (Hbpp = 2,2′-(1H-pyrazole-

3,5-diyl)bis(pyridine), which had the two ruthenium ions in close proximity thus avoiding the Ru-O-Ru bridge that was present in the blue dimer.

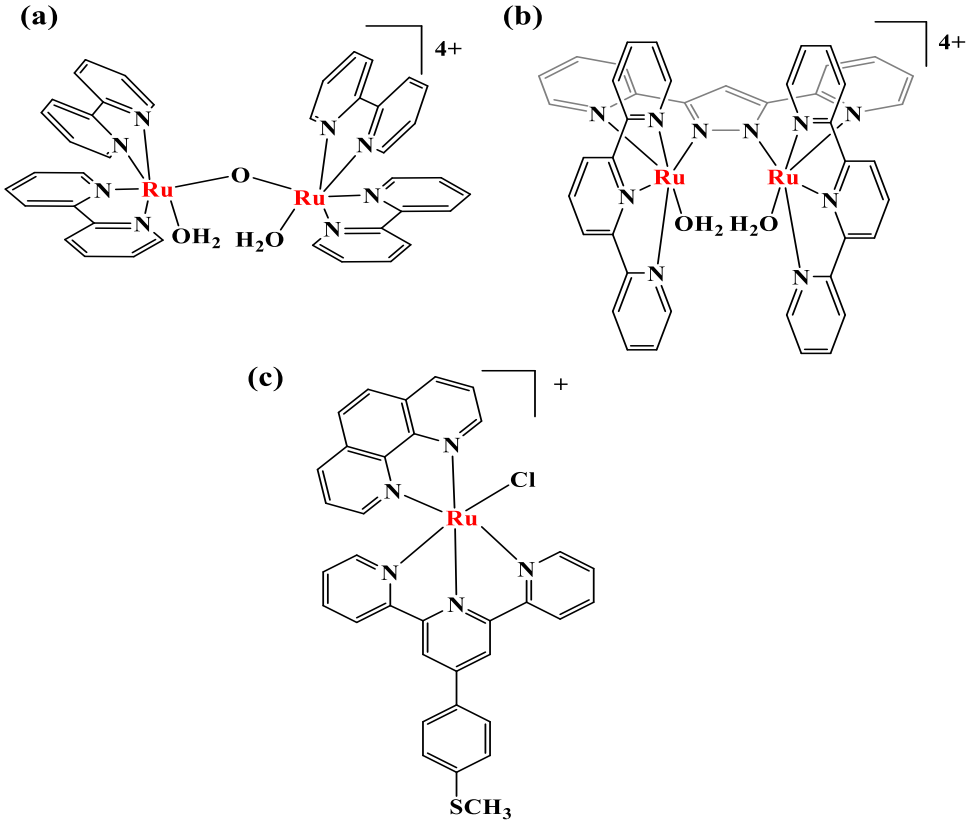

Figure 1.9. Selected homogeneous ruthenium-based catalysts for water oxidation.

The unique modification of the μ-oxo bridge in the terpy-Ru-bpp dimer enhanced the activity of the catalyst for homogeneous oxygen evolution and avoided decomposition. Thummel[35,85,86] and coworkers introduced a new type of binuclear and a variety of single site ruthenium derived water oxidation complexes They proposed a mechanism involving a seven-coordinate Ru^{IV} species which suggested the O – O bond formation occurs at an electrophilic Ru^{VI}=O bond. However, a detailed and critical evaluation of the mechanistic pathways for these catalysts is either lacking or are solely based on DFT computations. Verani[12] and coworkers studied substituent effect on water oxidation for a series of $[Ru^{II}(terpy)(phen)Cl]^{+}$ catalysts

(Figure 1.9c). When the authors compared the effects of substituted phenanthroline with electron-donating and electron-withdrawing groups on the catalytic activities of their catalysts, they concluded that catalytic activity was enhanced by the presence of electron-donating groups on the phenanthroline moiety, while the presence of electron-withdrawing substituents impedes the catalytic activity. They also observed an induction period for catalysis and ruled out a ligand-exchange mechanism. Based on their findings, they proposed a mechanism of water oxidation involving a seven-coordinate ruthenyl (Ru^{IV}=O) similar to the mechanism proposed by Thummel, supported by experimental evidence.

1.6.2 Molecular Water Oxidation Catalysts based on Manganese Complexes

Manganese-based water oxidation catalysts **(Figure 1.10)** have unique relevance because this ion has a broad range of oxidation states and is abundant in the Earth's crust.[87] Manganese is also the main transition element that constitutes the OEC in Photosystem II, and therefore, has been used extensively.

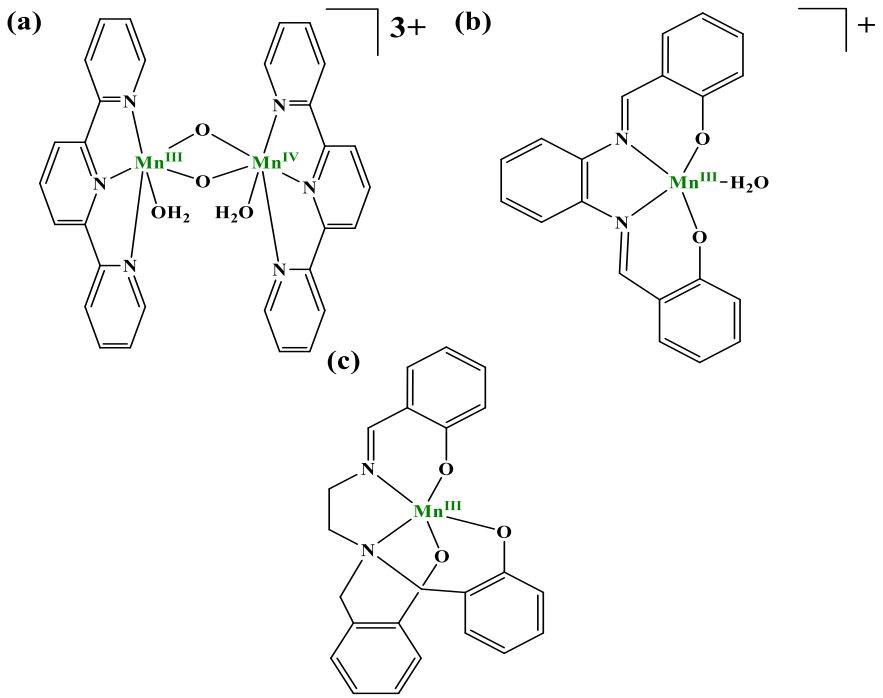

Figure 1.10. Selected homogeneous manganese-based catalysts for water oxidation.

Brudvig[88] and coworkers, reported the so-called "terpy-dimer" **(Figure 1.10a),** a di-terpyridine di-manganese complex, $[(terpy)(H_2O)Mn(\mu\text{-}O)_2Mn(terpy)\ (H_2O)]^{3+}$, in 1997 with a $3d^4$ Mn^{III} as one of the metal centers and a $3d^3$ Mn^{IV} as occupying the other center. The oxygen evolution activity of this catalyst in the presence of sodium hypochlorite was studied, utilizing ceric ammonium nitrate (Ce^{IV}), and observed a low (TON) of 4 after six hours of catalysis. This was due to the decomposition of the Mn dimer to form permanganate ions in solution.[88]

However, when Oxone (HSO_5^-) was used as the chemical oxidant, continuous water oxidation activity was observed. They proposed a mechanism **(Figure 1.11)** where Oxone first binds to the Mn(III, IV) dimer

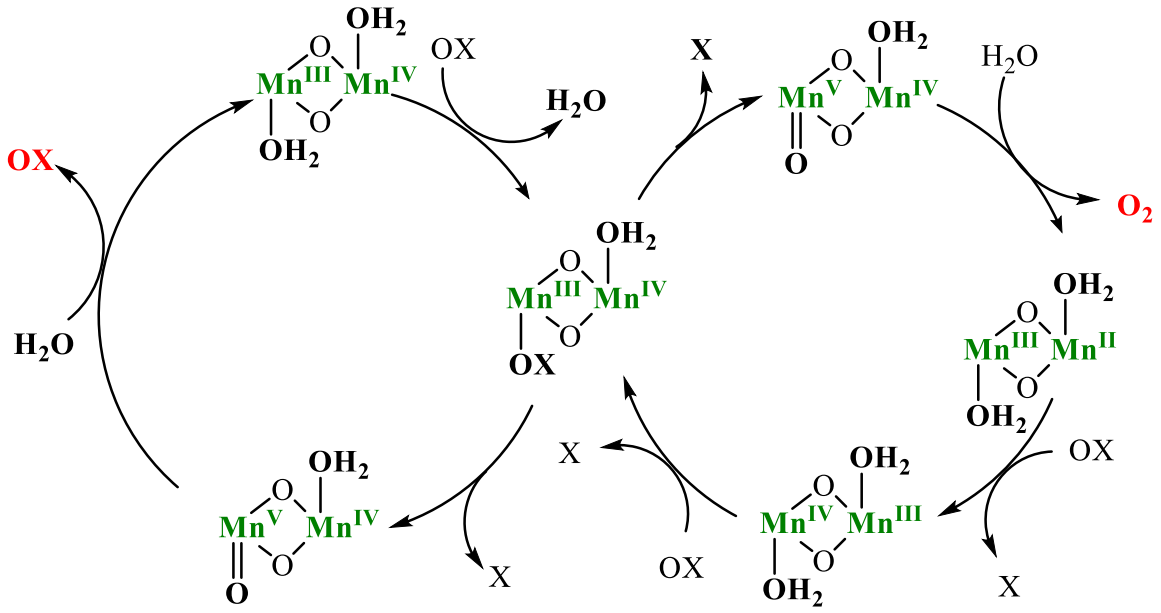

Figure 1.11. Proposed mechanism by Brudvig *et al* for the reaction between $[(terpy)(H_2O)Mn(\mu\text{-}O)_2Mn(terpy)\ (H_2O)]^{3+}$ and chemical oxidants XO (XO = NaOCl or $KHSO_5$).

After binding there are two mechanistic pathways possible due to the presence of two manganese centers, one in which no oxidation occurs when (HSO_5^-) binds to Mn(IV), because a two-electron oxidation would give a Mn(VI) which is inaccessible in that ligand environment. The second pathway involves the (HSO_5^-) binding to the Mn(III) and produces oxygen. The bound

sulfate (SO_4^{2-}) from the (HSO_5^-) is released, resulting in a two-electron oxidation of the manganese(III) to form the key high–valent manganese(V) necessary for the formation of the O–O bond. The highly reactive manganese(V)–oxo or manganese(IV)–oxyl intermediate involve in these pathways could be due to trans influence. The Collomb[89] group tried unsuccessfully to perform electrochemical water oxidation of the same Mn-terpy dimer because the complex transforms into an inactive tetranuclear analog.

It has been proposed by various reports that the incorporation of phenolate moieties into manganese species could lead to enhanced catalytic activity.[90,91,92] Akermark[93-94] and coworkers has shown impressive progress in this design, incorporating bimetallic [Mn_2] and multimetallic [RuMn][95] and studying charge, and electron transfer rates between photosensitizer and electron donor moieties. The study of electron-transfer rates in the [RuMn] triads, for instance, were conducted in an effort to mimic the photosynthetic process. The study revealed that the manganese ion has intrinsic properties that are favorable for creating and maintaining a long-lived charge separated state for electron transfer to occur from the Mn electron donor to the Ru ion. A similar approach based on modifications of the triazacyclononane ligand was undertaken by Wieghardt[96] and collaborators who found out that Mn^{II}, Mn^{III}, and Mn^{IV} redox states in their complexes were accessible and Ru(II) centers could be reversibly oxidized to Ru^{III}. Interestingly enough, it was also observed that the coordinated phenolate ligand could be oxidized to a phenoxyl radical. Fujii[79, 97-98] *et al*. have also studied examples of Mn^{IV} stabilization using [N_2O_2] salen platforms **(Figure 1.10b).** These systems build on an equilibrium between [Mn^{III}/phenoxyl] and [Mn^{IV}/phenolate] species relying on the energy of their frontier orbitals. It was initially suggested by Åkermark *et al*[99] that formation of Mn^{IV} leads to a Mn^{III}/phenoxyl species where radical decay is prevented by coordination to the metal center **(Figure 1.10c)**, but Fujii[100] proposes that the [Mn^{III}/phenoxyl]

state is favored upon coordination with water and the metal-centered high oxidation is only achieved by water deprotonation or formation of a Mn^{IV}=O moiety. A study from Anxolabéhère-Mallart *et al.*[80] proposed that an alternative and milder mechanism for water oxidation might involve the formation of Mn^{III}-oxyl species in pentadentate ligands similar to those developed by the groups of Pecoraro[101] and Åkermark.[99]

1.6.3 Molecular Water Oxidation Catalysts based on Cobalt Complexes

Though the cobalt ion plays no significant role in photosystem II to aid water oxidation, it has become a reliable water oxidation catalyst over the past decade because it can effectively stabilize multiple oxidation states, from $3d^8$ Co^I through $3d^5$ Co^{IV}. Whilst several heterogeneous cobalt oxide water oxidation catalysts have been reported in the literature, only a few molecular cobalt-based water oxidation catalysts have been reported **(Figure 1.12)**. Berlinguette[21] and his group, in 2010, reported on the electrocatalytic water oxidation of a homogeneous cobalt catalyst, ($[Co(Py_5)(OH_2)]^{2+}$) in basic medium (pH 9.2) with an overpotential of 0.5 V [Py_5 = 2,6-(bis(bis-2-pyridyl)-methoxymethane)pyridine)] **(Figure 1.12a).** They observed that their catalyst undergoes a series of (PCET) steps during catalysis to yield a $3d^5$ Co^{IV} intermediate, which is then attacked by a molecule of water under basic conditions producing oxygen. The catalyst remains stable at neutral through mildly basic pH conditions of 7-10. Under strong alkaline conditions, however, it was observed that there was deposition of CoO_x on the surface of the electrode. The authors concluded that whilst the catalyst is a molecular catalyst under mildly basic conditions, the catalyst transforms to nano-particulate cobalt oxide under harsh basic conditions. This phenomenon was attributed to the possibility of the metal–ligand bond *trans* to the M–O bond being "compromised at higher redox levels"[21] hence the decomposition of the molecular catalyst. Nam[102] and coworkers observed similar results when they studied $[Co^{II}(Me_6tren)(OH_2)]^{2+}$ and

$[Co^{III}(Cp^*)(bpy)(OH_2)]^{2+}$ [Me_6tren = tris(N,N′,N″-dimethyl aminoethyl) amine, Cp* = η^5-pentamethylcyclopentadienyl] in water over the 6–10 pH range.

Llobet[84] modified a known Ru-bpp water oxidation catalyst shown in **Figure 1.9b**, with cobalt and studied its catalytic activity towards water oxidation.[103] Several attempts to just replace the metal center and maintain the aqua axial ligands proved unsuccessful, producing an end-on peroxo bridge between the two cobalt centers **(Figure 1.12b)**, which remained stable in aqueous 0.1 M, pH 2.1 phosphate buffer over a period of several hours with no signs of degradation or decomposition. Its redox behavior during catalysis suggests that the $Co^{III}Co^{III}$ dimer undergoes a 2-electron oxidation before catalytic current enhancement is observed.

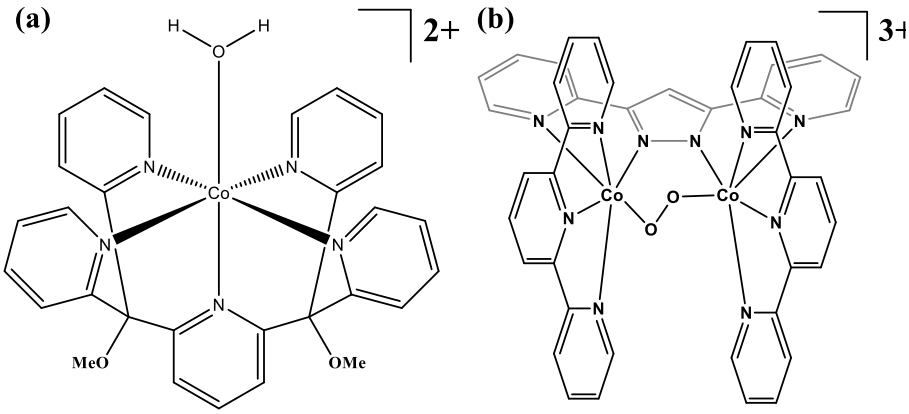

Figure 1.12. Selected homogeneous cobalt-based catalysts for water oxidation.

A mechanistic pathway was proposed by the authors in which the $Co^{III}Co^{III}$ parent dimer undergoes a one-electron oxidation to form a peroxo-bridged $Co^{III}Co^{IV}$ species which then follows two PCET steps to yield a dioxo-$Co^{IV}Co^{IV}$ intermediate, attacked by water, followed by the formation of an O–O bond to yield oxygen and regenerates the peroxo-bridged $Co^{III}Co^{III}$ complex, suggesting that both bpp-ligated Co and Ru complexes appear to catalyze water oxidation by “similar mechanisms”.

1.7. Outlook and Prospects

Efficient water splitting using energy from the sun is central to efforts toward a future based on a renewable and sustainable energy supply. For the development of a system that can harvest the energy of the sun and use it to split water, there must be a systematic effort targeted at the design and evaluation of catalytic systems which can utilize the photons to mediate the multi electronic processes involved in water splitting. Whilst significant progress has been made, questions persist as to how to identify and characterize key intermediates, as well as optimize the efficiency of these catalysts in order to utilize energy from the sun to split water. The prospect of designing a *bonafide* molecular catalyst that can efficiently use energy from the sun to split water remains the ultimate goal of achieving a sustainable hydrogen economy for the future. The Verani group at Wayne State University has focused its research interests towards achieving that goal. The results discussed in this dissertation constitute part of the research efforts.

1.8. Research Statements and Objectives

It is essential to understand the mechanistic processes governing water oxidation and water/proton reduction to achieve efficient electro- or photocatalysis. In the Verani group, we design ligands containing redox-active frameworks for the formation of metal complexes capable of water reduction and water oxidation. Cobalt and manganese complexes are important as water-splitting catalysts to generate dioxygen and dihydrogen stabilizing highly nucleophilic reduced species, and high-valent oxidative species respectively.

The focus of this dissertation was to design, and evaluate the redox, electronic, catalytic, and mechanistic properties of cobalt, and manganese complexes in various redox-active ligand frameworks towards efficient electrocatalytic water oxidation and reduction. These systematic studies are geared towards the eventual design of excellent photocatalysts based on affordable

Earth-abundant metal complexes. To obtain this objective, the following specific goals have been pursued.

- **Goal # 1:** ***Probing the Versatility of a Quinoline-based Pentadentate Co(II) Complex for Electrocatalytic Water Splitting.*** The primary focus was to synthesize, characterize and evaluate the stability and robustness of the cobalt(II) complex of a pentadentate quinoline-based polypyridine ligand towards water splitting. I hypothesized that modifying the ligand architecture by incorporating a more rigid quinoline ligand, which has increased aromaticity, stabilized by mesomeric and inductive effects, yielded a robust catalyst capable of efficient catalysis. The results of this goal are addressed in **Chapter 3** of my dissertation.
- **Goal # 2:** ***Evaluating Electronic Communication and Cooperativity in a Dicobalt Complex for Proton Reduction.*** The principal objective is to study whether distance and topology enhance the electronic communication and thereby cooperativity between two cobalt centers in a dicobalt complex towards efficient proton reduction. I hypothesized that cooperativity will be dependent on (i) the distance between the Co centers, (ii) the relative topology of the coordination environments, and (iii) the degree of orientation and overlap between redox-active orbitals. **Chapter 4** of my dissertation discusses the results.
- **Goal # 3:** ***Investigating Valence Tautomerism on Coordination Preferences in Manganese Complexes for Water Oxidation.*** The principal objective is to investigate whether the coordination environments around a manganese center can determine high-valent states relevant for electrocatalytic water oxidation. The hypothesis is that, by incorporating redox-active ligands such as phenolates and a redox-active metal ion such as Mn, valence tautomeric transitions can occur through intramolecular electron transfer,

yielding two different valence tautomers or redox isomers. This valence tautomerism can lead to the formation of Mn(IV) species, and support catalytic water oxidation. The results of this project constitute **Chapter 5** of my dissertation.

CHAPTER 2:

MATERIALS, METHODS AND INSTRUMENTATION

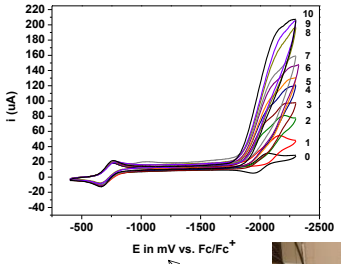

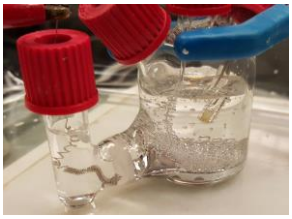

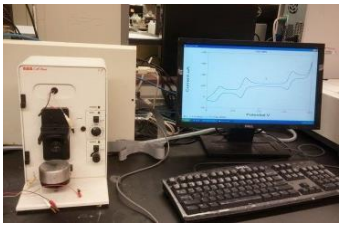

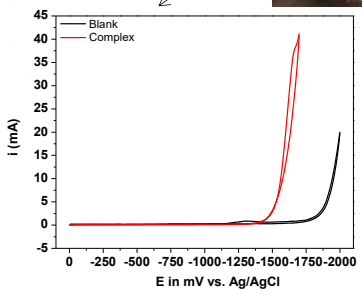

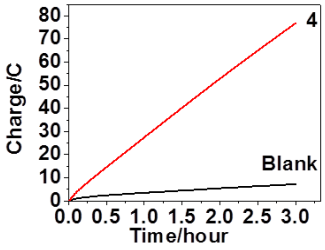

CHAPTER 2: MATERIALS, METHODS, AND INSTRUMENTATION

2.1. Materials

The research described in this dissertation consisted of the organic synthesis of ligand precursors, ligands, inorganic transition metal complexes, and where possible their intermediates. Chemical reagents were purchased from various commercial sources such as Sigma-Aldrich, Oakwood Chemicals, and Alfa Aesar. Safe and appropriate reaction protocols were strictly followed to obtain ligands and their complexes. Solvents and reagents were received and used from commercial sources without further purification unless otherwise stated.

2.2 Methods and Instrumentation

All the ligands and complexes used in the dissertation described in this dissertation were synthesized and characterized using a variety of synthetic, spectroscopic, and spectrometric methods and techniques to study the composition, electronic structure, redox properties, catalytic behavior, and mechanistic pathways.

These methods and techniques include, but are not limited to, proton nuclear magnetic resonance spectroscopy (1H-NMR), Fourier transform infrared spectroscopy (FTIR), electrospray ionization mass spectrometry (ESI-MS), elemental analysis, UV-visible spectroscopy, cyclic voltammetry, electron paramagnetic resonance spectroscopy (EPR), gas chromatography (GC), scanning electron microscopy (SEM), single crystal x-ray diffraction analysis (SC-XRD), and energy-dispersive electron microscopy (EDS).

2.2.1 Nuclear Magnetic Resonance Spectroscopy (NMR)

NMR is a widely used method of characterization in organic compounds, because it affords a versatile way to determine the structure of the organic compound. It has gradually become an effective technique in inorganic chemistry for providing valuable structural information about

diamagnetic metal complexes. The nuclei of various atomic isotopes each possess a unique spin (I), which in turn is associated with nuclear magnetic resonance. Some of these spins are fractional, such as I = 1/2, 3/2, 5/2. Isotopes such as ^{1}H, ^{13}C, ^{19}F and ^{31}P all have I = ½ and hence magnetic moment. They act as subatomic magnets and therefore can be analyzed by NMR spectroscopy. The resonance produced when these isotopic nuclei are placed in an external magnetic field can be detected and converted into an NMR spectrum. Generally, the peak positions in an NMR spectrum are reported relative to a standard signal, like that of tetramethylsilane (TMS). This ensures uniformity in signal output. The position and multiplicity of an NMR peak is dependent on the local chemical environment of the isotope. Peak integration is used to determine the number of isotopes (i.e. protons) present in a particular compound. In this dissertation, ^{1}H-NMR was used predominantly to identify organic ligands, ligand precursors, and metal complexes when appropriate, such as $3d^6$ $^{LS}Co^{III}$ and $4d^6$ $^{LS}Ru^{II}$ due to their diamagnetic nature**.** ^{1}H NMR spectra were obtained in deuterated solvents such as $CDCl_3$, CD_3CN, and DMSO-d6 at room temperature**,** using a Varian 400 MHz instrument.

2.2.2 Fourier Transform Infrared Spectroscopy (FTIR)

FTIR is an important technique used in identifying functional groups in organic compounds and in some cases inorganic complexes. This technique relies on the principle of infrared transmittance. For instance, when a sample is placed in an IR beam, some radiation is absorbed by the sample and some of it is transmitted. The detected signal is converted into a spectrum from which functional groups can be identified as well as the unique 'fingerprint' region of the sample. The utility of infrared spectroscopy is derived from different molecules' different FTIR fingerprints.[104] FTIR samples are prepared liquids or as potassium bromide (KBr) pellets for analysis by the spectrophotometer. In this dissertation, FTIR was used to confirm the presence of

the following major functional groups; C=N, C=O, C=C, and inorganic counter ions such as the perchlorate (ClO_4^-), and the hexafluorophosphate (PF_6^-). The FTIR data was measured from 4000 to 400 cm^{-1} as KBr pellets on a Bruker Tensor FTIR spectrophotometer, with spectra plotted as percent transmittance (% T) of IR radiation against centimeter wave numbers (cm^{-1}).

2.2.3 Electrospray Ionization Mass Spectrometry (ESI-MS)

Electrospray mass spectrometry (ESI-MS) is an essential analytical tool used to quantify known compounds, but also to elucidate structural and chemical properties of unknown compounds within a sample. The principle of MS includes the ionization of a sample into gaseous ions. These ions are then categorized according to their mass to charge ratios (m/z) and relative abundances.[105] Since ESI ionization techniques preclude the fragmentation of gaseous ions, this method is useful in identifying molecular ion peaks of organic ligands and inorganic complexes. ESI-MS was used extensively in this dissertation to ascertain the identity of ligands, inorganic metal complexes, post-catalytic species, or transformed catalytic intermediates. A typical sample for ESI-MS analysis is dissolved in polar solvents such as acetonitrile or methanol. The sample is then bombarded with high-energetic electrons to produce charged species. Low-resolution modes are convenient for organic compounds, whereas for inorganic metal complexes, the high resolution modes with isotopic distribution capabilities are more useful. Low resolution ESI-MS data was obtained on a Nexera X2 LC system with a LC-MS 8040 triple quadrupole mass spectrometer, and high resolution data on a Waters Micromass LCT Premier TOF (time of flight) instrument with a Waters HPLC 2695 Alliance LC system. These analyses were performed with the help of Drs. Lew Hryhorczuk, from 2012- 2013, Yuri Danylyuk, from 2013-2014, and Nicole Lenca 2014-2017 at the Lumigen instrument center (LIC) of the Department of Chemistry at Wayne State University.

2.2.4 Electron Paramagnetic Resonance Spectroscopy (EPR)

Electron paramagnetic resonance (EPR), is a spectroscopic tool which employs microwave radiation to analyze species with an odd number of electrons, such as organic radicals, radical cations, and metal cations such as $3d^9$ Cu^{II} , $3d^7$ Co^{II}, $3d^5$ Co^{IV}, $3d^5$ Fe^{III} in an applied external magnetic field.[106] The basic principles of this technique are analogous to the NMR technique described in section 2.2.1. Electrochemically generated catalytic intermediates during the research described in this dissertation, were characterized using the EPR technique. EPR samples are usually prepared under inert conditions depending on the nature of the species under study. A 10^{-3} M aliquot of the sample is then put in suprasil quartz capillary EPR tubes which are then frozen in liquid N_2. Continuous wave (CW) X-band (9-10 GHz) EPR experiments are then performed on a Bruker ELEXSYS E580 EPR spectrometer (Bruker Biospin, Rheinstetten, Germany), equipped with a Bruker ER 4102ST resonator or a Bruker ER 4122SHQ resonator. A temperature-controlled device equipped with a helium gas-flow cryostat (ICE Oxford, UK) and an ITC (Oxford Instruments, UK) helps keep the samples at low temperature. Data is processed on Xepr (Bruker BioSpin, Rheinstetten) and Matlab 7.11.2 (The MathWorks, Inc., Natick) software. Simulated spectra are generated using the EasySpin software package (version 4.5.5).[107] These analyses were done in collaboration with Dr. Oleg Poluektov and Dr. Jens Niklas of Argonne National Laboratory (ANL).

2.2.5. Ultraviolet-visible Spectroscopy (UV-visible)

UV-visible spectroscopy is a technique used to analyze the electronic transitions of complexes absorbing radiation. The absorption of UV or visible radiation is associated with the excitation of valence electrons. There are three main types of electronic transition: (i) transitions relating to π, σ, and n electrons; (ii) charge-transfer transitions – the transfer of an electron from

the orbital of an electron donor moiety to an orbital associated with an electron acceptor; (iii) *d-d* transitions – electron transfer from d-orbital in a metal complex to another d-orbital of higher energy. When a compound absorbs radiation, valence electrons get excited and are promoted from the ground state energy level to an excited state energy level. These transitions can be spin and Laporte allowed, or forbidden, depending on selection rules. Transition metal complexes typically exhibit electronic transitions such as intraligand-charge transfers (ILCT), ligand-to-ligand charge transfers (LLCT), metal-to-ligand charge transfers (MLCT), ligand-to-metal charge transfers (LMCT), and *d-d* transitions. The ligand-based transitions usually occur in the ultraviolet region, at low wavelengths with intense molar absorptivities ($\varepsilon \sim 20000 - 60000$), whereas the charges transfer transitions occur in the mid-visible region with medium molar absorptivities ($\varepsilon \sim 5000 - 20000$). The *d-d* transitions are usually weak as they are forbidden transitions according to the selection rules described, and hence have notably low absorptivities ($\varepsilon \sim 50 - 1000$). In this dissertation, UV–visible spectroscopy was used to track the electronic behavior of ligands and metal complexes. UV-visible spectra were typically obtained at room temperature using a Shimadzu 3600 UV-visible-NIR spectrophotometer operating in the range of 190 to 3600 nm with samples prepared in quartz cells as methanolic solutions. Other solvents used are dichloromethane, acetonitrile, and dimethyl formamide as needed. Spectral data is plotted as absorbance, or molar absorptivity (ε) in M^{-1} cm^{-1} when concentration is known, versus wavelength in nanometers.

2.2.6. Elemental Analyses (EA)

The technique of elemental analysis operates on the principle that during combustion, at elevated temperatures, all available carbon will easily decompose to become carbon dioxide, all hydrogen will decompose to become water and all nitrogen will decompose to nitric oxides. This will enable the determination of any compound's relative percent of carbon, hydrogen, and

nitrogen. These elemental analyses (C, H, and N) for metal complexes used during this dissertation were performed on an Exeter Analytical 440 elemental CHN analyzer by Midwest Microlab: Indianapolis, Indiana. Elemental analysis values are presented as percentages. A CHN elemental analysis sample calculation is shown:

Anal. Calc. for [$\mathbf{C_{30}H_{31}}$CoCl$\mathbf{N_6}$$O_5$]: C, 50.22; H, 4.36; N, 11.71%. Found: C, 50.37; H, 4.32; N, 11.57%.

C	**H**	**N**
50.37 g/12.00 $gmol^{-1}$	4.32 g/ 1.00 $gmol^{-1}$	11.57 g/ 14.00 $gmol^{-1}$
= 4.19 moles	= 4.32 moles	= 0.83 moles

Now dividing through by the lowest number of moles;

4.19/0.83	4.32/0.83	0.83/0.83
= 5.04	= 5.2	= 1

Now multiply by 6 (number of nitrogen atoms in the formula above)

= 30.24	= 31.20	= 6

Hence the CHN formula is $\mathbf{C_{30}H_{31}N_6}$.

In order to get a good elemental analysis result, purity is important. All samples must be pure and thoroughly dried. The following are sources of impurities and must be avoided at all cost.

1. Inorganic salts
2. Water of hydration

2.2.7. Single Crystal X-Ray Crystallography (SC-XRD)

Single crystal X-ray diffraction (SC-XRD) is one of the most authoritative techniques for obtaining detailed insight into the structure-to-function relationship of transition metal complexes in the solid state.[108] In the research reported in my dissertation, the single crystal X-ray structures

of inorganic complexes were obtained whenever possible. X-ray quality crystals were grown by either vapor diffusion, slow evaporation, or solvent layering when applicable. Diffraction patterns were measured on a Bruker X8 APEX-II[109] kappa geometry diffractometer with Mo radiation and a graphite monochromator SAINT[110] collection suite. The OLEX2[111] structure solution suite was used to solve various structures with refinements and absorption correction techniques utilized using SHELX[112] and SADABS[113] software. Dr. Mary J. Heeg, and Kenneth K. Kpogo solved all the crystal structures.

2.2.8. Cyclic Voltammetry (CV)

Cyclic voltammetry was extensively used in the course of my dissertation. It has become an indispensable analytical tool in studying electron transfer phenomena. In the context of this dissertation, cyclic voltammetry was used predominantly to evaluate the effects of ligand design on metal-centered redox potentials as well as probe the mechanistic details of electrocatalytic water splitting. In a typical CV experiment, the potential at a working electrode immersed in a solution containing a sample and a supporting electrolyte is scanned linearly with time; the current is monitored and plotted as a function of either time or potential. The use of CV as a successful technique depends on a few parameters such as choice of solvent, supporting electrolyte, choice of working electrode, reference electrode, and choice of standard reference material. CV experiments were conducted using a three-electrode setup comprised of a glassy carbon working electrode (W.E.), a saturated Ag/AgCl as reference electrode (R.E.), and a Pt wire as an auxiliary electrode (A.E.) on a BASi 50W potentiostat. Typical organic solvents used to obtain cyclic voltammograms were dichloromethane (CH_2Cl_2), acetonitrile (CH_3CN), and *N*,*N*'-dimethylformamide (DMF) when possible. Supporting electrolytes such as 0.1 M of *n*-Bu_4NPF_6 or *n*-Bu_4NBF_4 were used. CV experiments were conducted under an inert atmosphere at room

temperature. The ferrocene/ferrocenium (Fc/Fc^+) couple (E^o = 400 mV *vs* NHE)[114] was used as a standard reference material (SRM) and added as an internal standard. Usually, $E_{1/2} = (E\text{pc} + E\text{pa})/2$ are reported for reversible redox couples, whereas Epc (cathodic peak potential) and Epa (cathodic peak potential) are used to designate irreversible process. Peak-to-peak redox potential separations ($\Delta E\text{p} = |E\text{pc} - E\text{pa}|$) and |ipa / ipc| values are often measured to assess reversibility of redox processes [ipa = anodic peak current; ipc = cathodic peak current].

2.2.9 Spectroelectrochemistry (SEC)

Spectroelectrochemistry is an electroanalytical technique which combines electrochemical reactions with species-focused spectroscopy. Spectroelectrochemistry (SEC) gives a more detailed analysis of single and multiple electron-transfer processes during an electrochemical experiment. Spectroelectrochemical experiments were conducted in an optically transparent cuvette (*ca.* 0.1 mm) using a procedure described as follows:[115] a flat platinum wire (W.E.) in a "U" shape is sandwiched between two indium-tin oxide (ITO) (8-12 Ω/sq) coated glass slides. Redox potentials were measured vs. Ag/AgCl (R.E) and a second platinum wire (A.E.). Potentials were applied using a BASi 50W potentiostat, and the accompanying UV-visible spectra collected on a Varian Cary 50 spectrophotometer at 25 °C, over a period of time.

2.2.10. Bulk Electrolysis (BE)

Controlled potential electrolysis or bulk electrolysis is a technique where either a constant current or constant potential is applied to an electrochemical cell in order to assess significant changes in oxidation states or evaluate electrochemical robustness of a redox-active sample.[116] The total charge consumed by the system during electrolysis is obtained by plotting the current versus time.[116] Products of catalytic bulk electrolysis experiments are typically identified and quantified by gas chromatography. Other methods such as EPR, NMR, and sometimes ESI-MS, are used in

the case of complete or partially oxidized/reduced species. Bulk electrolysis was done based on a modified method[73, 117] in a custom-made airtight H-type cell with two chambers separated by a frit. A mercury-pool (Hg-pool) W.E. and Ag/AgCl R.E. were placed in the larger, major chamber, while a Pt wire A.E. was placed in the minor auxiliary chamber. Tetrabutylammonium hexafluorophosphate ($TBAPF_6$) was used as a supporting electrolyte. The major chamber was filled with the electrolyte solution and the sample. The auxiliary chamber contained only electrolyte solution.

In a typical experiment, the cell is evacuated with N_2 gas for approximately 15 minutes, after which the headspace is sampled with gas chromatography (GC) to ensure an O_2 free environment before applying a potential. A blank solution containing only supporting electrolyte was then electrolyzed over a period of time, at an appropriately applied potential (i.e. -1.7 V vs. Ag/AgCl). After electrolysis, the headspace gas was again sampled to measure the amount of dihydrogen generated. The cell was subsequently degassed with N_2 gas for another 15 minutes and the experiment repeated, this time containing the catalytic sample.

2.2.11 Gas Chromatography (GC)

Gas chromatography (GC) is an analytical technique which analyses the content of a gaseous compound. In a typical experiment, a sample is injected into a gas chromatograph, then enters a gas stream which transfers the sample into a column. A carrier gas (helium or nitrogen) aids this transfer. Separated components in the column are detected and quantified. To analyze an unknown sample, standard samples are injected, and their peak retention times and areas are compared to the unknown sample to determine its concentration. Gas chromatography was used to analyze and quantify electrocatalytic products of water splitting such as hydrogen (H_2), and O_2. A Gow-Mac 400 equipped with a thermal detector and an 8’ x 1/8” long 5Å molecular sieve

column working at 60°C was used, with N_2 as the carrier gas for hydrogen, whilst He was used as carrier gas for O_2.

2.2.12. Scanning Electron Microscopy and Energy Dispersive Spectroscopy (SEM-EDS)

Scanning electron microscopy (SEM) is one of the most versatile techniques available for analyzing the morphology of surface materials.[118] Images are formed from signals generated when the surface of a sample is scanned with a focused electron beam.[118] The electron beam and specimen interactions produce many signals that are processed to obtain useful information about the surface topography and composition of the sample.[119] Energy dispersive spectroscopy (EDS) supplements SEM by identifying particular elements in a scanning electron micrograph and determining their relative proportions.[120] EDS analysis involves the generation of X-ray spectra from the scanned SEM and plotted as number of X-rays processed by the detector *vs* the energy level of the X-rays.[121] SEM and EDS were used to characterize the nature and composition of post-catalytic electrodes in this dissertation to determine if catalyst deposition has occurred. Data was taken on a JSM-7600 FE SEM instrument, equipped with a Pegasus Apex 2 integrated EDS and EBSD system.

2.2.13. Density Functional Theory Calculations (DFT)

Density functional theory (DFT) finds utility in almost every aspect of science.[122] DFT effectively complements experimental studies and provides a theoretical approach to determining electronic structures of molecules. DFT can also provide insight into a great variety of molecular properties such as relative energies of molecular orbitals, reaction pathways, and reaction dynamics as a support for experimental reactions and design. DFT computations were used to predict the nature of catalytic intermediates that are often difficult to isolate experimentally, as well as predict energetically favorable reaction pathways. Calculations ultimately aimed to

elucidate plausible mechanistic pathways based on experimental observations. DFT calculations were performed in collaboration with the Schlegel group at Wayne State University, using the Gaussian suite with revisions H.31,[123] using B3LYP/6-31G(d,p)[124-125], and the BPW91[125] functional with SDD,[126,127] and the 6-31G(d,p)[128] basis set by Dr. Shivnath Mazumder, and Dr. Bishnu Thapa, for different projects described in my dissertation.

CHAPTER 3:
VERSATILITY OF A QUINOLINE-BASED PENTADENTATE Co(II) COMPLEX FOR ELECTROCATALYTIC WATER SPLITTING

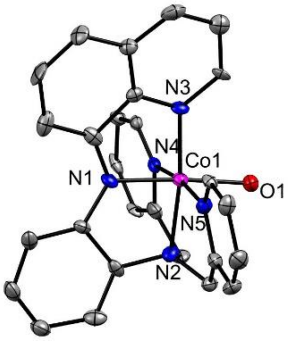

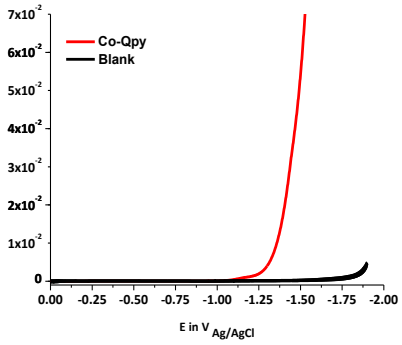

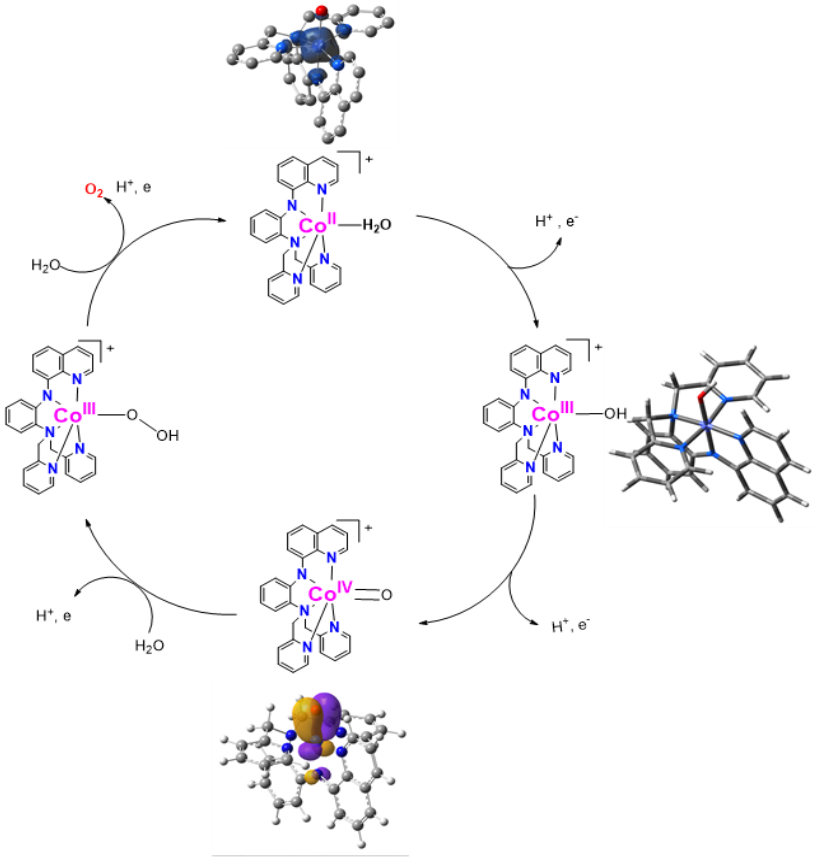

CHAPTER 3: VERSATILITY OF A QUINOLINE-BASED PENTADENTATE Co(II) COMPLEX FOR ELECTROCATALYTIC WATER SPLITTING

3.1. Introduction

Earth-abundant transition metals like cobalt, nickel, and iron have attracted attention due to their ability to generate H_2 and O_2 from water.[129,17,59,130] Among these, cobalt is particularly relevant because it can effectively stabilize the catalytically active species $3d^8$ Co^I and the cobalt/hydride intermediate Co^{III}–H^- which is pivotal for H^+ reduction to H_2.[14,131,46,132,133] The production of H_2 from Co^{III}-H follows either heterolytic or homolytic pathways shown in **Figure 3.1**.[46,16,47] The former mechanism relies on a single Co^{III}–H^- reacting with another H^+, while homolytic mechanisms involve two independent Co^{III}–H^-moieties.[48]

The reliance on a particular mechanism is governed by factors such as the concentration of acid used,[49] catalyst design, applied potential,[50] the rate constants for hydride formation,[51] and whether H_2 is evolved by hydride protonation or dimerization.[52]

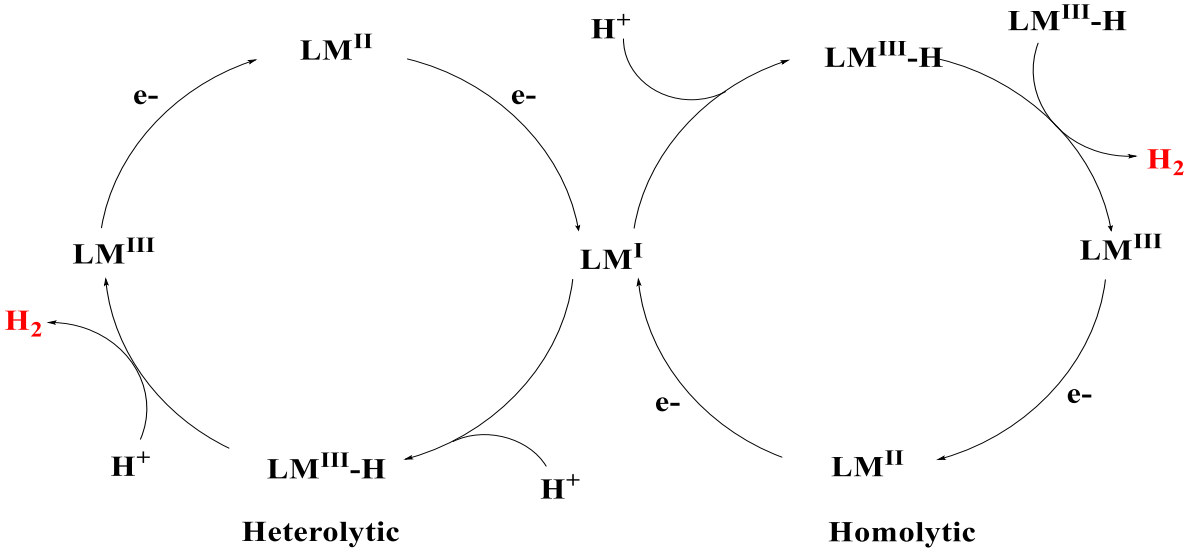

Figure 3.1. Generalized Catalytic mechanisms of H_2 generation.

Cobalt-based catalysts are also expected to oxidize water to dioxygen in basic media undergoing a well-defined PCET steps **(Figure 3.2)** to a tetravalent intermediate which is electrophilic enough to be attacked by a nucleophilic water molecule.

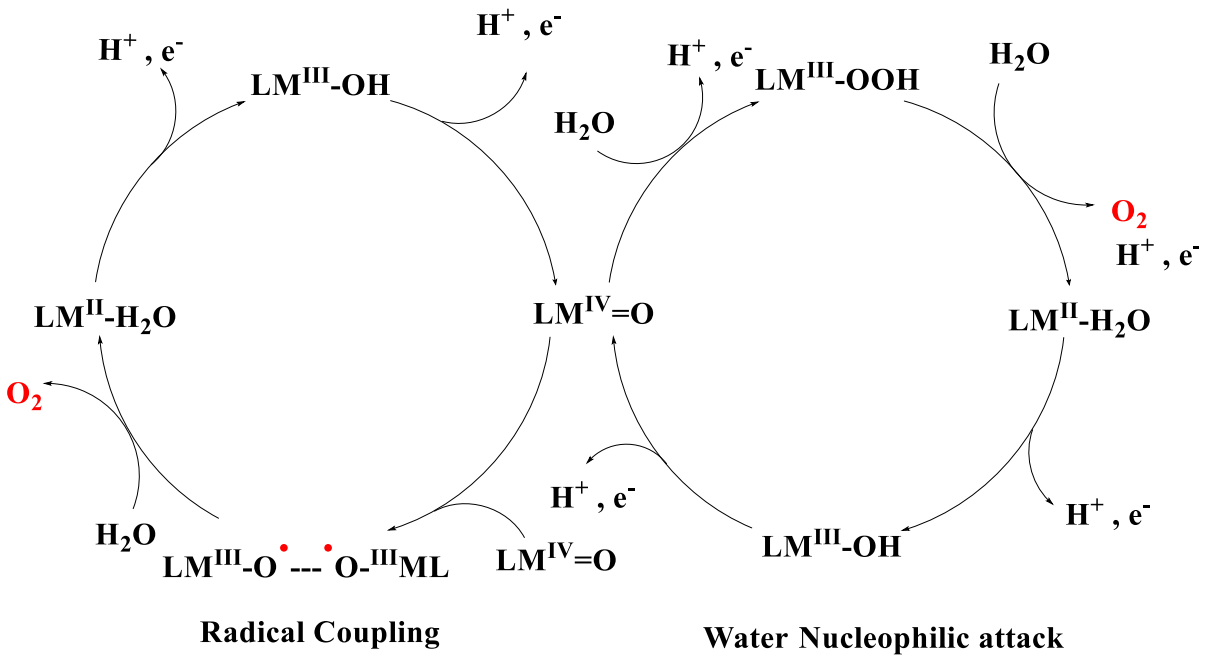

Figure 3.2. Generalized Catalytic mechanisms of O_2 generation.

For this step, two main mechanisms have been generally reported: (i) The water nucleophilic attack (WNA) pathway, where water attacks an oxo ligand bound to a high valent species,[134,135,21,136,137] and (ii) The radical homo-coupling (RC) pathway, where two metal–oxo species having radical character predominantly on the oxo group.[138]

Other mechanisms have been proposed, such as the expanded coordination sphere (seven-coordinate Ru).[86,12] The ability to isolate, identify and track key intermediate species during catalysis using analytical and spectroscopic techniques such as EPR and UV-visible spectrophotometry enables a systematic study of the various interactions that occur during catalysis and guide the design of better catalysts.

Finally, photocatalytic water splitting is viewed as the ultimate goal of developing a sustainable hydrogen economy. The ability of a well-studied electrocatalyst to work in tandem with a requisite photosensitizer to produce hydrogen from water, using solar energy is therefore highly desired.

In a recently published report on cobalt catalysts with pentadentate pyridine-rich ligands catalysts for proton and water reduction, The Verani group discussed how ligand architecture influences catalytic activity.[73] In that report we observed that one of the aminopyridine ligands transformed into an amido derivative through a hydroxy intermediate formed from addition of adventitious aqueous solvent to the imine moiety.[73] I therefore hypothesize that modifying the ligand architecture by incorporating a more rigid ligand, which has increased aromaticity, stabilized by mesomeric and inductive effects, will yield a robust second generation catalyst capable of efficient catalysis.

3.2 Experimental

3.2.1 Synthesis of N,N′-Mono(8-quinolyl) bispyridine-phenylenediamine (HL^{Qpy})

The synthesis of the pentadentate quinolyl-bispyridine ligand, $\mathbf{HL^{Qpy}}$, with a phenylenediamine backbone was adapted from the literature[139] and modified by treating one equivalent of 8-hydroxyquinoline with an equivalent of *ortho*-phenylenediamine in the presence of sodium metabisulfite ($Na_2S_2O_5$), triethylamine, and water under reflux for 7 days. The resulting orange solution was extracted with dichloromethane.

The pale yellow crystalline solid obtained was reacted with an aqueous solution of 2-(chloromethyl) pyridinium chloride (two equivalents) in the presence of sodium hydroxide and catalytic amounts of hexadecyltrimethyl ammonium chloride under inert conditions for 24 hours. Yield: 56%. ESI (m/z+) in CH_3OH for $[\mathbf{HL^{Qpy}} + H^+]^+$ = 418, ^1H NMR ($CDCl_3$): δ 8.90 (d, 1H,

QnH), 8.46 (d, 2H, 2-ArH), 8.17 (d, 1H, QnH) 7.78 (d, 2H, ArH), 7.62 (m, 4H, QnH), 7.41 (m, 4H, Ar H), 7.15 (m, 3H, ArH), 6.88 (m, 1H, Ar H), 4.53 (s, 4H, CH_2), 1.24 (s, 1H, sec-amine), IR (KBr, cm^{-1}) 3350(ν_{N-H}), 1610 ($\nu_{C=C}$, aromatic), 1580 (ν_{N-H},) 1589 ($\nu_{C=N}$), 1342 (ν_{C-N} aromatic), 750 (ν_{C-H}).

3.2.2 Synthesis of $[Co^{II}(L^{Qpy})H_2O]ClO_4$

A water-soluble Co(II) complex was prepared from the pentadentate **HL^{Qpy}** ligand. The complex was obtained by treating one equivalent of **HL^{Qpy}** with one equivalent of $Co(ClO_4)_2 \cdot 6H_2O$ in the presence of triethylamine in methanol under inert conditions for three hours at room temperature. Yield: 49%. ESI (m/z+) in CH_3OH for **$[Co^{II}(L^{Qpy})H_2O]ClO_4]H^+$** = 476 (100%), Anal. Calc. for $[C_{30}H_{31}CoClN_6O_5]$: C, 50.22; H, 4.36; N, 11.71%. Found: C, 50.37; H, 4.32; N, 11.57%. IR (KBr, cm^{-1}) 1610 ($\nu_{C=C}$, aromatic), 1580 (ν_{N-H},) 1589 ($\nu_{C=N}$), 1342 (ν_{C-N} aromatic), 1090 (ν_{ClO4}), 665($\nu_{C=C}$, aromatic).

3.2.3 X-Ray Structural Determinations

Yellow colored hexagonal X-ray quality crystals of **(HL^{Qpy})** precursor were grown by vapor diffusion of the complex dissolved in a 1 : 1 dichloromethane : pentane solvent mixture. A suitable crystal was selected and mounted on a mitogen loop, and diffraction data was collected on a Bruker X8 SMART APEX II CCD[140] diffractometer using a monochromatic graphite-Mo Kα radiation source (0.7107 Å) and SMART/SAINT[108] software. The crystal was kept at 100.1 K during data collection and a total of 87619 reflections were measured, with 4402 unique reflections. Using the Olex2 structure solution suite,[111] the structure was solved with the ShelXT[112] structure solution program using Intrinsic Phasing and refined with the ShelXL[112] refinement package using Least Squares minimization.[112] Hydrogen atoms were calculated using the riding model.

For the **2[Co^{II}(L^{Qpy})H$_2$O]ClO$_4$** complex, pink colored oblong X-ray quality crystals of were grown by vapor diffusion of the complex dissolved in a 1 : 1 methanol : isopropanol solvent mixture. A suitable crystal was selected and mounted on a mitogen loop, and diffraction data were collected as described above. The crystal was kept at 100.1 K during data collection and a total of 83673 reflections were measured, with 23563 unique reflections.

Using the Olex2 structure solution suite,[111] the structure was solved with the ShelXT[112] structure solution program using Intrinsic Phasing and refined with the olex2.refine refinement package using Gauss-Newton minimization.[111] Hydrogen atoms were placed in calculated positions. There are two independent dimeric octahedral complexes in the asymmetric unit. Each dimer has a trans-peroxo bridge connecting the monomeric units through the axial position.

Each of the dimers has two perchlorate anions consistent with the solid state oxidation of +2 for the cobalt center in each of the monomeric units. Selected crystallographic data for both the precursor and complex are shown in **Table 3.1.**

Table 3.1. **Summary of Crystallographic Data for** (HL^{Qpy}) **and** 2[Co^{II}(L^{Qpy})H$_2$O]ClO$_4$**.**

	(HL^{Qpy})	**4[Co^{II}(L^{Qpy})O]ClO$_4$**
Formula	$C_{15}H_{13}N_3$	$C_{113}H_{88}Cl_4Co_4N_{19}O_{20}$
M	235.28	2409.62
Temperature/K	100.1	100.1
Crystal system	Orthorhombic	Monoclinic
Space group	*Pca2$_1$*	*P*2$_1$
a/Å	10.6800(5)	13.5658(14)
b/Å	11.0757(5)	30.847(3)
c/Å	10.0873(5)	13.6410(13)
α/°	90	90

β/°	90	90.009(7)
γ/°	90	90
Volume/Å^3	1193.21(10)	5708.3(10)
Z	4	2
D_{calc} / g cm^{-3}	1.310	1.4018
μ/ mm^{-1}	0.080	0.740
R(F) (%)	3.68	8.28
Rw(F) (%)	10.38	18.99

[a] $R(F) = \sum \| F_o| - |F_c\| / \sum |F_o|$; $Rw(F) = [\sum w(F_o^2 - F_c^2)^2 / \sum w(F_o^2)^2]^{1/2}$ for $I > 2\sigma(I)$

3.2.4 Computational Details

The electronic structure calculations were performed in collaboration with the Schlegel group at WSU, by Dr. Bishnu Thapa, using the BP86 density functional[141-142] implemented in the Gaussian 09 (revision E.01) suit of package.[143] SDD basis set and an effective core potential (ECP)[144-145] was used for cobalt atom, and 6-31+G(d,p) basis set[146-150] was used for all the other atoms. All the structures were optimized in aqueous environment, modeled by using SMD implicit solvation.[151] The optimized structures were confirmed to be the minima on the potential energy surface by performing harmonic frequency calculations and had no imaginary normal mode frequency. Wave functions were tested for their stability. GaussView[152] was used to visualize the isodensity plot of canonical and biorthogonal orbitals, and spin density.

3.2.5. Electrocatalytic Studies

Electrocatalytic water reduction was performed in the previously described custom-made air-tight H-type cell **(Chapter 2)** under inert conditions,[73, 117, 130] where one side of the frit the working (mercury pool) and reference electrodes (Ag/AgCl) were placed, while the auxiliary electrode (coiled 12 inch Pt wire) was placed on the other side. During electrocatalysis the cell was

purged with N_2 gas for 10-15 minutes followed by sampling of the head space gas (100 μL) to ensure an O_2 free environment in the gas chromatograph.

The amount of hydrogen generated was determined in a Gow-Mac 400 gas chromatograph (GC) equipped with a thermal conductivity detector, and an 8 ft. x 1⁄8 in., 5 Å molecular sieve column operating at a temperature of 60 ℃. Nitrogen was used as a carrier gas at a flow rate of 30 mL/min. The amount of H_2 produced was quantified using a calibration curve of moles of hydrogen versus peak area. Turnover numbers and the Faradaic efficiency of the metal complex were calculated from the amount of H_2 released and the charge consumed.

For water reduction, a 1.0 M phosphate buffer was prepared by mixing NaH_2PO_4 (0.454 mol, 27.24 g) and Na_2HPO_4 (0.545 mol, 38.695 g) in ultrapure water. Then, the pH was adjusted to 7 by adding suitable amounts of NaOH or HCl. For the bulk electrolysis experiment, the main chamber was filled with 20 mL of phosphate buffer solution and mercury-pool electrode (working electrode) whereas the glass-fitted chamber was filled with 5 mL of solution. Bulk electrolysis was performed with an appropriate potential (i.e. -1.7 $V_{Ag/AgCl}$) applied in the presence of the same set of electrodes to generate H_2.

Electrocatalytic water oxidation was performed under similar conditions as described for water reduction, but in borate buffer (0.1 mol•L^{-1}, pH 8) using a fluorine-doped tin oxide (1.27 cm^2) glass working electrode, a Pt wire as the auxiliary electrode and Ag/AgCl as the reference electrode.

3.2.6. Photocatalytic Studies

Samples for photocatalytic water reduction were prepared in 15 mL clear cylindrical vials with gas tight screw caps fitted with septa. All the samples were filled with a 10 mL aliquot of 0.1 M pH 4 acetate buffer containing the $[Ru(bpy)_3]^{2+}$ photosensitizer (5.0 x 10^{-4} M), ascorbic acid

(1.1 M) and catalyst **[$Co^{II}(L^{Qpy})H_2O]ClO_4$** (1.0 10^{-4}M). The vials and their contents were then thoroughly degassed with nitrogen gas, and verified by GC prior to light irradiation. The vials were then placed in a water-jacketed beaker with a constant temperature of 20 °C.[153] The contents of the vials were irradiated by an 18 module blue LED strip (λ_{max} = 460 nm) wrapped around the beaker and connected to a 12 V power controller.

The headspace gas was analyzed in triplicates at 30 minute intervals over 4 hours by a GOW MAC GC with a TCD detector to determine the amount of hydrogen produced over time. Nitrogen was used as the carrier gas at a flow rate of 30 mL/min. The amount of H_2 produced was quantified using a calibration curve of moles of hydrogen versus peak area.

3.2.7. Electron paramagnetic resonance (EPR) studies

All samples were prepared under inert conditions atmosphere. A 10^{-3} M solution of the ($^{HS}Co^{II}$, d^7 S = 3/2) parent **[$Co^{II}(L^{Qpy})H_2O]ClO_4$** complex was transferred into a suprasil-quartz EPR capillary tube having a 4 mm outer diameter and frozen in liquid nitrogen. A series of one-electron and 2-electron electrochemical oxidation experiments were conducted to generate ($^{LS}Co^{III}$, d^6 S = 0) and ($^{HS}Co^{IV}$, d^5 S = 5/2) species, respectively.

Continuous wave (CW) X-band (9.48 GHz) EPR experiments were carried out by Drs. Oleg Poluektov and Jens Niklas at Argonne National Laboratories, with a Bruker ELEXSYS E580 EPR spectrometer (Bruker Biospin, Rheinstetten, Germany), equipped with a Bruker ER 4102ST resonator or a Bruker ER 4122SHQ resonator. The temperature was controlled using a helium gas-flow cryostat (ICE Oxford, UK) and an ITC (Oxford Instruments, UK). Data processing was done using Xepr (Bruker BioSpin, Rheinstetten) and Matlab 7.11.2 (The MathWorks, Inc., Natick) environment.

3.3 Results and Discussion

3.3.1 Synthesis and Characterization

An asymmetric, pentadentate quinolyl-bispyridine ligand, **HL^{Qpy}**, with a phenylenediamine backbone was synthesized and characterized by spectroscopic and spectrometric techniques (**Scheme 3.1)**. The ligand synthesis was adapted from the literature[139] and modified by treating one equivalent of 8-hydroxyquinoline with an equivalent of *o*-phenylenediamine in the presence of sodium metabisulfite, triethylamine (TEA) and water under reflux for 7 days. The resulting solution was extracted with dichloromethane yielding a pale-yellow crystalline precursor.

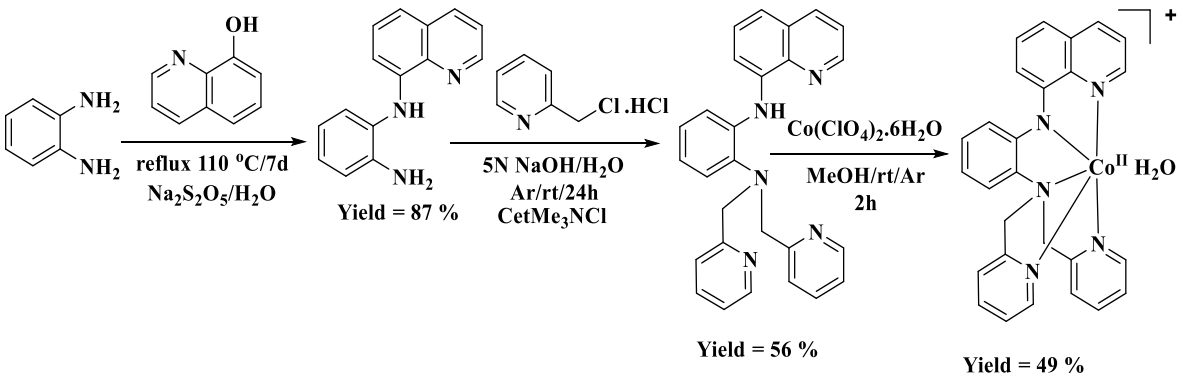

Scheme 3.1. Synthesis of the complex $[Co^{II}(L^{Qpy})H_2O]ClO_4$.

The pale yellow crystalline solid was reacted with an aqueous solution of 2-(chloromethyl) pyridinium chloride in the presence of NaOH and catalytic amounts of hexadecyltrimethyl ammonium chloride under inert conditions for 24 h to generate the crude ligand. The pure ligand was obtained by column chromatography on silica using a 3 : 1 EtOAc : hexanes solvent mixture. The ^{1}H-NMR spectrum of the ligand recorded in deuterated chloroform is shown in **Figure 3.3**, and the proton assignments detailed in **section 3.2.1** above.

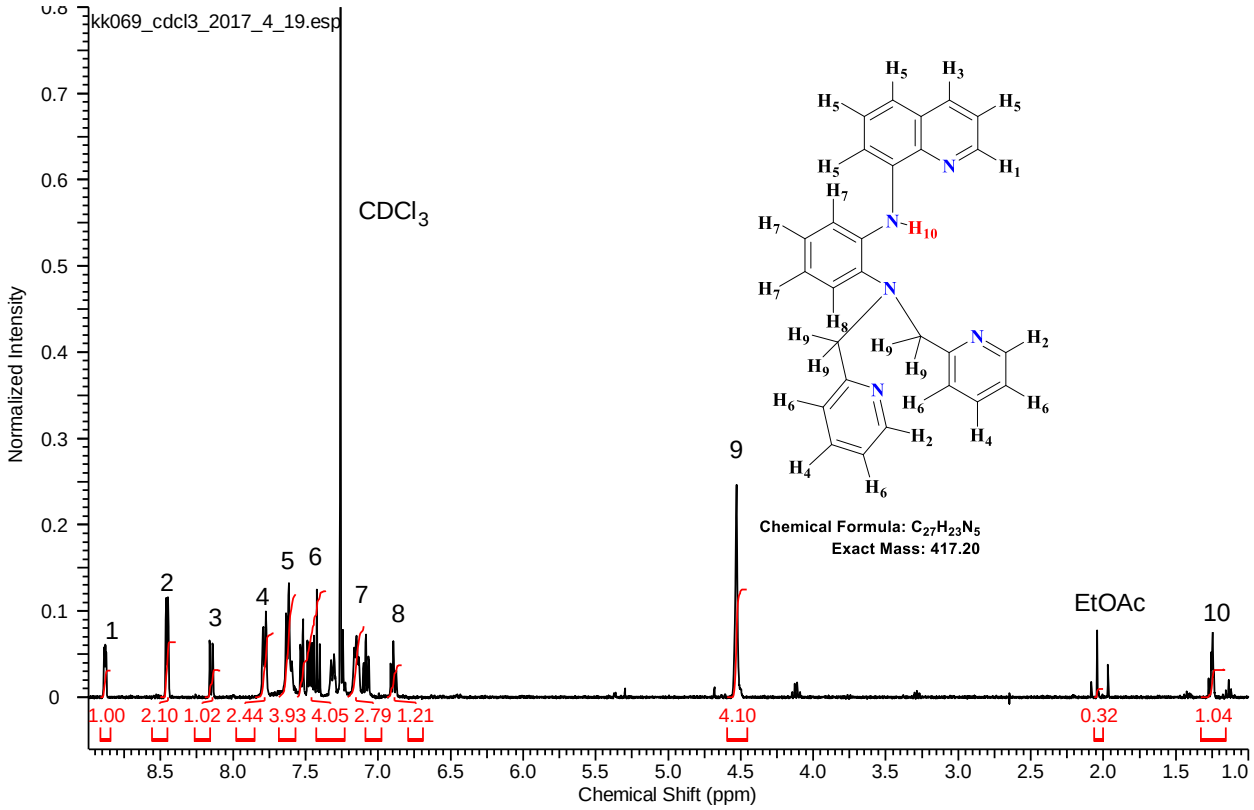

Figure 3.3. ^{1}H-NMR of **HL^{Qpy}** showing proton peaks with integration.

The water-soluble 3d^{7} ^{HS}Co^{II} complex was obtained by treating one equivalent of the pentadentate L^{Qpy} ligand with one equivalent of $Co(ClO_4)_2$ salt in presence of triethylamine (TEA) in methanol under inert conditions for 3 h. The ^{HS}Co^{II} aqua complex was characterized by FT-IR, ESI-MS, and elemental analyses. The disappearance of the N-H peak at 3350 cm $^{-1}$ in the FT-IR spectrum indicates the deprotonation of the secondary amine proton in the ligand from coordination to cobalt **Figure 3.4**. A sharp peak near 600 cm^{-1} and a very strong, and broad band at 1100 cm^{-1} both show the presence of a perchlorate counterion.

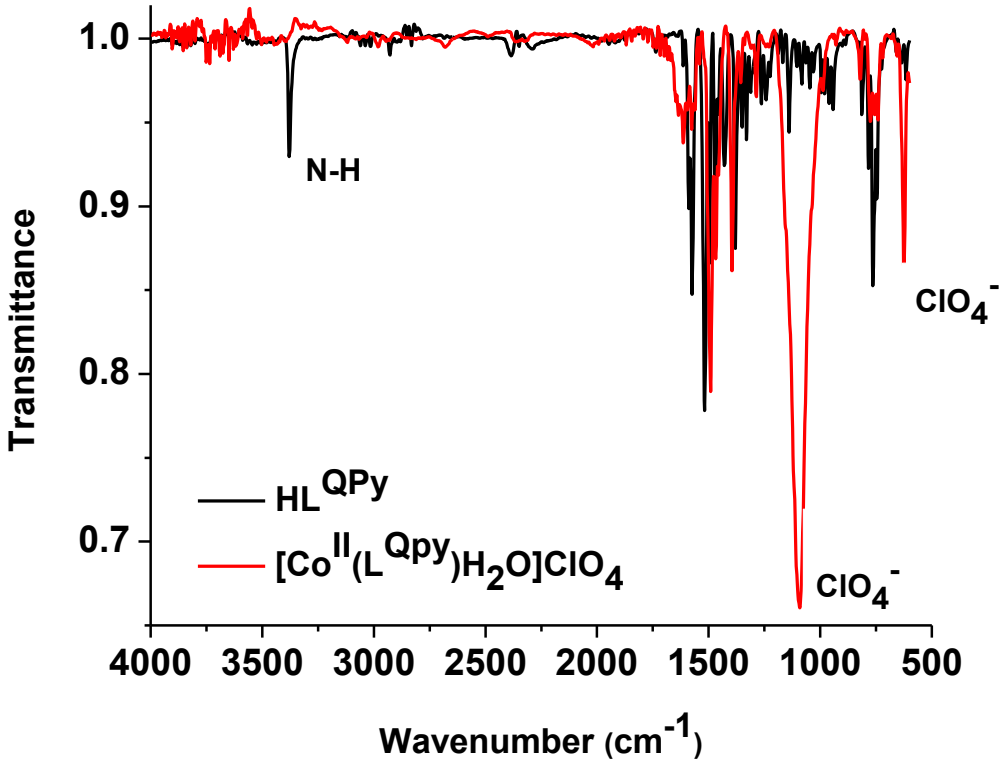

Figure 3.4. FTIR of **HL^{Qpy}** and **[Co^{II}(L^{Qpy})H$_2$O]ClO$_4$** showing relevant functional groups.

3.3.2 Geometric and Electronic Structures

The molecular structures of **HL^{Qpy}** and [Co^{II}(L^{Qpy})H$_2$O]ClO$_4$ were both determined by single crystal X-ray crystallography. Yellow colored hexagonal X-ray quality crystals of **(L^{Qpy})** precursor were grown by vapor diffusion of the complex dissolved in a 1 : 1 dichloromethane pentane solvent mixture for the structural determination (**Figure 3.5**). For **[Co^{II}(L^{Qpy})H$_2$O]ClO$_4$**, X-ray quality crystals grown by slow evaporation from 1 : 1 methanol : isopropanol were used for the structural determination. However it is important to state that, the crystal structure obtained from the diffraction studies indicate a dimeric form of the complex with an end-on transperoxo bridge. The formation of this dimer could be the oxidation of the complex dring the crystalization

process. The dimeric structure is shown in the Oak Ridge Thermal-Ellipsoid Plot (ORTEP)[154] representations at 50% probability in (**Figure 3.6**).

The **HL^{Qpy}** crystalized in an orthorhombic lattice with a *pca*2$_1$ space group. The asymmetric unit cell has one neutral molecule of a phenyldiamino-quinoline. Selected bond lengths for both crystal structures are shown in **Table 3.2.** The C-N bond lengths fall within the range of 1.323(1) Å and 1.421(1) Å consistent with reported C-N bonds for similar systems.[73,155]

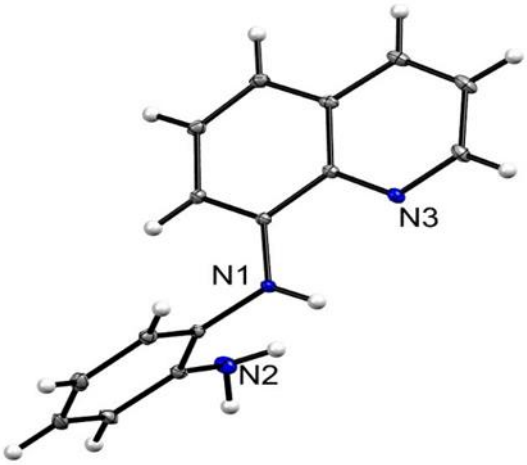

Figure 3.5. ORTEP[154] representations of **HL^{Qpy}** precursor at 50% probability. H atoms are shown for emphasis.

The structure is consistent with the presence of the characteristic secondary amine hydrogen (N-H) bonded to the nitrogen linking the phenylenediamine backbone and the quinoline moiety observed in FT-IR. The primary amine on the benzene ring does not form hydrogen bonds with the quinoline nitrogen in the solid state.

The **2[Co^{II}(L^{Qpy})O]ClO$_4$** complex crystallized with a *trans*-μ-peroxo bridge between the two cobalt centers, each of which adopts a distorted octahedral geometry with the ligand.

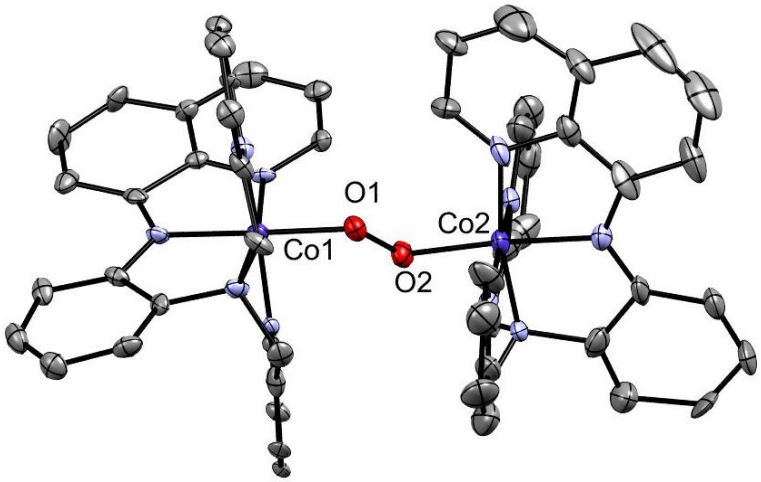

Figure 3.6. ORTEP[154] representations of dimeric form of **2[Co^{II}(L^{Qpy})O]ClO$_4$** at 50% probability H atoms are omitted for clarity.

The asymmetric unit cell consists of two dimeric cationic complexes with two perchlorate anionic moieties per each dimeric unit. The Co–N bond lengths fall in the range of the expected values of 1.88-1.95 Å.[156,73,155-159] The Co–O bond lengths range from 1.862(5) to 1.87(5) Å, which are similar to those reported.[70, 160-161] The O−O bond length of 1.422(8) Å, is typical for dinuclear Co−peroxo complexes.[103,162,155]

Table 3.2. Selected bond lengths (Å) and angles (°) from crystal data for (**HL^{Qpy}**) and **2[Co^{II}(L^{Qpy})O]ClO$_4$**

(L^{Qpy})			2[Co^{II}(L^{Qpy})O]ClO$_4$		
N3	C8	1.364(1)			
N3	C12	1.323(1)	Co1	O1	1.862(5)
N1	H1	0.880(1)	Co1	N1	1.885(6)
N1	C3	1.381(1)	Co1	N2	1.945(6)
N1	C7	1.421(1)	Co1	N3	1.900(6)

C3	C8	1.432(1)	Co1	N4	1.953(6)
C3	C11	1.384(1)	Co1	N5	1.928(6)
C4	C5	1.417(1)	Co2	O2	1.875(5)
C4	C8	1.421(1)	Co2	N6	1.896(6)
C4	C10	1.415(1)	Co2	N7	1.928(9)
			Co2	N8	1.943(9)
			Co2	N9	1.908(7)
			Co2	N10	1.939(9)

3.3.3 Electronic Spectroscopy

To probe metallation and gain insight into the electronic behavior of the complex before catalytic evaluation, a UV-visible spectrum was recorded in methanol and compared with that of the ligand (**Figure 3.7**). The ligand displays two bands at *ca.* 290 nm (ε = 38,500 L•mol^{-1}•cm^{-1}) and 380 nm (ε = 10,000 L•mol^{-1}•cm^{-1}) which are associated with $\pi \rightarrow \pi^*$ ILCT. The complex retained the band at 290 nm (ε = 22,000 L•mol^{-1}•cm^{-1}) associated with $\pi \rightarrow \pi^*$ ILCT, albeit with reduced intensity of the molar absorptivity due to coordination of the cobalt metal to the ligand. A new LMCT appears band at 330 nm (ε = 24,800 L•mol^{-1}•cm^{-1}) is assigned as quinoline $\pi \rightarrow {}^{HS}Co^{II}$–$d\sigma^*$.[163] The third band at 527 nm (ε = 6,650 L•mol^{-1}•cm^{-1}) is associated with a MLCT. The MLCT involves the promotion of an electron from the metal's d-orbital to the π^*-orbital of the ligand. A more rigid and planar ligand results in greater π-delocalization, producing the longest wavelength absorption.[164] These attributions are in agreement with similar published reports in the literature.[139, 164]

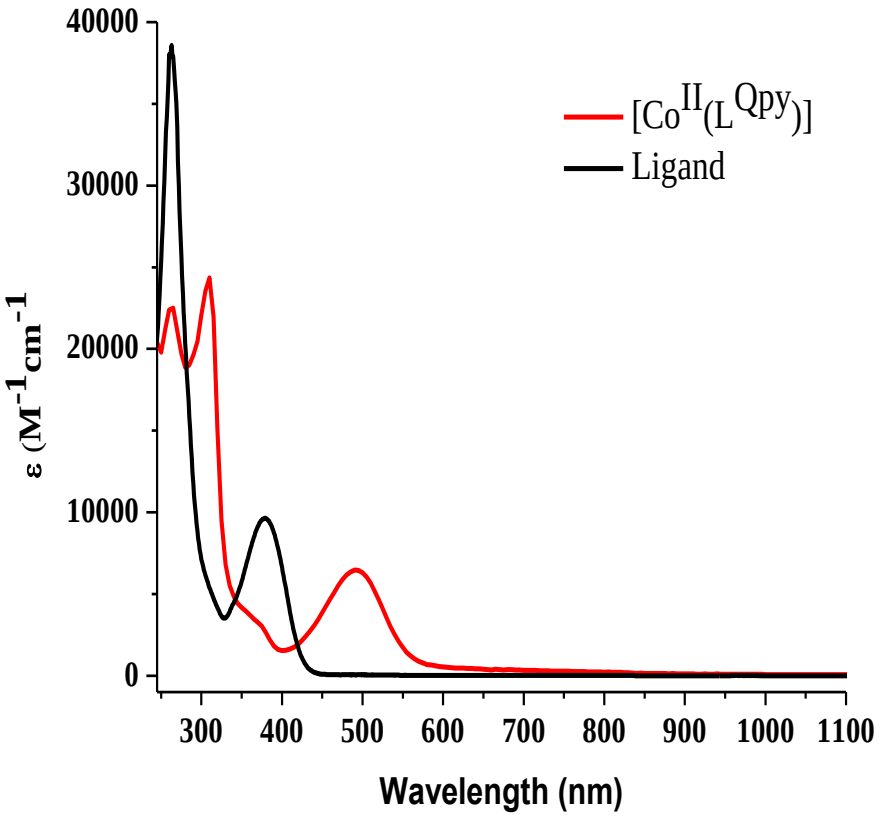

Figure 3.7. Electronic behavior of **HL^{Qpy}** and **[Co^{II}(L^{Qpy})H$_2$O]ClO$_4$** in 1.0 × 10^{-4} mol•L^{-1} methanol solution.

3.3.4 Electrochemical Properties

To probe the redox behavior of the metal complex, cyclic voltammograms were measured in 1.0 × 10^{-3} mol•L^{-1} acetonitrile solution using TBAPF$_6$ as the electrolyte (**Figure 3.8**). Redox potentials are reported versus Fc$^+$/Fc and are summarized in **Table 3.3**. The CV of **[Co^{II}(L^{Qpy})]** showed one quasi-reversible reduction event at -1.15 V$_{Fc+/Fc}$ attributed to a metal-based Co^{II}/Co^{I} reduction, with a second irreversible reduction peak arising at -2.2 V$_{Fc+/Fc}$ likely associated with ligand reduction. A quasi-reversible oxidation process observed at 0.60 V$_{Fc+/Fc}$ is assigned to a Co^{II}/Co^{III} oxidation event. [67,165]

Table 3.3. Electrochemical parameters for $[Co^{II}(L^{Qpy})H_2O]ClO_4$.

Redox Couples	E (V) vs. Fc/Fc^+	ΔE_p (V)	i_{pa} / i_{pc}
Co^{III}/Co^{II}	0.54	0.11	1.85
Co^{II}/Co^{I}	-1.16	0.09	1.42
L/L^-	-2.25	0.15	-

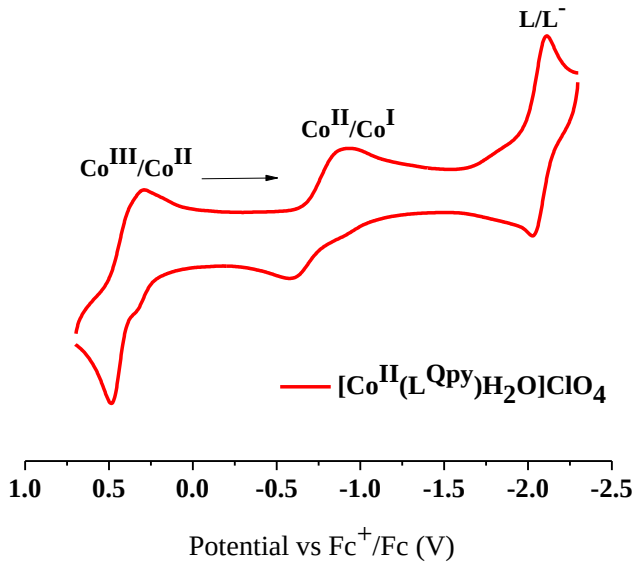

Figure 3.8. CV of **$[Co^{II}(L^{Qpy})H_2O]ClO_4$** in 1.0×10^{-3} mol•L^{-1} acetonitrile solution.

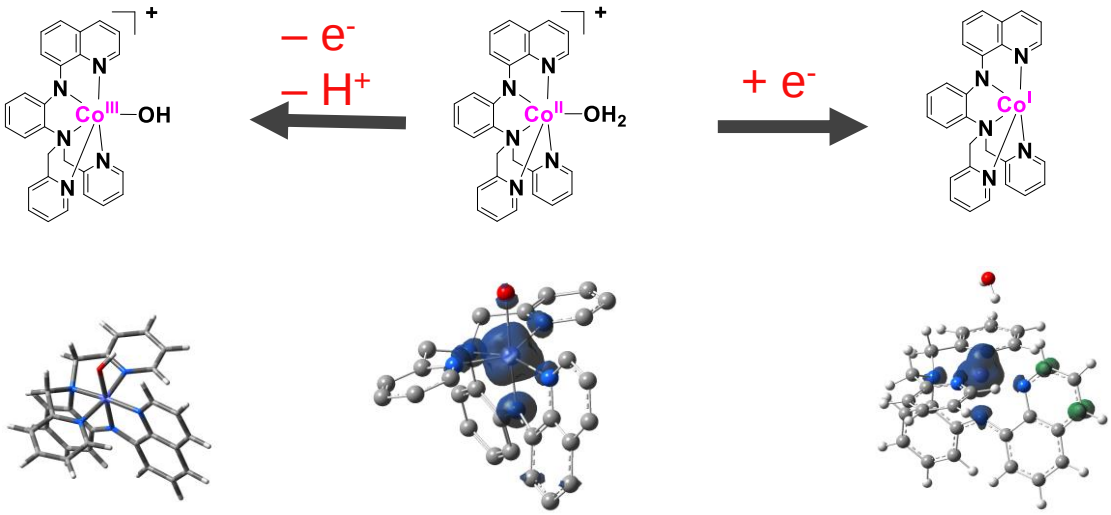

Figure 3.9. Spin density plots (isosurface value of 0.004 a.u.) of the redox-intermediate species generated during the electrochemical reduction, and oxidation of the complex.

The one-electron reduction potential of -1.15 $V_{Fc+/Fc}$ is affordable for water reduction based on,[133,71] and hence theoretical calculations were computed for an electronic comparison **(Figure 3.9).** Mulliken spin density plots show that the parent $3d^7$ Co^{II} is high spin.

Upon a one-electron reduction, a five-coordinate, $3d^{8\,LS}Co^{I}$ was found to be more favorable than a six-coordinate $3d^{7\,LS}Co^{II}$-$L^{\bullet}$ intermediate species by 10 kcal/mol. The one-electron oxidation of the parent $3d^{7\,HS}Co^{II}$ yielded a closed shell $3d^{6\,LS}Co^{III}$ which was favorable by 21.1 kcal/mol.

3.3.5 Electrocatalytic Studies

3.3.5.1. Water Reduction Electrocatalysis

The complex was evaluated for dihydrogen production in aqueous media by conducting cyclic voltammetry experiments in aqueous pH 7 phosphate buffer (0.1 mol•L^{-1}) using a three-electrode setup: Ag/AgCl as the reference electrode, a platinum wire auxiliary electrode, and Hg-pool as the working electrode due to its low affinity for water reduction and large reductive window[165]. A CV sweep was done for the blank buffer without the catalyst, with no catalytic current enhancement observed until -1.85 $V_{Ag/AgCl}$ **(Figure 3.10).**

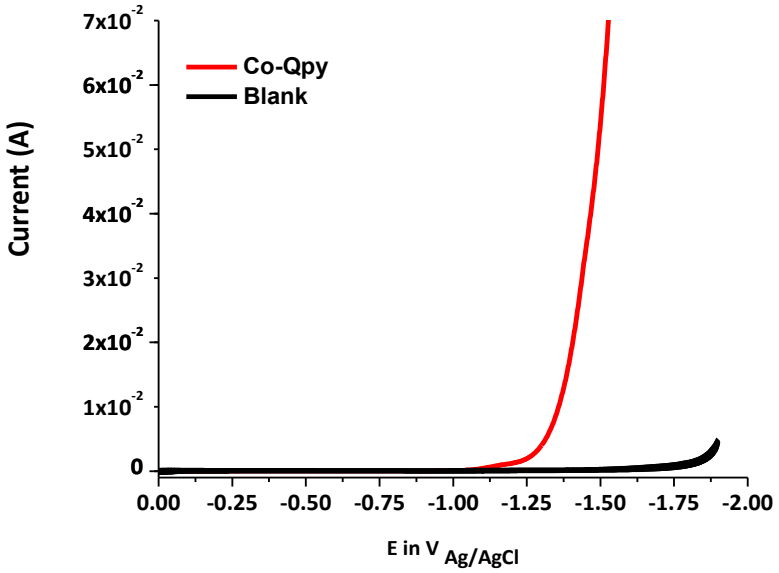

Figure 3.10. Catalytic water reduction CV of **$[Co^{II}(L^{Qpy})H_2O]ClO_4$** in 0.1 mol•$L^{-1}$ phosphate buffer at neutral pH.

In the presence of the catalyst, however, a current enhancement was observed at -1.15 $V_{Ag/AgCl}$ accompanied by evolution of bubbles. The identity of the bubbles was confirmed as hydrogen by gas chromatography.

An onset potential for catalysis of –1.20 $V_{Ag/AgCl}$ was observed, yielding an overpotential of 0.65 V. The identity of the gas was determined to be H_2 by injecting the headspace into a gas chromatograph. To ascertain the efficiency of the catalyst for H_2 production and quantify the amount of H_2 produced, a 3 h bulk electrolysis was performed to determine the (TON) and (%FE) at an applied potential of -1.7 $V_{Ag/AgCl}$ **(Figure 3.11)**.

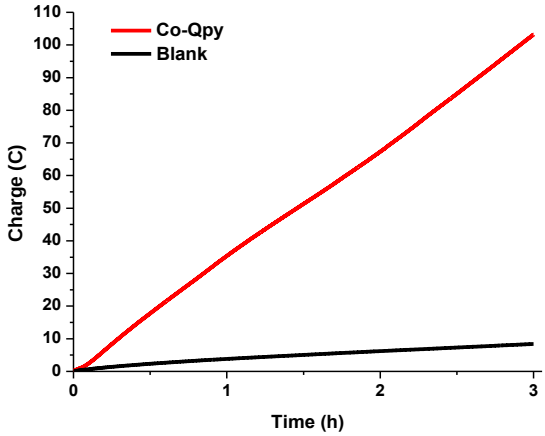

Fi**gure 3.11.** Charge consumption vs. time during BE (0.2 umol•L^{-1}) of **$[Co^{II}(L^{Qpy})H_2O]ClO_4$** in 0.1 mol•$L^{-1}$ phosphate buffer at pH 7 at –1.7 $V_{Ag/AgCl}$ for 3 hours.

After 3 h, the catalyst operated at 98% Faradaic efficiency with a TON of 2900, with no apparent loss in activity. The high Faradaic efficiency indicates that every electron transferred is utilized in the production of H_2.[165] The TON and high (%FE) are higher than those reported for cobalt catalysts with similar ligand architectures, and under similar experimental conditions by Chang *et al*,[18] Zhao *et al*.[166] and show a remarkable improvement on the TON reported by 1st-generation cobalt pyridine catalyst by Verani *et al*.[73]

To determine the robustness of the catalyst, bulk electrolysis was conducted under the same conditions for 18 h **(Figure 3.12)**. The 18-hour catalysis by **[$Co^{II}(L^{Qpy})$]** gave a TON of 12,100, with a (%FE) of 97, with negligible loss in activity by the charge versus time plot, suggesting a stable and robust catalyst.

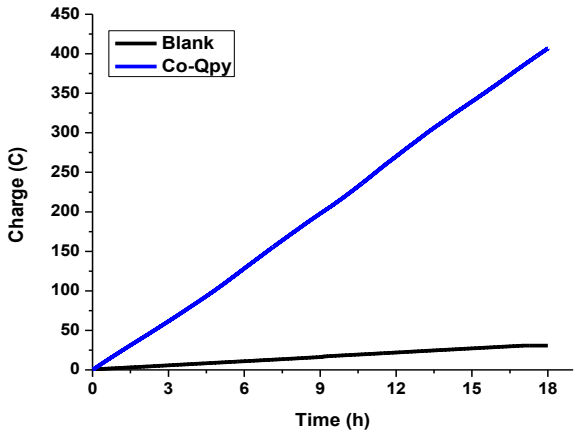

Figure 3.12. Charge versus time plot during controlled potential electrolysis of **[$Co^{II}(L^{Qpy})H_2O]ClO_4$** for 18 hours.

Post–catalytic analysis is often performed on molecular water-splitting catalysts to determine whether the catalyst has retained its molecular identity or it has been transformed to different species. Several techniques are employed for this analysis, including UV-visible spectroscopy, SEM and EDS. For the **[$Co^{II}(L^{Qpy})H_2O]ClO_4$** catalyst**,** UV-visible spectral analysis was performed in neutral water (pH 7.0, 1.0 M phosphate buffer) before and after bulk electrolysis to determine the fate of the catalyst **(Figure 3.13)**.

The post-catalysis spectrum remains practically the same as the spectrum before catalysis with only a slight increase of ~4% in the band around 300 nm and ~2% increase in 450 nm band. A plausible hypothesis for this slight increment in the spectral profile is the possibility of solvent percolation from the catalytic chamber to the auxiliary chamber through the semi-permeable frit.

To further confirm the molecular nature of the **[Co^{II}(L^{Qpy})H$_2$O]ClO$_4$** catalyst by SEM and EDS analyses, we performed BE experiments under identical experimental conditions but using a conductive grafoil sheet as the working electrode instead of the liquid Hg-pool electrode used for catalysis. The scanning electron microscope (SEM) images (**Figure 3.14**) show some formation of particulate species which were then analyzed by EDS to determine their composition.

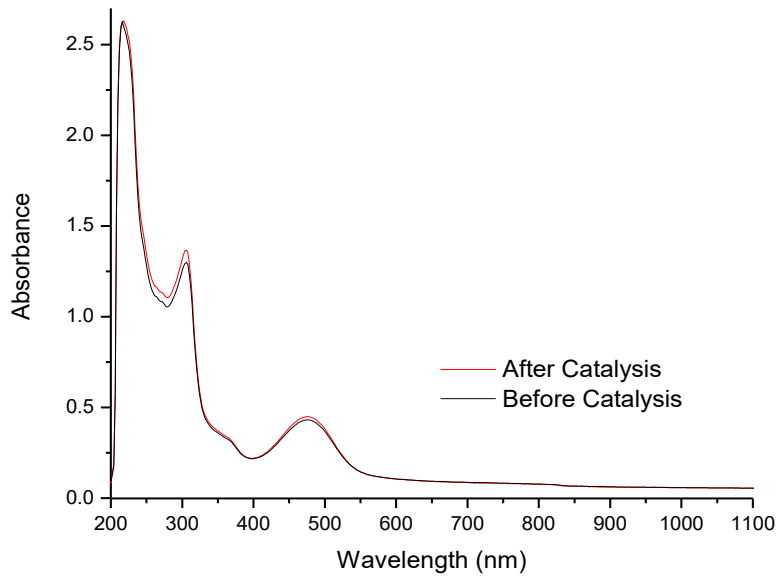

Figure 3.13. Spectral profile of **[Co^{II}(L^{Qpy})H$_2$O]ClO$_4$** before and after bulk electrolysis.

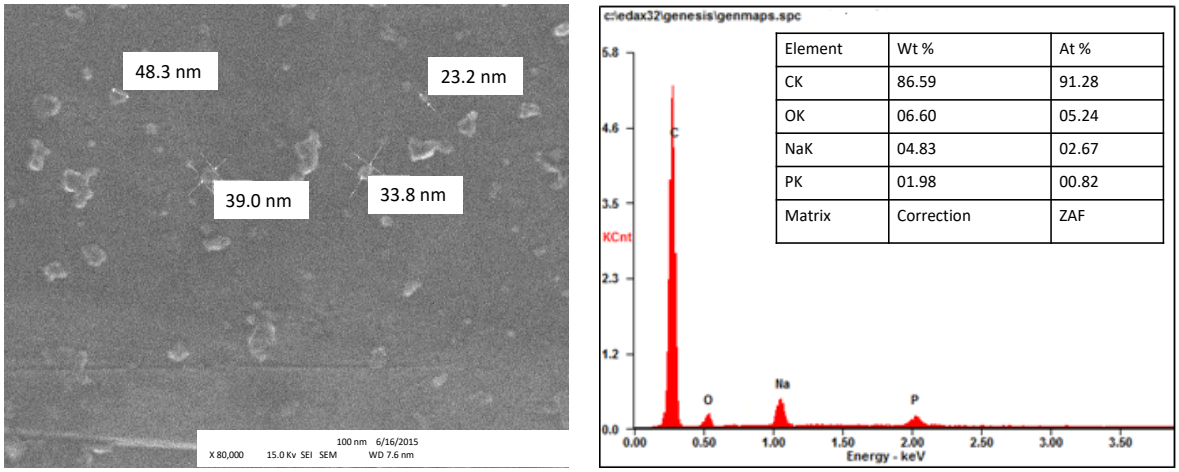

Figure 3.14. Post-catalytic SEM and EDX analysis of grafoil electrode surface.

The (EDS) analysis results indicate that the particulate species were composed of carbon and sodium phosphate, which are likely from the grafoil electrode and the phosphate buffer used for the catalysis. Cobalt nanoparticles were however not detected; thus ruling out catalyst transformation and suggesting the molecular nature of the catalyst.

3.3.5.2. Water Oxidation Electrocatalysis

To assess the capability of **$[Co^{II}(L^{Qpy})H_2O]ClO_4$** to catalyze water oxidation, a CV sweep was performed in borate buffer (0.1 mol•L^{-1}, pH 8.0) using a fluorine-doped tin oxide (FTO) glass working electrode, a Pt wire as the auxiliary electrode and Ag/AgCl as the reference electrode **(Figure 3.15)**. Upon scanning the borate buffer without the catalyst, a current enhancement peak of -0.5 mA was observed starting from 1.8 $V_{Ag/AgCl}$ to 2.0 $V_{Ag/AgCl}$. Upon the addition of the catalyst, two peaks were observed. An oxidation peak is observed at 1.25 $V_{Ag/AgCl}$ and is followed by a catalytic wave for water oxidation.

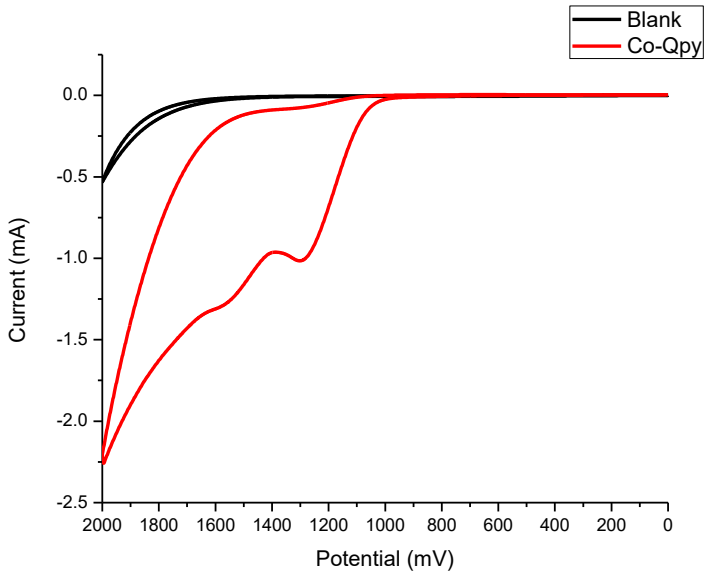

Figure 3.15. Catalytic water oxidation CV of **$[Co^{II}(L^{Qpy})H_2O]ClO_4$** in 0.1 mol•$L^{-1}$ borate buffer at pH 8.

Bulk electrolysis was performed under the same conditions **(Figure 3.16)**, using a 0.2 μ mol•L^{-1} concentration of the catalyst and 1.27 cm^2 FTO as working electrode, with an applied potential of 1.5 $V_{Ag/AgCl}$ for 3 h to quantify the oxidative catalytic product. After 3 h the catalyst gives a linear charge versus time consumption plot of 18 C/h, with no substantial loss in activity, and operates at 91% (F.E.) with a TON of 97. It is important to note that only a few reports exist on the catalytic activity of single-site molecular cobalt-based electrocatalysts for water oxidation,[167-169] and out of those, only a handful try to quantify the amount of oxygen produced during catalysis due to harsh oxidative conditions needed to perform water oxidation.[170-171] The TON of these catalysts range between 0 and 70 turnovers, with faradaic efficiencies ranging from 75% to 95%. Thus the high catalytic activity of this **$[Co^{II}(L^{Qpy})H_2O]ClO_4$** establishes it as one of the very few catalysts with TONs around 100 in 3 hours.

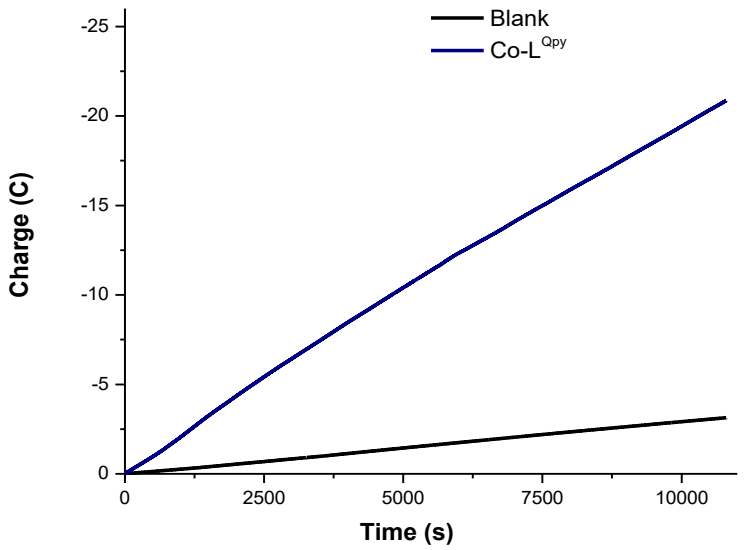

Figure 3.16. Charge versus time plot during bulk electrolysis of **$[Co^{II}(L^{Qpy})H_2O]ClO_4$** in 0.1 mol•$L^{-1}$ borate buffer at pH 8.

A BE experiment was performed again in borate buffer (0.1 mol•L^{-1}, pH 8.0) using an FTO electrode as the working electrode which was analyzed by SEM and EDS techniqes to ascertain whether the catalyst retained its molecular nature of during water oxidation because ligand transformations and catalyst degradation remain a challenge for most water oxidation electrocatlysts reported in the literature.

The SEM analysis results show no evidence of nanoparticles, with EDS analysis indicating only elements that constitute the FTO-glass electrode with no cobalt particles deposited on the electrode **(Figure 3.17)**. This lack of detectable nanoparticles suggests that the catalyst remains molecular during electrocatalysis.

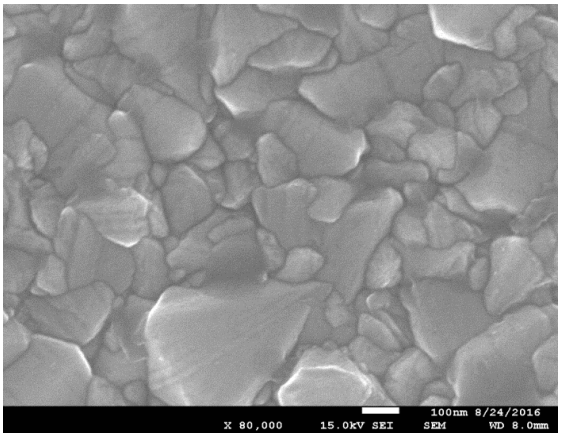

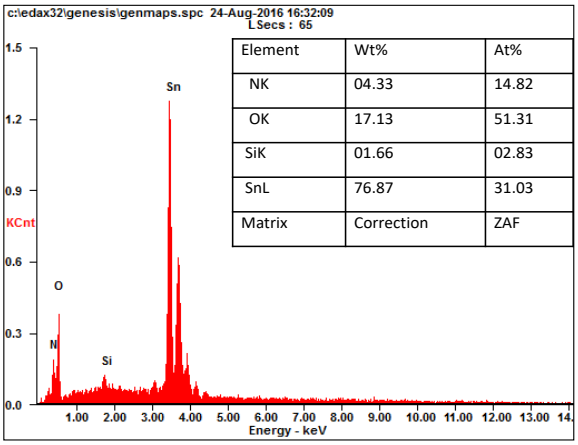

Figure 3.17. Post-catalytic SEM and EDX analysis of FTO electrode surface.

3.3.6 Characterization of Catalytic Oxidative Intermediates

Cobalt-based catalysts are expected to oxidize water to dioxygen in basic media undergoing well-defined PCET steps **(Figure 3.2)** to a tetravalent intermediate which is electrophilic enough to be attacked by a nucleophilic water molecule. The results from the redox behavior, and the electrocatalytic water oxidation of **$[Co^{II}(L^{Qpy})H_2O]ClO_4$**, shows that the $3d^7$ $^{HS}Co^{II}$ parent species complex undergoes a first one-electron oxidation event to yield a $3d^6$ [$^{LS}Co^{III}$-OH] species, and subsequently undergoes a second oxidation event after which a catalytic current

enhancement is observed. According to mechanisms reported by Berlinguette,[21, 81, 172] Nocera,[173] and Thapper,[170] the catalytic-active intermediate required for the crucial O – O bond formation in single-site cobalt catalyst for water oxidation is a $3d^5$ [Co^{IV}=O] species. To determine if the high-valent $3d^5$ [Co^{IV}=O] is involved in the catalytic pathway of the **[$Co^{II}(L^{Qpy})H_2O]ClO_4$** as well, I performed a series of independent one-electron, and 2-electron electrochemical oxidation experiments and used EPR to characterize the intermediate products (**Figure 3.18)**.

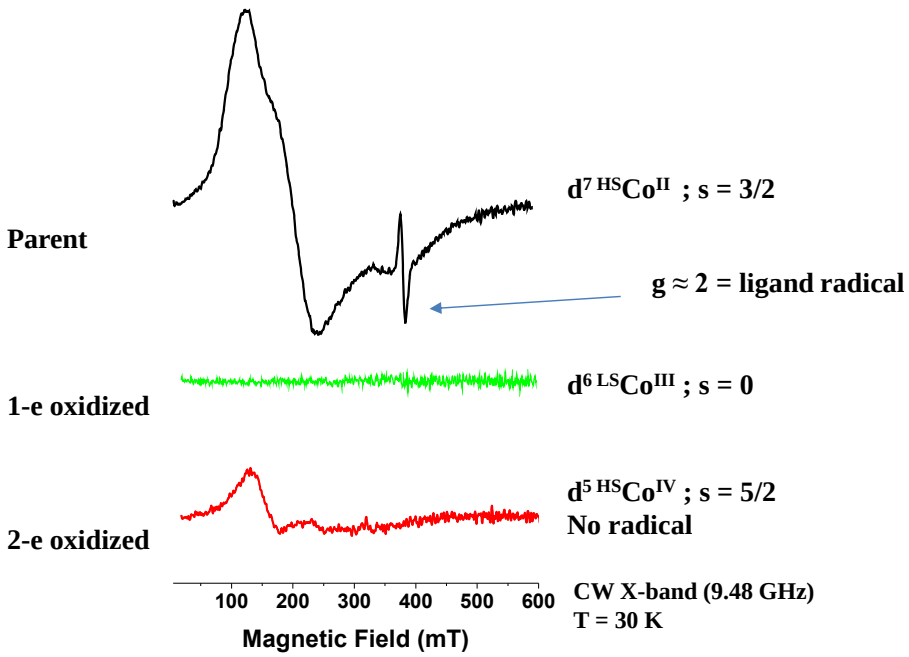

Figure 3.18. EPR spectra of catalytic oxidative **[$Co^{II}(L^{Qpy})H_2O]ClO_4$** intermediates.

The samples for EPR were prepared in CH_3CN under inert conditions and measured at the Argonne National Laboratory for analysis by Drs. Oleg Poluektov and Jens Niklas. The CW X-band (9.48 GHz) EPR analysis were performed at 30 Kelvin. The EPR data shows that, the main EPR signal for the parent complex (black trace) is from a $3d^7$ $^{HS}Co^{II}$ (S = 3/2) species with no sign of $^{LS}Co^{II}$ species. The narrow signal (line width peak-peak around 7 mT) close to g≈2 could be traces of ligand radical character. The one-electron oxidized sample gave no EPR signal suggesting

a closed shell $3d^6$ $^{LS}Co^{III}$ (S = 0) diamagnetic species. The 2-electron oxidized sample gives a signal characteristic of a $3d^5$ $^{HS}Co^{IV}$ (S = 5/2) species with no radical species visible.

The absence of a radical species suggests the presence of only the $^{HS}Co^{IV}$ species, thereby eliminating the possibility of the intermediate being a radical-bearing "[Co^{III}-L•]" species. These results constitute one of the few reports in the literature[174-175] that track, isolate and characterize experimentally, the oxidative intermediates for catalytic water oxidation.

3.3.7 Mechanism of Catalytic Water Oxidation

Based on the results from the water oxidation bulk electrolysis, the characterization of intermediate catalytic products, and DFT computations, we propose a 'water nucleophilic-attack' (WNA) mechanism of water oxidation for the **[$Co^{II}(L^{Qpy})H_2O]ClO_4$** complex **(Figure 3.19).** We propose that the parent $3d^7$ [$^{HS}Co^{II}$–OH_2] undergoes an oxidative one-electron, proton-coupled electron-transfer (PCET) step to yield $3d^6$ [$^{LS}Co^{III}$–OH] species.

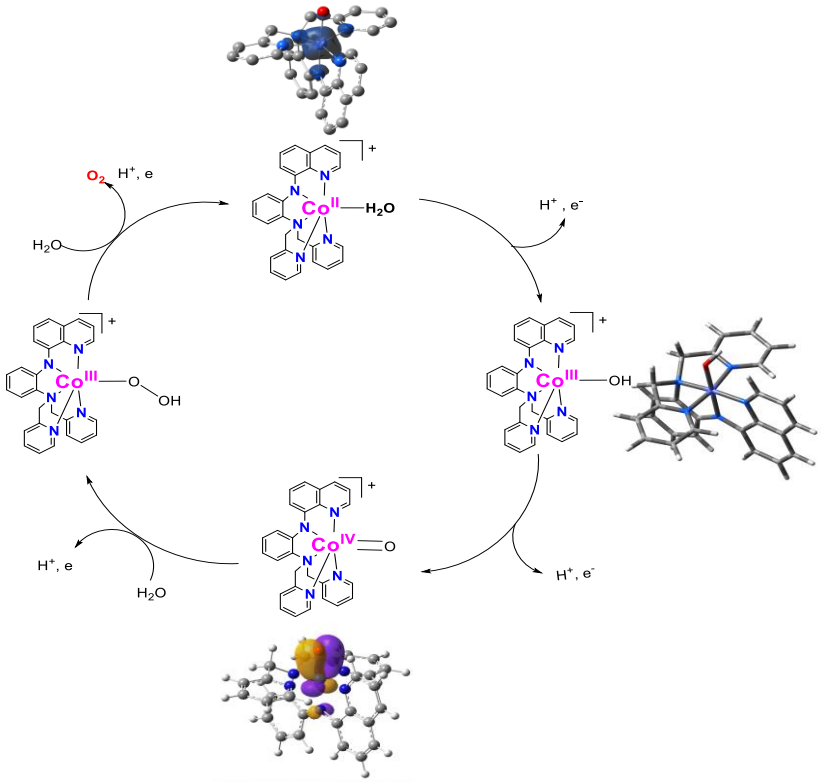

Figure 3.19. Proposed catalytic mechanism of O_2 generation by **[$Co^{II}(L^{Qpy})H_2O]ClO_4$.**

This intermediate further undergoes another one-electron oxidative process to yield the key $3d^5$ [$^{HS}Co^{IV}$=O], which is sufficiently electrophilic and very reactive. This intermediate is then attacked by a water molecule thus forming the essential O – O bond and releasing dioxygen in the process and yields he parent $3d^7$ [$^{HS}Co^{II}$–OH_2] catalyst.

The nucleophilic attack by the water molecule could be made possible by the interaction between the highest-occupied molecular orbital (HOMO) of water (σ symmetry) and (LUMO) of the pseudo-octahedral [$^{HS}Co^{IV}$=O] complex (dπ* character), accompanied by the breaking of the Co–O π bond and thus the two-electron reduction of the cobalt to yield the parent species.[174, 176-178] The non-detection of any radical character in the EPR spectrum of the $3d^5$ [$^{HS}Co^{IV}$=O] suggests that the catalysts does not undergo the oxidative mechanism, radical homo-coupling.

3.3.8 Photocatalytic Studies

To determine if **[$Co^{II}(L^{Qpy})H_2O]ClO_4$** could be an ideal candidate for eventual photocatalysis, preliminary photocatalytic activity was studied in acetate buffer (pH 4), using 1.0 $^{-4}$ of the catalyst, and $[Ru(bpy)_3]^{2+}$ (5.0 $^{-4}$ mol•L $^{-1}$) as the photosensitizer (P.S.) in the presence of ascorbic acid (1.1 mol•L $^{-1}$) as the sacrificial electron donor.[179] For an experiment, a series of 15 mL clear cylindrical vials with gas tight screw caps and septa were filled with a 10 mL aliquot of 0.1 mol•L $^{-1}$ pH 4 acetate buffer containing the P.S., ascorbic acid, and **[$Co^{II}(L^{Qpy})H_2O]ClO_4$**. The vials and their contents were then degassed with nitrogen. The absence of oxygen was verified by GC prior to light irradiation. The vials were then placed in a water-jacketed beaker with a constant temperature of 20 °C.[153] The contents of the vials were irradiated by an 18 module blue LED strip (λ_{max} = 460 nm) wrapped around the beaker and connected to a 12 V power controller.[180]

The headspace gas was analyzed in triplicate over in 30 m, intervals over 6 h by a GOW-MAC GC with a thermal conductivity detector (TCD) to determine the amount of hydrogen

produced over time using nitrogen gas as the carrier gas at a flow rate of 30 mL min $^{-1}$ **(Figure 3.20).** The amount of H_2 produced was calculated using a calibration curve of moles of hydrogen versus peak area. A TON of 294.40 was achieved with TOF of 50.00/h. Even though the preliminary TON is modest, it is comparable to those reported by Wang,[181] and Blackman,[179] using identical experimental conditions for the same period of time. A blank experiment was conducted under the same conditions without the catalyst as control and the negligible hydrogen produced was duly subtracted before calculating the TON.

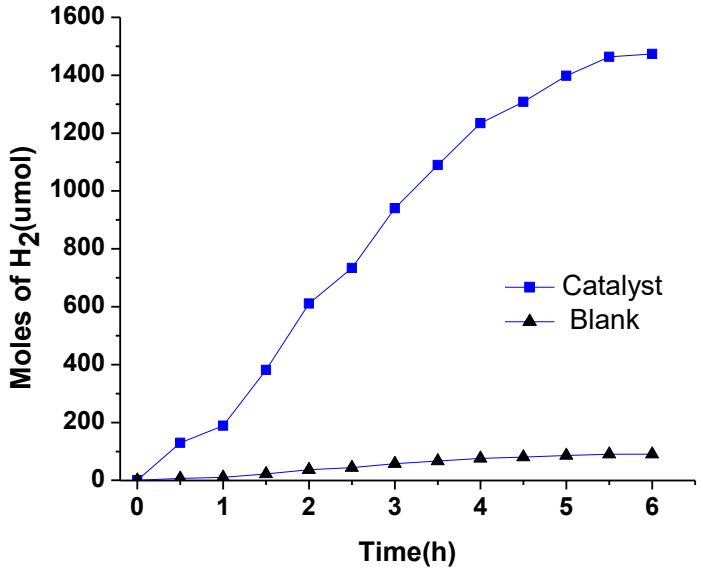

Figure 3.20. Plot of amount of H_2 produced over time during photocatalysis by **$[Co^{II}(L^{Qpy})H_2O]ClO_4$**.

To test whether the catalyst remains molecular during the photocatalytic experiment, a mercury-poison test was conducted on the samples to ensure that cobalt oxides or nanoparticles are not responsible for the photocatalytic activity **(Figure 3.21)**.[179, 182-183] Mercury was added to each sample after which the experiment was conducted under the same conditions. At the end of

the catalysis, the catalytic efficiency remained unchanged suggesting that the catalyst did not transform to cobalt oxides nor nanoparticles during the catalysis.

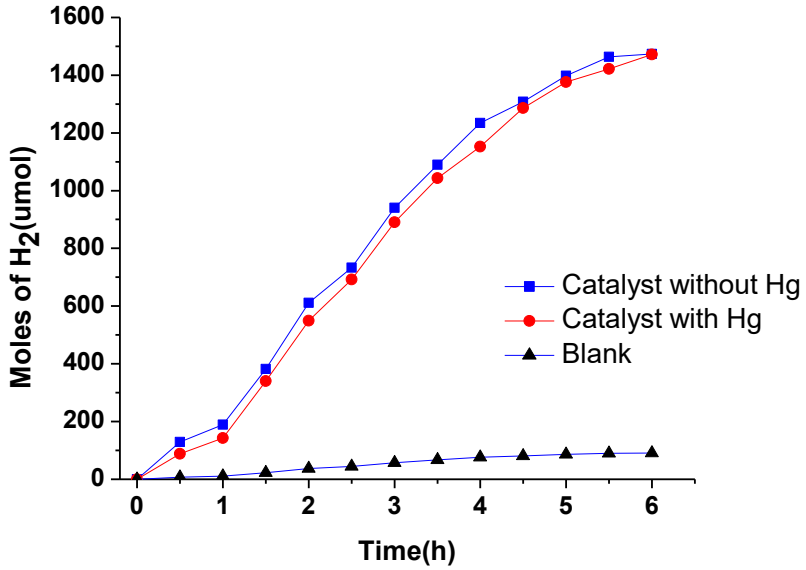

Figure 3.21. Plot of amount of H_2 produced by **[Co^{II}(L^{Qpy})H$_2$O]ClO$_4$** in the presence of Hg and without Hg over time.

3.4 Conclusions

In conclusion, I investigated an asymmetric, pentadentate quinolyl-bispyridine ligand **L^{Qpy}** with a phenylenediamine backbone and its water-soluble Co(II) complex **[Co^{II}(L^{Qpy})H$_2$O]ClO$_4$** that has been synthesized and characterized. This complex is active as an electrocatalyst as well as a photocatalyst. **[Co^{II}(L^{Qpy})H$_2$O]ClO$_4$** is catalytic towards H_2O reduction at a low overpotential of 0.63 V, giving a TON of 2900 with a Faradaic efficiency of 98%. An 18 h catalytic TON of 12,100 suggests a highly robust and stable catalyst. **[Co^{II}(L^{Qpy})H$_2$O]ClO$_4$** serves as a robust water oxidation catalyst as well, with a TON of 97 at 91% FE. By using a series of experimental and DFT techniques, I was able to isolate and characterize the catalytic oxidative intermediates for **[Co^{II}(L^{Qpy})H$_2$O]ClO$_4$**, and proposed a 'water nucleophilic-attack' (WNA) mechanism of water oxidation, where the highly electrophilic 3d^5 [^{HS}Co^{IV}=O] intermediate is attacked by a nucleophilic

water molecule thus forming an O-O bond and releasing dioxygen. Finally, the photocatalytic activity of **$[Co^{II}(L^{Qpy})H_2O]ClO_4$** in the presence of $[Ru(bpy)_3]^{2+}$, and ascorbic acid in an acetate buffer (pH 4) gave a TON of 295 with a TOF of 50/h.

CHAPTER 4

ELECTRONIC COMMUNICATION AND COOPERATIVITY IN A DICOBALT COMPLEX FOR PROTON REDUCTION

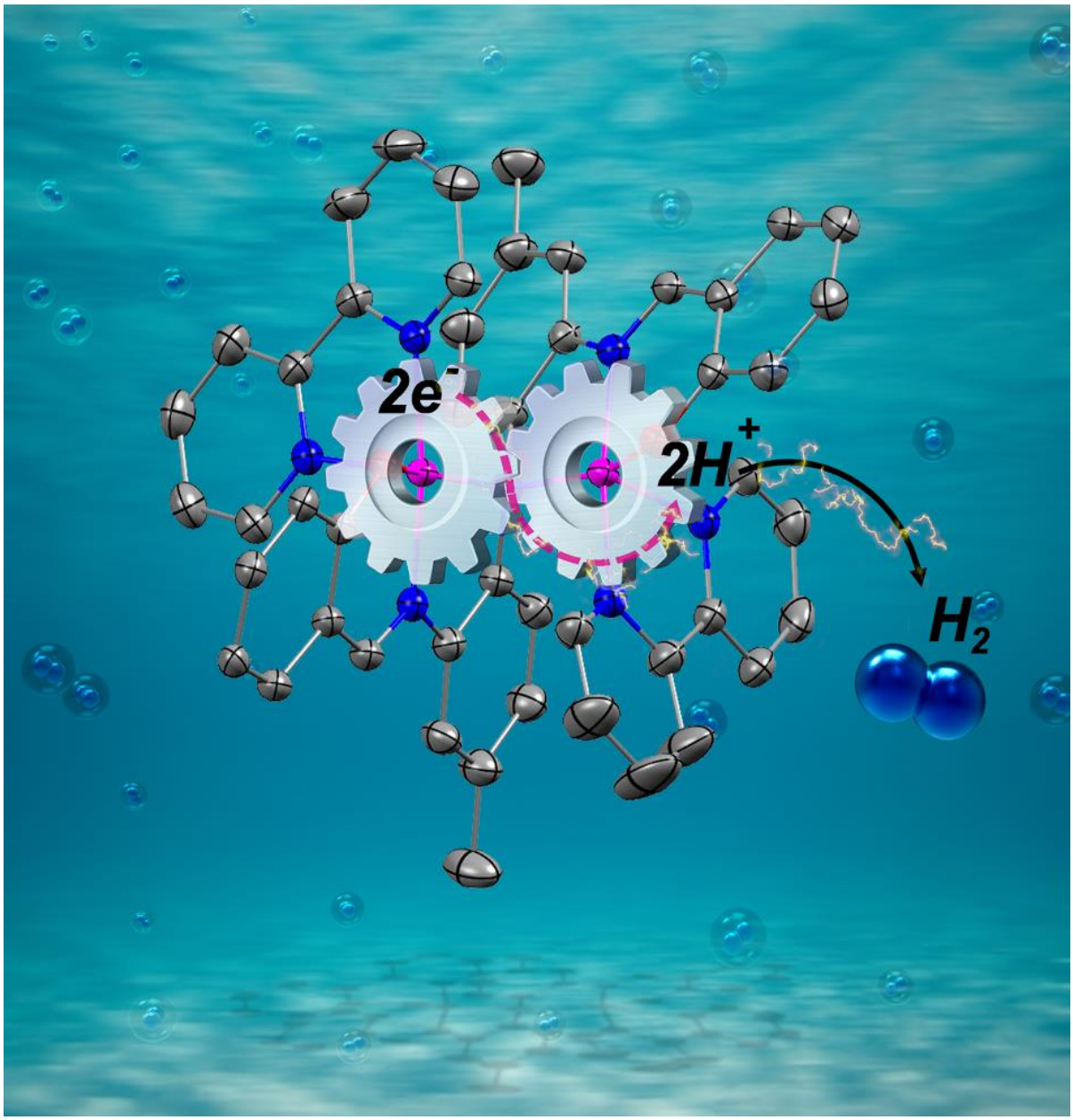

CHAPTER 4: ELECTRONIC COMMUNICATION AND COOPERATIVITY IN A DICOBALT COMPLEX FOR PROTON REDUCTION

4.1. Introduction

The widespread dependence of our society on fossil fuels and the impending depletion of carbon-based reserves have triggered the search for renewable and clean H-based energy.[184,1] Earth-abundant transition metals like cobalt, nickel, and iron have attracted attention due to their ability to generate H_2.[129,17,59,180] Among these metals, cobalt is particularly relevant because of its affordable redox potentials between the $3d^6$ Co^{III}, $3d^7$ Co^{II} and $3d^8$ Co^{I} states. The catalytically active monovalent species can be stabilized and yield the doubly-oxidized cobalt/hydride intermediate Co^{III}–H^-, which is pivotal for H^+ reduction to H_2 after reduction to more reactive Co^{II}–H^-.[14,131,46,132,133] Known cobalt catalysts follow either a heterolytic or a homolytic pathway.[46,16,47] The former mechanism relies on a single Co^{III}–H^- or a Co^{II}–H^- [51,185] reacting with another H^+ and is favored when the concentration of protons is not limiting. The latter involves the collision of two Co^{III}–H^- moieties from independent molecules.[48]

Enhanced activity is expected from some binuclear analogs of monometallic catalysts in which close proximity between two cobalt centers triggers cooperativity either by facilitating homolytic pathways[74] or by enabling electron transfer between the metal centers, thus avoiding the formation of a Co^{III}–H^- species.

Cooperative effects have been proposed by Dinolfo *et al.* [77] for a binuclear Co^{II} catalyst in a bicompartmental Robson/Okawa-type $[N_6O_2]$ macrocycle[186-187] with a Co-Co distance of 3.22 Å, while Gray *et al.* [75,188] evaluated oxime-based Co^{III} catalysts with both flexible hydrocarbon and rigid BO_4 bridges that revealed no significant catalytic enhancement. Similarly, the lack of cooperativity observed in dicobalt complexes featuring pyrazolato bridges[48,189] was attributed either to the large distance of 3.95 Å between the Co centers or to the flexibility of the ligand. To date, it is unclear what factors control metal cooperativity in proton reduction and this lack of understanding prevents a more rational design of Co_2 catalysts.

The Verani group has a long-standing interest in the mechanisms of H_2 generation by Co catalysts,[115,73,190,54] and continuing with that research focus, we collaborated with the Fiedler group from the University of Marquette who previously published the **$[Co^{II}_2(L^{1'})(bpy)_2]ClO_4$** complex **(Figure 4.1).** We hypothesized that cooperativity will be dependent on (i) the distance between the Co centers, (ii) the relative topology of the coordination environments, and (iii) the degree of orientation and overlap between redox-active orbitals. To evaluate this hypothesis, we analyzed the catalytic potential of the bimetallic complex **$[Co^{II}_2(L^{1'})(bpy)_2]ClO_4$**,[191] where $(L^{1'})^{3-}$ is the triply deprotonated ligand shown in **Figure 4.1**, by means of electrochemical, spectroscopic, and computational methods.

The complex **$[Co^{II}_2(L^{1'})(bpy)_2]ClO_4$** is a unique bimetallic species singularly suited for this study because of the short distance between the two vicinal Co centers along with the presence of a Co-$N_{arylamido}$-Co unit that may foster the proper orientation of Co orbitals involved in catalysis. Our results indicate that the two cobalt centers of $[Co^{II}_2(L^1)(bpy)_2]ClO_4$ function cooperatively in the electrocatalytic reduction of H^+, thus offering a viable mechanistic alternative to homolytic and heterolytic pathways employed by mononuclear cobalt catalysts.

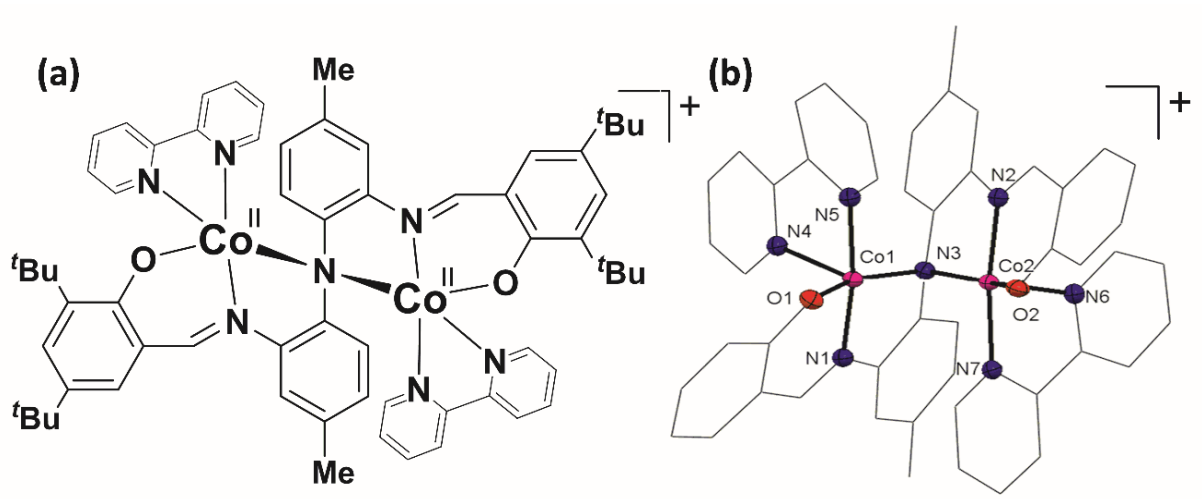

Figure 4.1. The complex **[Co^{II}$_2$(L$^{1'}$)(bpy)$_2$]ClO$_4$ (1)**: (a) Drawing and (b) ORTEP of the core showing a Co1-N3-Co2 angle of 86.9° expected to facilitate cooperativity.

4.2 Experimental

4.2.1 Materials and Methods

All reagents were used without further purification as purchased from commercial sources. **[Co^{II}$_2$(L$^{1'}$)(bpy)$_2$]ClO$_4$** was obtained by dissolving the ligand H_3L^1 (0.066 g, 0.10 mmol), 2,2'-bipyridine (bpy, 0.032 g, 0.20 mmol), and $Co(ClO_4)_2$•$6H_2O$ (0.073 g, 0.20 mmol) in a 1:1 mixture of CH_3CN and CH_2Cl_2 (10 mL). A detailed synthetic protocol and characterizations have been described recently.[191] ^{1}H NMR spectra were measured using a Varian 400 MHz instrument. Elemental analyses were performed by Midwest Microlab (Indianapolis, Indiana) in an Exeter-CE440 CHN analyzer. UV-visible spectra of 1.0×10^{-4} M and 1.0×10^{-5} M CH_2Cl_2 solutions were measured using a Shimadzu 3600 spectrophotometer in the range 190-1600 nm.

4.2.2 Redox Studies

The electrochemical behavior of **[Co^{II}$_2$(L$^{1'}$)(bpy)$_2$]ClO$_4$** was investigated with a BASi 50W potentiostat/galvanostat. Cyclic voltammograms (CV) were obtained at room temperature in CH_3CN containing 0.1 M of tetrabutylammonium hexafluorophosphate ($TBAPF_6$) as the

supporting electrolyte under argon atmosphere. The electrochemical cell employed three electrodes: glassy-carbon (working), platinum wire (auxiliary) and Ag/AgCl (reference). The ferrocene/ferrocenium (Fc/Fc^+) redox couple (E^o = 401 mV_{NHE}) was used as internal standard.

Bulk electrolysis (BE) was performed in a custom-made air-tight H-type cell under inert conditions according to the procedure reported by Basu *et al.*[73] The cell was comprised of two compartments separated by a frit. On one side of the frit was placed the Hg-pool working and Ag/AgCl reference electrodes, while a coiled 12-inch Pt wire serving as the auxiliary electrode was placed in the other compartment. BE experiments were performed in acetonitrile (20 mL) with $TBAPF_6$ as the supporting electrolyte until the calculated final charges were reached. All potentials were measured vs. Ag/AgCl. During BE, potentials were controlled with a BASi 50W potentiometer and UV-visible spectra were collected on a Shimadzu UV-3600 UV-visible-NIR spectrophotometer at room temperature.

4.2.3 Computational Studies

Electronic structure calculations were carried out by Dr. Shivnath Mazumder, using the BPW91 density functional[124,192] as implemented in a development version of Gaussian.[123] The SDD basis set and effective core potential[128] were used for Co atom and the 6-31G(d,p) basis set[126,127] was used for the other atoms. To streamline calculations, a slightly modified model was used where the *tert*-butyl substituents of $[Co^{II}_2(L^1)(bpy)_2]ClO_4$ were replaced by methyl groups. Geometry optimization was performed in the gas phase and all of the optimized structures were confirmed as minima by harmonic vibrational frequency calculations. The energies of the optimized structures were reevaluated by additional single point calculations on each optimized geometry in acetonitrile using the implicit SMD solvation model.[193] The converged wave functions in solvent were tested for SCF stability. The free energy in solution phase G(sol) was calculated

as follows: G(sol) = E_{SCF}(sol) + [zero-point energy(ZPE) + thermal correction – TS] (gas). E_{SCF} was calculated in the solvent while ZPE, thermal correction, and entropic contributions were calculated in the gas phase. The standard states of 1 M concentration were considered for all the reactants and products for calculating the free energies of reactions (ΔG(sol)). The spin density plots (isovalue = 0.004 au) and corresponding orbitals[194] (isovalue = 0.05 au) of the calculated structures were visualized using GaussView.[195] The literature value[196] of -264.6 kcal/mol was used for the free energy of proton in acetonitrile. The calculation of the reduction potentials (*E*, V in volts) of the complexes included ZPE, thermal correction, and entropic contribution. The standard thermodynamic equation ΔG(sol) = -nFE was used. The calculated potentials were referenced to a value of $E_{1/2}$ = 4.38 V for the ferrocene/ferrocenium couple calculated under our level of theory.

4.2.4 Catalytic Studies

Electrocatalytic experiments to determine the amount of H produced by the catalyst, turnover numbers, and Faradaic efficiencies was performed as previously described[73] in an H-type cell (Hg-pool; Ag/AgCl | Pt-coil). The main chamber was filled with $[Co^{II}_2(L^1)(bpy)_2]ClO_4$ (0.005 g; $4x10^{-6}$ moles), the $TBAPF_6$ electrolyte (1.56 g) and acetic acid (0.024 g; $4x10^{-4}$ moles; 100 equiv) were dissolved in 20 mL CH_3CN. The small chamber housing the auxiliary electrode was filled with 0.390 g $TBAPF_6$ in 5 mL ACN. In a typical run, the cell is purged for 20 minutes followed by sampling the head space gas with a Gow-Mac 400 gas chromatograph equipped with a thermal conductivity detector, and a 8 ft. x 1⁄8 in., 5 Å molecular sieve column operating at a temperature of 60 ºC. The amount of H_2 produced is determined *via* GC with a calibration curve obtained with known volumes of 99.999+ %H_2 gas. (**Figure 4.2 and Table 4.1**). A catalyst-free solution is electrolyzed for 3 h and analyzed by GC as a blank. The cell is then purged again and

the catalyst is added. Electrolysis ensues for 3 h and the headspace is analyzed by GC to determine the H_2 gas produced.

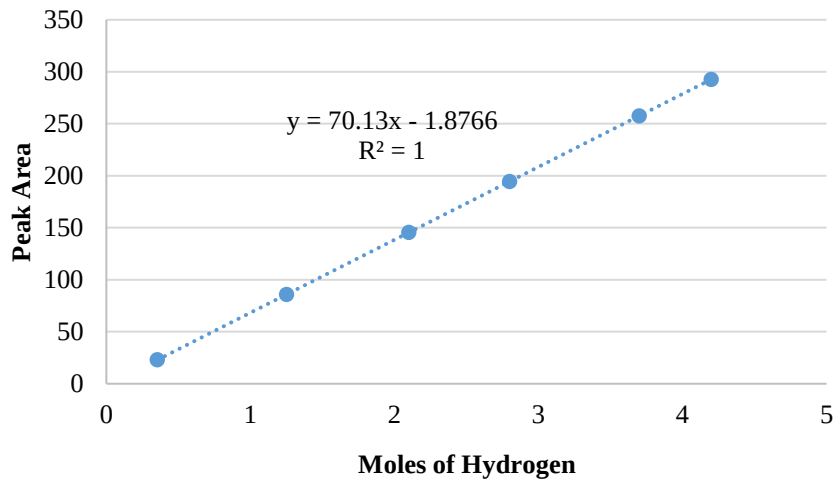

Figure 4.2. Calibration curve used for the determination of the amount of hydrogen.

The turnover number is then calculated after background subtraction as the ratio between moles of dihydrogen produced per mole of catalyst. Faradaic efficiency is calculated from the GC measurements.

Table 4.1. Sample Calculations:

Blank Peak Area	Catalyst Peak Area	Volume of the Cell (mL)	Volume of Solution (mL)	Volume injected into GC (µL)	Number of moles of catalyst (µmol)
8.0	34.7	46.2	27.4	100	4

$V_{headspace}$ = 46.2 - 27.4 = 18.8 mL

Number of moles of hydrogen in 100 µL of headspace for both blank ($n_{blank\ (100)}$) and catalyst ($n_{catalyst\ (100)}$):

$n_{blank\ (100)}$ (8.00 + 1.88)/70.13 = 0.14 µmol

$n_{catalyst\ (100)}$ (34.68 + 1.88)/ 70.13 = 0.52 µmol

The net amount of hydrogen produced by the catalyst in 100 µL of headspace $n_{net\ (100)}$, is equal to the difference between $n_{blank\ (100)}$ and $n_{catalyst\ (100)}$

$n_{net\ (100)} = n_{catalyst\ (100)} - n_{blank\ (100)} = 0.52 - 0.14 = 0.38$ µmol

The total net amount of hydrogen that was produced $n_{net\ (total)}$ is obtained by adjusting the injection volume to that of the total headspace volume

$$n_{net\ (total)} = \frac{n_{net\ (100)} \times V_{headspace}}{V_{injected}} = 71.56\ \mu mol$$

$$TON = \frac{n_{net\ (total)}}{n_{catalyst}} = 71.56/4 = 17.89$$

4.3 Results and Discussion

4.3.1 Synthesis and Characterization

The bimetallic **$[Co^{II}_2(L^{1'})(bpy)_2]ClO_4$** was prepared by treatment of 1 equiv of H_3L^1 with 2 equiv of $Co(ClO_4)_2{\cdot}6H_2O$ and pyridine in presence of Et_3N as the base. A detailed description of the synthesis of **$[Co^{II}_2(L^{1'})(bpy)_2]ClO_4$**, along with its thorough characterization and molecular structure, was recently reported by the Fiedler group.[191] **Figure 4.3** shows that the $(L^1)^{3-}$ ligand loses two phenolic and one amidic protons to support a dicobalt(II) core in which the metal centers lie at a short distance of 2.70 Å from each other, and bridged by the N3 atom of a diaryl amido unit with a Co1-N3-Co2 angle of 86.9°. Each of the five-coordinate Co^{II} centers is bonded to the N atom of an azomethine (N1 or N2) and the O atom of a phenolate (O1 or O2), with a bidentate bipyridine (bpy) completing the coordination sphere. This mono-cationic unit is neutralized by a single ClO_4^- counterion.

The low-spin (S = 1/2) nature of both Co^{II} centers is indicated by relatively short metal–ligand bond distances, ranging between 1.89 and 2.06 Å (the average Co–N/O bond length is 1.95 Å). The Co(II) centers are antiferromagnetically coupled, which was discovered by the sharpness of the ^1H NMR features.[191] The UV-visible spectrum of **$[Co^{II}_2(L^{1'})(bpy)_2]ClO_4$** was recorded in acetonitrile (**Figure 4.4**). The catalyst presents a yellowish brown color due to the presence of

tense intraligand charge transfers. The initial spectrum shows bands below 320 nm tentatively attributed to σ* ← σ and π* ← σ ILCT processes, while the shoulders around 343 and 452 nm are attributed to low-intensity π–π* transitions typical of distorted environments.[191]

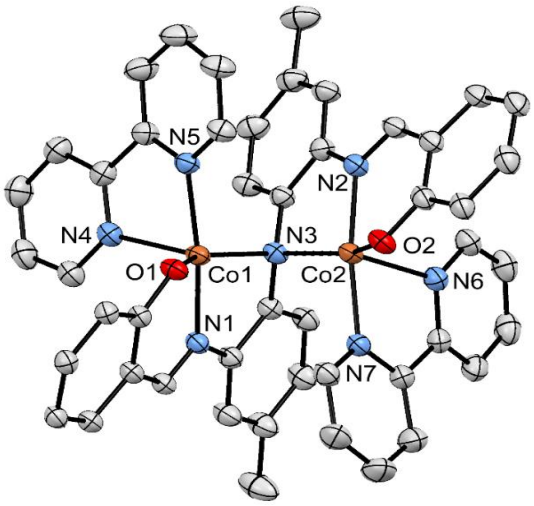

Figure 4.3. ORTEP of the complex **[Co^{II}$_2$(L$^{1'}$)(bpy)$_2$]ClO$_4$** with ellipsoids at 30% probability. Hydrogen atoms and *tert*-butyl groups removed for clarity. Used with permission from reference 28.

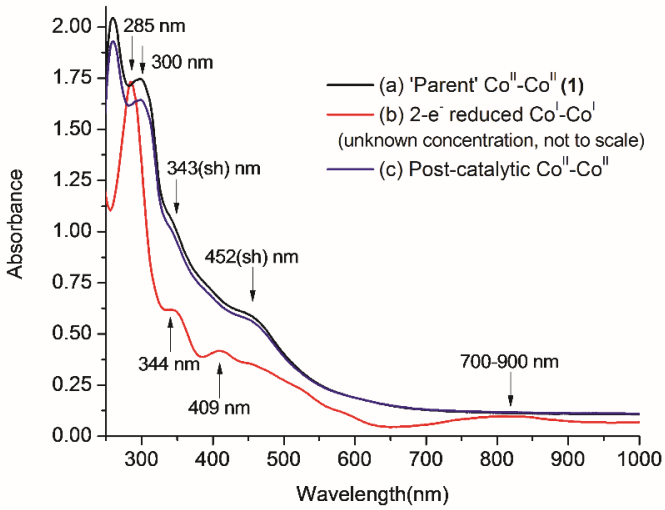

Figure 4.4. UV-visible spectra of **[Co^{II}$_2$(L$^{1'}$)(bpy)$_2$]ClO$_4$**: (a) Pre-catalytic [Co^{II}Co^{II}] at 1x10^{-3} M, (b) chemically reduced [Co^{I}Co^{I}], unknown concentration, (c) Post-catalysis.

4.3.2 Electrocatalytic H^+ Reduction

To study the possibility of **$[Co^{II}_2(L^{1'})(bpy)_2]ClO_4$** as a catalyst for the reduction of H^+ to H_2, we investigated the electrochemical response of **$[Co^{II}_2(L^{1'})(bpy)_2]ClO_4$** in anhydrous acetonitrile (CH_3CN) using a glassy carbon working electrode with increasing concentrations of acetic acid (HOAc, pK_a = 22.3 in CH_3CN) as the proton source.[24]

The standard reduction potential of H^+ in CH_3CN, $E°^{(H+/H2)}$ was determined via open circuit potential measurements as −0.028 ± 0.008 $V_{Fc+/Fc}$. [49] Under standard conditions, $E°^{(AH/A-;H2)}$ would be −1.35 $V_{Fc+/Fc}$ for HOAc; however, high concentrations can afford homoconjugation, leading to an incremental acidity and increasing the standard reduction potential.[197] As shown in **Figure 4.5**, a cyclic voltammogram of **$[Co^{II}_2(L^{1'})(bpy)_2]ClO_4$** shows three cathodic events.

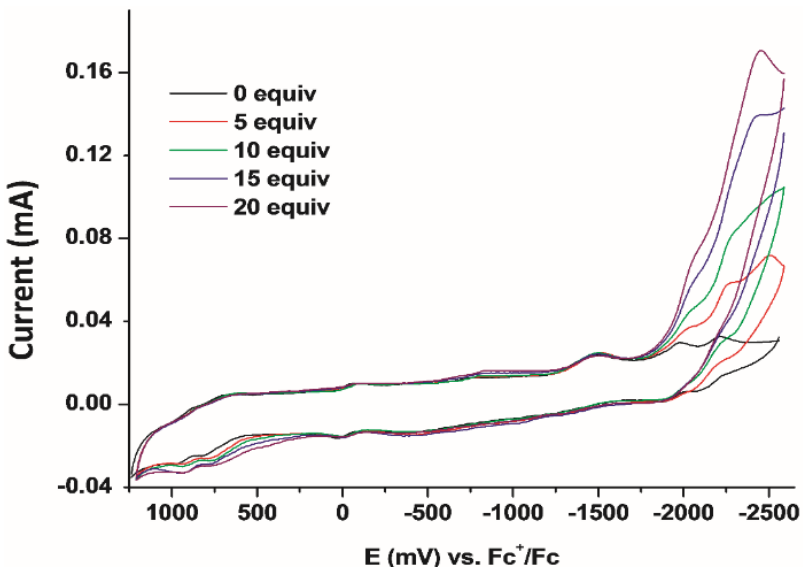

Figure 4.5. Cyclic voltammograms (CVs) of **$[Co^{II}_2(L^{1'})(bpy)_2]ClO_4$** (2.0 mM) measured vs. Ag/AgCl and plotted vs. Fc^+/Fc in the presence of increasing concentrations of HOAc. The CH_3CN solvent contained 0.1 M NBu_4PF_6 as the supporting electrolyte and a glassy carbon working electrode was employed.

Upon addition of HOAc (2.0 mM), an irreversible wave near –1.51 $V_{Fc+/Fc}$ (–0.99 $V_{Ag/AgCl}$) was observed and has been assigned to the reduction of the dicobalt(II) core [$Co^{II}Co^{II}$] to the formal

[$Co^{I}Co^{II}$] state. This [$Co^{I}Co^{II}$] state does not seem able to afford catalysis, which is observed at a potential of −1.86 $V_{Fc+/Fc}$ (–1.34 $V_{Ag/AgCl}$), thus requiring a [$Co^{I}Co^{I}$] state.

Upon increase of the HOAc concentration, this electrocatalytic current enhancement becomes evident and reaches its maximum at −2.08 $V_{Fc+/Fc}$ (–1.56 $V_{Ag/AgCl}$) with the addition of 20 equiv of acid. Control experiments where HOAc is added to CH_3CN in absence of **[$Co^{II}_2(L^{1'})(bpy)_2$]ClO_4** show negligible increase in current, even when more negative potentials are applied. These results validate the catalytic role of **[$Co^{II}_2(L^{1'})(bpy)_2$]ClO_4** and support our hypothesis of homogeneous H^+ reduction using **[$Co^{II}_2(L^{1'})(bpy)_2$]ClO_4** as an electrocatalyst. The experimentally determined redox events were further studied using DFT calculations in model compounds. **[$Co^{II}_2(L^{1'})(bpy)_2$]ClO_4** was modeled with two low-spin Co^{II} centers in agreement with NMR data.[191] Each center contained one unpaired electron and the [$Co^{II}Co^{II}$] core was antiferromagnetically coupled to provide a singlet (S = 0) ground state.[191] For simplicity, the *t*-Bu groups on the phenolates were replaced by methyl groups.[122] The results for relevant species are shown in **Figure 4.6** as calculated spin density plots with Mulliken spin density values.

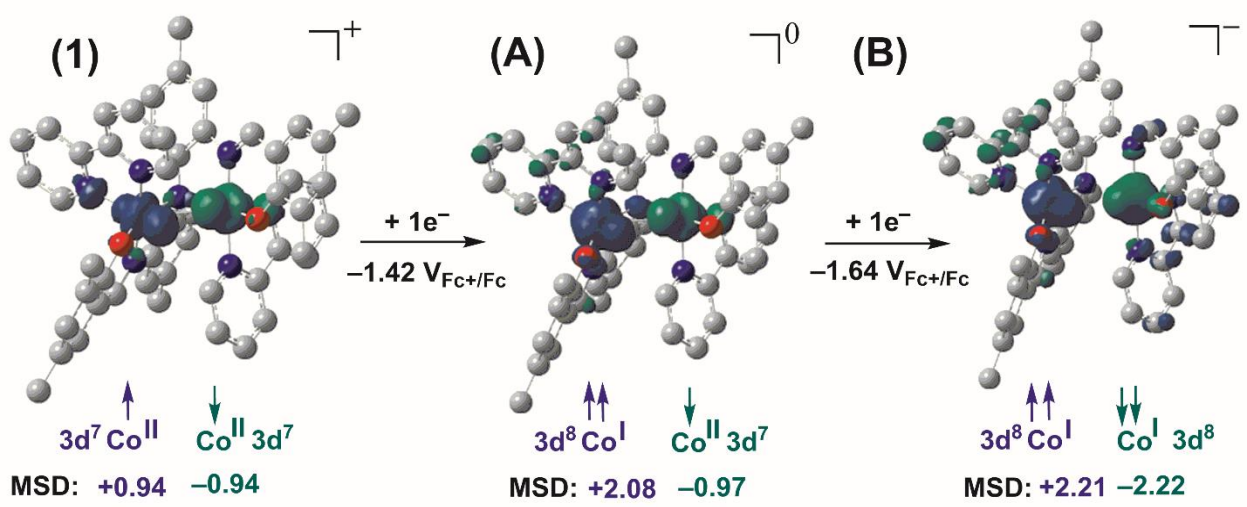

Figure 4.6. DFT-calculated spin density plots (isodensity 0.004 au), reduction potentials, and the Mulliken spin density (MSD) values showing reduction of [$Co^{II}Co^{II}$] **[$Co^{II}_2(L^{1'})(bpy)_2$]ClO_4** to [$Co^{I}Co^{II}$] (**A**) to [$Co^{I}Co^{I}$] (**B**). H atoms are omitted for clarity.

The initial singlet [$Co^{II}Co^{II}$] $^{LS}3d^7$–$^{LS}3d^7$ core in **[$Co^{II}_2(L^{1'})(bpy)_2]ClO_4$** is reduced to the doublet [$Co^{I}Co^{II}$] $^{HS}3d^8$–$^{LS}3d^7$ core in **A**. Species **A**, therefore, contains a high-spin $3d^8$ Co^I with two unpaired electrons and can be further reduced to the singlet [$Co^{I}Co^{I}$] **B** with a $^{HS}3d^8$–$^{HS}3d^8$ core at a calculated potential of –1.64 $V_{Fc+/Fc}$. The presence of the monovalent species **B** was confirmed experimentally via UV-visible spectroscopy by reducing chemically a sample of [$Co^{II}Co^{II}$] **(1)** with 2 equivalents of KC_8 under inert atmosphere. The resulting spectrum is shown in **Figure 4.4b** and displays bands typical of previously reported Co^I species; based on similarities to the spectrum of the Co^{II}-containing species, the band at 285 nm is attributed to ILCT processes. Bands at 344, 409, and 700-900 nm are comparable to those observed for a Co^I tetraaza-macrocyclic catalyst[183] and associated with d-d bands. In an octahedral Co^I bis(pyridine-2,6-diimine) complex these broad bands were attributed to d-π* CT processes,[198] and several shoulders in the 500-600 nm range were diagnostic of the presence of radical species. Similar shoulders were observed for **B** between 450-650 nm, thus suggesting that ligand reduction may have taken place to some extent.

To ascertain experimentally the overpotential at which **[$Co^{II}_2(L^{1'})(bpy)_2]ClO_4$** shows electrocatalytic activity, a series of 2-minute bulk electrolyses (BE) were run at applied potentials ranging between –0.7 and –1.6 $V_{Ag/AgCl}$ **(Figure 4.7).** The experiment was performed in an airtight H-type cell using a Hg-pool working electrode, Ag/AgCl as reference and a Pt-coil auxiliary electrode placed in an adjacent compartment separated by a frit. The main chamber was filled with **[$Co^{II}_2(L^{1'})(bpy)_2]ClO_4$**, $TBAPF_6$ electrolyte solution and HOAc in 20 mL CH_3CN. The auxiliary chamber was filled with the electrolyte solution only.

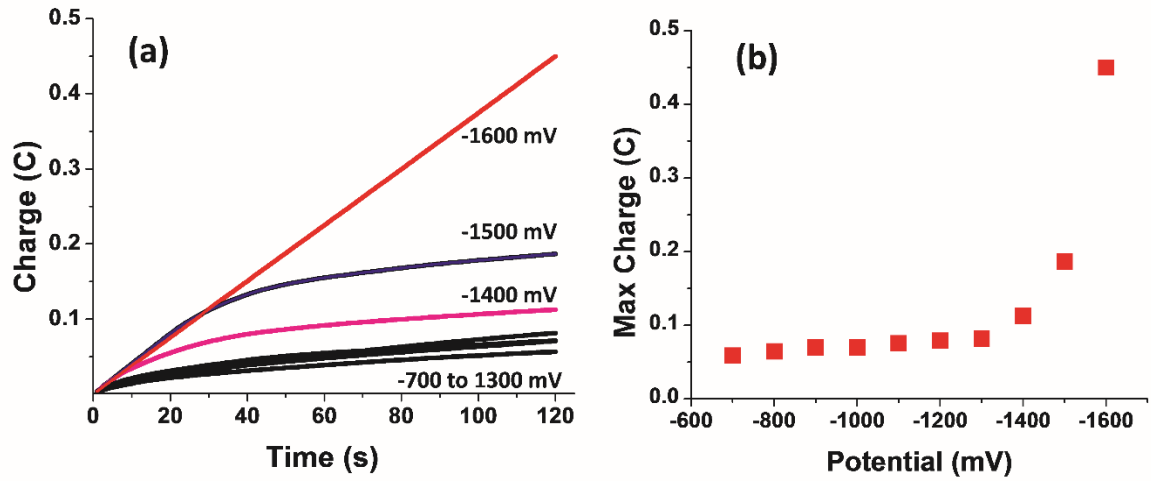

Figure 4.7. (a) Charge consumed at variable potentials (vs. Ag/AgCl) with 2 min. BE; (b) Maximum charge consumed vs. potential (vs. Ag/AgCl).

Figure 4.7a illustrates the total charge consumed by **[$Co^{II}_2(L^{1'})(bpy)_2]ClO_4$** in the presence of acid during BE; charge consumption remained constant up to –1.4 $V_{Ag/AgCl}$, after which it increased significantly until –1.6 $V_{Ag/AgCl}$, concomitant with evolution of H_2 gas, as confirmed by gas chromatography (GC). **Figure 4.7b** shows a plot of charge consumed vs. applied potential. The graph indicates that the onset potential for catalysis is –1.4 $V_{Ag/AgCl}$. This overpotential is comparable to that of the mononuclear cobalt polypyridyl catalyst recently published by the Verani group[73] and investigated under similar conditions that enable comparison. The plot of current vs. concentration of HOAc at a potential of –2.08 $V_{Fc+/Fc}$ is provided in **Figure 4.8**. The measured current increases linearly with concentration of HOAc, whereas negligible current increase was observed in absence of **[$Co^{II}_2(L^{1'})(bpy)_2]ClO_4$**. An apparent overpotential of 0.63 V has been calculated assuming homoconjugation (E_{Fc/Fc^+} AcOH in CH_3CN = -1.23 V), and a rate of H_2 generation[197] (k_{obs}) of 6.33 s^{-1}results.

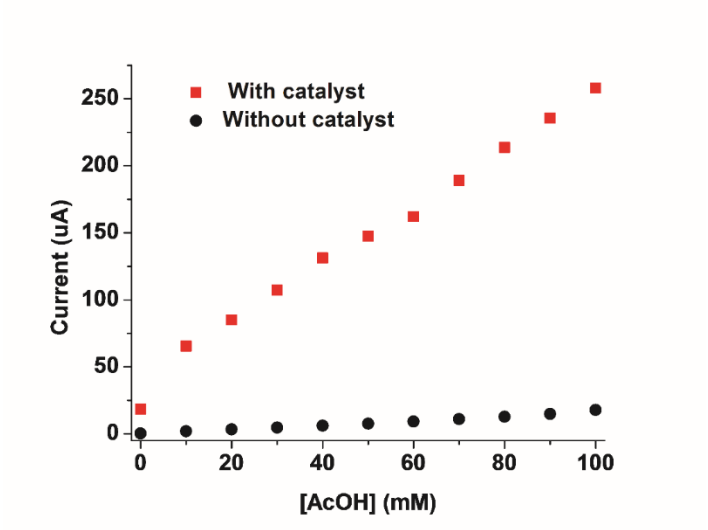

Figure 4.8. *Squares*: CV current at –2.08 $V_{Fc+/Fc}$ as a function of HOAc concentration for solutions of **[$Co^{II}_2(L^{1'})(bpy)_2]ClO_4$** (2.0 mM) in CH_3CN. *Circles*: corresponding data measured under identical conditions but in the absence of **[$Co^{II}_2(L^{1'})(bpy)_2]ClO_4$**.

A charge consumption plot over 3 h is shown in **Figure 4.9.** The slight curvature observed within the first 10 minutes is typical for proton reduction and tentatively associated with solvent dissociation.[190] The amount of H_2 produced over the same period of time was determined by BE as already discussed, using 100 equiv of acid at an applied potential of –1.6 $V_{Ag/AgCl}$.

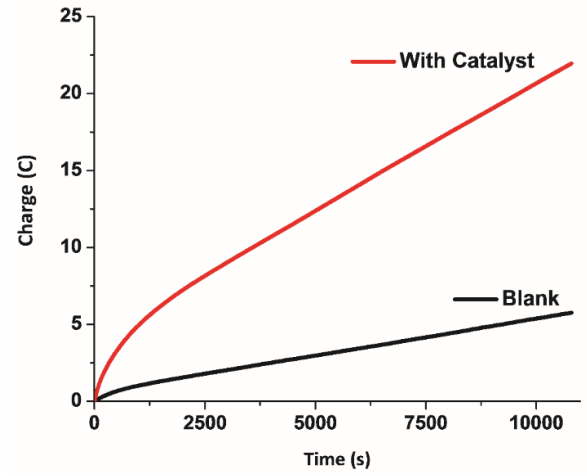

Figure 4.9. Charge consumption versus time during BE by **[$Co^{II}_2(L^{1'})(bpy)_2]ClO_4$** with ($TBAPF_6$: 1.560 g, HOAc: 0.024 g [0.400 mmol], **1:** 0.0047 g [0.0040 mmol], 20 mL CH_3CN) at –1.6 $V_{Ag/AgCl}$.

A sample of 100 μL of the headspace gas was injected into a GC to quantify the amount of H_2 produced and repeated in triplicate. A calibration curve (Figure 4.2) was used to standardize the calculations.

An average amount of 0.072 mmol of H_2 was calculated after background correction which is associated with a turnover number (TON) of 18, equivalent to ca. 40% conversion rate. Faradaic efficiency (FE) was calculated at 94% from the maximum charge consumed. BE experiments were performed under similar conditions as described above using an incremental concentration of acid leading to an increase in the calculated TONs. Accordingly, the use of 200 equiv of acid led to TON of 75, (Figure 4.10) whereas 300 equiv led to TON of 97. In both cases, the Faradaic efficiency remained consistent at > 90%.

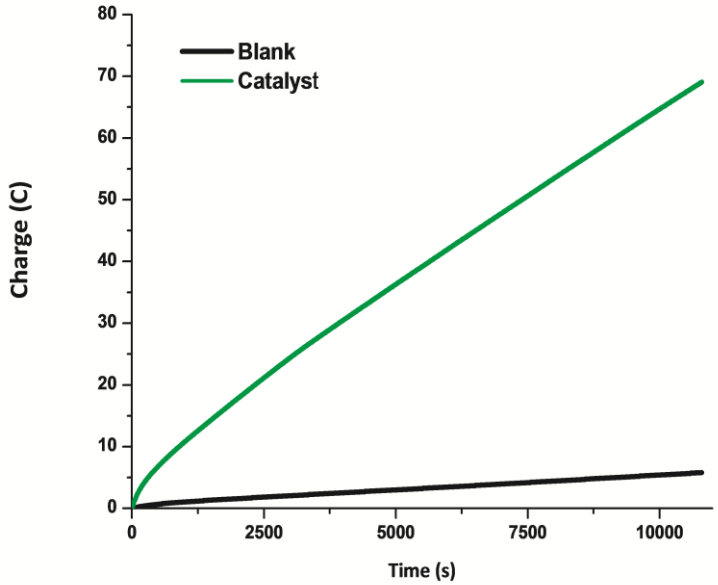

Figure 4.10. Charge consumption versus time by **[$Co^{II}_2(L^{1'})(bpy)_2]ClO_4$** during BE with 200 equivalents of HOAc.

As expected, high yields were observed when the concentration of acid was not a limiting factor, and the use of 400 equiv of acid led to the highest TON of 120 with an associated drop in %FE to *ca.* 85%. The charge vs. time plots for the 300 and 400 equiv experiments are shown in **Figures 4.11 and 4.12**. The initial lagging observed in **Figure 4.9** is almost a linear charge consumption behavior in the 200 and 300 equiv graphs. The plot with 400 equiv shows slightly increased activity after the first 10 minutes followed by a decrease after *ca.* 2.5 h, likely related to slow degradation of the catalyst under such acidic conditions.

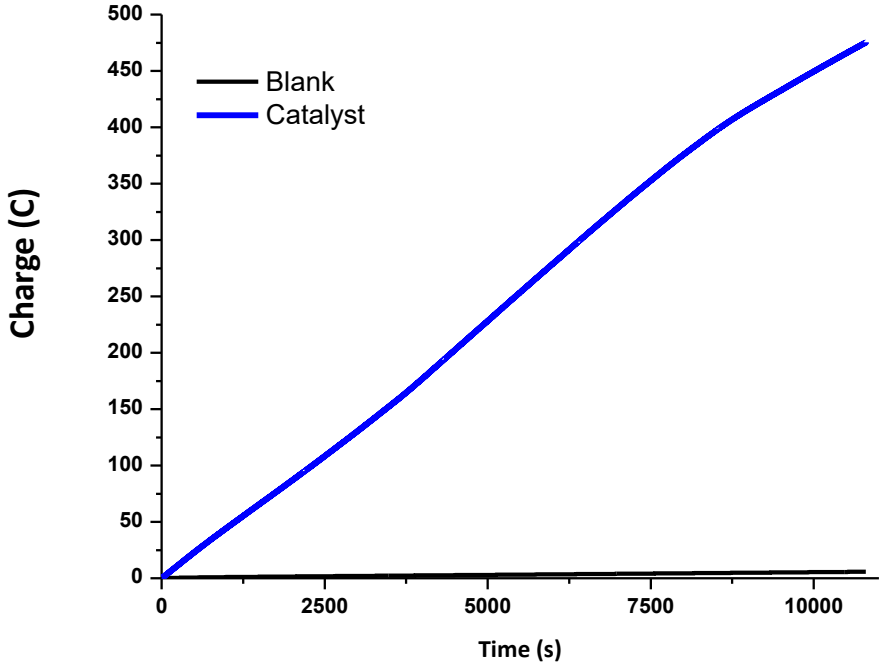

Figure 4.11. Charge consumption versus time by [CoII2(L1')(bpy)2]ClO4 with 300 equivalents of HOAc.

Considering the near-linearity of the graph in **Figure 4.10** the system seems optimized in the presence of 200 equiv of acid. Comparison of activity with other reported bimetallic species [48,77,75,161] is hampered by the lack of information on directly measured TONs by those reports. However, simple assessment of this system (without considering variables such as proton source

and applied potential) reveal that the TON, rate of conversion, and Faradaic efficiency values compare favorably with mono cobalt catalysts. [115,73]

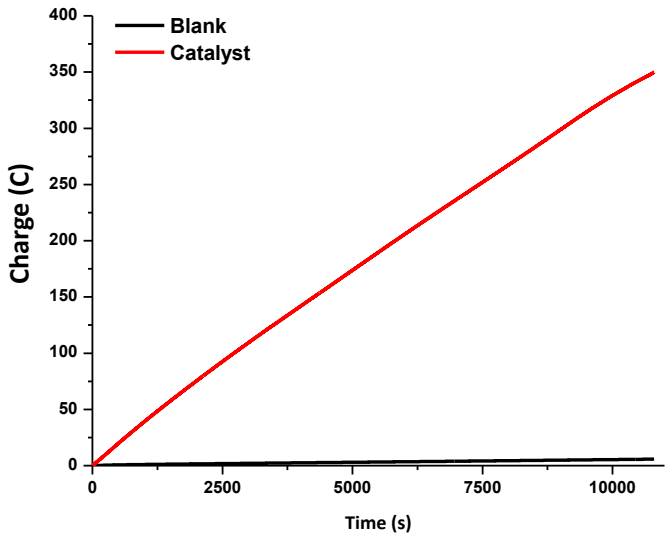

Figure 4.12. Charge consumption versus time by **[$Co^{II}_2(L^{1'})(bpy)_2]ClO_4$** with 400 equivalents of HOAc.

4.3.3 Mechanism of H^+ Reduction

A catalytic mechanism of H^+ reduction (**Figure 4.14)** was proposed based on the results from the redox studies, electrocatalytic studies and the electronic structure calculations carried out using the BPW91 density functional.[124,192] Orbital plots (isovalue = 0.05 au) of the singly occupied molecular orbitals (SOMOs) of complexes **1**, **A**, **B**, and **C** are shown in **Figure 4.13**. Each $^{LS}3d^7$ ion in **[$Co^{II}_2(L^{1'})(bpy)_2]ClO_4$** displays one unpaired electron in the d_{z2}-based singly occupied MO (SOMO) yielding an antiferromagnetically coupled singlet (S = 0). The reduction of **[$Co^{II}_2(L^{1'})(bpy)_2]ClO_4$** generates [$Co^{I}Co^{II}$] (**A**) with a Co^{I} ($^{HS}3d^8$) and a Co^{II} ($^{LS}3d^7$). The Co^{I}-based d_{x2-y2} orbital is now occupied by an electron leading to an overall doublet (S = 1/2) ground state. On further reduction the second Co^{II} center in **A** accepts an electron to its empty d_{x2-y2} orbital and is transformed into a second $^{HS}3d^8$ ion in [$Co^{I}Co^{I}$] (**B**).

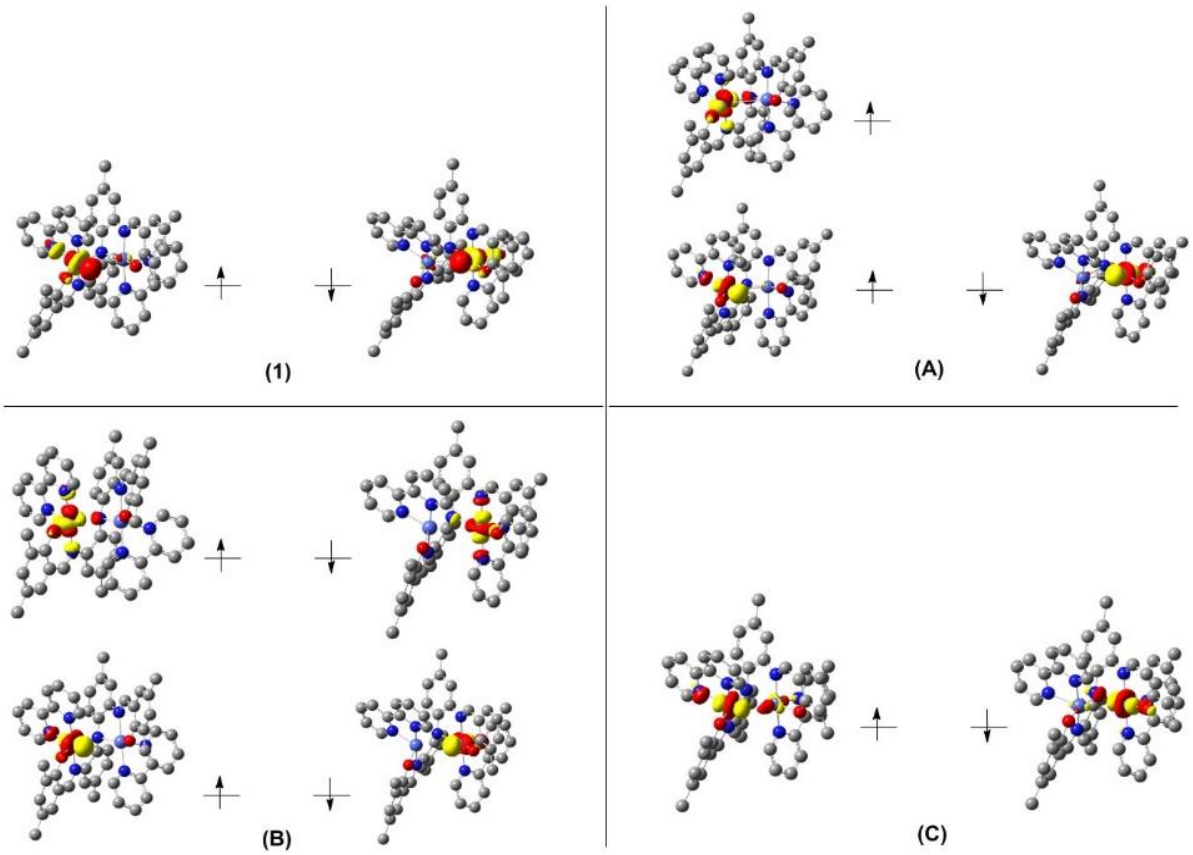

Figure 4.13. The corresponding orbital plots (isovalue= 0.05 au) of the SOMOs (singly occupied molecular orbitals) of **[$Co^{II}_2(L^{1'})(bpy)_2$]ClO_4**, and species **A**, **B**, and **C.**

This is the proposed catalytically active species. The two adjacent d_{x2-y2} SOMOs in **B** do not overlap spatially and therefore are not coupled with each other. As a consequence, each of these electrons can be transferred onto an incoming H^+ to reduce it to a hydride (H^-). As a result, protonation of **B** is favorable by 28 kcal/mol (ΔG). Each of the two $^{HS}Co^{I}$ centers transfers one electron from its d_{x2-y2} SOMO and the resulting complex is described as the species [$Co^{II}Co^{II}(H^-)$] (**C**). The hydride moiety is bound more tightly to one of the Co^{II} ions, rather than symmetrically bridged between the two centers. The shortest Co^{II}–H^- distance is calculated at 1.54 Å, while the other distance has a computed value of 1.85 Å. It is noteworthy that the cooperativity between both centers in species **B** leads to **C**, [$Co^{II}Co^{II}(H^-)$], thereby precluding formation of a [$Co^{I}Co^{III}(H^-)$] intermediate.

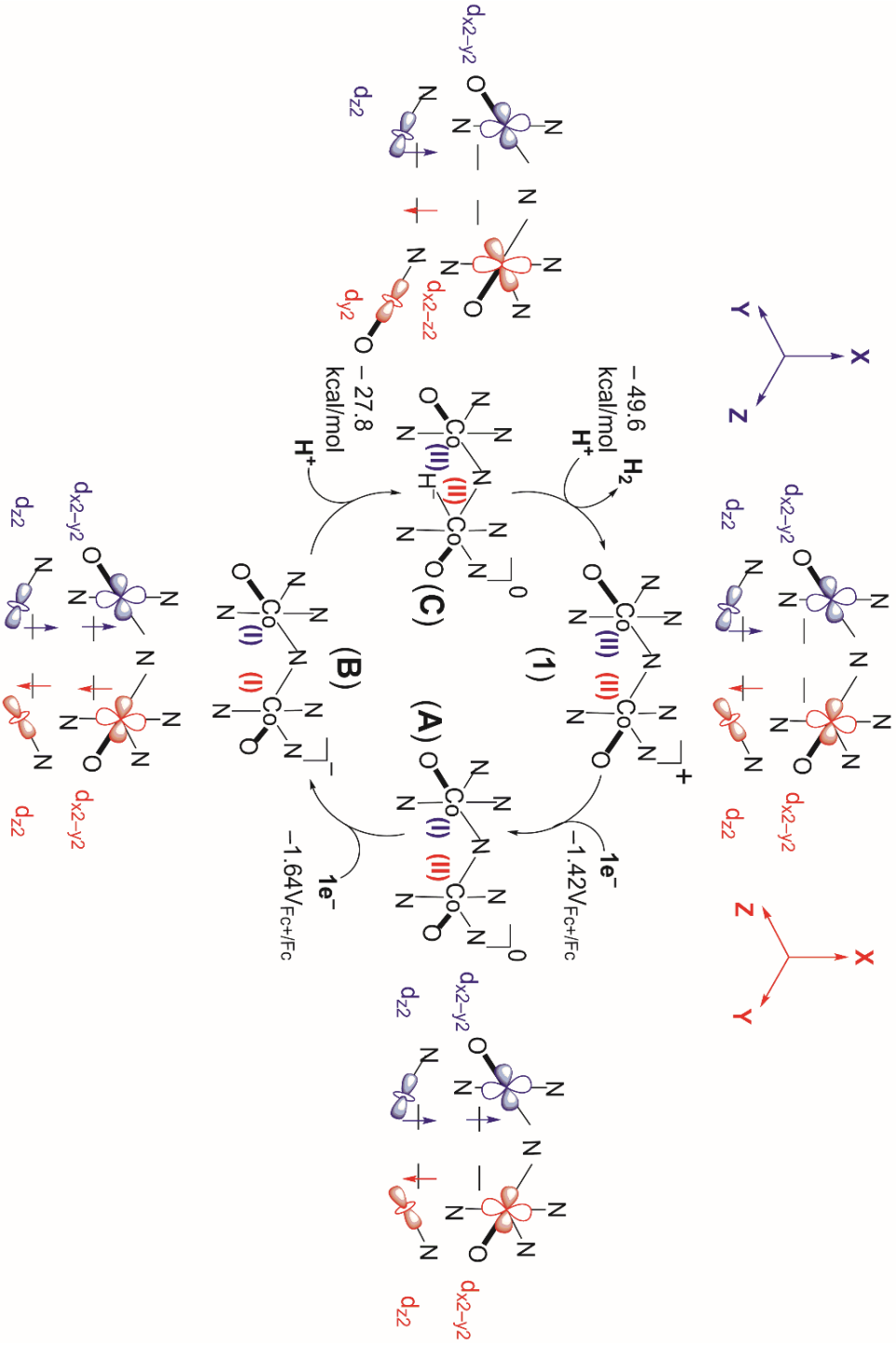

Figure 4.14. Catalytic mechanism of H_2 generation by **$[Co^{II}_2(L^{1'})(bpy)_2]ClO_4$** in CH_3CN. Protonation of the [CoICoI] intermediate B causes each CoI center to donate 1e– to H+, resulting in the formation of the [CoIICoII]-hydride complex C. Free energies (kcal/mol)199 and potentials (volt) calculated at the BPW91/SDD/6-31G(d,p) level of theory.[200]

The latter species, containing the trivalent $3d^6$ Co^{III} ion, can only be invoked if there is no cooperativity and the two metal centers function independently. Succinctly, protonation of one of the Co^{I} centers in **B** prompts a $2e^-$ transfer where each of the two Co^{I} centers donates an electron to the H^+. As a result, the more reactive $Co^{II}(H^-)$ unit is achieved without prior or concurrent formation of the $Co^{III}(H^-)$ moiety.

4.3.4 Fate of $[Co^{II}_2(L^{1'})(bpy)_2]ClO_4$ after Catalysis

The post-catalysis spectrum shown in **Figure 4.3c** displays the similar features observed in the $[Co^{II}Co^{II}]$ state, (**Figure 4.3a**) thus attesting to the catalytic nature of $\mathbf{[Co^{II}_2(L^{1'})(bpy)_2]ClO_4}$ along with a decrease of *ca.* 10% in the UV bands and of 2% in the 450 nm band. This small discrepancy is explained by slow percolation of solution between the chambers and through the frit of the electrochemical cell. Alternatively, a fraction of the catalyst may be deactivated and evaluation of a grafoil sheet electrode was performed by SEM and EDS to assess the possibility of nanoparticle formation **(Figure 4.15)**.

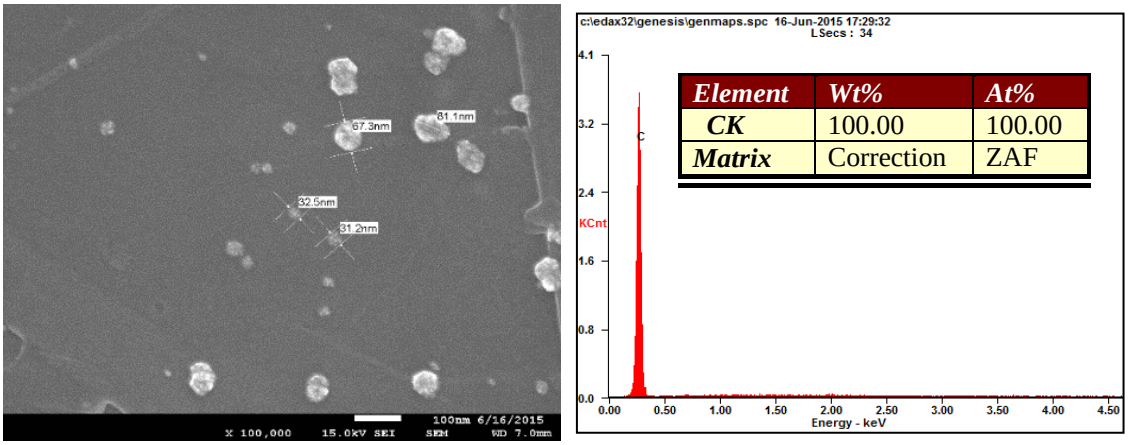

Figure 4.15. Micrograph of post-catalytic grafoil sheet electrode by SEM and EDS of $\mathbf{[Co^{II}_2(L^{1'})(bpy)_2]ClO_4}$.

Notwithstanding evidence for formation of organic nanoparticles, no Co was detected on the surface of the electrode. Thus, UV-visible, SEM, and EDX analyses support the presence of a catalyst that is molecular in nature.

4.4 Conclusions

In conclusion, we have investigated both experimentally and theoretically the bimetallic complex **[Co^{II}_2($L^{1'}$)(bpy)$_2$]ClO_4**. This species supports the catalytic H^+ reduction to H_2 in CH_3CN when in the presence of a weak acid such as HOAc at an overpotential of 0.63 V. This catalytic activity relies on a $2e^-$ reduction of the parent species [$Co^{II}Co^{II}$] to form a [$Co^{I}Co^{I}$] complex. Each of these Co^{I} centers contributes with the donation of one electron to a single incoming H^+, thus forming a reactive Co(II)-hydride. The novel bimetallic cooperativity exhibited by this system arises from the close proximity of the cobalt centers and an appropriate orbital topology that avoids the formation of the Co^{III}–H^- moiety required for proton reduction in monometallic catalysts. The second Co^{I} center plays a pivotal role in the catalytic reduction of H^+, acting as an electron reservoir to donate the second electron necessary for formation of the Co^{II}–H^- unit that favorably accepts another H^+ and releases H_2. Post-catalytic SEM and EDX analyses support the molecular nature of the catalyst. Therefore, the observations resulting from this work lead to considerations on how to optimize topology and orbital overlap to promote the use of a neighboring metal center as electron reservoir. These factors will become pivotal in the development of new and improved bimetallic catalysts.

CHAPTER 5:

EFFECT OF VALENCE TAUTOMERISM ON COORDINATION PREFERENCES IN MANGANESE COMPLEXES WITH [N_2O_3] LIGANDS FOR WATER OXIDATION

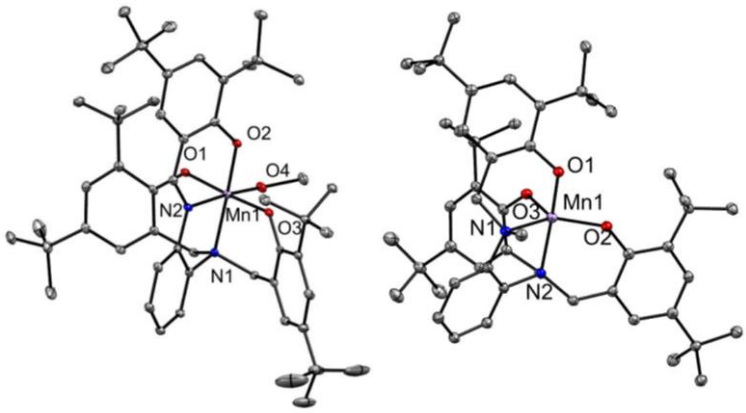

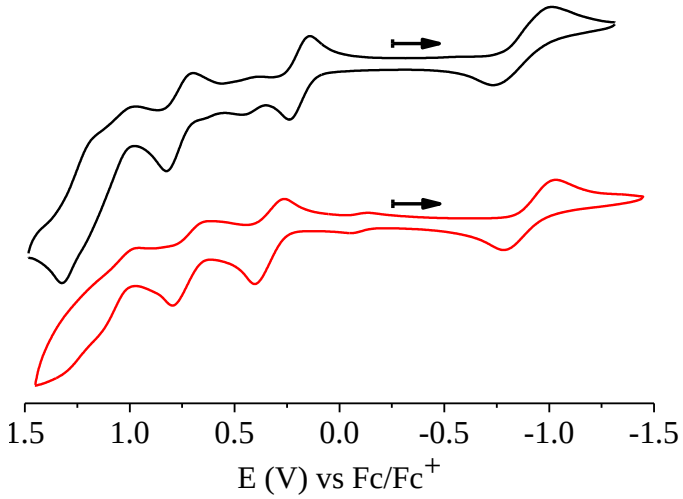

CHAPTER 5: EFFECT OF VALENCE TAUTOMERISM ON COORDINATION PREFERENCES IN MANGANESE COMPLEXES WITH [N_2O_3] LIGANDS FOR WATER OXIDATION

Portions of the text in this chapter were reprinted or adapted from a manuscript under preparation. Dr. Rajendra Shakya is acknowledged for his intellectual contributions.

5.1. Introduction

The manganese ion, with its broad range of oxidation states and considerable Earth-abundance, is an appropriate choice for the study of the electron transfer processes involved in catalytic water oxidation. It has been proposed that incorporation of phenolate moieties into manganese species could lead to catalytic activity,[91, 201-202]As described in Chapter 1, Akermark[93, 95, 203] and coworkers have used the phenolate ligand moiety with bimetallic [Mn_2] and heterometallic [RuMn] to study electron transfer rates. A similar approach based on modifications of the triaza-cyclononane ligand was undertaken by Wieghardt[96] and collaborators.

Fujii[79, 98] *et al.* have shown remarkable examples of Mn(IV) stabilization using [N_2O_2] salen platforms. These systems build on an equilibrium between [Mn^{III}/phenoxyl] and [Mn^{IV}/phenolate] species. It was initially suggested by Åkermark[99] and coworkers that formation of Mn(IV) leads to a Mn^{III}/phenoxyl species where radical decay is prevented by coordination to the metal center, but Fujii[204] proposes that the [Mn^{III}/phenoxyl] state is favored upon coordination with water and the metal-centered high oxidation is only achieved by water deprotonation or formation of a Mn(IV)=O moiety. A study from Anxalabehere-Mallart *et al.*[205] proposed that an alternative and milder mechanism for water oxidation might involve the formation of Mn(III)-oxyl species in pentadentate ligands. It has been reported that valence tautomeric transitions can occur similarly via a stimulated intramolecular electron transfer, between redox-active ligands such as

phenolates and a redox-active metal center, yielding two different valence tautomers or redox isomers.[206]

Continuing in the Verani group's success in designing mononucleated and pentadentate [N_2O_3] ligands containing three phenol moieties attached through rigid spacers that coordinate to trivalent 3*d* transition metals such as iron(III) and gallium(III), and form multiple phenoxyl radicals through sequential oxidations,[115, 207-211] we explore in this chapter the manganese chemistry of these ligands to improve our understanding of (i) how metal identity influences the physical and spectroscopic properties of complexes with these [N_2O_3] ligands, (ii) how valence tautomerism affects the coordination preferences in the formation of Mn(IV) species, and (iii) to determine if this pentadentate ligand framework is robust enough to support catalytic water oxidation at the vacant metal site.[209, 211]

To achieve these goals, we synthesized, and characterized two new trivalent manganese complexes, the hexacoordinate [$Mn^{III}(L^1)(CH_3OH)$] (**1**) and the pentacoordinate [$Mn^{III}(L^2)$] (**2**) **(Scheme 5.1)**, and evaluated their catalytic water oxidation properties.

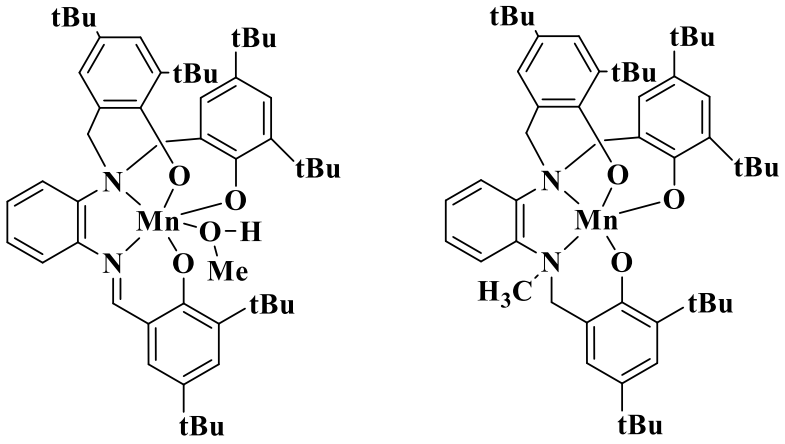

Scheme 5.1. Mononuclear manganese complexes hexacoordinate [$Mn^{III}(L^1)(CH_3OH)$] 1 (left) and the pentacoordinate [$Mn^{III}(L^2)$] 2 (right).

Spectroelectrochemical measurements were combined with DFT calculations to provide detailed insight into the spectroscopy of these complexes as well as the balance between metal- and ligand-based oxidation.

5.2 Experimental Section

5.2.1 Materials and Methods

Spectroelectrochemical measurements were done in an optically transparent thin-layer cell (*ca.* 0.1 mm) constructed according to a procedure described as follows: a u-shaped flat platinum wire was sandwiched between two glass slides. The inner parts were coated with indium-tin oxide (ITO) (8-12 Ω/sq.). The Pt-wire acted as the working electrode and extended outside of the slides for electrical contact. The solutions were prepared and degassed under inert atmosphere (argon) and introduced into the cell through a capillary. The working electrode was located within 4-6 mm of the cell bottom to minimize ohmic potential (iR) drop. All potentials were measured vs. an Ag/AgCl reference electrode and a second platinum wire (counter electrode). Potentials were applied to the cell via a BASi 50W potentiostat/galvanostat, and the spectra were collected with a Varian Cary 50 apparatus at the room temperature.

5.2.2 X-Ray Structural Determinations

Diffraction studies were done on a Bruker *X8 APEX-II* kappa geometry diffractometer equipped with Mo radiation and a graphite monochromator. Diffraction patterns were collected at 100 K with the detector at 40 mm and 0.3 degrees between each reflection for 5-10 s. *APEX-II*[212] and *SHELX*[112] software were used for structure solution and refinement. A total 135,874 reflections were measured, yielding 35,599 unique data (R_{int} = 0.093). Hydrogen atoms were placed in calculated positions. The refinement included 26% racemic twinning. There were some partial occupancy (50/50) atoms placed in the disordered *tert*-butyl groups and held isotropically. Each

complex coordinates to a neutral methanol ligand. The asymmetric unit contains 3 complexes and one methanol solvate. Compound **2** crystallized as dark needles and 79,319 *hkl* data points were harvested which averaged to 11,683 data (R_{int} = 0.107). Hydrogen atoms were calculated. The neutral complex crystallized without solvent. Selected crystallographic data are shown in **Table 5.1.**

Table 5.1. Summary of Crystallographic Data for complexes **1**·1/3CH_3OH and 2.

	1·1/3CH_3OH	**2**
Formula	$C_{52.33}H_{74.33}Mn_1N_2O_{4.33}$	$C_{52}H_{73}MnN_2O_3$
FW	855.74	829.06
Space group	*Cc*	*P21/c*
a (Å)	28.8966(17)	13.9076(7)
b (Å)	17.2405(17)	27.1291(14)
c (Å)	29.9927(19)	14.1947(7)
α (deg)	90	90
β (deg)	98.392(5)	117.731(2)
γ (deg)	90	90
V (Å^3)	14782.1(19)	4740.5(4)
Z	12	4
Temp (K)	100(2)	100(2)
λ (Å)	0.71073	0.71073
ρ(g cm^{-3})	1.154	1.162
μ (mm^{-1})	0.312	0.321
R(F) (%)	6.69	5.94
Rw(F)(%)	15.50	11.18

$R(F) = \sum \| F_o | - | F_c \| / \sum | F_o |$, $Rw(F) = [\sum w (F_o^2 - F_c^2)^2 / \sum w (F_o^2)^2]^{1/2}$

5.2.3 Computational Details

Electronic structure computations were performed using density functional theory (DFT)[122] as implemented in a development version of Gaussian.[143] Geometry optimizations were

performed at the B3LYP/6-31G(d,p)[141, 213-214] level of theory employing the IEF-PCM[215] variant for the continuum solvation model (CH_2Cl_2) with no symmetry constraints. The ligand phenols were substituted with *tert*-butyl groups experimentally; we replaced the *tert*-butyl groups with methyl for computational efficiency while capturing the electronic properties of the alkyl substituents.[215] All optimized structures were confirmed to have stable wave functions, and to be local minima by analyzing the harmonic frequencies.[152] Cartesian coordinates and frequencies for all species can be found in the Appendix B. TD-DFT[214] was employed to estimate vertical electronic excitation energies and intensities, and the results were visualized and fit with Gaussians using GaussView.[23] Single point energies for thermodynamics and TD-DFT calculations were performed using a larger basis set, 6-311+G(d,p).[149]

5.2.4 Catalytic Studies

To test the catalytic activity of $[Mn^{III}L^1CH_3OH]$ (1) for water oxidation, bulk electrolysis was performed in a CH_3CN:phosphate 10:90% buffered solution at neutral pH. in a custom H-type cell. A 3-electrode system consisting of a 1.30 cm^2 FTO plate as the working electrode and Ag/AgCl and platinum wire as the reference and auxiliary electrodes, respectively. The quantification of oxygen was measured by gas chromatography and calculated from the ratio of O_2 and N_2 in the headspace according to equation 5.1.[155] A sample calculation is shown.

$$\Delta A = [(r_2 - r_1)]/r_0 \times A \qquad \text{(Equation 5.1)}$$

ΔA= number of moles of O_2 produced by catalyst (25 µM) after 10800 seconds

A = number of moles of O_2 in the headspace before electrolysis (113 µmol for 13 mL headspace)

r_0 = ratio of O_2 and N_2 in the headspace before electrolysis

r_1 = ratio of O_2 and N_2 in the headspace after electrolysis without catalyst

r_2 = ratio of O_2 and N_2 in the headspace after electrolysis with catalyst

r_0, r_1, and r_2 are 0.257, 0.261, and 0.266, respectively. ΔA =2.20 µmol

TON = moles of O_2 produced/moles of catalyst used

TON = 2.20 µmol / 0.075 µmol =30

5.2.5 Synthetic Procedures

The ligands, *N*,*N*,*N*'-tris-(3,5-di-*tert*-butyl-2-hydroxybenzyl)-benzene-1,2-diamine ($H_3L^{1'}$), and, 6,6'-(((2-((3,5-di-*tert*-butyl-2-hydroxybenzyl)(methyl)amino)phenyl)azanediyl) bis(methylene))bis(2,4-di-tert-butylphenol) (H_3L^2) were prepared according to literature procedures.[115, 207-211] We demonstrated that $H_3L^{1'}$ transforms into the related L^1 containing an azomethine (C=N) group when coordinated to a trivalent metal under oxidizing conditions in earlier reports.[208-209, 211]

5.2.5.1 Synthesis of [$Mn^{III}(L^1)(CH_3OH)$] (1)

$H_3L^{1'}$ (0.380 g, 0.500 mmol) was dissolved in a solvent mixture of anhydrous CH_3OH:CH_2Cl_2 (20 mL, 1:1) and treated with $NaOCH_3$ (0.0810 g, 1.5000 mmol) under argon atmosphere. A methanol solution of $MnCl_2{\cdot}4H_2O$ (0.0990 g, 0.5000 mmol) was transferred via cannula, heated at 50 ºC, and stirred for 2 h. The resulting light brown solution was cooled to room temperature. Oxygen gas was bubbled through the cooled solution for 15 min where the color immediately changed to dark brown. Upon slow solvent evaporation, dark brown crystals suitable for X-ray analysis were isolated from the solution. Yield: 70% (0.295 g, 0.350 mmol). ESI-MS (m/z^+; CH_3OH) = 813.4572, 100%, for [$C_{51}H_{69}N_2O_3Mn + H^+$]. IR (KBr, cm^{-1}) 2954(s), 2904(m), 2866(m), ν(C-H); 1610(m) ν(C=N), 1584(s), 1528(s), 1465(s), 1413(s), 1389(s),1360(s), ν(C=C); 1250(s), 1200(s), ν(C–O). Anal. calc. for $C_{52.33}$ $H_{74.33}$ $N_2O_{4.33}Mn$: C,73.45; H, 8.76; N, 3.27%. Found: C, 72.99; H, 8.13; N, 3.41%. UV-visible (λ / nm; ε / $M^{-1}cm^{-1}$): 290 (22,000); 440 (6,068); 527 (4,450); 609 (3,408).

5.2.5.2 Synthesis of $[Mn^{III}(L^2)]$ (2)

Complex **2** was prepared analogously to **1**, except that H_3L^2 was used as the ligand and anhydrous $MnCl_2$ was used as the salt. Brown X-ray suitable single crystals of **2** were obtained by slow crystallization in a CH_3OH : CH_2Cl_2 mixture (1 : 1). Yield: 70% (0.290 g, 0.350mmol). ESI (m/z^+) = 829.5061, 100%, for $[C_{52}H_{73}N_2O_3Mn + H^+]$. IR (KBr, cm^{-1}) 2955(s), 2904(m), 2867(m), ν(C-H); 1602(m), 1527(s), 1463(s), 1413(s), 1390(s),1360(s), ν(C=C); 1265(s), 1237(s), ν(C–O). Anal. calc. for $C_{52}H_{73}N_2O_3Mn$: C,75.33; H, 8.87; N, 3.38%. Found: C, 75.41; H, 8.78; N, 3.54%. UV-visible (λ / nm; ε / $M^{-1}cm^{-1}$): 285 (24,700); 390 (6,632); 532 (2,622); 815 (1,634).

5.3 Results and Discussion

5.3.1 Synthesis and Characterization

Ligands H_3L^1 and H_3L^2 were synthesized according to reported procedures.[115, 207-211] The hexacoordinate complex $[Mn^{III}(L^1)(CH_3OH)]$ was synthesized by combining H_3L^1 with $MnCl_2{\cdot}4H_2O$ in the presence of $NaOCH_3$ followed by a 15 min O_2 purge. The IR spectrum of **1** lacked an N–H band at *ca.* 3200 cm^{-1} indicative of the amine group but did show an absorption band at 1610 cm^{-1} consistent with the C=N group. Oxidation of the amine $(L^1)^{3-}$ to form the imine $(L^1)^{3-}$ was previously observed for an iron(III) complex.[207, 209] Elemental analysis, ESI mass spectra, and the X-ray crystal structure confirmed a hexacoordinate manganese complex containing $[Mn^{III}(L^1)(CH_3OH)]$, where the coordinated methanol occupies the last position.

Complex $[Mn^{III}L^2]$ **(2)** was synthesized by reaction of equimolar amounts of H_3L^2 and anhydrous $MnCl_2$ under similar conditions. The ligands L^1 and L^2 are the 2,4-di-*tert*-butyl-6-[(2-[(3,5-di-tert-butylbenzyl)(methyl)amino]phenyl)imino]methylphenolate and 2,4-di-*tert*-butyl-6-(1-methyl-1*H*-benzo[*d*]imidazol-2-yl)phenolate, respectively. The use of anhydrous $MnCl_2$ yielded **2** as the only product. The compound showed an IR spectrum lacking the C=N band at

1619 cm^{-1}, evidence that ligand oxidation was prevented by the N-attached methyl group present in $(L^2)^{3-}$. The $[M+H]^+$ peak was observed at 829.51 in the ESI mass spectrum along with an appropriate isotopic distribution pattern. Elemental analysis data supports that **2** has no coordinated CH_3OH or any other ligand occupying the sixth coordination site. The X-ray crystal structure determination confirmed **2** as a pentacoordinate manganese species.

5.3.2 Geometric and Electronic Structures

The molecular structures of hexacoordinate $[Mn^{III}L^1CH_3OH]$ **(1)** and pentacoordinate $[Mn^{III}L^2]$ **(2)** were solved by X-ray and are plotted as ORTEP[216] representations at 50% probability in **Figure 5.1**. The unit cell of **1** consists of an asymmetric unit with three $[Mn(L^1)(CH_3OH)]$ molecules and one uncoordinated methanol in the lattice.

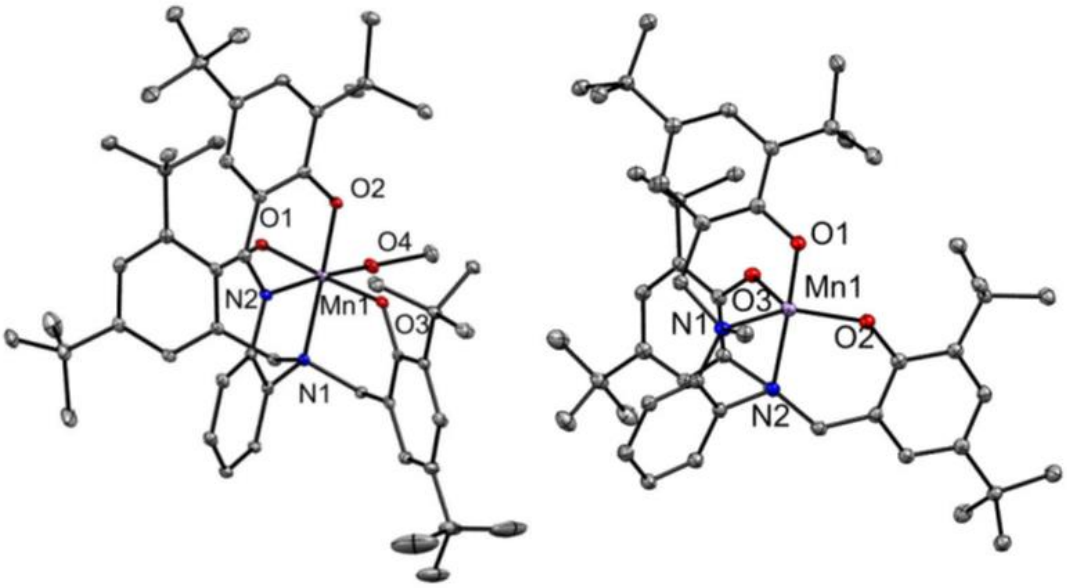

Figure 5.1. ORTEP[216] representations of **1** (left) and **2** (right).

These three manganese complexes are chemically equivalent with slight differences in the bond lengths and angles, with a notable exception for the $Mn–O_{CH3OH}$ bond which shows a longer bond length. This elongation of the bond is consistent with the weak nature of the bound CH_3OH and rules out the possibility of the methoxylated coordination. The ORTEP[216] representation of **1**

in **Figure 5.1** (left) contains a single molecule (Mn2 center). Complex **2** crystallized in the monoclinic space group $P2_1/c$, **(Figure 5.1)** (right). Selected bond lengths and angles for **1** and **2** are given in **Table 5.2.**

Table 5.2. Selected bond lengths (Å) and angles (°) from crystal data for **1** (Mn2 center) and **2**.

[$Mn^{III}(L^1)(CH_3OH)$]		**[$Mn^{III}(L^2)$]**	
Mn(2)-O(6)	1.865(3)	Mn(1)-O(2)	1.8934(17)
Mn(2)-O(5)	1.916(3)	Mn(1)-O(1)	1.8382(16)
Mn(2)-N(4)	2.126(3)	Mn(1)-N(2)	2.061(2)
Mn(2)-N(3)	2.151(4)	Mn(1)-N(1)	2.139(2)
Mn(2)-O(7)	1.887(3)	Mn(1)-O(3)	1.9235(16)
Mn(2)-O(8)	2.201(4)		
N(3)-C(59)	1.302(5)	N(1)-C(7)	1.493(3)
N(4)-C(73)	1.504(5)	N(2)-C(22)	1.508(3)
N(4)-C(66)	1.509(5)	N(2)-C(15)	1.511(3)
N(4)-C(65)	1.469(5)	N(2)-C(14)	1.473(3)
N(3)-C(60)	1.417(5)		
O(6)-C(72)	1.341(5)	O(2)-C(21)	1.338(3)
O(5)-C(53)	1.300(5)	O(1)-C(1)	1.350(3)
O(7)-C(79)	1.319(5)	O(3)-C(28)	1.344(3)
O(6)-Mn(2)-O(5)	90.58(13)	O(2)-Mn(1)-O(1)	90.06(7)
O(6)-Mn(2)-O(7)	170.00(14)	O(2)-Mn(1)-O(3)	121.62(7)
O(7)-Mn(2)-O(5)	89.16(13)	O(1)-Mn(1)-O(3)	96.13(7)
O(6)-Mn(2)-N(4)	92.32(13)	O(2)-Mn(1)-N(2)	92.21(7)
O(5)-Mn(2)-N(4)	166.90(13)	O(1)-Mn(1)-N(2)	168.20(7)
O(7)-Mn(2)-N(4)	90.17(12)	O(2)-Mn(1)-N(1)	132.36(7)
O(6)-Mn(2)-N(3)	92.08(14)	O(1)-Mn(1)-N(1)	87.09(7)
O(7)-Mn(2)-N(3)	97.91(13)	O(3)-Mn(1)-N(1)	105.95(7)
N(4)-Mn(2)-N(3)	78.41(13)	N(2)-Mn(1)-N(1)	82.82(7)
O(6)-Mn(2)-O(8)	86.54(13)		
O(5)-Mn(2)-O(8)	99.70(13)		
O(7)-Mn(2)-O(8)	83.65(13)		
N(4)-Mn(2)-O(8)	93.23(13)		
N(3)-Mn(2)-O(8)	171.47(13)		

In **[$Mn^{III}L^1CH_3OH$] (1),** the N_2O_3 moiety of L^1 consists of an amine nitrogen, an imine nitrogen, and three phenolate oxygens (based on C–O bond lengths of 1.30-1.34 Å) for an overall trianionic, pentadentate ligand. The three phenolates are chemically distinct, and display Mn–O

bond lengths of 1.865(3), 1.887(3) and 1.916(3) Å, respectively. The π-withdrawing imine makes the iminophenolate less electron rich than the aminophenolates, as evidenced by a shorter C–O bond length of 1.300(5), which leads to weaker electrostatic interactions with the manganese(III) ion. The Mn–N_{amine} bond length (2.126(3) Å) is also shorter than Mn–N_{imine} (2.151(4) Å). Average Mn–N and Mn–O bond lengths of 2.14 and 1.89 Å are consistent with related manganese(III) complexes,[99, 217-218] and with those measured in an iron(III) complex that has an established $(L^1)^{3-}$ ligand oxidation state.[207] As discussed above, the Mn–O_{CH3OH} bond length of 2.201(4) Å is consistent with the presence of an axial CH_3OH rather than a methoxy anion.

Density functional theory (DFT) calculations were performed to evaluate the energetic and structural difference between a low spin S = 1 and high spin S = 2 manganese(III) center, denoted $3d^4$ $^{LS}Mn^{III}$ and $^{HS}Mn^{III}$, respectively. The computations predict the solution-phase free energy of the $^{HS}Mn^{III}$ complex to be 11.6 kcal mol^{-1} lower than for $^{LS}Mn^{III}$. Additionally, the computed geometry for $^{HS}Mn^{III}$ is more consistent with the X-ray structural information. Thus, we assign this species as pseudo-octahedral [$^{HS}Mn^{III}(L^1)(CH_3OH)$], consistent with experimental evidence offered by similar compounds available in the literature.[217-218]

The N_2O_3 donor moiety for **[$Mn^{III}L^2$] (2)** consists of two amine nitrogens and three phenolate oxygens to afford the pentadentate $(L^2)^{3-}$ ligand. **[$Mn^{III}L^2$] (2)** crystallized as a pentacoordinate molecule with no methanol coordinated, although it was synthesized and recrystallized in a 1 : 1 CH_3OH : CH_2Cl_2 solvent mixture. The τ value[219] of 0.7 indicates that the manganese(III) ion is a distorted trigonal bipyramidal geometry. A similar geometry was observed for a related manganese(III) complex with an [N_2O_3] pentadentate ligand. Average Mn–O and Mn–N bond lengths of 1.88 and 2.10 Å in **[$Mn^{III}L^2$] (2)** are comparable to **[$Mn^{III}L^1CH_3OH$] (1)** and other related complexes.[217-218]

DFT computations were carried out in the case of **[$Mn^{III}L^2$] (2)** to evaluate the relative energetic difference between low-spin and high-spin configuration for a manganese(III) ion bound to the L^2 ligand environment as well. A Gibb's free energy difference of 22.9 kcal mol^{-1} favors species **[$Mn^{III}L^2$] (2)** as [$^{HS}Mn^{III}(L^2)$] consistent with the expectation that the high-spin state is favored due to a lower coordination number and, in good agreement with other five-coordinate species.[99, 101]

5.3.3 Electronic Spectroscopy

The electronic spectra of the hexacoordinate **[$Mn^{III}L^1CH_3OH$] (1)** and the pentacoordinate **[$Mn^{III}L^2$] (2)** in CH_2Cl_2 are illustrated in **Figure 5.2** (solid lines) along with TD-DFT simulations for each species (dotted lines). Both compounds demonstrate high energy ligand-centered transitions ($\pi \rightarrow \pi^*$) below 300 nm. Complex **[$Mn^{III}L^1CH_3OH$] (1)** shows an intense band at 440 nm that was initially associated with a phenolate-to-manganese charge transfer. According to TD-DFT results, however, this absorption band is predominantly associated with an intra-ligand-charge-transfer (ILCT) involving the phenolates and azomethine group (phenolate $\pi \rightarrow$ imine π^*) which overlaps the phenolate-to-manganese charge transfer. The nature of this ILCT was confirmed by spectroelectrochemical measurements **(Section 5.3.5).**

Compound **[$Mn^{III}L^2$] (2)** lacks an imine functionality and therefore the band observed at 390 nm is assigned as a phenolate $\pi \rightarrow {}^{HS}Mn^{III}$–$d\sigma^*$ ligand-to-metal charge transfer (LMCT).[217-218, 220-221] TD-DFT results support assignment. It is important to note that the TD-DFT results suggest that each transition involves multiple donor (and sometimes acceptor) orbitals. A full description of the low energy transitions with appreciable intensity can be found in **Appendix B**, Tables C3-C5. Lower energy LMCT bands between 500 and 900 nm are observed at 437, 527, and

609 nm and at 532 and 815 nm, respectively for **[$Mn^{III}L^1CH_3OH$] (1)** and **[$Mn^{III}L^2$] (2)**. Similar features have been observed in related complexes reported in the literature.[218, 221-222]

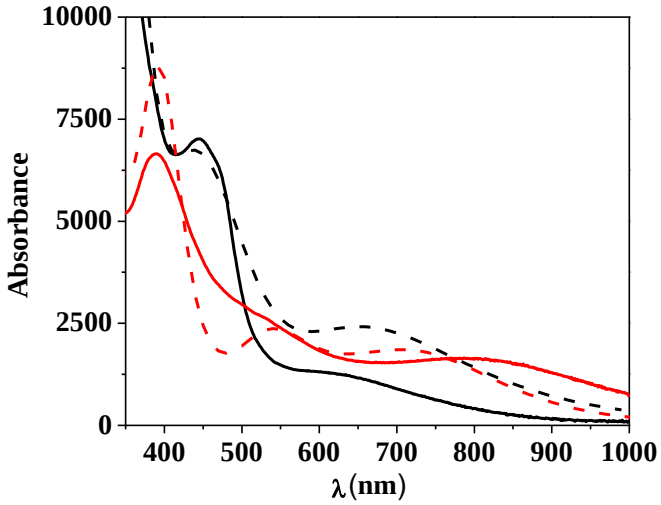

Figure 5.2. UV-visible spectra of [$Mn^{III}L^1CH_3OH$] **(1)** (black) and [$Mn^{III}L^2$] **(2)** (red) in CH_2Cl_2. Solid lines are experimental spectra, dotted lines are TD-DFT simulated spectra.

5.3.4 Electrochemical Properties

The redox behavior of the hexacoordinate [$Mn^{III}L^1CH_3OH$] **(1)** and the pentacoordinate [$Mn^{III}L^2$] **(2)** was studied by cyclic voltammetry (CV) in CH_2Cl_2 using tetrabutylammonium hexafluorophophate ($TBAPF_6$) as the supporting electrolyte. Redox potentials are reported versus Fc^+/Fc. Quasireversible one electron processes are observed at –0.88 and –0.92 V for **[$Mn^{III}L^1CH_3OH$] (1)** and **[$Mn^{III}L^2$] (2)**, respectively, and are attributed to the Mn(III/II) redox couple.[223] The potential difference of 0.04 V for the manganese reduction processes in **1** and **2** is likely associated to the different geometries of the metal ion. A first oxidative quasi-reversible process at 0.19 V is seen for **[$Mn^{III}L^1CH_3OH$] (1)**, whereas **[$Mn^{III}L^2$] (2)** shows the same process at a lower potential of 0.30 V. This process can be either attributed to the formation of a manganese(IV) species, or to ligand oxidation leading to a [Mn(III)/phenoxyl] species.

DFT calculations for hexacoordinate **[Mn^{III}L^{1}CH$_3$OH] (1)** show ligand oxidation to be thermodynamically favored over metal-based oxidation by 2.8 kcal mol^{-1}. This energy difference is within the experimental error of the DFT method and therefore metal-based oxidation could be favored as well. This could be attributed to proximity in the energy of the ligand and metal redox-active orbitals. Therefore, one-electron oxidation of some M^{+}–phenolate complexes afford either the M$^{(n+1)+}$–phenolate or the M^{n+}–phenoxyl valence tautomer.[224-226] Interestingly, no metal-based oxidized state could be located for the pentadentate **[Mn^{III}L^{2}] (2)**.

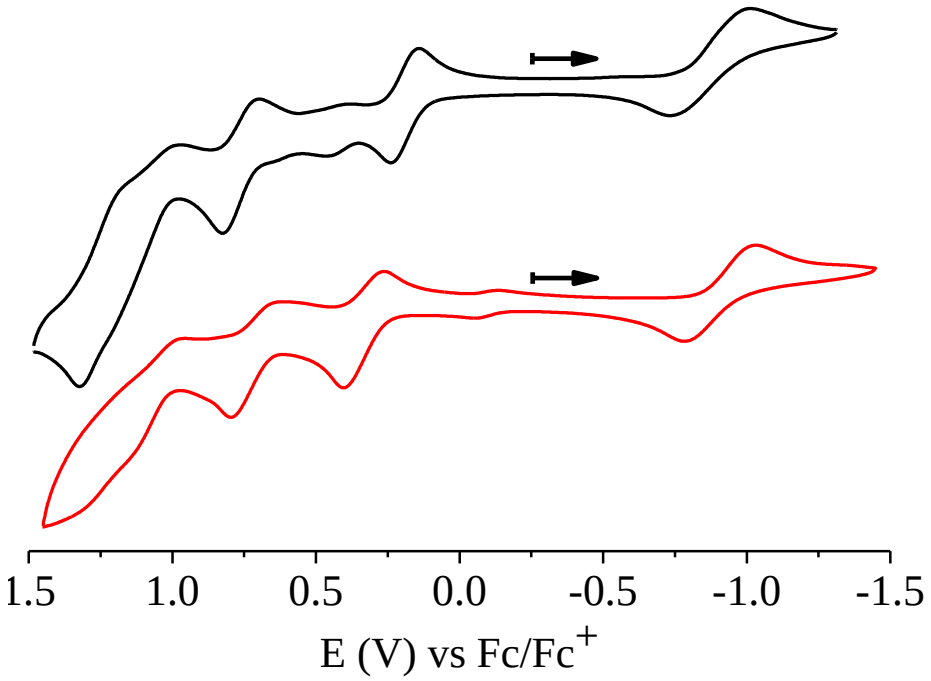

Figure 5.3. Cyclic voltammograms for **1** (top) and **2** (bottom) in CH_2Cl_2 with 0.1 M $TBAPF_6$ as supporting electrolyte.

Compound **[Mn^{III}L^{1}CH$_3$OH] (1)** also exhibits an anodic process at 0.42 V with a much smaller current response. The solution was prepared multiple times from isolated crystals and this redox process was reproducible. The amplitude of the process increases when the scan rate is decreased. This inverse proportionality could be associated with the formation of

Mn(IV)/phenolate from a [Mn(III)/phenoxyl] species because the energy of their frontier orbitals is similar; a necessary condition for valence tautomerism.[224]

Another quasi-reversible redox process centered at 0.76 and 0.68 V is observed for **1** and **2**. Based on our previous study of [$Ga^{III}L^1$] and [$Fe^{III}L^1$] complexes[207, 209], as well as other literature reports[115, 227-230] and DFT calculations, we assign these processes to oxidation of a second phenolate group. A scheme of the computed spin densities for these redox states is included in **Figure 5.4** and summarizes the sequence of redox events for these two molecules. The first oxidation occurs at the aminophenolate instead of the iminophenolate in **1** due to the π-withdrawing nature of the imine, while the first oxidation of **2** occurs at the phenolate attached to the methylamine due to inductive effect. This sequence is also observed for iron(III) species with similar ligands,[115, 207] and suggests that ligand electronic properties precede coordination preferences. In both the hexa and pentadentate complexes DFT suggests an antiferromagnetic coupling between the phenoxyl radicals and the high-spin manganese(III) ion to be favored for coupling constants, in agreement with the results proposed by Fujii[98] and coworkers.

Table 5.3. Electrochemical parameters for compounds **1** and **2**.

Complexes					
1			**2**		
E (V) vs. Fc/Fc^+	ΔE_p (V)	i_{pa} / i_{pc}	E (V) vs. Fc/Fc^+	ΔE_p(V)	i_{pa} / i_{pc}
-0.88	0.28	1.42	-0.92	0.20	1.62
0.19	0.11	0.91	0.30	0.07	0.86
0.42	0.09	0.74	-	-	-
0.76	0.13	0.80	0.68	0.10	0.42
1.08	0.18	-	1.01	0.11	-

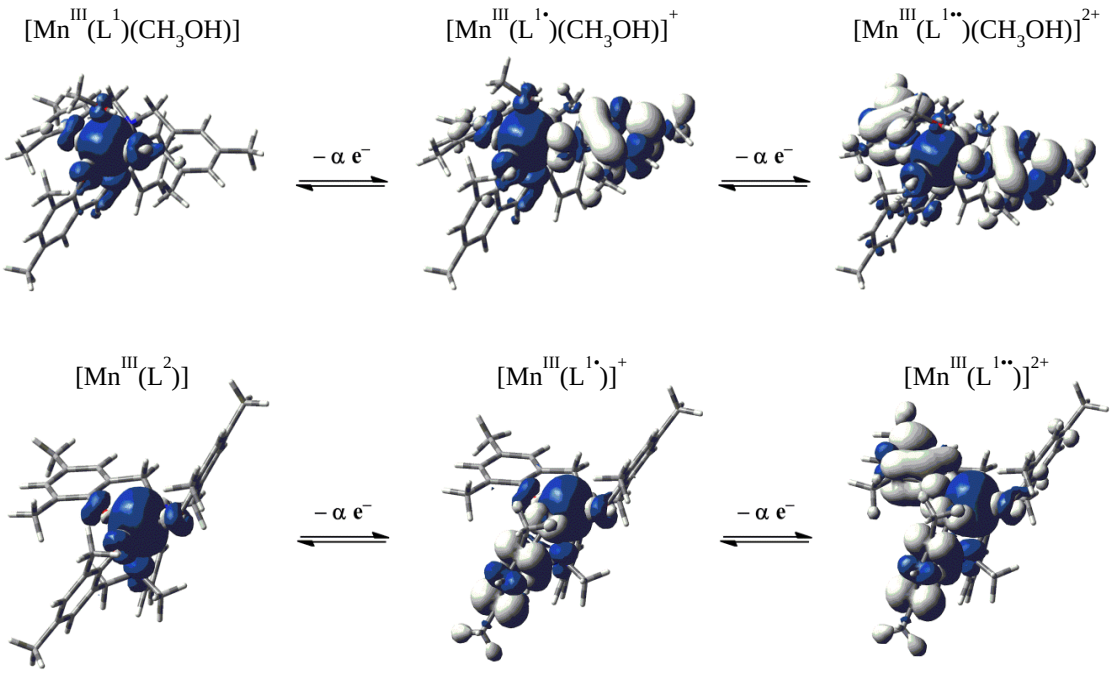

Figure 5.4. Summary of redox sequence based on predicted spin densities from DFT for **1** (top) and **2** (bottom). Spin densities are plotted with an isodensity value of 0.002 au, blue corresponds to excess α spin and white corresponding to excess β spin. The neutral species is on the left, the monocation is in the middle, and the dication is on the right.

5.3.5 Spectroelectrochemical Behavior

Spectral changes associated with electrochemical oxidations and reductions were collected under variable and stepwise potential conditions and were assessed to confirm the assignment of various bands in the UV-visible spectra. We were particularly interested in the ligand- versus metal-based character of the first anodic process. The spectral changes observed for the reduction of the hexacoordinate $[Mn^{III}L^{1}CH_3OH]$ **(1)** at an applied potential of –1.41 V vs. Fc^{+}/Fc are shown in **Figure 5.5** (left). The LMCT absorption bands decrease between 500 and 750 nm, in agreement with a Mn(III) + e^{-} → Mn(II) reduction process, where the unoccupied $d_{x^2-y^2}$-based molecular orbital accepts an electron and becomes half-filled. Isosbestic points are observed at 400 and 490 nm with an increase in the absorption band at 450 nm.

No isosbestic points were observed for the reduction of the pentacoordinate [$Mn^{III}L^2$] **(2)** under similar conditions (**Figure 5.5**, right), and instead, a continuous decrease of the spectral intensity is observed. Collectively, the disappearance of all LMCT bands in **1** and **2** upon reduction suggests the band at ~ 450 nm for **1** does not involve the metal, supporting the TD-DFT assignment of intraligand charge transfer ($\pi_{phenolate} \rightarrow \pi^*_{imine}$). This band has been commonly attributed to an LMCT in recent literature, but in view of these observations, it becomes apparent that an ILCT is more appropriate to explain the nature of the band.[115]

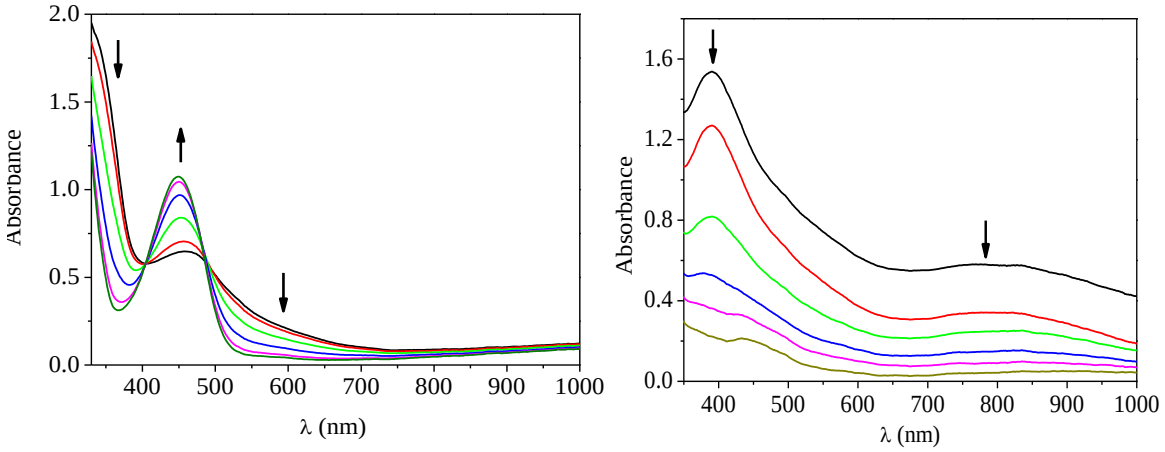

Figure 5.5. Spectral changes upon electrochemical reduction of **1** (left) and **2** (right) in CH_2Cl_2. The applied potential was –1.41 V vs. Fc^+/Fc for a period of 6 minutes.

We scanned the potential for oxidation of **1** instead of using a fixed potential due to the nearly overlapping oxidations at 0.19 and 0.42 V. This approach allows helps in deducing overlapping spectral contributions from the two oxidation processes. Oxidation between 0.20 to 0.30 V gives rise to two clear isosbestic points at 535 and 660 nm (**Figure 5.6**), with an increase in intensity below 535 nm and above 660 nm, and a decrease in between these values. The increased intensity in the low-energy region of the spectrum (> 660 nm) is consistent with ligand-based oxidation as phenolate π → phenoxyl radical π* transitions occur in this region.[96, 220 79, 208, 229]

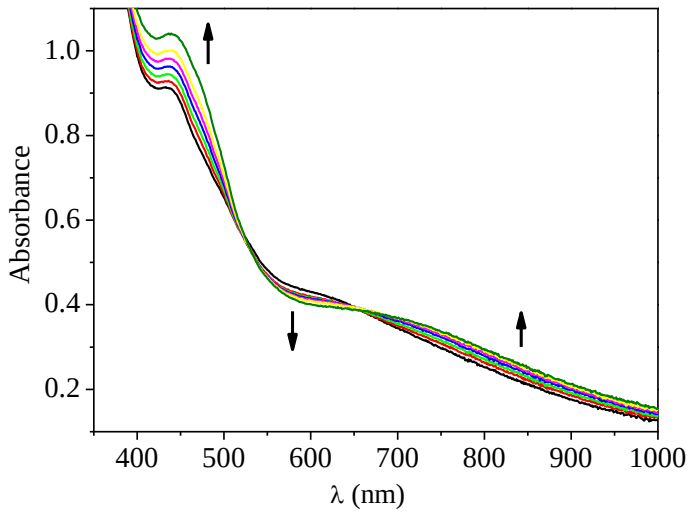

Figure 5.6. Spectral changes upon stepwise oxidation of **1** in CH_2Cl_2 in the potential range 0.20 to 0.30 $V_{Fc+/Fc.}$

Oxidation of pentadentate **2** at a fixed potential of 0.5 V vs. Fc^+/Fc **(Figure 5.7)** generates a spectral response similar to **1**. Two isosbestic points are seen at 435 and 500 nm, with increased intensity above 500 and below 435 nm and decreasing intensity between these regions. The intensity increase at low-energy is again consistent with a phenolate π → phenoxyl radical π* charge transfer band, suggesting ligand-based oxidation, rather than manganese(IV) formation.

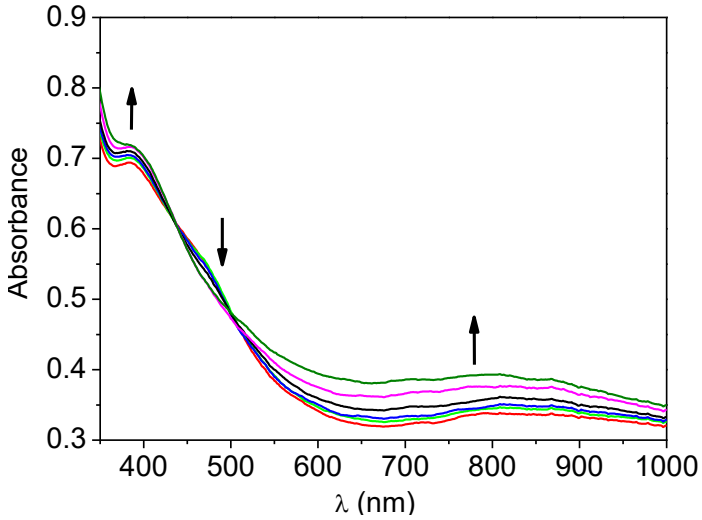

Figure 5.7. Spectral changes upon electrochemical oxidation of **2** in CH_2Cl_2. An applied potential of 0.5 V vs. Fc^+/Fc was applied for eight minutes.

5.4. Catalytic Studies

Based on the spectroscopic results described in the sections above both [$Mn^{III}L^{1}CH_3OH$] **(1)** and [$Mn^{III}L^{2}$] **(2)** were screened for their catalytic activity towards water oxidation using a CH_3CN (10%) : phosphate (90%) buffered solution at neutral pH.[155, 170, 231] The experiment was conducted in a custom H-type cell with a 3-electrode system consisting of a 1.30 cm^2 FTO plate as the working electrode, and Ag/AgCl and a platinum wire as the reference and auxiliary electrodes, respectively. The quantification of oxygen was measured by gas chromatography and calculated from the ratio of O_2 and N_2 in the headspace according to **equation 5.1** described in the experimental **section 5.2.4**. Upon scanning the phosphate buffer without the catalyst, no current enhancement was observed until 1800 mV $_{Ag/AgCl}$.

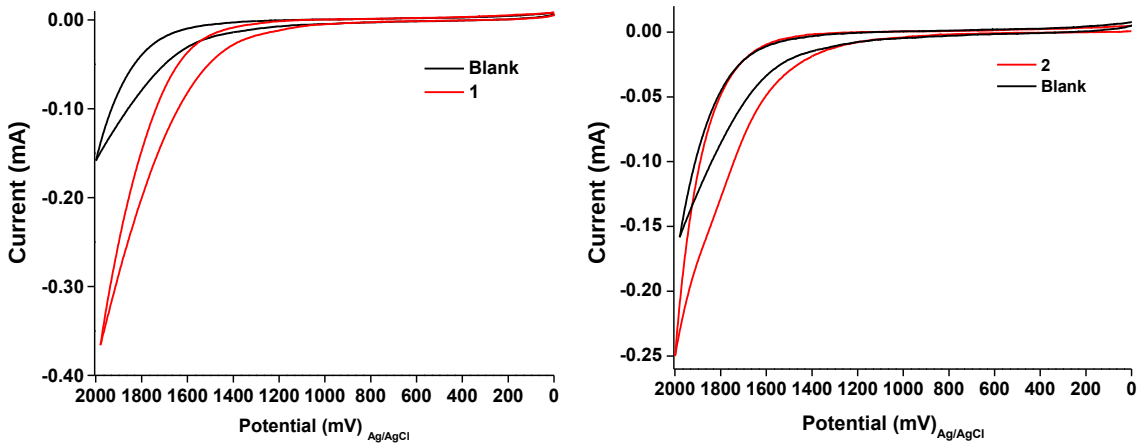

Figure 5.8. Catalytic water oxidation CV in (0.1 mol•L^{-1}) CH_3CN : Phosphate buffer at pH 7

Upon addition of **[$Mn^{III}L^{1}CH_3OH$] (1)** and the pentacoordinate **[$Mn^{III}L^{2}$] (2)** catalytic current enhancement was observed for **[$Mn^{III}L^{1}CH_3OH$]**, while **[$Mn^{III}L^{2}$]** gave a current enhancement comparable to the blank solution. These results suggest that **[$Mn^{III}L^{1}CH_3OH$]** can afford the $3d^3$ [Mn(IV)/phenolate] intermediate needed for water oxidation whilst [$Mn^{III}L^{2}$] is in capable of doing so (**Figure 5.8)**. Bulk electrolysis was performed for [$Mn^{III}L^{1}CH_3OH$] **(1)** (**Figure 5.9)** under the same conditions, using 1.0 μmol•L^{-1} of catalyst and 1.30 cm^2 FTO as the

working electrode, with an applied potential of 1.7 $V_{Ag/AgCl}$ for three hours.[231] It was observed after three hours that the catalyst operates at 85% Faradaic efficiency with a TON of 53.

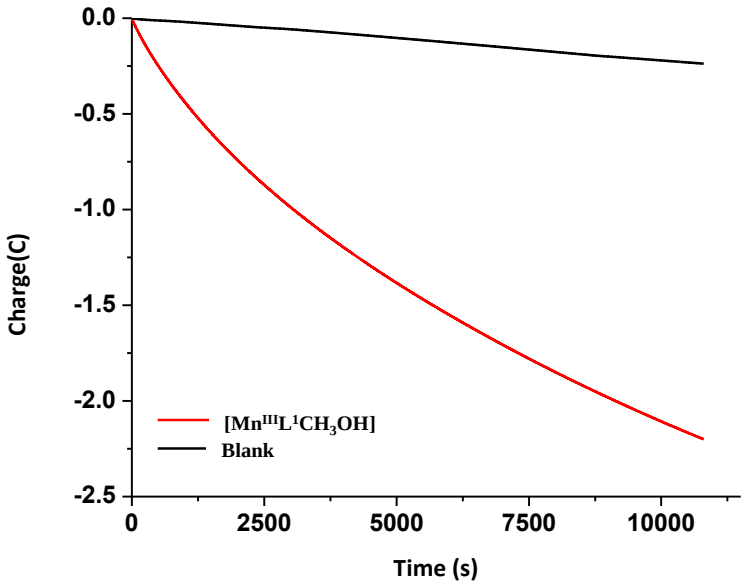

Figure 5.9. Charge consumption vs. time during BE with (0.1 mol•L^{-1} CH_3CN : phosphate buffer at pH 7 [1.0 umol•L^{-1}]) at 1.7 VAg/AgCl.

Even though the TON and %FE are considered low, they are better than others reported in the literature where TONs ranged from 16–24 with %FE of 74–81. [231-232] considering the fact that a thermodynamic barrier of 1.23 V needs to be overcome.[168]

5.5. Conclusions

I synthesized and investigated the effect of valence tautomerism on water oxidation in two manganese complexes, the hexacoordinate [$Mn^{III}L^1CH_3OH$] and the pentacoordinate [$Mn^{III}L^2$] using [N_2O_3] pentadentate ligands containing three phenolate donors. Detailed structural, electrochemical, and spectroscopic measurements suggest that whilst both complexes show ligand-based oxidations favoring formation of a [Mn(III)/phenoxyl] species, the hexacoordinate analog also shows a possibility of forming a [Mn(IV)/phenolate] species specifically due to the

degree of the interaction between the metal center and the redox-active phenolate ligands, and the similarity between the energy of their frontier orbitals (>5 kcal/mol), essential attributes of valence tautomerism. I, therefore, tested the hexacoordinate [$Mn^{III}L^{1}CH_3OH$] for water oxidation catalysis and observed an overpotential of 0.77 V and TON of 53 in three hours with the catalyst operating at a Faradaic efficiency of 85%. Such a compound is thus particularly useful to better understand the way in which ligands could be designed to favor either a radical or a high-valent metal pathway for catalytic water oxidation.

CHAPTER 6:

CONCLUSIONS

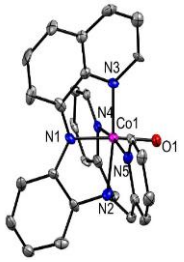

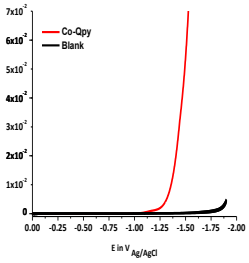

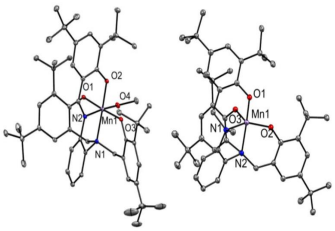

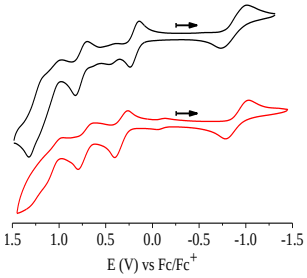

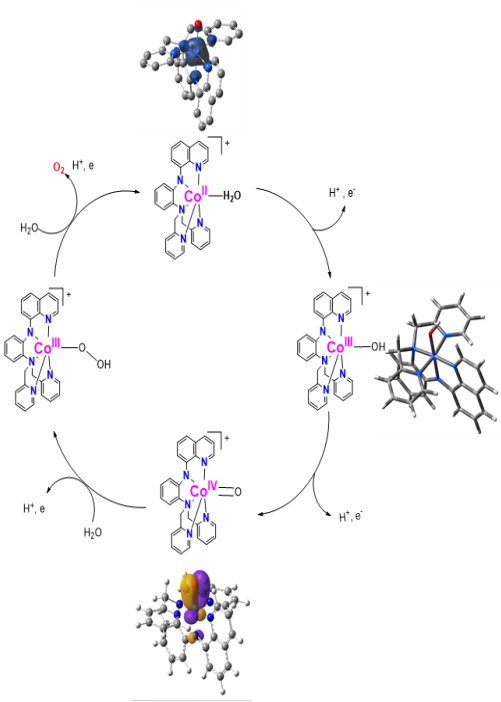

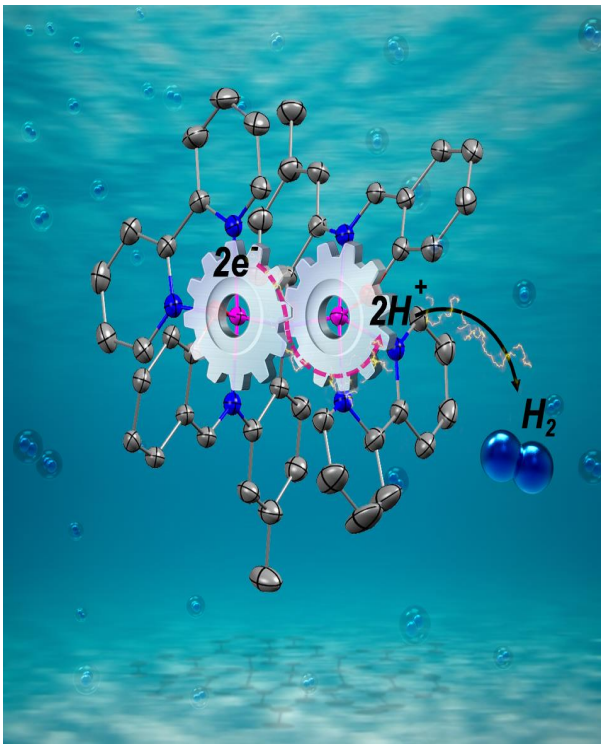

CHAPTER 6: CONCLUSIONS

The focus of this dissertation was to design and evaluate the redox, electronic, catalytic, and mechanistic pathways of $3d^7$ Co^{II}, and $3d^4$ Mn^{III} complexes with various redox-active ligand frameworks in an effort towards efficient electrocatalytic water oxidation and reduction. These systematic studies were geared towards the eventual design of excellent photocatalysts based on affordable Earth-abundant metal complexes.

In Chapter 3, I described the synthesis and characterization an asymmetric, pentadentate quinolyl-bispyridine ligand **HL^{Qpy}** with a phenylenediamine backbone and its water-soluble $3d^7$ $^{HS}Co^{II}$ complex **$[Co^{II}(L^{Qpy})H_2O]ClO_4$**. The complex is active as an electrocatalyst **(Figure 6.1)**, as well as a photocatalyst.

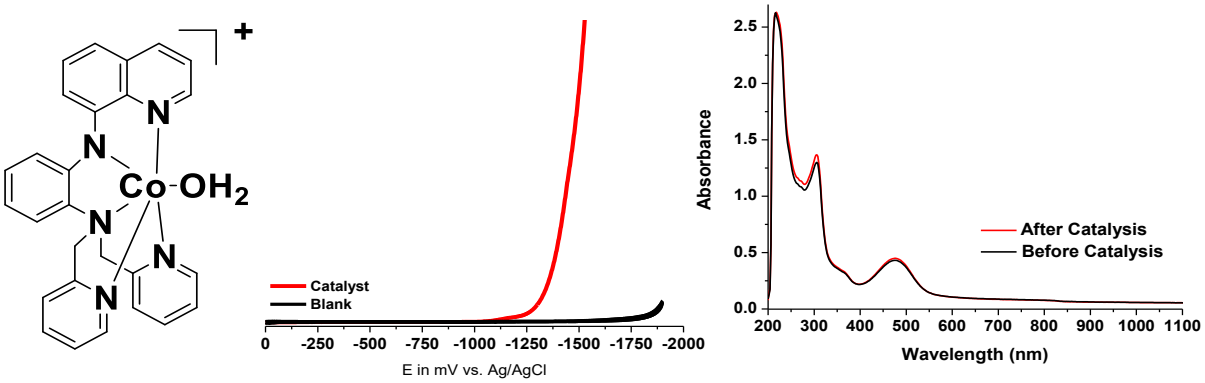

Figure 6.1. Robust and stable **$[Co^{II}(L^{Qpy})H_2O]ClO_4$** complex and its electrocatalytic water reduction activity.

$[Co^{II}(L^{Qpy})H_2O]ClO_4$ is catalytic towards H_2O reduction at a low overpotential of 0.63 V, giving a TON of 2900 with a Faradaic efficiency of 98%. An 18 h catalytic TON of 12,100 suggests a highly robust and stable catalyst. **$[Co^{II}(L^{Qpy})H_2O]ClO_4$** serves as a robust water oxidation catalyst as well, with a TON of 97 at 91% FE.

By using a series of experimental methods as well as DFT techniques, I isolated and characterized the catalytic oxidized intermediates for **[Co^{II}(L^{Qpy})H$_2$O]ClO$_4$** and proposed a 'water nucleophilic-attack' (WNA) mechanism of water oxidation **(Figure 6.2)**. The highly electrophilic 3d^5 [^{HS}Co^{IV}=O] intermediate is attacked by a nucleophilic water molecule thus forming the essential O-O bond and releasing dioxygen.

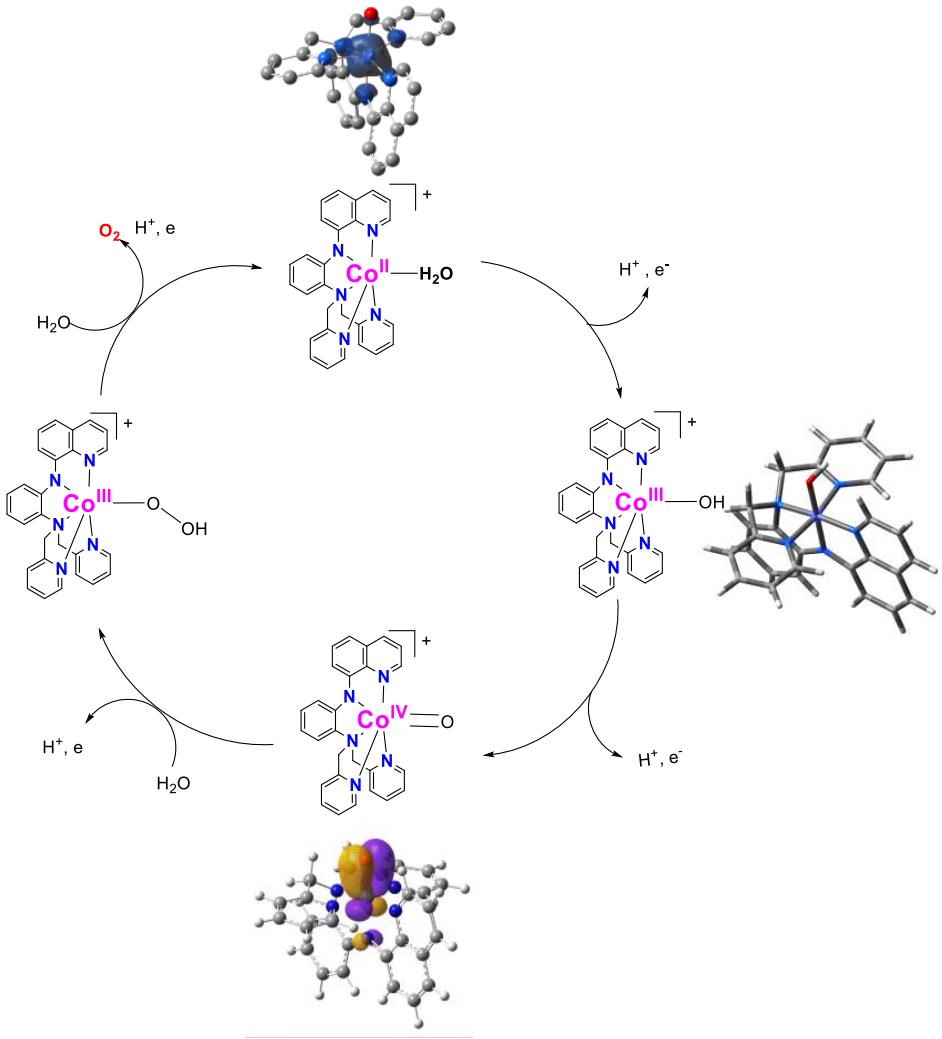

Figure 6.2. Proposed catalytic mechanism of O_2 generation by **[Co^{II}(L^{Qpy})H$_2$O]ClO$_4$**.

Finally, the photocatalytic activity of **[Co^{II}(L^{Qpy})H$_2$O]ClO$_4$** in the presence of $[Ru(bpy)_3]^{2+}$ and ascorbic acid acetate buffer (pH 4) shows a TON of 295 with a TOF of 50/h.

In Chapter 4, the principal objective was to study the effect that distance and topology have on the electronic communication, and thereby cooperativity between two cobalt centers in a dicobalt complex towards efficient proton reduction **(Figure 6.3)**. In collaboration with the Fiedler group of Marquette University, I investigated both experimentally and theoretically the catalytic properties of the bimetallic complex **$[Co^{II}_2(L^{1'})(bpy)_2]ClO_4$**, a dicobalt(II) complex in which the metal centers lie at a short distance of 2.70 Å away from each other and bridged by a nitrogen atom of a diarylamido unit with a Co1-N3-Co2 at an angle of 86.9°.

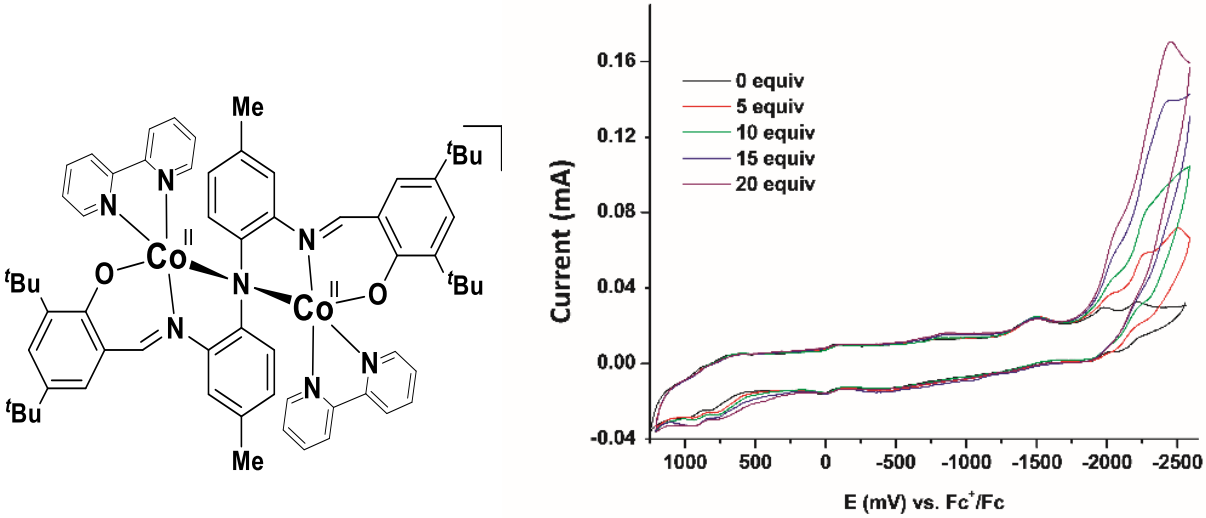

Figure 6.3. $[Co^{II}_2(L^{1'})(bpy)_2]ClO_4$ and its catalytic response to H^+ in CH_3CN.

Each metal center is a five-coordinate Co^{II} bonded to two N atoms and the O atom of a phenolate, with a bidentate bipyridine (bpy) completing the coordination. **$[Co^{II}_2(L^{1'})(bpy)_2]ClO_4$** supports the catalytic reduction of H^+ to H_2 in CH_3CN in the presence of a weak acid such as HOAc at an overpotential of 0.63 V. This catalytic activity relies on a $2e^-$ reduction of the parent species $[Co^{II}Co^{II}]$ to form a $[Co^{I}Co^{I}]$ complex with each of these Co^{I} centers contributing cooperatively with the donation of $1e^-$ to an incoming H^+, thus forming a reactive Co(II)-hydride.

The novel bimetallic cooperativity exhibited by this system arises from the close proximity of the cobalt centers and an appropriate orbital topology that allows interaction between the frontier orbitals and facilitate intramolecular electron transfer between the two centers thus avoiding the formation of the Co^{III}–H^- moiety required for proton reduction in monometallic catalysts. The second Co^{I} center plays a pivotal role in the catalytic reduction of H^+, acting as an electron reservoir to donate the second electron necessary for formation of the Co^{II}–H^- unit that favorably accepts another H^+ and releases H_2 **(Figure 6.4)**.

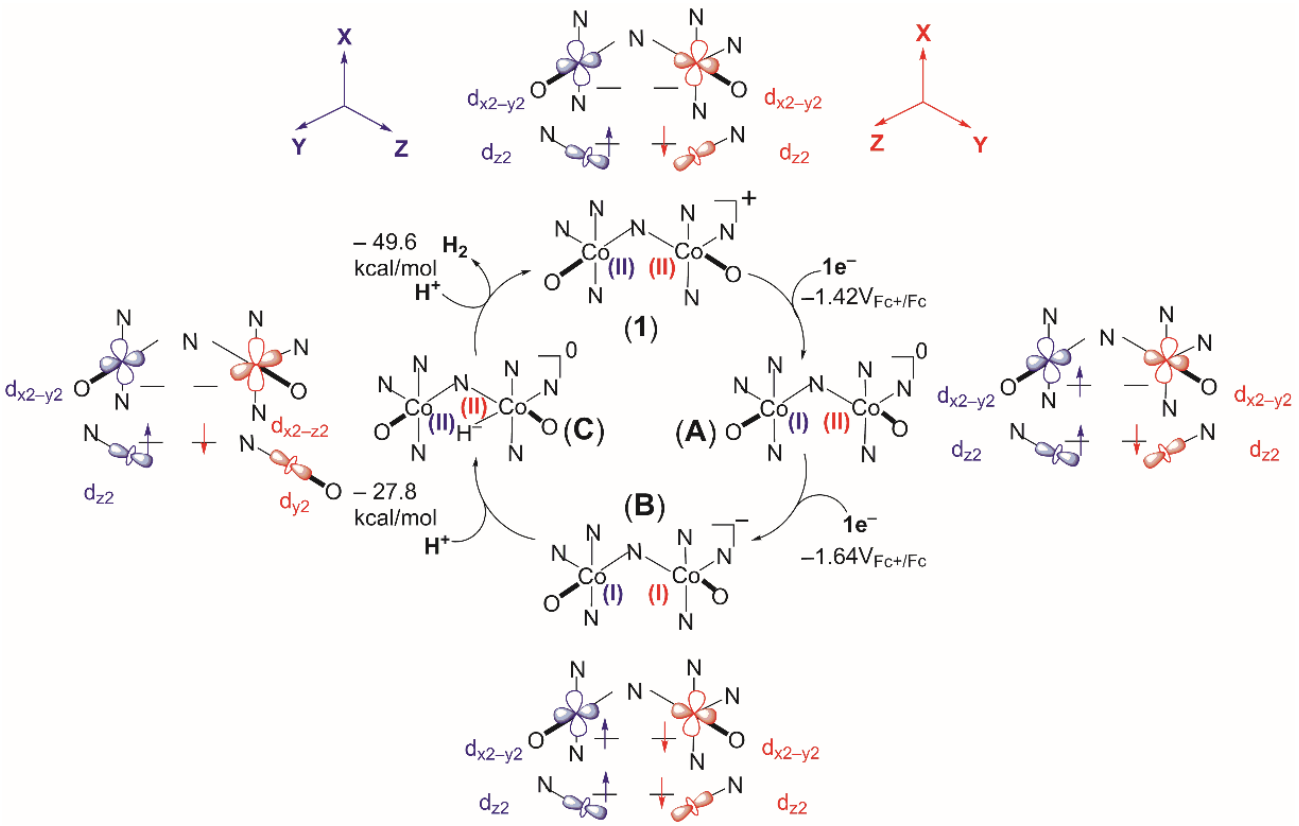

Figure 6.4. Catalytic mechanism of H_2 generation by **$[Co^{II}_2(L^{1'})(bpy)_2]ClO_4$** in CH_3CN.

Post-catalytic SEM and EDX analyses support the molecular nature of the catalyst. I utilized a wide array of experimental techniques aided by extensive theoretical computations to conclude that (i) topology, (ii) orbital overlap, and (iii) oxidation states play relevant roles in a cooperative mechanism and not merely the distance between two metals. Being the first report of

the evaluation of mechanistic cooperativity for proton reduction,[233] the implications of this study are essential to the design of ligand platforms that can support the appropriate topology, afford the crucial orbital overlap necessary for cooperative catalysis, and ensure that the metals used maintain low oxidation states, which is essential for affordable catalytic proton and water reduction

In Chapter 5, the principal objective was to investigate whether the coordination environments around a manganese center can determine high-valent states relevant for electrocatalytic water oxidation. I synthesized two manganese complexes, the hexacoordinate [$Mn^{III}L^{1}CH_3OH$] and the pentacoordinate [$Mn^{III}L^{2}$] using [N_2O_3] pentadentate ligands containing three phenolate donors, and probed the implications of valence tautomerism in these complexes on water oxidation **(Figure 6.5)**.

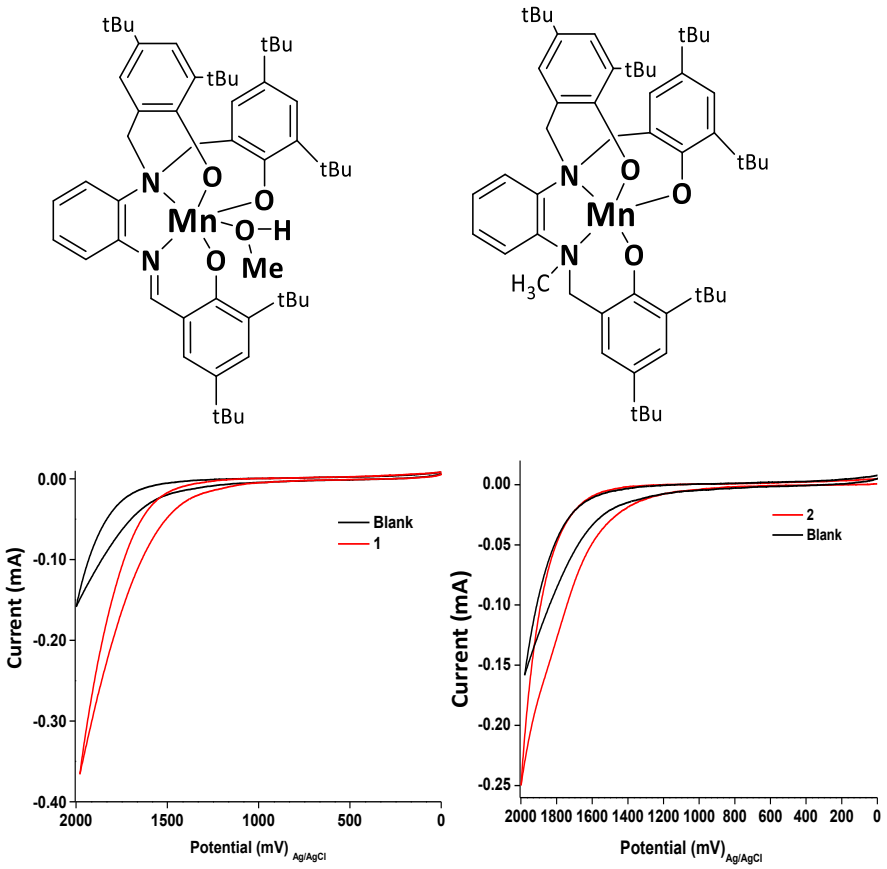

Figure 6.5. [$Mn^{III}L^{1}CH_3OH$] (1) and**[$Mn^{III}L^{2}$] (2)** and their respective catalytic responses to water oxidation.

Detailed structural, electrochemical, and spectroscopic measurements suggest that whilst both complexes show ligand-based oxidations favoring formation of a [Mn^{III}/phenoxyl] species, the hexacoordinate analog could form a [Mn^{IV}/phenolate] species. This is specifically due to the low energy difference between the frontier orbitals (<5 kcal/mol) of the metal center, and the redox-active phenolate ligands. This low energy barrier allows electronic interaction between the Mn ion, and the phenolate ligand, causing valence tautomerism through electron transfer. We therefore tested the hexacoordinate [$Mn^{III}L^{1}CH_3OH$] for water oxidation catalysis and observed an overpotential of 0.77 V and TON of 53 in three hours with the catalyst operating at a Faradaic efficiency of 85%. This study is particularly useful because it provides a basis for ligand design that favors either a radical or a high-valent metal pathway for catalytic water oxidation.

In summary, I have evaluated molecular Earth-abundant monometallic and bimetallic complexes for their efficient activity towards catalytic water reduction and oxidation during the course of my stay in the Verani group and the results are reported in this dissertation. Results from these evaluations are critically important for the future design of molecular catalysts capable of producing dioxygen and dihydrogen as fuels from water using the sun’s energy.

APPENDIX A (CHAPTER 4)

Bimetallic Cooperativity in Proton Reduction with an Amido-bridged Cobalt Catalyst

1. Copyright Details

JOHN WILEY AND SONS LICENSE
TERMS AND CONDITIONS

Jul 23, 2017

This Agreement between WAYNE STATE UNIVERSITY -- Kenneth KPOGO ("You") and John Wiley and Sons ("John Wiley and Sons") consists of your license details and the terms and conditions provided by John Wiley and Sons and Copyright Clearance Center.

License Number	4154920231119
License date	Jul 23, 2017
Licensed Content Publisher	John Wiley and Sons
Licensed Content Publication	Chemistry - A European Journal
Licensed Content Title	Bimetallic Cooperativity in Proton Reduction with an Amido-Bridged Cobalt Catalyst

Licensed Content Author	Kenneth K. Kpogo, Shivnath Mazumder, Denan Wang, H. Bernhard Schlegel, Adam T. Fiedler, Cláudio N. Verani
Licensed Content Date	Jun 23, 2017
Licensed Content Pages	8
Type of use	Dissertation/Thesis
Requestor type	Author of this Wiley article
Format	Print and electronic
Portion	Full article
Will you be translating?	No
Title of your thesis / dissertation	EVALUATION OF EARTH-ABUNDANT MONOMETALLIC AND BIMETALLIC COMPLEXES FOR CATALYTIC WATER SPLITTING
Expected completion date	Dec 2017
Expected size (number of pages)	206
Requestor Location	WAYNE STATE UNIVERSITY 5101 CASS AVENUE DETROIT, MI 48202

	United		States
	Attn: KENNETH KPOGO		
Publisher Tax ID	EU826007151		
Billing Type	Invoice		
Billing Address	WAYNE	STATE	UNIVERSITY
	5101	CASS	AVENUE
	DETROIT,	MI	48202
	United		States
	Attn: KENNETH KPOGO		
Total	0.00 USD		

Terms and Conditions

TERMS AND CONDITIONS

This copyrighted material is owned by or exclusively licensed to John Wiley & Sons, Inc. or one of its group companies (each a “Wiley Company") or handled on behalf of a society with which a Wiley Company has exclusive publishing rights in relation to a particular work (collectively "WILEY"). By clicking "accept" in connection with completing this licensing transaction, you agree that the following terms and conditions apply to this transaction (along with the billing and payment terms and conditions established by the Copyright Clearance Center Inc., ("CCC's Billing and Payment terms

LOSS OF PROFITS, DATA, FILES, USE, BUSINESS OPPORTUNITY OR CLAIMS OF THIRD PARTIES), AND WHETHER OR NOT THE PARTY HAS BEEN ADVISED OF THE POSSIBILITY OF SUCH DAMAGES. THIS LIMITATION SHALL APPLY NOTWITHSTANDING ANY FAILURE OF ESSENTIAL PURPOSE OF ANY LIMITED REMEDY PROVIDED HEREIN.

Should any provision of this Agreement be held by a court of competent jurisdiction to be illegal, invalid, or unenforceable, that provision shall be deemed amended to achieve as nearly as possible the same economic effect as the original provision, and the legality, validity and enforceability of the remaining provisions of this Agreement shall not be affected or impaired thereby.

The failure of either party to enforce any term or condition of this Agreement shall not constitute a waiver of either party's right to enforce each and every term and condition of this Agreement. No breach under this agreement shall be deemed waived or excused by either party unless such waiver or consent is in writing signed by the party granting such waiver or consent. The waiver by or consent of a party to a breach of any provision of this Agreement shall not operate or be construed as a waiver of or consent to any other or subsequent breach by such other party.

This Agreement may not be assigned (including by operation of law or otherwise) by you without WILEY's prior written consent.

Any fee required for this permission shall be non-refundable after thirty (30) days from receipt by the CCC.

These terms and conditions together with CCC's Billing and Payment terms and conditions (which are incorporated herein) form the entire agreement between you and

WILEY concerning this licensing transaction and (in the absence of fraud) supersedes all prior agreements and representations of the parties, oral or written. This Agreement may not be amended except in writing signed by both parties. This Agreement shall be binding upon and inure to the benefit of the parties' successors, legal representatives, and authorized assigns.

In the event of any conflict between your obligations established by these terms and conditions and those established by CCC's Billing and Payment terms and conditions, these terms and conditions shall prevail.

WILEY expressly reserves all rights not specifically granted in the combination of (i) the license details provided by you and accepted in the course of this licensing transaction, (ii) these terms and conditions and (iii) CCC's Billing and Payment terms and conditions. This Agreement will be void if the Type of Use, Format, Circulation, or Requestor Type was misrepresented during the licensing process.

This Agreement shall be governed by and construed in accordance with the laws of the State of New York, USA, without regards to such state's conflict of law rules. Any legal action, suit or proceeding arising out of or relating to these Terms and Conditions or the breach thereof shall be instituted in a court of competent jurisdiction in New York County in the State of New York in the United States of America and each party hereby consents and submits to the personal jurisdiction of such court, waives any objection to venue in such court and consents to service of process by registered or certified mail, return receipt requested, at the last known address of such party.

WILEY OPEN ACCESS TERMS AND CONDITIONS

2. Results from DFT Calculations

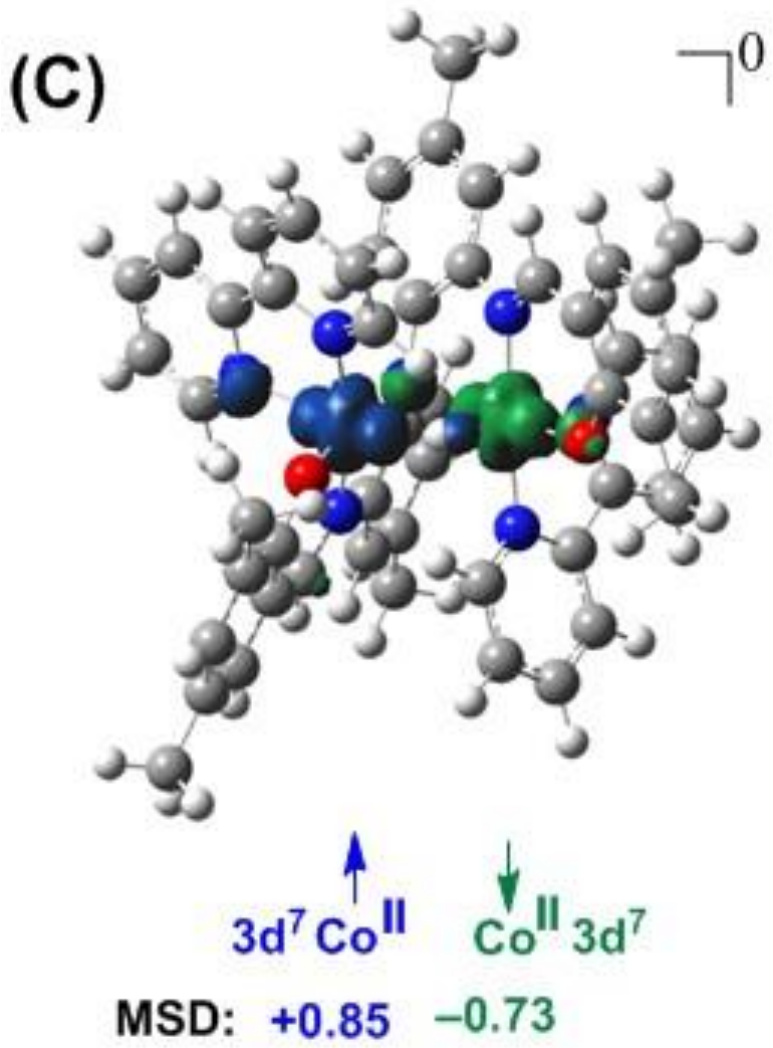

Figure A1. Spin density plot (isovalue = 0.004 au) with Mulliken spin density (MSD) values for $[Co^{II}(H^{-})Co^{II}]$ complex **C.**

Table A1. The XYZ coordinates of the calculated structures

Complex 1

C	-3.951477000	-1.891537000	-5.683427000
C	-1.807016000	-0.739353000	-4.948893000
C	-3.143563000	-1.107098000	-4.673090000
C	-1.061485000	0.010015000	-4.036197000
C	2.099288000	-3.170152000	-3.579661000
C	0.514639000	3.992578000	-3.848998000
C	2.759769000	-1.944622000	-3.408098000
C	2.737539000	5.221416000	-3.708622000
C	-4.324957000	4.777346000	-2.867479000
C	-3.677739000	5.953272000	-2.459893000
C	-0.377411000	3.007615000	-3.418425000
C	-3.704631000	-0.705685000	-3.451762000
C	0.936086000	-3.419010000	-2.845266000
C	1.759857000	4.180988000	-3.208076000
C	-1.631463000	0.420849000	-2.814755000
C	-3.948918000	3.566872000	-2.277559000
C	-2.965367000	0.059090000	-2.522814000
C	-2.691630000	5.873696000	-1.472255000
C	2.220955000	-1.012316000	-2.516419000
C	-0.052453000	2.175708000	-2.328713000
C	0.461069000	-2.440704000	-1.953768000
C	2.075731000	3.358336000	-2.116495000
C	-2.376551000	4.622780000	-0.912044000
C	1.184414000	2.357734000	-1.671148000
C	-1.413988000	-3.820237000	-0.928108000
C	-0.717974000	-2.608821000	-1.081881000
C	-4.629095000	0.197210000	-0.808628000
C	-2.455075000	-3.906993000	0.000655000
C	-1.397555000	4.419042000	0.173743000
C	-0.787988000	5.466252000	0.886035000
C	2.446864000	1.603262000	0.215847000
C	-2.769742000	-2.779109000	0.769861000
C	-2.049737000	-1.599159000	0.560363000
C	-5.191291000	0.555112000	0.447694000
C	-6.514176000	0.102609000	0.748541000
C	0.047211000	5.173508000	1.967994000
C	-0.380142000	2.836495000	1.569615000
C	-4.449073000	1.299390000	1.433094000
C	2.752646000	0.814688000	1.359556000
C	0.243770000	3.833268000	2.325735000
C	-7.115186000	0.356885000	1.971033000
C	-8.518673000	-0.104721000	2.291310000
C	1.879203000	-0.235071000	1.818501000
C	3.937484000	1.124931000	2.097945000
C	-5.065111000	1.545387000	2.710033000
C	-6.356552000	1.080918000	2.937277000
C	2.228042000	-0.936990000	3.025105000
C	4.280137000	0.440764000	3.253438000
C	1.318133000	-2.031770000	3.521989000
C	3.397046000	-0.588791000	3.693786000
C	5.535871000	0.754368000	4.034798000
C	-4.293597000	2.308774000	3.756790000
H	-4.169304000	-1.284834000	-6.578057000
H	-3.405289000	-2.783646000	-6.028617000
H	-1.349058000	-1.042364000	-5.894431000
H	-4.912588000	-2.225002000	-5.266738000
H	2.484335000	-3.920378000	-4.273097000
H	0.246875000	4.621721000	-4.702309000
H	-0.032202000	0.289260000	-4.266107000
H	-3.937216000	6.916613000	-2.903291000
H	3.166861000	4.929891000	-4.681664000
H	-5.106729000	4.792710000	-3.628685000
H	2.246699000	6.196313000	-3.855574000
H	3.675326000	-1.710369000	-3.953740000
H	-1.329757000	2.868801000	-3.932396000
H	0.403611000	-4.362737000	-2.968324000
H	-4.741513000	-0.979495000	-3.245432000
H	3.572681000	5.366409000	-3.008382000
H	-4.417514000	2.624034000	-2.565089000
H	-2.171137000	6.774895000	-1.146236000
H	-1.124606000	-4.696398000	-1.508831000
H	2.692818000	-0.041536000	-2.354540000
H	3.046566000	3.490225000	-1.634464000
H	-5.250488000	-0.456835000	-1.431675000
H	-0.989018000	6.502970000	0.615176000
H	-2.997046000	-4.845351000	0.134544000
H	-7.058221000	-0.458004000	-0.019238000
H	3.131982000	2.436851000	0.021823000
H	-3.558249000	-2.801131000	1.523020000
H	0.519242000	5.979516000	2.533437000
H	-2.258190000	-0.694859000	1.133252000
H	4.585108000	1.926453000	1.726876000
H	-0.257169000	1.779777000	1.809254000
H	0.868107000	3.551993000	3.174536000
H	-6.815444000	1.288193000	3.910203000
H	3.652865000	-1.138840000	4.605981000
Co	-2.250355000	1.763026000	-0.417932000
Co	0.134366000	0.047288000	-0.497465000
N	-0.923875000	1.160753000	-1.809047000
N	1.098860000	-1.244316000	-1.803110000
N	-2.998657000	3.480574000	-1.323189000
N	-3.436380000	0.544583000	-1.275141000
N	-1.062065000	-1.500601000	-0.357505000
N	1.410298000	1.454425000	-0.599288000
N	-1.163212000	3.111913000	0.502590000
O	-3.232132000	1.750827000	1.234646000
O	0.768454000	-0.573029000	1.204929000
H	6.092727000	1.589282000	3.585538000
H	5.304587000	1.027285000	5.077623000
H	6.212673000	-0.115134000	4.075257000
H	1.713938000	-2.490155000	4.439194000
H	0.307659000	-1.646633000	3.734734000
H	1.195301000	-2.820618000	2.762581000
H	-3.996502000	3.302434000	3.384719000
H	-4.890473000	2.442418000	4.669835000
H	-3.360585000	1.787285000	4.025860000
H	-8.537912000	-0.750382000	3.184708000
H	-9.185286000	0.748483000	2.499669000
H	-8.955949000	-0.673039000	1.457738000

==========

Complex A

C	-4.154663000	-1.710038000	-5.781181000
C	-1.897384000	-0.806544000	-5.032106000
C	-3.265551000	-1.025840000	-4.764453000
C	-1.090922000	-0.138566000	-4.107685000
C	1.953436000	-3.274462000	-3.552647000
C	0.576171000	3.860282000	-4.009580000
C	2.680916000	-2.084560000	-3.387450000
C	2.658661000	5.299178000	-3.726022000
C	-4.038342000	4.926390000	-2.942650000
C	-3.415015000	6.106681000	-2.490079000
C	-0.270386000	2.826066000	-3.615038000
C	-3.779196000	-0.578523000	-3.538953000
C	0.799897000	-3.471702000	-2.788923000
C	1.751943000	4.170558000	-3.284399000
C	-1.608340000	0.334047000	-2.881732000
C	-3.713307000	3.718722000	-2.329390000
C	-2.976948000	0.081391000	-2.577592000
C	-2.506067000	6.017503000	-1.434677000
C	2.216619000	-1.137949000	-2.470064000

C	0.028530000	2.041843000	-2.472956000
C	0.402934000	-2.482185000	-1.870554000
C	2.048313000	3.401629000	-2.152378000
C	-2.235088000	4.768187000	-0.844282000
C	1.215919000	2.333484000	-1.750433000
C	-1.493021000	-3.776861000	-0.774467000
C	-0.768118000	-2.589773000	-0.981301000
C	-4.582305000	0.111147000	-0.835582000
C	-2.534928000	-3.794978000	0.156932000
C	-1.335541000	4.565179000	0.296771000
C	-0.813916000	5.610351000	1.083267000
C	2.499392000	1.600207000	0.133541000
C	-2.821252000	-2.625458000	0.874488000
C	-2.071547000	-1.473404000	0.615185000
C	-5.155607000	0.416512000	0.438507000
C	-6.445488000	-0.133307000	0.717145000
C	-0.025691000	5.315684000	2.197091000
C	-0.326824000	2.976788000	1.689922000
C	-4.469294000	1.177991000	1.464184000
C	2.793222000	0.842025000	1.306114000
C	0.213108000	3.965249000	2.512452000
C	-7.085669000	0.041952000	1.934935000
C	-8.458878000	-0.529134000	2.212142000
C	1.885849000	-0.148642000	1.823857000
C	4.002110000	1.124994000	2.010405000
C	-5.137110000	1.339759000	2.737504000
C	-6.397785000	0.789470000	2.934674000
C	2.225715000	-0.807932000	3.057303000
C	4.338109000	0.477025000	3.191168000
C	1.270324000	-1.831928000	3.616666000
C	3.420988000	-0.488199000	3.694921000
C	5.623076000	0.774042000	3.932571000
C	-4.428692000	2.122027000	3.814445000
H	-4.220401000	-1.129224000	-6.716602000
H	-3.766496000	-2.706212000	-6.051708000
H	-1.464971000	-1.151533000	-5.976172000
H	-5.177832000	-1.843169000	-5.399953000
H	2.276711000	-4.032482000	-4.269363000
H	0.318907000	4.450649000	-4.894372000
H	-0.038200000	0.043171000	-4.333882000
H	-3.632785000	7.070560000	-2.955022000
H	3.059747000	5.126645000	-4.739278000
H	-4.764211000	4.943337000	-3.758167000
H	2.121758000	6.262270000	-3.756162000
H	3.590395000	-1.889660000	-3.958843000
H	-1.181332000	2.621595000	-4.179225000
H	0.205840000	-4.378116000	-2.914942000
H	-4.844738000	-0.723371000	-3.344039000
H	3.515542000	5.418620000	-3.046207000
H	-4.165931000	2.777120000	-2.646768000
H	-1.997568000	6.913099000	-1.073118000
H	-1.222606000	-4.684200000	-1.316028000
H	2.737650000	-0.191377000	-2.311900000
H	2.952301000	3.640218000	-1.587340000
H	-5.165594000	-0.610070000	-1.429283000
H	-1.049056000	6.647426000	0.837455000
H	-3.102842000	-4.711728000	0.330569000
H	-6.940235000	-0.708921000	-0.074564000
H	3.224943000	2.385129000	-0.111851000
H	-3.617350000	-2.588191000	1.618768000
H	0.379977000	6.118123000	2.817241000
H	-2.265549000	-0.534380000	1.137093000
H	4.675734000	1.884188000	1.597069000
H	-0.160021000	1.917584000	1.893113000
H	0.812964000	3.678355000	3.377886000
H	-6.885556000	0.937944000	3.905583000
H	3.666092000	-1.008003000	4.628324000
Co	-2.220517000	1.911879000	-0.410328000
Co	0.148831000	0.070102000	-0.505380000
N	-0.808461000	1.042871000	-1.940834000
N	1.108642000	-1.323112000	-1.721761000
N	-2.832314000	3.615329000	-1.301743000
N	-3.433322000	0.554599000	-1.326658000
N	-1.081037000	-1.443235000	-0.303684000
N	1.442590000	1.465143000	-0.656456000
N	-1.075114000	3.246436000	0.590040000
O	-3.285368000	1.698396000	1.311921000
O	0.757269000	-0.472757000	1.238415000
H	6.208451000	1.554991000	3.424543000
H	5.428983000	1.120240000	4.962051000
H	6.263354000	-0.121054000	4.013691000
H	1.661843000	-2.276190000	4.543713000
H	0.286915000	-1.383474000	3.833544000
H	1.084433000	-2.639829000	2.890514000
H	-4.200557000	3.145301000	3.474634000
H	-5.036231000	2.181081000	4.729913000
H	-3.457485000	1.664857000	4.065480000
H	-8.452225000	-1.209362000	3.081373000
H	-9.193607000	0.263447000	2.436167000
H	-8.838766000	-1.096893000	1.349312000

==========

Complex B

C	-4.319398000	-1.430997000	-5.828205000
C	-2.058631000	-0.501166000	-5.107525000
C	-3.413942000	-0.768152000	-4.811295000
C	-1.232903000	0.141483000	-4.184266000
C	2.015408000	-3.413404000	-3.697098000
C	0.776486000	3.864086000	-3.987597000
C	2.650371000	-2.157433000	-3.550427000
C	3.100169000	4.903495000	-3.867525000
C	-4.169841000	5.050811000	-2.940678000
C	-3.550721000	6.245163000	-2.502449000
C	-0.187653000	2.958501000	-3.543495000
C	-3.891011000	-0.391241000	-3.548603000
C	0.893486000	-3.683511000	-2.915094000
C	2.033193000	3.961719000	-3.349829000
C	-1.710542000	0.551015000	-2.913014000
C	-3.817586000	3.851720000	-2.330288000
C	-3.067838000	0.241177000	-2.588490000
C	-2.617793000	6.167671000	-1.469095000
C	2.125985000	-1.244169000	-2.642069000
C	0.045826000	2.101931000	-2.437351000
C	0.416183000	-2.721987000	-2.000152000
C	2.264858000	3.141482000	-2.237273000
C	-2.312329000	4.923457000	-0.879815000
C	1.296195000	2.230956000	-1.755650000
C	-1.393036000	-4.151153000	-0.932595000
C	-0.735680000	-2.916302000	-1.120908000
C	-4.572911000	0.109082000	-0.765724000
C	-2.446017000	-4.247669000	-0.023743000
C	-1.369058000	4.736610000	0.222062000
C	-0.794696000	5.790325000	0.964335000
C	2.410181000	1.632416000	0.248987000
C	-2.822076000	-3.096758000	0.700554000
C	-2.138732000	-1.904962000	0.463236000
C	-5.119769000	0.394951000	0.530205000
C	-6.347048000	-0.242134000	0.876980000
C	0.050699000	5.506076000	2.036343000
C	-0.290133000	3.160798000	1.583488000
C	-4.444721000	1.223345000	1.509916000
C	2.676911000	0.890078000	1.448531000
C	0.302306000	4.156251000	2.359647000
C	-6.950684000	-0.087785000	2.119758000
C	-8.265437000	-0.755284000	2.461227000
C	1.816446000	-0.173732000	1.927908000
C	3.798379000	1.291679000	2.231551000
C	-5.071890000	1.362605000	2.807479000
C	-6.281965000	0.729948000	3.072858000
C	2.154141000	-0.779633000	3.198693000
C	4.125629000	0.690557000	3.441743000
C	1.258926000	-1.879155000	3.712167000
C	3.275294000	-0.352837000	3.902781000
C	5.333636000	1.115822000	4.248350000
C	-4.371833000	2.213237000	3.837218000
H	-4.384164000	-0.849108000	-6.764496000
H	-3.956322000	-2.436585000	-6.104728000
H	-1.647141000	-0.797246000	-6.078480000
H	-5.342957000	-1.546646000	-5.439415000
H	2.388017000	-4.152740000	-4.410237000
H	0.553565000	4.506018000	-4.846640000
H	-0.190152000	0.341614000	-4.437212000
H	-3.789365000	7.205543000	-2.965821000
H	3.520208000	4.564298000	-4.831823000
H	-4.910838000	5.054825000	-3.743366000
H	2.699910000	5.917917000	-4.035722000
H	3.535583000	-1.895257000	-4.134485000
H	-1.151557000	2.898805000	-4.051771000
H	0.371128000	-4.637115000	-3.019071000
H	-4.945846000	-0.563617000	-3.315766000
H	3.938161000	4.991291000	-3.158679000
H	-4.262387000	2.902124000	-2.636569000
H	-2.110109000	7.070315000	-1.121929000
H	-1.060646000	-5.034839000	-1.481678000
H	2.578946000	-0.260131000	-2.500037000
H	3.241688000	3.191184000	-1.747470000
H	-5.099508000	-0.686965000	-1.318368000
H	-1.031437000	6.826404000	0.712661000
H	-2.957778000	-5.200979000	0.131799000
H	-6.828014000	-0.873781000	0.119324000
H	3.038147000	2.529855000	0.119617000
H	-3.635277000	-3.117392000	1.428258000
H	0.496722000	6.315730000	2.619776000
H	-2.400897000	-0.988089000	0.994104000
H	4.422892000	2.108897000	1.848770000
H	-0.116030000	2.103346000	1.791596000
H	0.953003000	3.877075000	3.190204000
H	-6.737067000	0.865720000	4.062393000
H	3.510168000	-0.841092000	4.857288000
Co	-2.268407000	2.055261000	-0.442937000
Co	0.133192000	-0.188209000	-0.608247000
N	-0.906158000	1.187091000	-1.946340000
N	1.034588000	-1.490515000	-1.868995000

N	-2.913306000	3.757596000	-1.319630000
N	-3.501240000	0.655562000	-1.311481000
N	-1.126601000	-1.788372000	-0.431279000
N	1.475610000	1.375513000	-0.648113000
N	-1.099936000	3.419565000	0.527203000
O	-3.310031000	1.821974000	1.300068000
O	0.758479000	-0.592903000	1.299506000
H	5.841097000	1.976277000	3.784535000
H	5.061130000	1.408892000	5.277955000
H	6.079114000	0.304909000	4.338754000
H	1.609322000	-2.260290000	4.684388000
H	0.220733000	-1.525548000	3.824058000
H	1.212318000	-2.718247000	2.998432000
H	-4.215993000	3.238846000	3.464091000
H	-4.946226000	2.259789000	4.775852000
H	-3.365391000	1.820708000	4.058064000
H	-8.180301000	-1.409350000	3.347500000
H	-9.057815000	-0.019245000	2.688463000
H	-8.625716000	-1.377122000	1.626754000

==========

Complex C

C	-4.153755000	-1.825119000	-5.626349000
C	-2.099237000	-0.411265000	-5.108478000
C	-3.339148000	-0.954179000	-4.693899000
C	-1.334881000	0.390739000	-4.261920000
C	2.018149000	-2.992001000	-3.757397000
C	0.879487000	4.027705000	-3.823643000
C	2.585981000	-1.722593000	-3.553693000
C	3.244593000	4.918739000	-3.523313000
C	-4.283331000	4.629950000	-3.112538000
C	-3.525162000	5.792990000	-2.904228000
C	-0.162778000	3.170809000	-3.461507000
C	-3.785415000	-0.661121000	-3.398345000
C	0.898917000	-3.351719000	-3.004784000
C	2.099365000	4.017437000	-3.113589000
C	-1.789465000	0.702639000	-2.954924000
C	-4.030878000	3.513769000	-2.307786000
C	-3.041597000	0.169795000	-2.532276000
C	-2.559307000	5.795176000	-1.893913000
C	2.006071000	-0.867571000	-2.615475000
C	-0.040777000	2.275410000	-2.374977000
C	0.364613000	-2.443942000	-2.072100000
C	2.222907000	3.140642000	-2.025705000
C	-2.382862000	4.639073000	-1.110136000
C	1.169234000	2.286503000	-1.619696000
C	-1.423379000	-3.963402000	-1.097494000
C	-0.785390000	-2.714929000	-1.206560000
C	-4.589552000	0.231563000	-0.711071000
C	-2.467712000	-4.131537000	-0.186742000
C	-1.434984000	4.546490000	0.017645000
C	-0.919662000	5.672957000	0.683862000
C	2.167125000	1.600624000	0.410220000
C	-2.841049000	-3.038812000	0.613476000
C	-2.177444000	-1.821999000	0.455661000
C	-5.067849000	0.536213000	0.598459000
C	-6.355060000	0.045100000	0.974715000
C	-0.101779000	5.498128000	1.803567000
C	-0.378481000	3.118515000	1.535052000
C	-4.295705000	1.302038000	1.545645000
C	2.498348000	0.788534000	1.533487000
C	0.165161000	4.194416000	2.243498000
C	-6.892884000	0.261189000	2.235581000
C	-8.256058000	-0.264378000	2.628555000
C	1.881923000	-0.497206000	1.805345000
C	3.500729000	1.291945000	2.423342000
C	-4.852723000	1.517676000	2.858081000
C	-6.108521000	1.003382000	3.163768000
C	2.331182000	-1.219562000	2.980896000
C	3.920746000	0.594713000	3.543879000
C	1.700579000	-2.557481000	3.270676000
C	3.310845000	-0.671675000	3.795456000
C	4.985951000	1.129520000	4.475101000
C	-4.046236000	2.305107000	3.859926000
H	-4.473027000	-1.272045000	-6.526402000
H	-3.576462000	-2.696989000	-5.977820000
H	-1.723219000	-0.635775000	-6.111572000
H	-5.061060000	-2.205117000	-5.133414000
H	2.440944000	-3.685501000	-4.487449000
H	0.749806000	4.705578000	-4.672769000
H	-0.369063000	0.772227000	-4.596159000
H	-3.678078000	6.679194000	-3.524301000
H	3.513881000	4.776619000	-4.582971000
H	-5.055772000	4.584820000	-3.882848000
H	2.983424000	5.983798000	-3.401109000
H	3.464818000	-1.395464000	-4.112406000
H	-1.099490000	3.181125000	-4.022532000
H	0.436331000	-4.330258000	-3.141983000
H	-4.732417000	-1.094408000	-3.067292000
H	4.144962000	4.728330000	-2.920643000
H	-4.586688000	2.582632000	-2.437898000
H	-1.935231000	6.674966000	-1.728214000
H	-1.086649000	-4.801741000	-1.709150000
H	2.412854000	0.126439000	-2.427039000
H	3.181801000	3.094946000	-1.503325000
H	-5.285190000	-0.337237000	-1.341159000
H	-1.192632000	6.674781000	0.349273000
H	-2.969478000	-5.096770000	-0.090719000
H	-6.924977000	-0.527901000	0.233981000
H	2.723576000	2.547721000	0.357151000
H	-3.639989000	-3.118200000	1.352334000
H	0.299135000	6.363711000	2.335922000
H	-2.432473000	-0.948343000	1.052371000
H	3.951590000	2.264543000	2.191874000
H	-0.207187000	2.084387000	1.834764000
H	0.783974000	4.000992000	3.121087000
H	-6.512594000	1.183816000	4.166769000
H	3.632287000	-1.239093000	4.677149000
Co	-2.156774000	1.755096000	-0.387516000
Co	-0.017012000	-0.105532000	-0.494714000
N	-1.067959000	1.395984000	-1.983001000
N	0.915051000	-1.199775000	-1.885942000
N	-3.107203000	3.505962000	-1.325342000
N	-3.410080000	0.556034000	-1.224083000
N	-1.181248000	-1.637568000	-0.448174000
N	1.265311000	1.378230000	-0.539905000
N	-1.140447000	3.278031000	0.430767000
O	-3.122003000	1.816788000	1.284691000
O	0.963758000	-1.026852000	1.065829000
H	5.342270000	2.119156000	4.151100000
H	4.612254000	1.232643000	5.508591000
H	5.862771000	0.460541000	4.521158000
H	2.108014000	-3.000457000	4.191787000
H	0.607439000	-2.464636000	3.376481000
H	1.864973000	-3.262438000	2.438976000
H	-3.824794000	3.317614000	3.484268000
H	-4.580590000	2.395774000	4.817216000
H	-3.069771000	1.829178000	4.047563000
H	-8.199782000	-0.931904000	3.505546000
H	-8.948211000	0.552689000	2.895724000
H	-8.717948000	-0.833731000	1.807867000
H	-0.945698000	0.653413000	0.467688000

==========

APPENDIX B (CHAPTER 5)

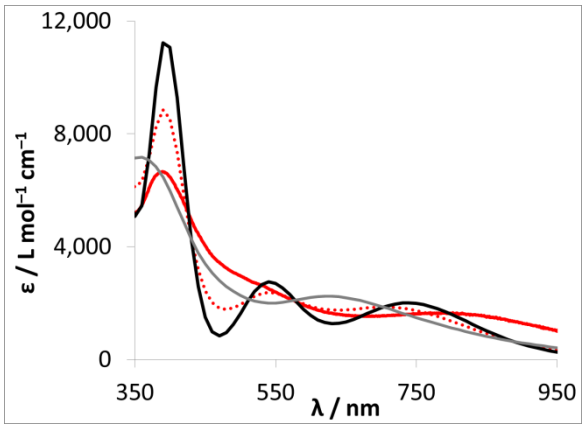

Figure B1. Plot of TD-DFT predicted spectrum of isomer 1 (black) and isomer 2 (gray) for species **2**.

Neither individual isomer's spectrum matched the intensities well for the experimental spectrum (solid red). These two species are predicted to be isoenergetic $\Delta G \sim 0.4$ kcal mol^{-1}, so we averaged their spectra (dotted red), and this average spectrum matches experiment quite well.

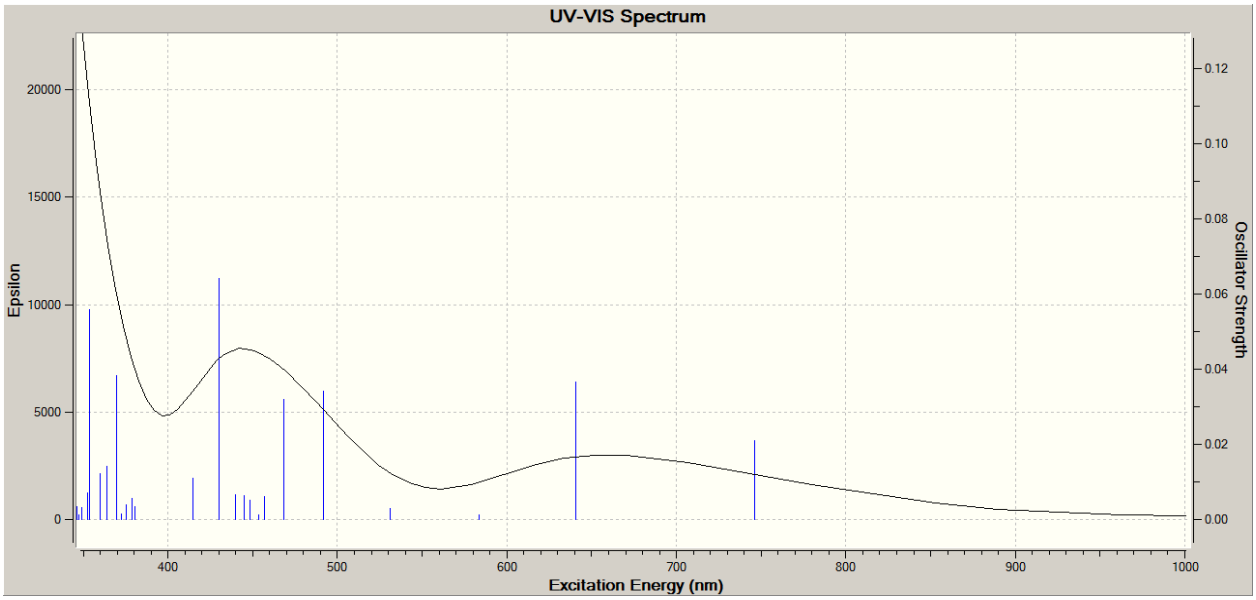

Figure B2. Simulated UV-visible spectrum for **1** with individual transitions shown as sticks. A half-width at half-max of 0.2 eV was employed for the Gaussian fittings.

Table B1. Assignments for TD-DFT transitions of **1**. Contributions > 10% are shown. Orbitals are only listed once with label, then labels are repeated thereafter.

Excited State	**λ / nm**	**Osc. Str.**	**% Cont.**	**Occ. MO**	**Unocc. MO**
2	746	0.0211	43	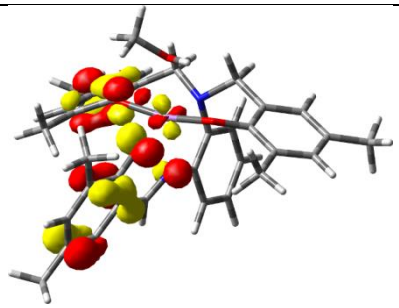 157α	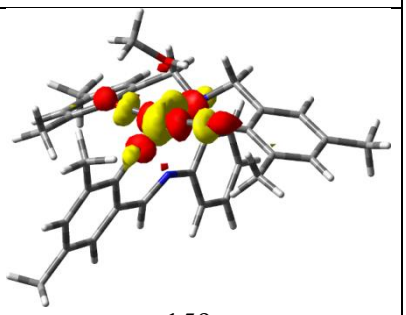 159α
			31	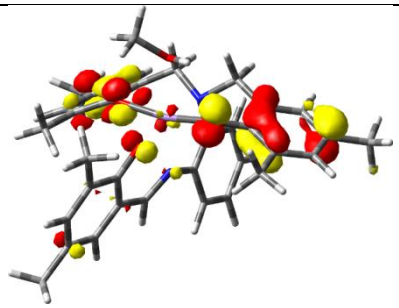 158α	159α
			18	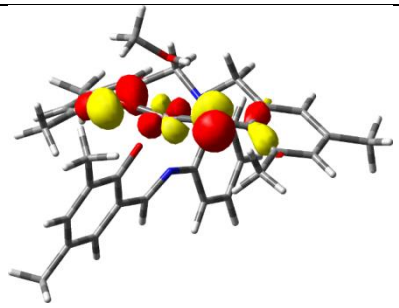 151α	159α
3	640	0.0367	64	158α	159α
			21	157α	159α
			10	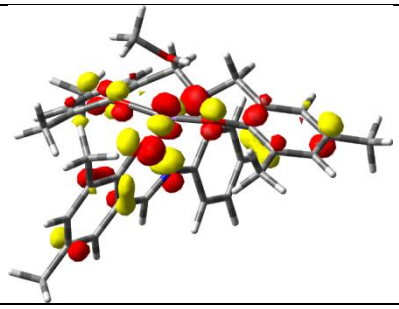	159α

				156α	
6	492	0.0342	63	151α	159α
			17	157α	159α
			10	156α	159α
7	468	0.0320	44	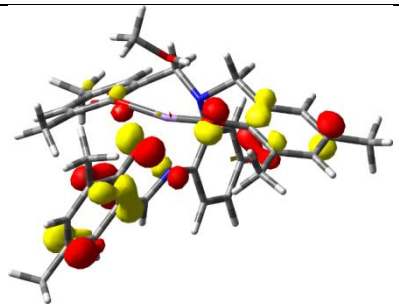 154β	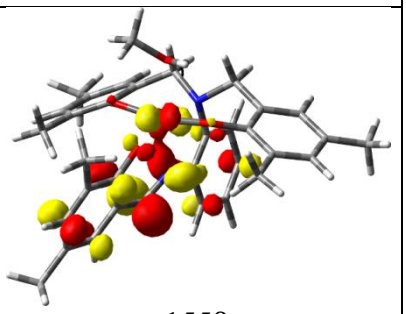 155β
			21	157α	159α
			16	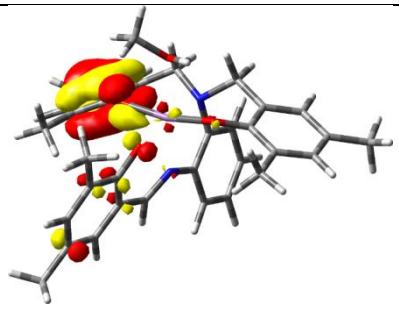 153β	155β
13	430	0.0640	35	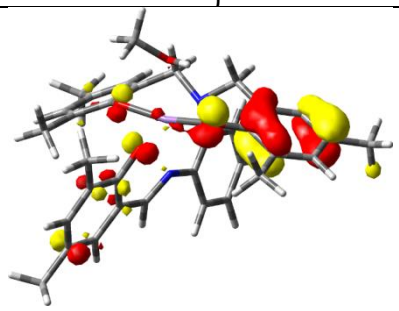 152β	155β

			19	157α	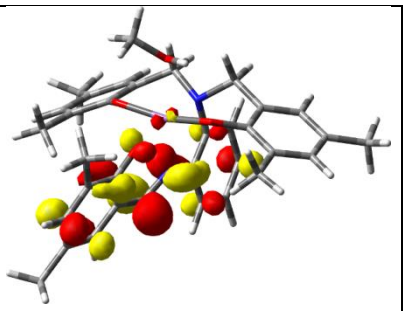 160α
			15	156α	160α
			10	153β	155β

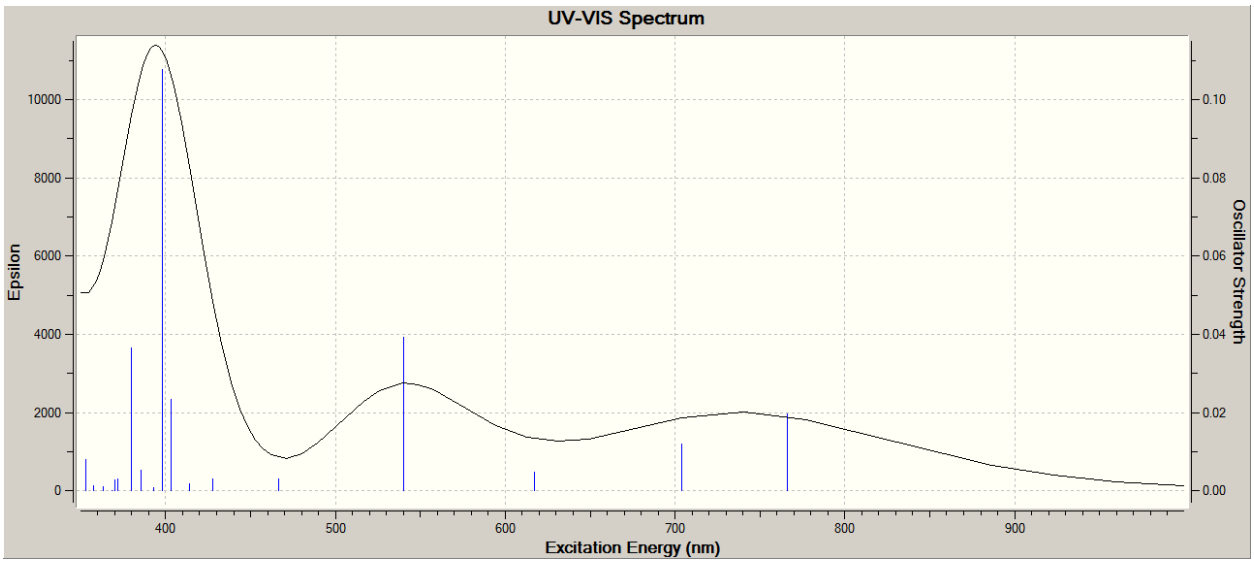

Figure B3. Simulated UV-visible spectrum for isomer 1 of **2** with individual transitions shown as sticks. A half-width at half-max of 0.2 eV was employed for the Gaussian fittings.

Table B2. Assignments for TD-DFT transitions of Isomer 1 for **2**. Contributions > 10% are shown. Orbitals are only listed once with label, then labels are repeated thereafter.

Excited State	**λ / nm**	**Osc. Str.**	**% Cont.**	**Occ. MO**	**Unocc. MO**
1	766	0.0196	44	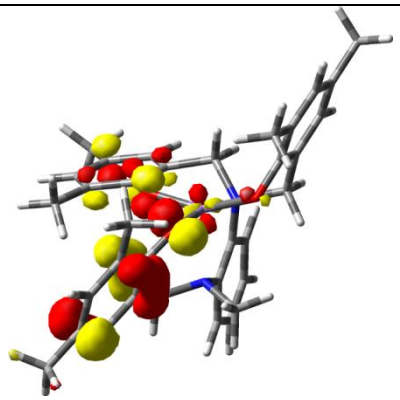 154α	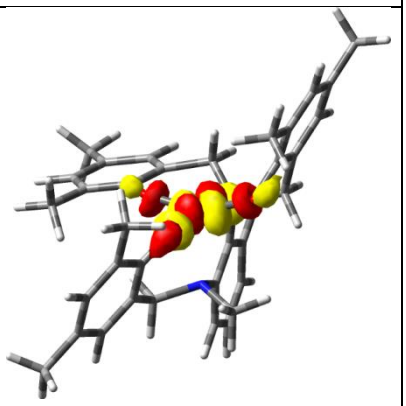 155α
			19	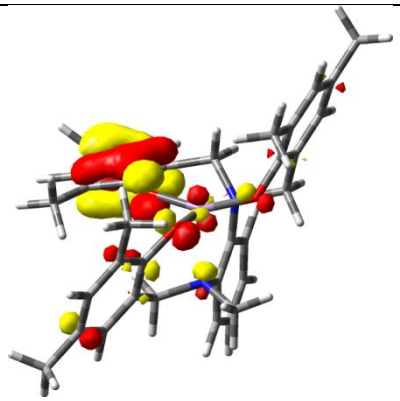 153α	155α
			18	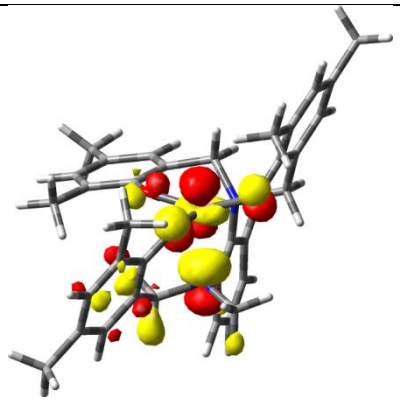 151α	155α

			10	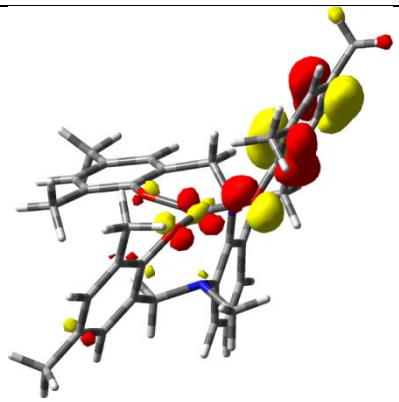 152α	155α
2	704	0.0119	38	154α	155α
			28	153α	155α
			20	151α	155α
4	540	0.0392	49	153α	155α
			28	151α	155α
			18	152α	155α
9	398	0.1078	68	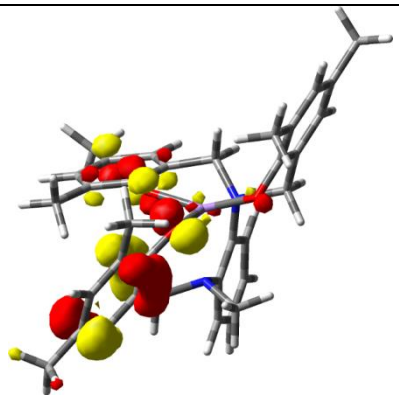 150β	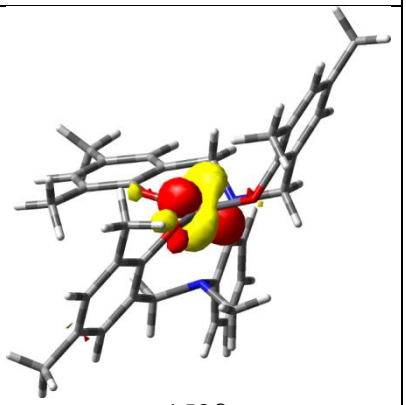 152β

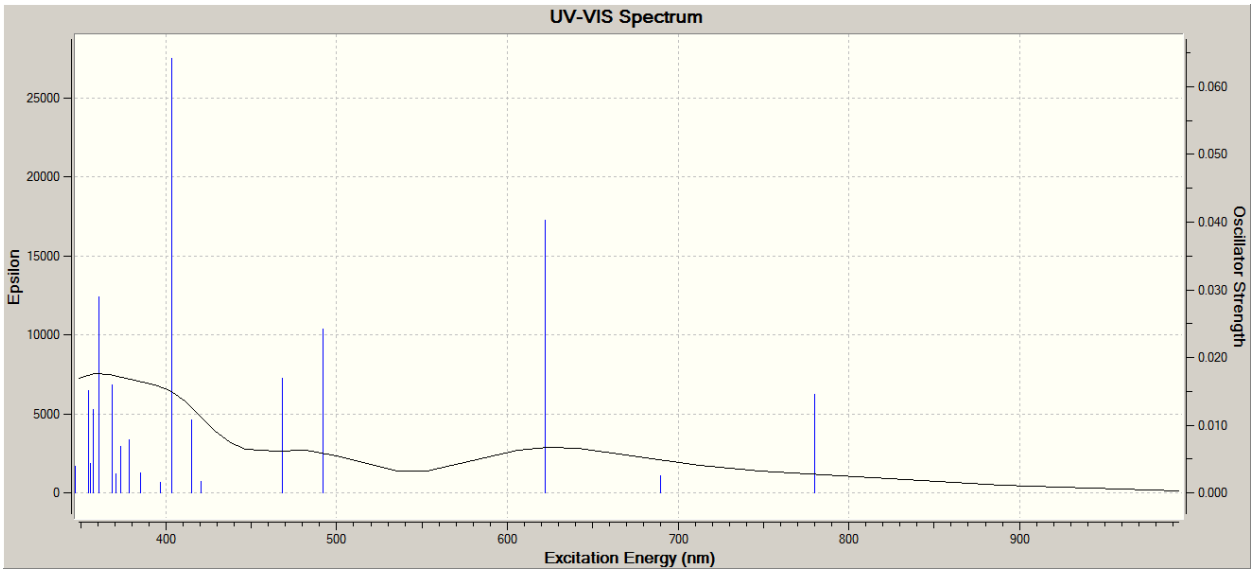

Figure B4. Simulated UV-visible spectrum for isomer 2 of **2** with individual transitions shown as sticks. A half-width at half-max of 0.2 eV was employed for the Gaussian fittings

Table B3. Assignments for TD-DFT transitions of Isomer 2 for **2**. Contributions > 10% are shown. Orbitals are only listed once with label, then labels are repeated thereafter.

Excited State	**λ / nm**	**Osc. Str.**	**% Cont.**	**Occ. MO**	**Unocc. MO**
1	780	0.0145	46	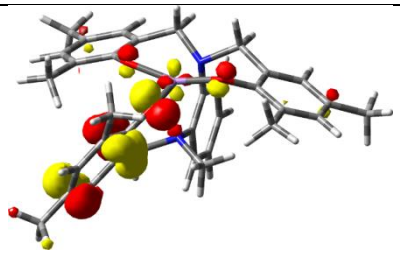 154α	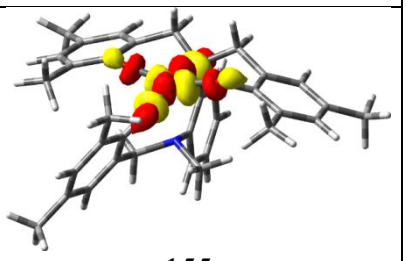 155α
			30	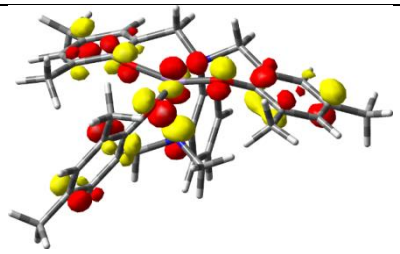 152α	155α

			17	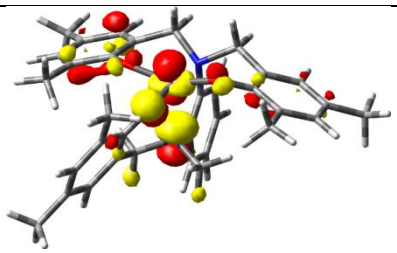 150α	155α
3	622	0.0403	68	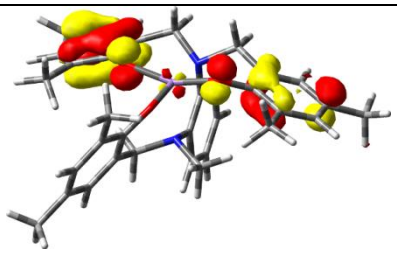 153α	155α
			19	154α	155α
4	492	0.0242	46	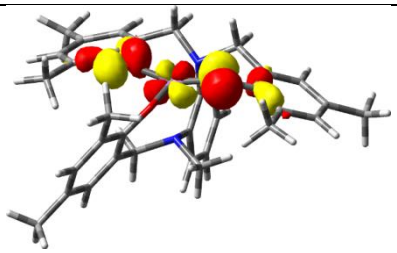 147α	155α
			22	150α	155α
			14	153α	155α
5	468	0.0170	37	150α	155α
			23	152α	155α
			21	147α	155α

Table B4. Cartesian coordinates (Å) for all optimized structures.

[$^{HS}Mn^{III}(L^1)(CH_3OH)]^0$ *S*=2

Mn	0.01004400	-0.44509200	1.01807900
N	1.38563600	1.24523400	0.69499500
N	-0.15048800	-0.15029800	-1.13460200
C	1.52526000	1.52439700	-0.74095000
C	2.41602700	2.49683900	-1.19806400
C	0.75065800	0.79025400	-1.66374700
C	2.57244300	2.73498300	-2.56218100
H	3.00139200	3.07113800	-0.48754100
C	0.94289600	1.01630100	-3.03865800
C	1.83988600	1.98175500	-3.48225100
H	3.27315200	3.49036300	-2.90251700
H	0.40231600	0.41663300	-3.76267900
H	1.97437700	2.13908900	-4.54789800
C	0.83118700	2.43652300	1.43923600
H	0.76571500	2.11968100	2.48617200
H	1.55258300	3.26017200	1.38567400
C	2.71571100	0.87349700	1.31325500
H	2.49026900	0.63654100	2.35855900
H	3.37525200	1.74879900	1.31018500
C	-0.50996400	2.88981600	0.93669600
C	-1.58398600	1.97764300	0.97064800
C	-0.71882200	4.20220300	0.50157300
C	-2.87821500	2.41074600	0.59310800
C	-1.98402600	4.64892400	0.11271300
H	0.12407200	4.89006300	0.47708800
C	-3.04515800	3.73279000	0.17696500
H	-4.04247700	4.06180100	-0.11033600
O	-1.40403400	0.72253700	1.40897600
C	-1.18802600	-0.56273600	-1.80497000
H	-1.37530600	-0.15385500	-2.80288400
C	-2.16542300	-1.51239300	-1.35306100
C	-3.21689100	-1.81477400	-2.26092500
C	-2.13890900	-2.14837000	-0.06625300
C	-4.22142700	-2.71257600	-1.96075700
H	-3.21533600	-1.31508800	-3.22758400

C	-3.18248100	-3.07813100	0.24292500
C	-4.17384300	-3.33342400	-0.68981300
H	-4.95613700	-4.04457700	-0.42904100
O	-1.20701700	-1.95253300	0.83134100
O	0.37453200	-0.59385800	3.28366100
C	-0.65314600	-0.66438200	4.28500400
H	-1.22674700	-1.59256500	4.20062000
H	-0.21935100	-0.58868000	5.28706400
H	-1.31450200	0.18226500	4.10525800
C	-3.16603900	-3.75832500	1.58674800
H	-2.25090500	-4.34553000	1.72384200
H	-3.18777500	-3.02644200	2.40207500
H	-4.02407200	-4.42640100	1.69861600
C	-5.33267500	-3.03161300	-2.93215100
H	-5.34711000	-4.09675100	-3.19230600
H	-6.31663400	-2.79401400	-2.51056400
H	-5.22253900	-2.46396800	-3.86026300
C	-4.04162700	1.45529200	0.66876400
H	-3.87591500	0.57194100	0.04349400
H	-4.18890100	1.08772600	1.69096100
H	-4.96692200	1.93966500	0.34473600
C	-2.20501800	6.06145800	-0.37742700
H	-2.34143300	6.09541500	-1.46581900
H	-3.10035900	6.50740400	0.06928400
H	-1.35369700	6.70435900	-0.13535100
C	3.38553100	-0.28251100	0.62666300
C	4.67789800	-0.17283400	0.10476300
C	2.69619400	-1.50908600	0.55017700
C	5.32099300	-1.26295600	-0.48710200
H	5.19309800	0.78346200	0.16923100
C	3.32506300	-2.62669200	-0.04895900
C	4.62081900	-2.47760400	-0.54659700
H	5.10283000	-3.34140300	-1.00154000
O	1.47205300	-1.64229000	1.08212200
C	2.59571600	-3.94352600	-0.12137900
H	2.34277800	-4.31722900	0.87764600
H	1.64845900	-3.84460200	-0.66277700
H	3.20251900	-4.70082700	-0.62528000
C	6.71025900	-1.13635100	-1.06880200
H	7.32739400	-2.00903400	-0.82982500
H	6.68486700	-1.05323500	-2.16290100
H	7.22237200	-0.24824400	-0.68691000
H	0.93609300	-1.38297200	3.31884100

$[^{LS}Mn^{III}(L^{1})(CH_3OH)]^0$ *S*=1

Mn	-0.11291200	-0.26236000	-0.92202600
N	1.39461000	1.17756700	-0.69014400
N	-0.30011900	-0.08734900	1.01366400
C	1.55512900	1.40712200	0.75155100
C	2.54312500	2.25258200	1.25572800
C	0.67126000	0.74613400	1.62312200
C	2.67258000	2.44490700	2.62916700
H	3.21953800	2.76147000	0.57723700
C	0.81974100	0.93533700	3.00813700
C	1.80828600	1.77971000	3.50200000
H	3.44585400	3.10117200	3.01457300
H	0.17622100	0.41776800	3.70955000
H	1.90790900	1.91232900	4.57466500
C	2.66948000	0.66763600	-1.32298100
H	2.40053600	0.45122100	-2.36206400
H	3.41000900	1.47540100	-1.33731300
C	1.02100600	2.45965000	-1.40225100
H	0.90703800	2.18053900	-2.45524400
H	1.86327700	3.15731500	-1.33606300
C	3.24469600	-0.54191100	-0.64485300
C	2.41789500	-1.66365900	-0.43647600
C	4.59247200	-0.58347600	-0.27071800
C	2.97448000	-2.83575700	0.13700100
C	5.16071600	-1.72639800	0.29470500
H	5.21094100	0.29712300	-0.43474900
C	4.32541300	-2.83915000	0.48364400
H	4.74411500	-3.74367300	0.92235700
O	1.13092500	-1.65992500	-0.79390800
C	-1.25763600	-0.66083800	1.69715900
H	-1.32838600	-0.45070400	2.76403100
C	-2.24518200	-1.55887300	1.19755900
C	-3.18262500	-2.06289100	2.14553500
C	-2.31783000	-1.98705800	-0.17331500
C	-4.16815100	-2.96097700	1.80201600
H	-3.10229800	-1.71953800	3.17485000
C	-3.34305600	-2.92880300	-0.52243900
C	-4.21933500	-3.37908300	0.44703700
H	-4.98984300	-4.09057700	0.15401300
O	-1.52143500	-1.57439600	-1.11505900
O	0.03807700	-0.25664900	-3.02009600
C	0.03929600	-1.48899200	-3.77329000
H	-0.82827600	-2.09709900	-3.51243900
H	0.04815100	-1.26127600	-4.84216600
H	0.95033800	-2.01623900	-3.49660500
C	-3.43443000	-3.39764200	-1.95059300
H	-3.59114700	-2.55665300	-2.63553400
H	-2.50677800	-3.88713600	-2.26802700
H	-4.25804200	-4.10500700	-2.07875300
C	-5.16050400	-3.49462100	2.80692500
H	-6.19160200	-3.25589300	2.52011500
H	-5.09922000	-4.58608400	2.89306800
H	-4.98485900	-3.07192500	3.80002100
C	2.10244200	-4.04676600	0.34783900
H	1.23580500	-3.81092900	0.97523100
H	1.70179900	-4.42271800	-0.60090500
H	2.66299300	-4.85563200	0.82480800
C	6.61506500	-1.76687400	0.70451200
H	6.72867800	-1.82848300	1.79410000
H	7.13004700	-2.63763200	0.28252600
H	7.14682800	-0.87146000	0.36963900
C	-0.22891000	3.10277100	-0.87726200
C	-0.24594800	4.43384400	-0.44834200
C	-1.41507100	2.34431100	-0.88390900
C	-1.43034300	5.04929300	-0.03632400
H	0.68292900	5.00114500	-0.44779700
C	-2.62850100	2.94765800	-0.47379600
C	-2.60576400	4.28213100	-0.06436300
H	-3.54168200	4.74236200	0.24885200
O	-1.40606100	1.07491400	-1.31297600
C	-3.90802300	2.15130500	-0.50119400
H	-4.16409600	1.84007700	-1.52099200
H	-3.82066000	1.23162000	0.08736000
H	-4.74314200	2.73668500	-0.10650900
C	-1.45016000	6.48291500	0.44235200
H	-2.26758900	7.05008300	-0.01664700
H	-1.59031000	6.54573600	1.52894400
H	-0.51322000	6.99485500	0.20403700
H	-0.77220100	0.24642600	-3.20917300

[^{HS}Mn^{III}(L^{1})(CH$_3$OH)]$^+$ *S*=3/2

Mn	-0.02484200	-0.43457900	0.98078100
N	1.34076900	1.23802600	0.67982500
N	-0.21368300	-0.13279900	-1.14603800
C	1.48700000	1.51292000	-0.76259200
C	2.38476300	2.47953700	-1.21764400
C	0.70409200	0.78526200	-1.68344800
C	2.54583300	2.70729200	-2.58258400
H	2.97040600	3.05606800	-0.50961800
C	0.90028400	1.00242000	-3.05896400
C	1.80799200	1.95709600	-3.50197600
H	3.25351000	3.45474200	-2.92483600
H	0.35051800	0.41074900	-3.78220100
H	1.94522800	2.11168600	-4.56725200
C	0.77977900	2.44015500	1.41648400
H	0.73799200	2.14258800	2.46982000
H	1.48943200	3.26929600	1.32980900
C	2.66670900	0.89428500	1.30911300
H	2.44471100	0.60899800	2.34276600
H	3.30177400	1.78521700	1.34374600
C	-0.57450300	2.85794700	0.92449700
C	-1.63077400	1.93057400	1.01792000
C	-0.81749800	4.14724100	0.44420100
C	-2.94358400	2.31347000	0.65715200
C	-2.10276600	4.54836500	0.06972000
H	0.00828700	4.85128400	0.37278800
C	-3.14449500	3.61508600	0.19581700
H	-4.15371400	3.91544300	-0.07848600
O	-1.39976900	0.69676900	1.50529700
C	-1.23998700	-0.57720900	-1.81360500
H	-1.42287800	-0.20524100	-2.82520200
C	-2.20612100	-1.52178500	-1.32767600
C	-3.27999700	-1.83893400	-2.19993900
C	-2.14306500	-2.14047500	-0.03707000
C	-4.27424600	-2.73301400	-1.85014200
H	-3.30974900	-1.35526700	-3.17341700
C	-3.16867800	-3.06022000	0.32829400
C	-4.18857200	-3.33110100	-0.57215700
H	-4.96178100	-4.03735000	-0.27602200
O	-1.16281000	-1.94046600	0.82209200
O	0.52201100	-0.70204200	3.19343800
C	-0.40045400	-0.51363100	4.28814600
H	-1.04117400	-1.39104900	4.41179400
H	0.14744400	-0.31729900	5.21372800
H	-1.01339600	0.34640600	4.02547200
C	-3.10978200	-3.72225900	1.67988300
H	-2.19700400	-4.31806400	1.79081200
H	-3.09798900	-2.97940000	2.48476700
H	-3.96927800	-4.38004500	1.82952900
C	-5.41448000	-3.06902100	-2.78006900
H	-5.43222500	-4.13850500	-3.01937100
H	-6.38296300	-2.82705500	-2.32763500
H	-5.33644000	-2.51666000	-3.72004400
C	-4.08542200	1.34052000	0.79953200
H	-3.92742200	0.44450600	0.19116400
H	-4.19023900	1.00073700	1.83589100
H	-5.02857700	1.80101800	0.49480400
C	-2.36801100	5.93418300	-0.46899600
H	-2.53458100	5.91634000	-1.55320500
H	-3.26207300	6.37541800	-0.01620200
H	-1.52573600	6.60455500	-0.27721800
C	3.40348500	-0.21135700	0.60583900
C	4.72098100	-0.07749500	0.23311400
C	2.74082800	-1.47539300	0.39018900
C	5.43949900	-1.14951000	-0.35730000
H	5.23250700	0.86599600	0.39882500
C	3.46247200	-2.57975500	-0.21055500
C	4.78408800	-2.38357500	-0.56108900
H	5.33895800	-3.20127600	-1.01163800
O	1.51759700	-1.65505400	0.74212800
C	2.74990000	-3.87996900	-0.42663400
H	2.37976400	-4.28404800	0.52160700
H	1.87311000	-3.74087900	-1.06807300
H	3.41053600	-4.61577000	-0.88808600
C	6.86303900	-0.95625200	-0.78408900
H	7.39423700	-1.90732400	-0.86014100
H	6.89568600	-0.47929700	-1.77310200
H	7.40080500	-0.29878800	-0.09528500
H	1.03766200	-1.50588400	3.34982100

[Mn^{IV}(L^{1})(CH$_3$OH)]$^+$ *S*=3/2

Mn	0.01636700	-0.42313600	-0.89047400
N	-1.33940000	1.19092100	-0.72527700
N	0.20523300	-0.17191200	1.03248300
C	-1.53441000	1.44092100	0.71133300
C	-2.45561000	2.37322600	1.18439500
C	-0.76627100	0.68825000	1.60803000
C	-2.63554800	2.53492900	2.55669800
H	-3.04322800	2.96591900	0.49272400
C	-0.97655700	0.82650600	2.98753700
C	-1.90432500	1.75203500	3.45337100
H	-3.35889000	3.25522700	2.92275600
H	-0.43651300	0.20822900	3.69454800
H	-2.06273400	1.85442300	4.52155200
C	-0.79385900	2.41560300	-1.43892100
H	-0.69072800	2.11574300	-2.48678900
H	-1.55126800	3.20339500	-1.39149800
C	-2.65343300	0.82159100	-1.40123300
H	-2.38430200	0.55811700	-2.42809100
H	-3.27717400	1.71859600	-1.44790700
C	0.50871000	2.90659200	-0.88521800
C	1.58812300	2.00930800	-0.83308400
C	0.68699400	4.23538200	-0.49249300
C	2.86698700	2.45208900	-0.42648200
C	1.93582800	4.70054800	-0.07184800
H	-0.15784300	4.91877300	-0.53077400
C	3.00556900	3.79150500	-0.05848000
H	3.98776400	4.14104900	0.25243100
O	1.41602500	0.72850200	-1.22171100
C	1.22237400	-0.63969100	1.71210700
H	1.32035100	-0.32076200	2.74793000
C	2.22527500	-1.52652800	1.23162500
C	3.29141100	-1.86473600	2.10746400
C	2.16847400	-2.10431600	-0.06976100
C	4.28517300	-2.74436600	1.72640100
H	3.31291500	-1.41310100	3.09541200
C	3.17651100	-3.02073700	-0.46614100
C	4.19645200	-3.30836800	0.43163700
H	4.96860400	-4.00767300	0.11833800
O	1.17609600	-1.86000000	-0.90964100
O	-0.28552000	-0.60091400	-2.90797100
C	0.79074500	-0.57302400	-3.88663800
H	1.44386900	-1.43522200	-3.74564300
H	0.34873200	-0.57608700	-4.88367500

H	1.33997900	0.34782600	-3.71088700
C	3.11646500	-3.65214400	-1.83160400
H	2.17301000	-4.18796300	-1.97929500
H	3.18024100	-2.89520800	-2.62093900
H	3.93868700	-4.35759400	-1.96936100
C	5.42911600	-3.10751500	2.64071900
H	5.45504700	-4.18561100	2.83392400
H	6.39309000	-2.83775600	2.19526200
H	5.34759600	-2.59458600	3.60212600
C	4.04085100	1.50744700	-0.42127200
H	3.88471400	0.67211000	0.26867800
H	4.20190300	1.06958400	-1.41233200
H	4.95496100	2.02815400	-0.12597000
C	2.13620300	6.13351700	0.36061000
H	2.35087600	6.19973400	1.43385900
H	2.98092900	6.59420200	-0.16276000
H	1.24689300	6.73758200	0.16266100
C	-3.38804400	-0.28564700	-0.70847700
C	-4.74030300	-0.17122100	-0.37448400
C	-2.69526200	-1.47183600	-0.41720400
C	-5.42681500	-1.22666600	0.23103800
H	-5.26601200	0.75372100	-0.59928600
C	-3.35803500	-2.55234300	0.20920700
C	-4.71087900	-2.40204600	0.51234600
H	-5.22765100	-3.23045500	0.99227600
O	-1.39900400	-1.60712700	-0.75371500
C	-2.60810500	-3.82070900	0.52133900
H	-2.22212600	-4.29061200	-0.39012900
H	-1.74187000	-3.62388200	1.16229600
H	-3.25446800	-4.54086200	1.02874900
C	-6.89357900	-1.11748900	0.57320000
H	-7.49930600	-1.78519000	-0.05107000
H	-7.08235800	-1.39712800	1.61529300
H	-7.26309200	-0.09946100	0.42454800
H	-0.82271600	-1.40197900	-3.02753100

$[^{HS}Mn^{III}(L^1)(CH_3OH)]^+$ *S*=5/2

Mn	-0.00859900	-0.29982600	1.11033800
N	1.46873800	1.24866200	0.68379600
N	-0.19091200	-0.13737500	-1.06258200
C	1.61668500	1.42923000	-0.76147600
C	2.57930400	2.29777700	-1.27663700
C	0.77893500	0.70757700	-1.64014500
C	2.74147800	2.44246300	-2.65207500
H	3.21537900	2.86144300	-0.60316500
C	0.97789200	0.83791300	-3.02859000
C	1.94463200	1.69922900	-3.52773900
H	3.49691800	3.11847400	-3.03807700
H	0.39404800	0.24390400	-3.72157600
H	2.08503600	1.78351800	-4.60012300
C	1.00469800	2.51772000	1.36148200
H	0.92717200	2.27022200	2.42627700
H	1.77992100	3.28423300	1.25631300
C	2.76475400	0.79245400	1.31751900
H	2.52704800	0.61367400	2.37211200
H	3.49510900	1.60786100	1.28268500
C	-0.30676600	3.02767700	0.83315300
C	-1.43933800	2.19330600	0.90703300
C	-0.43167100	4.32507900	0.32711800
C	-2.70157000	2.67694900	0.49261900
C	-1.66572500	4.82630400	-0.09404100
H	0.45154000	4.95730600	0.27142700
C	-2.78302800	3.98236400	0.00635000
H	-3.75508300	4.35644600	-0.30900700
O	-1.33914000	0.95060200	1.41932300
C	-1.19098200	-0.58300800	-1.76160100
H	-1.31426500	-0.25536000	-2.79538800
C	-2.20969400	-1.50452700	-1.31688500
C	-3.17902800	-1.87163300	-2.25082000
C	-2.27348800	-2.08395100	0.02432100
C	-4.20198500	-2.78544700	-1.95289400
H	-3.13611100	-1.44113900	-3.24713500
C	-3.32996600	-3.04494900	0.32295600
C	-4.24547900	-3.35880700	-0.65477700
H	-5.03538200	-4.07001700	-0.42933400
O	-1.45306300	-1.78828200	0.94302500
O	0.17274600	-0.52908700	3.26217600
C	-0.85659200	-0.34766300	4.25806600
H	-1.50280500	-1.22780000	4.31155400
H	-0.40022200	-0.15585500	5.23217200
H	-1.43688500	0.51570600	3.93873500
C	-3.37657000	-3.64286500	1.69662600
H	-2.44641300	-4.17556100	1.92136500
H	-3.48068500	-2.86164600	2.45715300
H	-4.21161200	-4.33912600	1.79091500
C	-5.23224300	-3.16194100	-2.97494300
H	-5.21673900	-4.24279300	-3.15782000
H	-6.23872100	-2.92006200	-2.61357400
H	-5.07188200	-2.64711800	-3.92369700
C	-3.92103900	1.79764000	0.60070200
H	-3.81754100	0.89112700	-0.00530300
H	-4.08427600	1.46751000	1.63248200
H	-4.81574300	2.32923000	0.26697400
C	-1.79955000	6.22465900	-0.64968700
H	-2.04028100	6.21000200	-1.71960200
H	-2.60150200	6.77940700	-0.15043300
H	-0.87265100	6.79146900	-0.52743200
C	3.33030700	-0.43881200	0.66532800
C	4.63551700	-0.45762400	0.16707500
C	2.53964500	-1.60503500	0.59711800
C	5.18582100	-1.61256100	-0.39603500
H	5.23571300	0.44733000	0.22666100
C	3.07069500	-2.78644600	0.02575000
C	4.38064600	-2.76153500	-0.45148100
H	4.79066200	-3.67112900	-0.88570500
O	1.29917000	-1.62862400	1.11326600
C	2.22732000	-4.03300400	-0.03819200
H	1.95066600	-4.38002600	0.96392200
H	1.28974600	-3.85243700	-0.57513900
H	2.76281600	-4.84119400	-0.54254600
C	6.59019900	-1.62367300	-0.95075500
H	7.13705700	-2.51939800	-0.63808700
H	6.58704100	-1.61811800	-2.04788100
H	7.15649600	-0.74900600	-0.61942700
H	0.68606300	-1.33047800	3.44379500

$[^{HS}Mn^{III}(L^1)(CH_3OH)]^{2+}$ *S*=1

Mn	0.11718800	-0.38456500	-0.94109200
N	-1.32620400	1.16990200	-0.70708900
N	0.23556400	-0.22711100	1.03831000
C	-1.51258900	1.39587800	0.73922200
C	-2.44058300	2.31739800	1.22385500
C	-0.73548300	0.63339500	1.62393600
C	-2.62313900	2.46205400	2.59693000

H	-3.03133000	2.91748400	0.54086100
C	-0.95053100	0.76043300	3.00534900
C	-1.88508800	1.67267900	3.48232600
H	-3.34966200	3.17434900	2.97170100
H	-0.40759200	0.14415200	3.71142200
H	-2.04158600	1.76156400	4.55190800
C	-0.85889300	2.43067200	-1.42051400
H	-0.69284000	2.14135500	-2.46243800
H	-1.67466800	3.15757900	-1.40471200
C	-2.63730900	0.76502400	-1.37027700
H	-2.38527000	0.52104100	-2.40583600
H	-3.29864000	1.63494800	-1.39171000
C	0.38001500	3.04958300	-0.83907400
C	1.59360200	2.26625500	-0.82667000
C	0.40852900	4.34429300	-0.38387000
C	2.82632500	2.84700800	-0.33163200
C	1.61561000	4.93092100	0.09262700
H	-0.49761300	4.94343400	-0.39032500
C	2.79678000	4.15923200	0.10446000
H	3.71104100	4.61289800	0.47520700
O	1.57452900	1.06075000	-1.26241900
C	1.19516100	-0.77883800	1.74538800
H	1.24913700	-0.53622400	2.80480100
C	2.19583000	-1.66819800	1.26793300
C	3.16694500	-2.13573100	2.19511800
C	2.24046400	-2.11631200	-0.08344600
C	4.15461000	-3.02298100	1.81770700
H	3.11681100	-1.77981800	3.22018900
C	3.24511000	-3.03088200	-0.48261100
C	4.16496000	-3.45329300	0.46986300
H	4.93644400	-4.15311800	0.15677500
O	1.35383000	-1.72830700	-0.99225800
O	-0.13054400	-0.45317900	-3.01695000
C	0.95794300	-0.33061800	-3.97665900
H	1.62678800	-1.18882900	-3.89471100
H	0.53360900	-0.26206400	-4.97897300
H	1.48757800	0.58507200	-3.72588800
C	3.29102000	-3.51586200	-1.90716300
H	2.35898300	-4.01979500	-2.18398300
H	3.42106000	-2.68117600	-2.60428200
H	4.11652800	-4.21554400	-2.05262100
C	5.19200800	-3.52997700	2.78872400
H	5.14723700	-4.62067300	2.88040400
H	6.20398100	-3.27685100	2.45427900
H	5.04809200	-3.10172300	3.78350900
C	4.07028700	2.01372100	-0.31473400
H	3.92091700	1.10333000	0.27534200
H	4.33372000	1.68904600	-1.32716200
H	4.90916900	2.57207900	0.10364800
C	1.61890800	6.35527200	0.55446900
H	0.74121600	6.57207000	1.17130600
H	2.52137800	6.59718000	1.11837200
H	1.57029600	7.02982000	-0.31083000
C	-3.34209700	-0.38354700	-0.70504000
C	-4.63599300	-0.28914200	-0.25828300
C	-2.65085500	-1.64781800	-0.60383100
C	-5.30995700	-1.41480400	0.29779400
H	-5.17024700	0.65339500	-0.33177200
C	-3.31795100	-2.79659900	-0.02164100
C	-4.62628100	-2.64395900	0.40042100
H	-5.14652200	-3.49481600	0.82966800
O	-1.45275000	-1.75480400	-1.04591600
C	-2.57344100	-4.09086800	0.08799100
H	-2.25145400	-4.43933100	-0.89917700
H	-1.66376700	-3.96606200	0.68544700
H	-3.19335100	-4.86184400	0.54789800
C	-6.72474700	-1.27147400	0.76602600
H	-7.12240000	-2.20968000	1.15537800
H	-6.79349100	-0.50907200	1.55149600
H	-7.36798500	-0.93143300	-0.05442700
H	-0.65633300	-1.24132800	-3.22983700

$[^{HS}Mn^{III}(L^1)(CH_3OH)]^{2+}$ *S*=3

Mn	-0.01419800	-0.29926600	-1.06081100
N	1.38208600	1.34197500	-0.66463600
N	-0.34714400	0.02026500	1.07598700
C	1.44987600	1.60711100	0.77650300
C	2.37301300	2.52100200	1.28583700
C	0.56541400	0.93565600	1.64936200
C	2.44696100	2.76436900	2.65488600
H	3.04300000	3.04771500	0.61532500
C	0.67078500	1.17273100	3.03245200
C	1.59686200	2.08063900	3.52784900
H	3.17123000	3.47495300	3.03779100
H	0.04480300	0.63036800	3.73064300
H	1.66255000	2.24763400	4.59749300
C	2.71483000	0.93158500	-1.23232200
H	2.53015600	0.65592600	-2.27666500
H	3.39585800	1.78850500	-1.24377500
C	0.89545600	2.56116800	-1.42746400
H	0.92387600	2.28020900	-2.48564400
H	1.60597300	3.38004800	-1.27999800
C	3.37194400	-0.21311200	-0.50605500
C	2.65462700	-1.45449100	-0.29724600
C	4.68238700	-0.13798200	-0.10946300
C	3.33372200	-2.59750100	0.29778400
C	5.35626100	-1.24547100	0.48788200
H	5.23585800	0.78448200	-0.25742500
C	4.65504000	-2.45603900	0.67048600
H	5.17215000	-3.29742900	1.12091300
O	1.42302200	-1.59176300	-0.62870700
C	-1.34954400	-0.45127800	1.74992800
H	-1.54188500	-0.08868200	2.76067300
C	-2.28724000	-1.46260000	1.30272300
C	-3.28074700	-1.83649900	2.19527500
C	-2.23117300	-2.13012200	0.00168500
C	-4.23114300	-2.84377200	1.89772200
H	-3.33160500	-1.34692900	3.16354800
C	-3.20573300	-3.17693700	-0.29799400
C	-4.16009200	-3.49574100	0.64592700
H	-4.88480100	-4.27253300	0.42177800
O	-1.37262900	-1.84419800	-0.88492100
O	0.38799300	-0.71829300	-3.13917200
C	0.67568200	-1.99687700	-3.75814400
H	-0.22515300	-2.61326000	-3.79928600
H	1.07277000	-1.83440200	-4.76181400
H	1.42704200	-2.48112300	-3.13748400
C	-3.12970200	-3.85450100	-1.62979100
H	-3.28159700	-3.13170200	-2.43913500
H	-2.13897000	-4.29358300	-1.78662800
H	-3.88358500	-4.63839200	-1.71293600
C	-5.29745400	-3.18901200	2.88941500
H	-6.10861300	-2.45010100	2.83642800
H	-5.73014200	-4.17122400	2.69092800

H	-4.91197200	-3.16485500	3.91256800
C	2.56825200	-3.86921300	0.48777000
H	1.70954000	-3.71008800	1.14929400
H	2.16511100	-4.22556700	-0.46614200
H	3.20226700	-4.64629800	0.91655200
C	6.78334600	-1.10056600	0.90840200
H	6.87805600	-0.31257300	1.66618700
H	7.18578400	-2.02800600	1.31748200
H	7.40429900	-0.78871300	0.05996800
C	-0.48817300	2.98594500	-1.02818600
C	-0.75687500	4.26000500	-0.52957200
C	-1.54416300	2.06984500	-1.20428400
C	-2.06534800	4.65269700	-0.22213600
H	0.06255400	4.95966200	-0.38687900
C	-2.87435900	2.43259600	-0.89885000
C	-3.10003400	3.72554000	-0.42406600
H	-4.12196400	4.02256200	-0.20036300
O	-1.27532700	0.84996800	-1.72339400
C	-4.00605600	1.46272400	-1.11738500
H	-4.03082700	1.10588300	-2.15212300
H	-3.90563400	0.57866500	-0.47901400
H	-4.96663100	1.93226100	-0.89411500
C	-2.35963100	6.02603100	0.32899300
H	-3.23198600	6.47174600	-0.15917900
H	-2.58074300	5.98158600	1.40234600
H	-1.51081700	6.70108400	0.19402600
H	-0.26202800	-0.23515400	-3.67251800

[$^{HS}Mn^{III}(L^2)]^0$ *S*=2, Isomer 1

Mn	-0.13126200	-0.74263400	-0.03845000
N	-1.53124300	0.70980300	0.67375800
N	1.04323100	0.03484600	1.73469600
C	-0.87729900	1.59293800	1.65357400
C	-1.52154200	2.75352100	2.09907300
C	0.35938500	1.23269400	2.20724100
C	-0.94634300	3.55313000	3.08200700
H	-2.47897500	3.03703400	1.67710500
C	0.92400200	2.03834700	3.20483900
C	0.28006600	3.19170300	3.64170600
H	-1.45769700	4.45181800	3.41107400
H	1.87701800	1.75959900	3.64148200
H	0.73416000	3.80505600	4.41317100
C	-2.04655100	1.46554100	-0.53321300
H	-2.42845300	0.69459300	-1.21150100
H	-2.90737100	2.07420700	-0.23727800
C	-2.69949000	0.02811600	1.37461000
H	-3.43292600	0.79596900	1.64147500
H	-2.28625000	-0.38059100	2.30113100
C	-1.00939400	2.32522100	-1.19839500
C	0.21787500	1.75208800	-1.58525900
C	-1.27454000	3.66962200	-1.48434600
C	1.16489100	2.54223700	-2.28322600
C	-0.35446500	4.46843000	-2.16534300
H	-2.22669400	4.09578800	-1.17434900
C	0.85629800	3.87500200	-2.55560200
H	1.58816700	4.47529900	-3.09360000
O	0.50074400	0.46539300	-1.33844100
C	2.38287500	0.39045700	1.16531500
H	2.19132200	1.17252900	0.42503900
C	3.15825100	-0.74792800	0.53276900
C	4.55618300	-0.70904200	0.65858600
C	2.56617400	-1.77375500	-0.23968900
C	5.39340600	-1.63269200	0.03564600
H	4.99883600	0.07934900	1.26483800
C	3.40373100	-2.72379700	-0.88443600
C	4.78506400	-2.63397400	-0.73656600
H	5.40955100	-3.37326900	-1.23550800
O	1.24295500	-1.95757600	-0.35256000
C	2.77269900	-3.81901800	-1.70537500
H	2.12896300	-4.45847300	-1.09068000
H	2.13393000	-3.40791100	-2.49508800
H	3.53633300	-4.44771000	-2.17151100
C	6.89584900	-1.56693100	0.18356300
H	7.30126000	-2.49228500	0.60994200
H	7.39125500	-1.42037900	-0.78383300
H	7.19512900	-0.74203800	0.83650900
C	2.46302700	1.92409000	-2.73561700
H	3.02251900	1.49477700	-1.89774400
H	2.28683100	1.10131600	-3.43832100
H	3.09749200	2.66452900	-3.23021900
C	-0.63717400	5.92318600	-2.46148400
H	-0.00501500	6.58893300	-1.86063000
H	-0.44393100	6.16503200	-3.51256600
H	-1.67895400	6.17787600	-2.24629900
C	-3.33598700	-1.06125900	0.56475900
C	-4.69067900	-1.04761400	0.21675500
C	-2.52310900	-2.15643200	0.21682700
C	-5.27007600	-2.11963200	-0.46599000
H	-5.30180400	-0.19107200	0.49400500
C	-3.08715100	-3.25395200	-0.47578000
C	-4.44495800	-3.20802500	-0.79584400
H	-4.87840900	-4.05232800	-1.32936300
O	-1.22470500	-2.16042400	0.56978000
C	-2.22056000	-4.43043500	-0.84280400
H	-1.35091000	-4.11347600	-1.42837400
H	-1.82657000	-4.93027700	0.04976200
H	-2.78178700	-5.16607600	-1.42513800
C	-6.73310200	-2.11589800	-0.84515000
H	-6.86849500	-2.18176900	-1.93121700
H	-7.26536700	-2.96807200	-0.40650300
H	-7.22942600	-1.20309700	-0.50390300
H	3.00716700	0.83381000	1.95099800
C	1.15346000	-0.99202800	2.80193900
H	0.15710600	-1.22671200	3.17882800
H	1.59227700	-1.89449800	2.37646800
H	1.78047900	-0.64680500	3.63307700

[$^{HS}Mn^{III}(L^2)]^0$ *S*=2, Isomer 2

Mn	-0.09986100	-0.43873600	-1.11740800
N	-1.22053000	1.37417500	-0.80449200
N	-0.08811100	-0.42569000	1.14708400
C	-1.26745900	1.69379900	0.63305800
C	-1.87869200	2.87686100	1.06661300
C	-0.71125100	0.81979900	1.57917200
C	-1.93747300	3.19643900	2.41939200
H	-2.31330800	3.55823900	0.34358400
C	-0.77604200	1.15114900	2.93932700
C	-1.38264600	2.32939300	3.36172800
H	-2.41475000	4.11873300	2.73415400
H	-0.34936000	0.47626500	3.67362000
H	-1.42289200	2.56804400	4.41958000
C	-0.55278800	2.48233100	-1.60072200
H	-0.53859800	2.11483400	-2.63364100
H	-1.19094400	3.37152500	-1.57863700

C	-2.61876100	1.21863400	-1.37416600
H	-2.47091900	1.06935600	-2.44957300
H	-3.15695800	2.16269100	-1.24247700
C	0.83425800	2.82091700	-1.14978700
C	1.80037600	1.79759000	-1.17525400
C	1.19562900	4.12491400	-0.79754200
C	3.15148200	2.10853800	-0.88530200
C	2.51710100	4.45119100	-0.48472400
H	0.43129800	4.89905400	-0.78136000
C	3.47249900	3.42468900	-0.54711600
H	4.51173700	3.66026700	-0.32405800
O	1.45775600	0.54569900	-1.51388900
C	1.36912900	-0.45182100	1.49124700
H	1.79847700	0.46711700	1.08138900
C	2.14071300	-1.66227800	0.99518600
C	3.20658900	-2.09918200	1.79848000
C	1.90898700	-2.30343800	-0.24561400
C	4.06416500	-3.12987200	1.41764200
H	3.36872300	-1.60504400	2.75481500
C	2.77344600	-3.35671300	-0.65010600
C	3.82263900	-3.74300000	0.17896200
H	4.47303400	-4.55210600	-0.14925400
O	0.87274700	-2.02796000	-1.05050200
C	2.52634800	-4.03970700	-1.97087400
H	1.54233600	-4.52167400	-1.99353700
H	2.53632100	-3.32241900	-2.79923000
H	3.28611000	-4.80175900	-2.16548700
C	5.20588900	-3.57853500	2.30015400
H	5.10237600	-4.63037200	2.59303000
H	6.17159400	-3.48596500	1.78895200
H	5.25812700	-2.98349300	3.21649600
C	4.20697100	1.03549400	-0.96664000
H	4.00301000	0.21209000	-0.27464200
H	4.24508000	0.59267700	-1.96832300
H	5.19506000	1.44297900	-0.73600700
C	2.90848800	5.85353900	-0.07933500
H	3.08467600	5.92781400	1.00131100
H	3.83158100	6.17250000	-0.57511600
H	2.12535200	6.57424500	-0.33209300
C	-3.40707000	0.07961800	-0.80385200
C	-4.66521300	0.26801000	-0.22454600
C	-2.88603500	-1.21873500	-0.96657700
C	-5.44324100	-0.81764500	0.18649200
H	-5.04767400	1.27988200	-0.10704200
C	-3.66404500	-2.33505000	-0.57630000
C	-4.92082800	-2.10538600	-0.01192500
H	-5.51699800	-2.96594800	0.28691400
O	-1.67785400	-1.39437300	-1.52081000
C	-3.13013100	-3.72886100	-0.78117400
H	-2.90401900	-3.91885300	-1.83642700
H	-2.19432000	-3.88079400	-0.23245600
H	-3.85104600	-4.47878500	-0.44467800
C	-6.79212500	-0.61761800	0.83802500
H	-7.52384100	-1.34910700	0.47934100
H	-6.73517500	-0.73053100	1.92826600
H	-7.18809400	0.38169600	0.63486500
H	1.48362100	-0.39592500	2.58174900
C	-0.78849900	-1.60688700	1.71548000
H	-1.85272900	-1.53537000	1.49269600
H	-0.38602700	-2.50830300	1.25398900
H	-0.64952200	-1.67054600	2.80153000

$[^{LS}Mn^{III}(L^2)]^0$ *S*=1

Mn	-0.06177200	-0.37226600	-1.00527800
N	-1.23602700	1.37668400	-0.76666500
N	0.00775300	-0.42642000	1.04000400
C	-1.26933200	1.66545800	0.67147000
C	-1.91758300	2.80100400	1.16947400
C	-0.62901600	0.79346000	1.55935300
C	-1.92481900	3.07159800	2.53441100
H	-2.41643500	3.48112600	0.48782900
C	-0.63951700	1.06912600	2.93138000
C	-1.28068000	2.20414300	3.41823500
H	-2.43004200	3.95724000	2.90550900
H	-0.15156300	0.39385900	3.62520200
H	-1.28002800	2.40689100	4.48411400
C	-0.61513300	2.52127200	-1.54451400
H	-0.58584600	2.17064300	-2.58290200
H	-1.28987400	3.38320300	-1.50891500
C	-2.62594700	1.19460900	-1.33417900
H	-2.47202200	1.04954900	-2.40985400
H	-3.18581700	2.12752600	-1.20720900
C	0.75697000	2.91520900	-1.09378300
C	1.75738600	1.92615300	-1.10101900
C	1.07421200	4.23786400	-0.77121400
C	3.09896600	2.28970000	-0.82978100
C	2.38553800	4.61573900	-0.47162900
H	0.28433000	4.98626700	-0.76954500
C	3.37624700	3.62266100	-0.51900900
H	4.40790600	3.89919800	-0.30834500
O	1.45442600	0.65586500	-1.40363300
C	1.47491000	-0.47674800	1.39850000
H	1.91342300	0.44404100	1.00911600
C	2.20569500	-1.70387800	0.89564700
C	3.21388200	-2.22640500	1.72182400
C	1.96055400	-2.29853200	-0.36829400
C	4.01201900	-3.30375400	1.34265800
H	3.37766900	-1.76460500	2.69419000
C	2.76176200	-3.40787600	-0.76242400
C	3.75935400	-3.87708400	0.08623200
H	4.35931600	-4.72564900	-0.23926300
O	0.99536300	-1.91426500	-1.20211700
C	2.50384000	-4.05297600	-2.09989100
H	1.48416500	-4.45031500	-2.16212600
H	2.60096900	-3.32972700	-2.91745900
H	3.20392100	-4.87355600	-2.28067700
C	5.10245700	-3.83958400	2.24125900
H	4.97439500	-4.91015400	2.44098800
H	6.09551800	-3.71848700	1.79095700
H	5.11336000	-3.32147300	3.20471200
C	4.19248300	1.25528900	-0.91237200
H	3.99970600	0.40205700	-0.25453700
H	4.27281700	0.84700800	-1.92657100
H	5.15990000	1.68793900	-0.64336500
C	2.72892100	6.03878900	-0.09622800
H	2.88096900	6.14614800	0.98535200
H	3.65242600	6.37080500	-0.58231700
H	1.93088600	6.72986500	-0.38298400
C	-3.40253300	0.04187100	-0.77483100
C	-4.70058400	0.20759400	-0.28220100
C	-2.84055300	-1.24491700	-0.87623400
C	-5.47939100	-0.88902400	0.09604600
H	-5.11386600	1.21166200	-0.20919200
C	-3.62106200	-2.37368600	-0.52544900

C	-4.91735400	-2.16689600	-0.04897400
H	-5.51299200	-3.03718900	0.22124500
O	-1.58900200	-1.41174100	-1.32534300
C	-3.04955500	-3.75895100	-0.68488200
H	-2.77591300	-3.95922500	-1.72705500
H	-2.13449600	-3.88621700	-0.09689100
H	-3.76943300	-4.51867500	-0.36871200
C	-6.87226900	-0.71129800	0.65468800
H	-7.56691700	-1.45204300	0.24473300
H	-6.88802400	-0.82823900	1.74584300
H	-7.26855400	0.28281700	0.42810600
H	1.56119700	-0.44271900	2.48979900
C	-0.68414400	-1.63396900	1.59397500
H	-1.75278300	-1.55183400	1.40738500
H	-0.29120200	-2.51933900	1.09993600
H	-0.50550000	-1.70824100	2.67074700

[^{HS}Mn^{III}(L^2)]$^+$ *S*=3/2, Isomer 1

Mn	0.02472400	-0.59484800	-0.16905500
N	-1.62808200	0.31104000	0.77354500
N	1.12146100	0.28191100	1.61171500
C	-1.13530200	1.30912000	1.73804700
C	-2.01372400	2.24794200	2.28952600
C	0.20303800	1.27958300	2.16145400
C	-1.57154600	3.15845400	3.24459500
H	-3.05050100	2.27232300	1.97550400
C	0.63373700	2.19378000	3.13038800
C	-0.24293400	3.13146500	3.66778000
H	-2.26577800	3.88287800	3.65686300
H	1.66202900	2.17142100	3.47394900
H	0.11058100	3.83385900	4.41511800
C	-2.49380400	0.92523600	-0.30911100
H	-2.73968900	0.10243600	-0.98903900
H	-3.44124300	1.24524300	0.13479800
C	-2.44358000	-0.73391000	1.52964100
H	-3.35799600	-0.25298000	1.89038000
H	-1.84043700	-1.00763800	2.39891800
C	-1.85198800	2.07494200	-1.03467200
C	-0.53449600	1.96712100	-1.51462900
C	-2.59038300	3.23660800	-1.29044900
C	0.02937000	3.02589400	-2.26436500
C	-2.06070600	4.29286500	-2.03275000
H	-3.60625800	3.30751600	-0.90810900
C	-0.74708000	4.15890300	-2.50748600
H	-0.31009000	4.96921600	-3.08774000
O	0.21189200	0.86498700	-1.29710500
C	2.33906100	0.93720200	1.03647000
H	1.98241200	1.63251300	0.27154600
C	3.34687500	-0.00762300	0.42044200
C	4.68245300	0.16252100	0.69581600
C	2.96827200	-1.03673300	-0.53258900
C	5.69697900	-0.60899000	0.06282100
H	4.98439100	0.92020800	1.41355200
C	3.99893300	-1.82924100	-1.19021200
C	5.32188700	-1.59116400	-0.87557300
H	6.09654500	-2.17879900	-1.35833000
O	1.75057200	-1.30680000	-0.81400200
C	3.57959200	-2.87631400	-2.17519300
H	2.92953400	-3.61882100	-1.70024900
H	2.99991200	-2.43195900	-2.99131100
H	4.44785600	-3.38575600	-2.59608200
C	7.13493400	-0.35672200	0.39472200
H	7.79649000	-1.08242600	-0.08069700
H	7.42986700	0.64773200	0.06520900
H	7.29419800	-0.38792700	1.47841800
C	1.43279600	2.90464300	-2.80072600
H	2.16382100	2.76078300	-1.99716000
H	1.53095300	2.04173800	-3.46900200
H	1.71468600	3.80128800	-3.35839100
C	-2.86909700	5.53519300	-2.32545800
H	-2.32431500	6.44402900	-2.04696700
H	-3.10350300	5.61856300	-3.39352500
H	-3.81627800	5.53160900	-1.77912900
C	-2.75855900	-1.95009600	0.70898800
C	-4.06667900	-2.37935700	0.46831000
C	-1.67065800	-2.70067800	0.22547500
C	-4.31671600	-3.56211000	-0.23338400
H	-4.89872300	-1.78938200	0.84533200
C	-1.89332600	-3.89719000	-0.49040500
C	-3.21453400	-4.29859200	-0.69733700
H	-3.39360900	-5.22103000	-1.24601700
O	-0.41061300	-2.27374400	0.48393700
C	-0.72693000	-4.70903000	-0.99121800
H	-0.06859200	-4.11068800	-1.63001200
H	-0.11102600	-5.07342900	-0.16113700
H	-1.07016300	-5.57360300	-1.56453900
C	-5.72580500	-4.04603000	-0.48196200
H	-5.89695600	-4.25202400	-1.54418400
H	-5.92908100	-4.97704000	0.06039800
H	-6.46362100	-3.30671100	-0.15936600
H	2.85847600	1.52133800	1.80285600
C	1.47827100	-0.73021600	2.64478600
H	0.56607700	-1.18403000	3.03025100
H	2.08797000	-1.51278800	2.19157000
H	2.03539600	-0.27754000	3.47279100

[^{HS}Mn^{III}(L^2)]$^+$ *S*=3/2, Isomer 2

Mn	-0.11305000	-0.35034200	-1.15092200
N	-1.24299500	1.40912200	-0.78397000
N	-0.03695000	-0.41104200	1.11901400
C	-1.25950500	1.70397900	0.65945500
C	-1.88207900	2.86895800	1.12267200
C	-0.65210800	0.83489200	1.57812300
C	-1.89984000	3.17621800	2.47925300
H	-2.35570000	3.54626300	0.42091900
C	-0.67513700	1.15405000	2.94183500
C	-1.29095200	2.31626600	3.39381400
H	-2.38698500	4.08429100	2.81824100
H	-0.21453300	0.48335100	3.65887300
H	-1.29875100	2.54564500	4.45409400
C	-0.59863100	2.53945200	-1.57532800
H	-0.58813500	2.18485000	-2.61255600
H	-1.25044300	3.41658400	-1.53189500
C	-2.64814100	1.23124700	-1.33424300
H	-2.51715500	1.11463200	-2.41583900
H	-3.20583300	2.15725900	-1.16766400
C	0.78778500	2.89061000	-1.12927500
C	1.76793900	1.88161000	-1.16420900
C	1.13814100	4.19294100	-0.76746900
C	3.11717900	2.19628100	-0.88439600
C	2.46035400	4.52702500	-0.45722400
H	0.36832900	4.96048200	-0.74093400
C	3.42651600	3.51359500	-0.53576800
H	4.46437800	3.75913600	-0.32059400

O	1.42879000	0.62230800	-1.50249400
C	1.41751900	-0.45123900	1.45805700
H	1.87585500	0.44145500	1.02277700
C	2.16396500	-1.68532800	0.98785100
C	3.15808000	-2.19137000	1.79473700
C	1.93541600	-2.32715500	-0.29756700
C	3.97776200	-3.28518700	1.40651300
H	3.33270400	-1.73774200	2.76661200
C	2.76580400	-3.45399200	-0.70025400
C	3.75636100	-3.89267100	0.15411400
H	4.37976500	-4.73104200	-0.14126400
O	0.99452900	-1.98422000	-1.09567200
C	2.50544700	-4.09643900	-2.02811900
H	1.48297500	-4.48550500	-2.07855500
H	2.60042700	-3.36679200	-2.83921900
H	3.20359600	-4.91584900	-2.20644300
C	5.05088500	-3.77541900	2.32929600
H	5.60144500	-4.61468100	1.90179500
H	5.76038400	-2.97101500	2.55693300
H	4.62010000	-4.09106300	3.28707900
C	4.18670000	1.14058600	-1.00027200
H	4.00095100	0.29219400	-0.33307700
H	4.23067700	0.73190400	-2.01605400
H	5.16846700	1.55406300	-0.75694100
C	2.83627300	5.92742600	-0.03394400
H	2.88218700	6.01583700	1.05886100
H	3.81979400	6.21136100	-0.42071000
H	2.10724700	6.66133900	-0.38899800
C	-3.40118800	0.05955500	-0.77839600
C	-4.66911900	0.20670800	-0.21122200
C	-2.85047500	-1.22560700	-0.94292300
C	-5.42193000	-0.90566600	0.17846000
H	-5.08109800	1.20546100	-0.08724600
C	-3.59635500	-2.36842200	-0.57722300
C	-4.86639100	-2.17746600	-0.02774600
H	-5.44481200	-3.05554500	0.25191700
O	-1.62305100	-1.36781300	-1.48029700
C	-3.02780300	-3.74517100	-0.80195600
H	-2.83800200	-3.92784000	-1.86563700
H	-2.06835400	-3.87108100	-0.28908500
H	-3.71416900	-4.51505600	-0.44115000
C	-6.78191300	-0.74680100	0.81606400
H	-7.47743100	-1.51829000	0.47127700
H	-6.72362700	-0.83143300	1.90849900
H	-7.21773500	0.22975200	0.58728700
H	1.54901600	-0.37919200	2.54375200
C	-0.74747100	-1.58732800	1.69680100
H	-1.81281000	-1.49914300	1.48952000
H	-0.37294000	-2.50035700	1.23418100
H	-0.59458800	-1.65128300	2.77962500

[^{HS}Mn^{III}(L^{2})]$^{+}$ *S*=5/2, Isomer 1

Mn	-0.09007000	0.51898200	-0.22879800
N	1.64918300	-0.09312600	0.76072200
N	-1.08386000	-0.43033400	1.56812900
C	1.28634800	-1.15457000	1.71469500
C	2.27708600	-1.96796000	2.27353700
C	-0.05056900	-1.30881900	2.11856200
C	1.94986400	-2.93634200	3.21829800
H	3.31081800	-1.84954600	1.97085400
C	-0.36532300	-2.28003800	3.07600500
C	0.62409800	-3.09333400	3.62128400
H	2.73040100	-3.56220400	3.63751200
H	-1.39092600	-2.39966800	3.40693700
H	0.35905200	-3.84174100	4.36051500
C	2.61642800	-0.56255000	-0.30851400
H	2.71238300	0.27946500	-1.00325300
H	3.60434900	-0.69980700	0.14170900
C	2.27219800	1.06566300	1.53257500
H	3.24726000	0.73714100	1.90511700
H	1.62074500	1.22981100	2.39439200
C	2.18934500	-1.82283400	-1.00946200
C	0.87141100	-1.96146500	-1.47963800
C	3.11802500	-2.84562200	-1.23856300
C	0.49638600	-3.12378500	-2.19252900
C	2.77625100	-3.99996900	-1.94379000
H	4.13187700	-2.72966400	-0.86184100
C	1.45734500	-4.11072400	-2.41049100
H	1.16580800	-5.00218400	-2.96238500
O	-0.05545200	-1.00148400	-1.28076800
C	-2.22827900	-1.21520200	1.00499800
H	-1.80568700	-1.87146400	0.23890500
C	-3.33239500	-0.37890400	0.39648500
C	-4.63886900	-0.63134000	0.73938500
C	-3.07130500	0.61848500	-0.63022800
C	-5.73495600	0.02822700	0.11434700
H	-4.85318500	-1.36991300	1.50674200
C	-4.18809300	1.28392000	-1.29059300
C	-5.47454800	0.97252900	-0.89905000
H	-6.31064300	1.47101700	-1.38006500
O	-1.89191400	0.95624400	-0.98574100
C	-3.89047700	2.29227400	-2.35668900
H	-3.29486800	3.11875900	-1.95425000
H	-3.29707700	1.84431500	-3.16084100
H	-4.81188000	2.69563800	-2.77952000
C	-7.13399900	-0.29485100	0.53896000
H	-7.87345000	0.27542100	-0.02518400
H	-7.33946800	-1.36376400	0.40519400
H	-7.26965100	-0.08344300	1.60653500
C	-0.91142300	-3.26646700	-2.71143700
H	-1.64572800	-3.25162200	-1.89789300
H	-1.17461600	-2.44268500	-3.38421200
H	-1.03151000	-4.20557700	-3.25743300
C	3.78188100	-5.09955700	-2.19337700
H	3.46155400	-6.04665000	-1.74373500
H	3.91571100	-5.28518800	-3.26527000
H	4.75975000	-4.84649900	-1.77475900
C	2.39570500	2.32529200	0.72585800
C	3.61724100	2.97425000	0.52461100
C	1.20817600	2.88875300	0.22274600
C	3.67982300	4.19170600	-0.15913700
H	4.52795500	2.52807700	0.91702800
C	1.24161800	4.11514500	-0.47595200
C	2.48001300	4.73777300	-0.64357300
H	2.51317900	5.68458500	-1.17877900
O	0.03396100	2.24441900	0.43689800
C	-0.03171400	4.72052100	-1.00707300
H	-0.54313300	4.03553800	-1.69210400
H	-0.73694600	4.93860800	-0.19728700
H	0.17176300	5.65172800	-1.54140000
C	4.99289700	4.90668100	-0.37463500
H	5.17464300	5.09747100	-1.43824000
H	5.00529000	5.87944800	0.13054600
H	5.83279000	4.32172100	0.00922000

H	-2.67810700	-1.84599600	1.77806700
C	-1.54765700	0.53939900	2.59996500
H	-0.69213600	1.09532800	2.98009400
H	-2.24440200	1.24580000	2.14774900
H	-2.04536800	0.02628700	3.43071300

[^{HS}Mn^{III}(L^{2})]$^{+}$ *S*=5/2, Isomer 2

Mn	-0.10351900	-0.29351700	-1.17826400
N	-1.23870500	1.44620600	-0.76625900
N	-0.01370600	-0.40608900	1.09360800
C	-1.23981100	1.71680600	0.68196600
C	-1.86097800	2.87204000	1.17080200
C	-0.61418700	0.83753600	1.57839700
C	-1.85786300	3.16106700	2.53143200
H	-2.34907900	3.55619000	0.48580000
C	-0.61558600	1.13922400	2.94634900
C	-1.22837000	2.29272400	3.42389800
H	-2.34416300	4.06177800	2.89062700
H	-0.14211400	0.46050100	3.64721600
H	-1.21909000	2.50813400	4.48708900
C	-0.61065900	2.59659600	-1.54272800
H	-0.60929700	2.26482400	-2.58708000
H	-1.26672800	3.46859300	-1.47292400
C	-2.64693900	1.26025900	-1.30446300
H	-2.52703700	1.16860200	-2.38991200
H	-3.21514100	2.17513100	-1.11300600
C	0.77942600	2.94511300	-1.10584100
C	1.76239400	1.94153200	-1.17735700
C	1.12956200	4.23895400	-0.71331100
C	3.11206300	2.25020700	-0.89886600
C	2.45374100	4.56818900	-0.40794700
H	0.35783600	5.00305700	-0.65798700
C	3.42154900	3.55916900	-0.51995200
H	4.46048000	3.80141800	-0.30604300
O	1.41928300	0.69149400	-1.55046100
C	1.44461800	-0.47148400	1.42051300
H	1.91926900	0.39921800	0.95938700
C	2.14753400	-1.73749600	0.97156600
C	3.08380500	-2.30166700	1.80609800
C	1.93331800	-2.35010900	-0.33180300
C	3.86144300	-3.43323600	1.43339300
H	3.24711800	-1.86800600	2.78887000
C	2.71994500	-3.51649100	-0.71759300
C	3.65494500	-4.01460900	0.16642400
H	4.24551400	-4.88047900	-0.11693500
O	1.05634200	-1.93735400	-1.16332900
C	2.47620600	-4.12841400	-2.06246100
H	1.43683700	-4.46064400	-2.15618700
H	2.64031600	-3.39503700	-2.85913900
H	3.13561500	-4.98214900	-2.22657100
C	4.88021700	-3.98050100	2.38467200
H	4.42812900	-4.18709400	3.36134900
H	5.33759100	-4.89638000	2.00730300
H	5.67415200	-3.24333500	2.55868800
C	4.18121600	1.19760700	-1.04605700
H	3.99168800	0.32856800	-0.40698700
H	4.22818000	0.82190700	-2.07438700
H	5.16282700	1.60143100	-0.78642100
C	2.83081900	5.95871400	0.04639600
H	2.90025400	6.01714200	1.13993200
H	3.80391400	6.25988900	-0.35362600
H	2.09001100	6.69745800	-0.27235100
C	-3.38227900	0.06886600	-0.76409400
C	-4.65220500	0.19741000	-0.19503700
C	-2.82367700	-1.21051000	-0.94810100
C	-5.39806800	-0.92492400	0.17704200
H	-5.07107400	1.19134300	-0.05627500
C	-3.56366600	-2.36324500	-0.60242100
C	-4.83462300	-2.18964500	-0.05002700
H	-5.40704000	-3.07602100	0.21552500
O	-1.59265500	-1.34113200	-1.48248100
C	-2.98655500	-3.73298100	-0.84795000
H	-2.78408700	-3.89391000	-1.91275200
H	-2.03262500	-3.86578300	-0.32650300
H	-3.67377500	-4.51241400	-0.51001200
C	-6.75959400	-0.78547400	0.81602000
H	-7.46044500	-1.53281200	0.43071700
H	-6.70731400	-0.92470500	1.90307500
H	-7.18584200	0.20485400	0.63341800
H	1.58991200	-0.37860200	2.50260000
C	-0.73385400	-1.58008500	1.66513100
H	-1.80051300	-1.47194500	1.47617200
H	-0.38132300	-2.49213400	1.18374700
H	-0.56518400	-1.66241600	2.74438300

[^{HS}Mn^{III}(L^{2})]$^{2+}$ *S*=1, Isomer 1

Mn	-0.14988700	0.51702000	-0.18597200
N	1.62176600	-0.02411000	0.86841300
N	-1.11807700	-0.50136500	1.57345900
C	1.27944500	-1.10288500	1.81408700
C	2.28976800	-1.86371100	2.41119800
C	-0.06302800	-1.32999400	2.16174800
C	1.97566600	-2.85515900	3.33651900
H	3.32932000	-1.68518500	2.16212200
C	-0.36406500	-2.32254300	3.10056000
C	0.64479500	-3.08601800	3.68150100
H	2.77099500	-3.43835400	3.78767200
H	-1.39330100	-2.49898500	3.39109000
H	0.38980000	-3.85208700	4.40561100
C	2.67377200	-0.44305800	-0.12509200
H	2.80894100	0.40251900	-0.80953400
H	3.63047300	-0.56763600	0.38857300
C	2.14716300	1.18458000	1.64609500
H	3.12496400	0.92299900	2.06038200
H	1.45247800	1.32363900	2.47683900
C	2.36097400	-1.69205400	-0.90610900
C	1.04732400	-1.90731800	-1.46998300
C	3.34808400	-2.60691700	-1.17467900
C	0.79896100	-3.04712300	-2.33603300
C	3.11823200	-3.73557300	-2.01477100
H	4.33884000	-2.47173900	-0.75018200
C	1.83881500	-3.92179400	-2.57916600
H	1.66948700	-4.78024600	-3.22117400
O	0.06367600	-1.11540800	-1.21763900
C	-2.22435200	-1.34299000	1.00707500
H	-1.77042500	-2.01691500	0.27465000
C	-3.34174700	-0.55902500	0.35648000
C	-4.64587800	-0.84453100	0.67533800
C	-3.08779600	0.43166600	-0.67281300
C	-5.74577100	-0.22126100	0.01570700
H	-4.85750100	-1.57685100	1.44900600
C	-4.20132300	1.06285800	-1.36716000
C	-5.48780800	0.71878600	-1.00200800
H	-6.32589700	1.19076700	-1.50497600

O	-1.90238500	0.79836200	-0.99969100
C	-3.90762000	2.07420600	-2.43043700
H	-3.35931900	2.92578500	-2.01285900
H	-3.27178600	1.64515800	-3.21188300
H	-4.82933800	2.43982800	-2.88509200
C	-7.14222400	-0.57874800	0.41333400
H	-7.88530900	-0.00262400	-0.13917100
H	-7.32628100	-1.64650800	0.24046000
H	-7.28997100	-0.40991400	1.48666400
C	-0.56498700	-3.23254700	-2.92424900
H	-1.30945700	-3.40256700	-2.13864600
H	-0.88028700	-2.33651700	-3.46842300
H	-0.57974000	-4.08419700	-3.60556400
C	4.23526000	-4.68932700	-2.29142400
H	4.65930500	-5.06752100	-1.35398700
H	3.91079900	-5.53405500	-2.90016900
H	5.05127500	-4.17413100	-2.81389700
C	2.22486100	2.42861700	0.80941200
C	3.41266000	3.13081100	0.60165300
C	1.02220000	2.90930800	0.25414400
C	3.42119200	4.31996700	-0.13736100
H	4.33835900	2.75415200	1.02858200
C	1.00051900	4.09678100	-0.50987600
C	2.20718400	4.77758900	-0.67673400
H	2.20477600	5.69919300	-1.25404300
O	-0.12140500	2.21922400	0.48992600
C	-0.29244300	4.60719400	-1.08936600
H	-0.77279000	3.85093400	-1.71885200
H	-1.00713300	4.85956800	-0.29826000
H	-0.12248700	5.50157900	-1.69255800
C	4.69503000	5.10033100	-0.34954600
H	4.84402800	5.33828700	-1.40795700
H	4.66668200	6.05345700	0.19125500
H	5.56792300	4.54444200	0.00106000
H	-2.66693000	-1.96294200	1.79193100
C	-1.65055700	0.45578800	2.59027900
H	-0.82890700	1.04085600	2.99930200
H	-2.35858900	1.13540600	2.11556200
H	-2.15454500	-0.07965500	3.40198200

[^{HS}Mn^{III}(L^2)]$^{2+}$ *S*=1, Isomer 2

Mn	-0.11541900	-0.37259300	-1.12032100
N	-1.25579900	1.39732900	-0.74537600
N	0.03722500	-0.36658400	1.14822300
C	-1.24647100	1.71272400	0.69676900
C	-1.88377600	2.87059500	1.15655500
C	-0.57912600	0.87989100	1.60666900
C	-1.85831000	3.20506200	2.50653300
H	-2.40050900	3.52216900	0.46092500
C	-0.55727900	1.22810400	2.96286200
C	-1.18795800	2.38307600	3.41308800
H	-2.35809100	4.10582200	2.84578000
H	-0.05204200	0.58646600	3.67595800
H	-1.16018100	2.63603400	4.46739500
C	-0.62630300	2.52817100	-1.55705600
H	-0.65003800	2.18321800	-2.59611200
H	-1.26457400	3.41212000	-1.48275100
C	-2.65873400	1.22250500	-1.28261100
H	-2.54848200	1.08334600	-2.36413500
H	-3.21592300	2.15102000	-1.13324900
C	0.77703200	2.85876000	-1.15547200
C	1.74825900	1.83635700	-1.25495200
C	1.15902200	4.13679700	-0.76350800
C	3.11849500	2.11357100	-1.00841800
C	2.50371100	4.43676000	-0.49504800
H	0.40770800	4.91658300	-0.67781300
C	3.45626100	3.41247700	-0.63425000
H	4.50174300	3.64067000	-0.44313900
O	1.37145700	0.60571700	-1.61742300
C	1.50757300	-0.38517900	1.42981800
H	1.94299500	0.49858800	0.95384900
C	2.23931600	-1.63149200	0.97031400
C	3.26509400	-2.11220000	1.75124800
C	1.95786100	-2.31291500	-0.28164300
C	4.06644600	-3.22153800	1.36304500
H	3.48032600	-1.62908400	2.70028000
C	2.76702100	-3.45320700	-0.68603200
C	3.79155100	-3.86722100	0.14012000
H	4.40061600	-4.71595700	-0.15474700
O	0.97759500	-1.99205800	-1.04830600
C	2.44963400	-4.13621100	-1.98023800
H	1.42720300	-4.52888600	-1.97229600
H	2.50692800	-3.43183500	-2.81675500
H	3.14134400	-4.95957900	-2.16338600
C	5.17445000	-3.68447000	2.25574900
H	5.70224700	-4.54264300	1.83798100
H	5.89581200	-2.87547700	2.42275400
H	4.78255500	-3.95883600	3.24263200
C	4.16071700	1.04348100	-1.19086400
H	3.96410700	0.16832500	-0.56305200
H	4.17846500	0.68680100	-2.22647900
H	5.15351100	1.42458300	-0.94357700
C	2.92425100	5.82836100	-0.10009900
H	3.72929600	5.80581500	0.64016700
H	3.30130400	6.38207600	-0.96902000
H	2.08815900	6.39736500	0.31395800
C	-3.44690500	0.07551400	-0.71728200
C	-4.72431600	0.25184800	-0.24370300
C	-2.91739400	-1.26195400	-0.81286700
C	-5.54292100	-0.85699600	0.11317900
H	-5.13448400	1.25409100	-0.16198200
C	-3.74795400	-2.40402700	-0.49383400
C	-5.03012700	-2.16316500	-0.03599500
H	-5.66529100	-3.00519400	0.22035500
O	-1.69610100	-1.46481000	-1.18273500
C	-3.19579900	-3.78629100	-0.66138700
H	-2.87304900	-3.95094200	-1.69484000
H	-2.31437800	-3.94042500	-0.03019100
H	-3.94443700	-4.53650700	-0.40328800
C	-6.93758700	-0.62351800	0.60070600
H	-7.39245300	-1.53588900	0.98896500
H	-6.95536300	0.14678700	1.37885000
H	-7.56406200	-0.25114000	-0.22070400
H	1.67970000	-0.27665000	2.50590500
C	-0.62726100	-1.53569900	1.79875300
H	-1.70702100	-1.43676700	1.70058800
H	-0.30539500	-2.45619200	1.31293000
H	-0.37719700	-1.58888600	2.86315200

[^{HS}Mn^{III}(L^2)]$^{2+}$ *S*=3, Isomer 1

Mn	-0.17863500	0.47724300	-0.21311300
N	1.61071500	0.08999600	0.83354800
N	-1.08031700	-0.56811900	1.56203600
C	1.35255900	-1.01281400	1.77897700

C	2.41795500	-1.70078700	2.36706700
C	0.03041400	-1.33328800	2.13369100
C	2.17926500	-2.71537100	3.29025600
H	3.44008300	-1.44601900	2.11268400
C	-0.19470000	-2.34885200	3.06879500
C	0.86976400	-3.04150000	3.64021400
H	3.01583400	-3.24241700	3.73572100
H	-1.20745400	-2.59804600	3.36417900
H	0.67369600	-3.82679200	4.36217300
C	2.67960300	-0.23710700	-0.17859000
H	2.70878000	0.60984000	-0.87389000
H	3.65456400	-0.25295600	0.31620500
C	2.04369300	1.33300900	1.61162500
H	3.03807800	1.14354800	2.02523400
H	1.34209500	1.41758600	2.44365700
C	2.48213000	-1.53252100	-0.92118800
C	1.17962400	-1.91348800	-1.42307300
C	3.55438200	-2.34535100	-1.19201200
C	1.02652900	-3.12888100	-2.20905300
C	3.42015600	-3.53777500	-1.96265600
H	4.53917100	-2.08065200	-0.81732800
C	2.14638000	-3.89613100	-2.45423700
H	2.04918900	-4.80388100	-3.04106400
O	0.12924000	-1.20836000	-1.19232700
C	-2.14966800	-1.46270900	1.00788400
H	-1.66891600	-2.11957100	0.27738800
C	-3.30218900	-0.73044000	0.35617400
C	-4.59126600	-1.03576000	0.71615900
C	-3.09757700	0.21675500	-0.72657900
C	-5.72294300	-0.47402200	0.05419100
H	-4.76616300	-1.74048900	1.52375100
C	-4.24517900	0.77779300	-1.42768600
C	-5.51291700	0.41919700	-1.01569000
H	-6.37405400	0.84048400	-1.52453600
O	-1.93076100	0.58851200	-1.10943000
C	-4.00303600	1.73368200	-2.55337000
H	-3.47802200	2.62683300	-2.19710900
H	-3.36449900	1.28038100	-3.31873100
H	-4.94386900	2.03993800	-3.01268100
C	-7.09992000	-0.84133400	0.50644000
H	-7.86969600	-0.41569000	-0.13857100
H	-7.21941200	-1.93051800	0.53426100
H	-7.26883300	-0.48537300	1.53089700
C	-0.33037900	-3.48902900	-2.72829900
H	-1.04621200	-3.60941500	-1.90817900
H	-0.72273700	-2.69408500	-3.37173700
H	-0.29400300	-4.41745900	-3.29956500
C	4.62344600	-4.38188100	-2.23236500
H	5.08528000	-4.70163100	-1.29022600
H	4.37952200	-5.26641200	-2.82182000
H	5.38476700	-3.80054300	-2.76692700
C	2.02617000	2.58433900	0.78321600
C	3.15364400	3.38527100	0.60003400
C	0.79193600	2.97780300	0.22765100
C	3.07061500	4.58623400	-0.11442500
H	4.10369500	3.07657100	1.02794200
C	0.67699200	4.17854400	-0.50666600
C	1.82563300	4.95718500	-0.65082100
H	1.75193100	5.88777200	-1.20855400
O	-0.29137900	2.18601700	0.43269300
C	-0.64992400	4.59537200	-1.08332100
H	-1.06615000	3.81490700	-1.72862700
H	-1.38540700	4.77625300	-0.29173200
H	-0.54920300	5.51088800	-1.67000000
C	4.27935400	5.46893600	-0.30321900
H	4.41971500	5.73062700	-1.35728000
H	4.16866600	6.41020400	0.24757000
H	5.19033600	4.98033300	0.05081600
H	-2.56198100	-2.09571500	1.79894800
C	-1.64766700	0.35909400	2.58780500
H	-0.85463200	0.99083500	2.98415800
H	-2.40068000	0.99584000	2.12392300
H	-2.10445100	-0.20378700	3.40873100

[$^{HS}Mn^{III}(L^2)]^{2+}$ *S*=3, Isomer 2

Mn	-0.07140400	-0.28814100	-1.14904400
N	-1.22571800	1.45258000	-0.73875600
N	0.03907800	-0.37490000	1.11459400
C	-1.20014900	1.74126100	0.70955100
C	-1.81367300	2.90150100	1.19505700
C	-0.54350400	0.87885100	1.59950800
C	-1.77328000	3.20987500	2.55086600
H	-2.32205700	3.57585900	0.51520100
C	-0.50661100	1.20100900	2.96167600
C	-1.11225700	2.35910200	3.43744100
H	-2.25381200	4.11335100	2.91004400
H	-0.01059100	0.53593600	3.65955800
H	-1.07289800	2.59182600	4.49600700
C	-0.61315000	2.60459300	-1.53915500
H	-0.64949600	2.28120700	-2.58445900
H	-1.25827200	3.48057100	-1.43847000
C	-2.63483400	1.27446800	-1.25823900
H	-2.54178700	1.16087900	-2.34399100
H	-3.19713400	2.19443300	-1.07751200
C	0.79138000	2.93325300	-1.13875400
C	1.75991800	1.91819000	-1.25573900
C	1.16923000	4.20454000	-0.71045300
C	3.12071100	2.18182200	-0.98207100
C	2.50849200	4.49753100	-0.42412700
H	0.41471400	4.97983200	-0.60995000
C	3.45740600	3.47448600	-0.57540800
H	4.50201000	3.69358600	-0.36774700
O	1.37695400	0.69398300	-1.67693800
C	1.51076400	-0.44512700	1.39822800
H	1.97899600	0.41265600	0.90640300
C	2.18211200	-1.73133700	0.95887200
C	3.11865500	-2.30542000	1.78373900
C	1.92914400	-2.35752500	-0.32872500
C	3.86078200	-3.46429900	1.41155400
H	3.31293100	-1.86355800	2.75683300
C	2.67609300	-3.54884400	-0.71647000
C	3.61373400	-4.05884600	0.15746600
H	4.17529500	-4.94404200	-0.12400500
O	1.04149200	-1.93220000	-1.14915500
C	2.38865600	-4.17260500	-2.04623300
H	1.33976200	-4.48123700	-2.11171600
H	2.55328500	-3.45439500	-2.85650400
H	3.02346800	-5.04415200	-2.21139800
C	4.88740800	-4.01733900	2.34751300
H	5.26048900	-4.98734700	2.01601700
H	5.73927400	-3.32828900	2.42005400
H	4.48068600	-4.11530400	3.35985400
C	4.16781600	1.11463500	-1.16918300
H	4.00097300	0.25556400	-0.51081900

H	4.16181700	0.73089600	-2.19477200
H	5.16351400	1.51032000	-0.95815500
C	2.92875600	5.88069200	0.00758000
H	3.71923200	5.83936400	0.76278500
H	3.32276300	6.45379000	-0.84063700
H	2.08779100	6.44331300	0.42110000
C	-3.40575400	0.10716200	-0.70711100
C	-4.66557700	0.26491900	-0.19035900
C	-2.87963900	-1.23128400	-0.86447700
C	-5.48021600	-0.85795200	0.15248000
H	-5.07376800	1.26242900	-0.05854000
C	-3.71200900	-2.38607800	-0.56119900
C	-4.97779500	-2.16066300	-0.05855600
H	-5.60826100	-3.00924200	0.18747700
O	-1.67504800	-1.42731000	-1.26578800
C	-3.16117200	-3.75767900	-0.79216600
H	-2.88571500	-3.88974100	-1.84413000
H	-2.24797300	-3.91761200	-0.20920700
H	-3.89074700	-4.52129000	-0.51993500
C	-6.85729300	-0.63458500	0.68573900
H	-7.30074900	-1.55307600	1.07229200
H	-6.85281300	0.12602600	1.47347500
H	-7.50683100	-0.24994400	-0.11259300
H	1.68805600	-0.32638200	2.47201200
C	-0.66373100	-1.53510500	1.74183200
H	-1.73946300	-1.38921600	1.65945800
H	-0.38537100	-2.45629100	1.23043700
H	-0.40541600	-1.62595300	2.80176000

Table B5. Frequencies (cm^{-1}) for all optimized structures.

$[^{HS}Mn^{III}(L^1)(CH_3OH)]^0$ *S*=2

15.6294	27.6272	29.8376	32.3668	34.8929	40.7550
42.3807	45.6158	48.5643	61.8792	74.5846	83.7317
90.3141	95.6249	104.2071	110.8661	118.1023	128.1257
131.9099	134.5866	135.0096	144.6642	148.7101	161.5423
174.6856	182.4604	188.5920	196.0452	201.1499	207.6627
218.2090	221.4539	223.0363	238.1232	243.3590	255.4313
265.1722	267.7617	282.6182	298.7640	303.0286	306.0318
310.4176	321.9974	329.8860	345.9204	357.9405	359.2917
369.5879	405.3065	422.5024	428.7050	440.3768	449.1116
481.3315	494.7620	501.1562	506.9326	522.0654	523.0502
530.5068	533.2055	542.8196	545.8328	553.6227	560.3966
570.1073	576.4368	580.9760	586.2255	587.2963	606.1792
615.0349	624.0813	633.0900	680.5852	686.6503	706.0243
751.7752	756.1026	762.9302	769.5545	781.2307	782.5448
820.4740	830.5602	833.4693	873.7556	878.5207	879.7345
881.1006	886.8286	906.6156	907.6392	924.4063	941.8322
954.7036	961.1770	970.3006	980.3684	980.6304	987.9248
990.0136	992.3236	995.3938	1009.7089	1030.2899	1035.6878
1036.3160	1038.1052	1040.3444	1046.0760	1059.6433	1060.1585
1061.4153	1061.9290	1062.4006	1064.2822	1066.5626	1067.8109
1075.2048	1076.1110	1080.1285	1127.5960	1180.0975	1185.6106
1186.8390	1188.6749	1190.6443	1204.4361	1230.7329	1239.9736
1266.5392	1273.1516	1280.3101	1280.7616	1289.7014	1296.1295
1302.6161	1312.8181	1326.4529	1336.0902	1343.4747	1347.9196
1350.5050	1354.3863	1357.2764	1360.5653	1398.9041	1417.9601
1418.7388	1419.7398	1420.7696	1423.1200	1424.6718	1424.8888
1427.6473	1450.3071	1453.4778	1454.0064	1457.0831	1477.0068
1477.4081	1480.3752	1483.8291	1485.2585	1488.4452	1489.5556
1490.6659	1491.0391	1492.0174	1497.1621	1499.8571	1502.4346
1508.5203	1509.6491	1510.5034	1512.0447	1513.3897	1516.9618
1520.3528	1529.4361	1579.7469	1619.0656	1620.4725	1628.9183
1636.6534	1658.8292	1659.1203	1660.9231	1671.7456	3030.6281
3030.8126	3032.8980	3038.6096	3039.5563	3039.8749	3041.6691
3045.6075	3046.4103	3084.8303	3085.9389	3086.8473	3088.1147
3089.0608	3091.4189	3092.0632	3093.0491	3096.3061	3116.2177
3117.6770	3117.8384	3121.3847	3123.3004	3124.2283	3125.0617
3157.9720	3158.0601	3158.9281	3164.0322	3164.2473	3165.0457
3175.5824	3192.3533	3199.4758	3210.7498	3218.0846	3786.1401

$[^{LS}Mn^{III}(L^1)(CH_3OH)]^0$ *S*=1

11.6241	24.6320	30.2606	33.9605	37.4899	40.9336
45.6484	52.4249	67.7882	77.9549	80.1408	88.3137
97.1325	99.1076	104.7993	116.2948	122.4420	131.1341
141.8333	148.4766	150.8510	161.1158	175.1151	181.2239
189.2458	195.6490	199.1287	204.2166	210.9726	216.8056
223.9451	233.7675	246.0401	253.4486	263.3176	267.7887
292.0270	297.4226	300.3949	311.9002	318.4130	328.5647
332.7671	343.5051	354.0359	361.9964	366.7415	387.0409
408.5493	426.5560	429.9649	437.6890	441.3438	468.9920
484.5642	494.4806	503.8590	510.2317	518.2446	531.1833
536.8464	537.9930	546.2754	558.3102	574.9959	575.8956
578.9107	583.2771	585.6163	587.4632	609.1885	614.6490
635.6606	654.7612	671.6276	682.7768	690.1941	709.7194
750.6700	753.7703	761.0427	767.4063	778.1996	784.7294
826.4279	830.6265	839.9669	868.9077	874.4799	880.1644
880.4781	898.5838	905.6777	906.5794	927.2808	942.1982
952.8448	964.1668	970.1529	972.0724	979.8887	982.1437
989.8012	990.1788	992.6970	1014.7318	1020.3765	1028.5730
1035.7073	1038.1537	1038.5389	1047.8579	1056.4698	1059.5711
1060.9203	1062.0219	1062.6780	1064.4150	1067.1106	1070.0560
1077.4534	1086.0602	1087.5712	1130.1678	1185.1506	1185.8571
1189.4702	1191.2741	1192.3242	1208.6421	1226.8285	1243.6620
1271.4044	1276.1507	1280.2446	1282.0183	1293.6723	1303.2364
1305.5409	1314.9367	1325.6035	1340.6235	1348.0282	1352.0447
1356.3149	1357.7474	1364.2189	1370.2254	1410.8186	1417.4347
1419.7804	1419.9117	1421.4201	1422.9248	1424.4750	1426.2718
1433.3688	1448.6605	1453.9276	1456.1300	1459.7223	1472.3788
1477.7802	1479.1183	1480.5465	1485.0976	1488.1168	1489.7807
1490.4699	1490.7782	1491.4517	1496.3769	1501.1731	1503.2910
1510.3362	1511.1169	1511.4262	1513.4444	1515.6265	1516.7174
1523.1861	1533.0418	1580.0395	1618.5722	1621.4573	1634.9311
1638.4274	1657.7063	1660.4906	1662.5309	1677.2792	3029.8265
3030.2193	3032.6067	3035.8607	3037.4352	3038.9746	3046.8454
3049.4961	3068.5170	3081.9106	3084.2725	3084.3597	3089.1952
3090.1479	3091.6056	3093.7231	3096.2664	3115.8256	3116.6851
3121.1408	3121.3254	3121.7321	3125.8566	3148.9062	3154.4673
3154.7741	3155.5718	3159.5578	3160.6858	3162.8528	3167.5115
3189.5708	3195.4355	3204.3398	3216.0697	3224.7681	3734.7110

$[^{HS}Mn^{III}(L^1)(CH_3OH)]^+$ *S*=3/2

15.9194	27.8867	30.4978	38.9541	40.8575	42.7179
43.9014	49.3042	50.2016	68.0759	75.2789	85.4297
95.5912	96.5821	112.4559	115.6286	121.6781	124.4874
125.9883	134.2891	136.2442	148.0592	154.8773	155.8453
171.4726	178.1114	190.1879	192.6380	193.7964	199.2805
207.2185	216.7210	223.5261	229.5622	240.0817	248.1080
263.8823	269.5019	285.2641	294.9676	302.2139	307.2472
308.5117	324.6672	332.1984	340.5949	344.1986	358.3761
369.0744	400.7051	417.0175	427.4469	439.1881	447.1745
473.0589	479.4215	487.0920	488.8810	498.2553	512.6210
520.1469	523.8388	530.8878	542.9055	552.1838	554.8839
567.0302	573.3472	575.0518	580.8246	585.7347	595.8250
606.8425	623.7328	637.6339	674.4970	684.6647	704.7045
749.9932	753.0442	759.9755	769.6720	777.3925	781.3568
811.0952	822.5369	826.4267	877.4526	881.8117	883.1186
888.0704	892.3646	907.7658	912.4976	931.2343	940.0491
958.1346	962.8757	967.2465	979.5380	983.0194	987.5734
989.0028	996.5898	1000.9020	1009.4037	1018.1573	1024.8923
1036.7016	1039.4956	1040.0181	1042.8424	1046.9610	1051.9456
1058.6171	1061.6226	1062.7463	1064.8551	1067.1502	1067.4589
1076.7008	1081.9739	1086.9737	1126.6341	1176.4551	1180.1078
1185.0737	1186.8014	1192.7588	1205.8822	1229.7647	1247.8803
1266.3479	1271.9236	1278.9496	1281.7014	1288.5148	1303.7124
1308.4167	1316.2118	1328.7859	1336.6893	1341.3150	1346.7264
1353.0923	1366.2758	1367.5423	1394.1157	1404.2006	1411.4498
1417.3718	1420.5612	1421.6668	1422.1743	1423.9800	1426.2438
1426.7549	1447.7149	1451.2513	1451.7605	1455.7503	1472.1546
1473.0606	1476.6093	1480.4174	1481.5602	1485.9921	1488.2053
1489.2490	1490.8729	1491.3491	1493.4163	1497.8790	1502.3271

1503.0923	1505.1232	1506.6002	1509.2965	1509.5630	1512.7218
1513.9272	1526.6116	1528.1229	1577.7972	1617.6724	1627.8042
1633.3290	1639.5391	1652.2513	1656.0359	1664.1280	3035.9085
3036.3415	3039.2924	3043.9123	3046.8170	3052.3118	3053.0164
3055.5026	3057.4994	3093.2383	3093.5975	3098.1120	3102.6984
3103.5940	3104.3282	3104.6402	3108.0250	3110.5129	3125.0055
3128.6216	3131.8706	3132.0089	3133.2625	3148.0112	3151.3530
3168.2951	3169.2089	3174.2702	3177.7768	3190.0042	3191.1013
3197.1009	3198.1537	3204.4613	3216.3612	3223.5274	3810.9636

$[Mn^{IV}(L^1)(CH_3OH)]^+$ *S*=3/2

16.2635	30.5743	32.4211	36.1537	43.3006	44.9738
52.2827	57.2760	76.6418	84.3497	88.2642	92.3895
96.0229	113.1535	118.2175	130.0802	131.3847	132.5491
141.1493	146.3845	150.8219	160.5993	173.0423	181.7910
190.0914	197.7552	203.7537	207.6845	213.4967	223.0429
233.0577	242.4657	246.9727	259.2057	266.2893	273.5894
291.4274	298.6788	304.3452	307.4813	328.7719	331.4651
338.5652	342.4783	356.0654	363.0036	365.4020	391.9203
413.4185	426.5819	435.0490	442.7188	443.4878	461.8589
489.4188	494.9948	511.5774	514.3592	523.7283	532.9483
536.1049	541.0293	549.5530	560.2072	572.4140	574.5014
578.3044	583.7344	585.2930	593.1773	609.8684	614.7448
633.7533	647.9068	665.0145	682.0628	686.5177	708.0189
744.6279	748.8981	751.4572	764.5039	777.6757	782.3974
834.3052	839.3014	846.1341	873.7446	881.1741	883.4197
887.9395	901.5664	913.1964	915.5404	936.2773	938.8347
960.3723	962.6602	968.7780	978.8541	981.6383	983.2110
988.3501	989.1351	992.2597	1003.6484	1004.4908	1018.0153
1038.3562	1040.2022	1041.2601	1043.4208	1060.8683	1061.1865
1062.4967	1062.8222	1063.1349	1065.4863	1068.9501	1072.4139
1075.5793	1093.5099	1093.6389	1125.1119	1175.5470	1182.9716
1186.4217	1188.8756	1193.6129	1208.4374	1231.4193	1238.0482
1265.1956	1271.6276	1275.3569	1282.5161	1284.2961	1296.3099
1306.8592	1315.1524	1323.5690	1335.0421	1341.8166	1350.3246
1352.2890	1355.2053	1358.0988	1361.3430	1398.2236	1416.0183
1418.3357	1421.7977	1422.4777	1423.5852	1425.7692	1427.6981
1428.6406	1446.3599	1451.4222	1451.5973	1452.7015	1466.7242
1481.1419	1481.7634	1482.8264	1484.6046	1486.1019	1488.5509
1489.4147	1489.5213	1489.7262	1494.1117	1495.8325	1501.8286
1507.1051	1509.0785	1510.0786	1511.1477	1511.9756	1512.5306
1515.8777	1531.7118	1581.0337	1622.7118	1624.7599	1625.9549
1642.9501	1650.3328	1654.2404	1655.1060	1663.7684	3039.3343
3039.4659	3044.1353	3044.3770	3048.3772	3048.5050	3064.3258
3070.2417	3087.0206	3095.0297	3095.1573	3097.8373	3100.8728
3104.1495	3105.7740	3114.4610	3117.1918	3127.4682	3127.4969
3133.1808	3133.7096	3133.9059	3140.3591	3170.2684	3170.4401
3172.5851	3175.5199	3175.7875	3176.6938	3177.8260	3190.5469
3206.6709	3214.8213	3218.1851	3223.8057	3229.9514	3759.7097

$[^{HS}Mn^{III}(L^1)(CH_3OH)]^+$ *S*=5/2

9.6679	21.6790	27.0645	30.7028	32.2638	33.9808
35.7944	43.5697	49.4118	53.3967	74.8491	77.9203
84.2436	88.5693	102.8254	109.1525	121.3851	123.2156
126.2924	130.7640	135.5974	138.1158	140.8563	163.8381
170.6704	176.0939	183.8530	191.6779	197.1039	203.8414
210.0400	221.6773	236.1075	239.2378	244.0749	255.6023
269.0649	272.3866	282.0253	292.2383	297.9462	305.5347
315.8735	317.9932	330.3150	343.6469	356.7109	360.5581
371.0640	390.9149	425.4405	427.0698	438.3673	445.8903
460.3416	481.0590	495.5864	498.3339	505.7147	512.8606
523.6293	525.9519	538.2462	544.9640	549.2231	554.7542
564.6389	568.4959	572.3151	584.4757	586.3770	608.2505
611.2055	626.7058	628.6562	678.4427	681.5462	695.2367
748.5247	751.8634	761.3725	770.9956	777.1828	782.7039
806.3994	828.5701	831.4184	875.2655	881.3401	882.3974
886.0628	894.1446	910.9227	913.1373	920.9096	944.0154
960.9220	964.2760	969.9751	974.2804	979.3321	979.5433
990.5571	995.1641	1004.5349	1008.4384	1019.2934	1030.6822
1036.6133	1037.4206	1040.7006	1044.4481	1045.4777	1054.3767
1059.5967	1059.7019	1060.8837	1061.3494	1062.6341	1064.9865
1068.2987	1080.6267	1088.2852	1131.2221	1180.3300	1181.1044
1184.5950	1188.1957	1194.7703	1196.6898	1226.7732	1241.5685
1268.7304	1271.4250	1277.1058	1284.3781	1285.8475	1290.4817
1301.7050	1309.5314	1317.5358	1330.3405	1343.3088	1346.8929
1352.1217	1356.7851	1361.6492	1367.6281	1392.5810	1411.6990
1414.4933	1417.6656	1419.9936	1421.8614	1423.5600	1425.6543
1438.4454	1450.0540	1452.3250	1453.7386	1470.7500	1472.0571
1472.9104	1474.8082	1476.6585	1480.7667	1481.2853	1484.9761
1489.8747	1490.3445	1492.0692	1494.6617	1497.3028	1500.4916

1502.9790	1509.2334	1510.3043	1511.2550	1511.6490	1513.4385
1516.7080	1522.9036	1531.9585	1603.0715	1612.2015	1619.4546
1626.5279	1633.3017	1649.7413	1653.8763	1657.8342	3035.6444
3036.6874	3041.8309	3041.9111	3043.0928	3044.1673	3051.6130
3051.9005	3062.1359	3090.8371	3091.5178	3092.5632	3095.2565
3095.3593	3096.4581	3098.1819	3107.3185	3124.6610	3125.1439
3125.4489	3129.3906	3129.9473	3139.5404	3149.9271	3150.9558
3166.0298	3167.0193	3171.5744	3174.8494	3191.8838	3192.9429
3193.4592	3203.6379	3211.6465	3220.5997	3227.3529	3798.6288

$[^{HS}Mn^{III}(L^1)(CH_3OH)]^{2+}$ *S*=1

13.0242	32.2204	34.0591	40.7640	43.3763	45.8227
54.0839	59.9638	69.0895	76.4293	80.8273	88.2434
91.5540	106.0513	111.8737	116.2903	120.3710	131.0814
139.1919	142.1891	144.1836	159.8717	168.5405	170.9270
173.8637	181.3039	189.0063	191.3692	202.3936	206.1223
206.6940	212.9179	225.6131	235.6526	246.4558	261.2000
283.2565	286.1825	292.2569	293.6579	296.2530	315.5261
325.1923	330.7363	339.8016	348.9699	350.7369	371.2138
374.0384	389.8404	399.6122	430.6278	435.3918	450.0106
473.2039	479.8880	481.3095	483.5446	500.2797	513.2982
517.7708	522.7903	537.2769	546.6887	565.6375	567.1596
572.1740	573.8862	575.9285	585.8102	588.4580	602.8966
626.5391	630.3880	660.8081	668.9249	674.6299	709.1812
741.1293	751.0165	754.1146	765.5680	775.0354	781.1415
806.5174	810.4547	848.5120	869.1205	878.0712	894.0026
903.5896	904.4150	910.7636	923.2690	938.9033	940.7617
954.3637	957.3079	961.6833	976.2146	983.6754	984.8996
986.7098	990.8032	993.2126	1004.1516	1007.5072	1009.4307
1029.1924	1036.1819	1040.3476	1040.6707	1042.7101	1044.1019
1050.0096	1053.2630	1055.0500	1065.6814	1068.4743	1069.4823
1076.0103	1096.3025	1107.7375	1121.4860	1178.2330	1178.4356
1180.9941	1187.7604	1195.0219	1211.4694	1227.5224	1259.8528
1261.0275	1277.2482	1279.1495	1297.3837	1303.6163	1311.2515
1311.9187	1332.6096	1338.5508	1339.7972	1343.4515	1357.5433
1368.4000	1371.9259	1400.3725	1407.1432	1408.2647	1410.8906
1414.2944	1417.6660	1421.3798	1423.3457	1424.6738	1429.5489
1440.5349	1442.7494	1450.8083	1459.5053	1464.5045	1471.9597
1473.8198	1475.4036	1475.4493	1477.9187	1481.4147	1483.0217
1484.9586	1485.8111	1487.2724	1494.7540	1496.0987	1501.1442
1505.0522	1506.6081	1508.5363	1509.1320	1509.7718	1514.1497
1517.4010	1528.4967	1529.6731	1531.0622	1579.3649	1622.8468
1638.6922	1645.3874	1647.5150	1648.9289	1663.9425	3037.6718
3040.4453	3046.2561	3049.4290	3052.6693	3054.9911	3077.4329
3081.2055	3084.0779	3092.9687	3102.6758	3103.5017	3104.8535
3107.4327	3111.8577	3127.1355	3132.2606	3135.6675	3143.1467
3153.8327	3153.8663	3155.4734	3155.6898	3172.9651	3176.2334
3180.7070	3193.5536	3197.3909	3199.0686	3200.3395	3204.1546
3209.0922	3210.4987	3216.2371	3226.5209	3233.2788	3770.0199

$[^{HS}Mn^{III}(L^1)(CH_3OH)]^{2+}$ *S*=3

17.3001	23.6165	32.3020	38.5294	40.8628	45.7709
48.1886	50.0887	59.2296	70.2038	75.3489	84.1030
89.4766	93.0117	94.2844	102.9788	109.6525	114.5771
124.6458	132.5549	135.7758	142.5462	149.0772	159.4875
168.1081	173.4192	181.6238	190.6212	191.3731	197.9810
200.3277	210.8004	226.0107	235.7589	245.6769	253.5777
265.3389	271.1508	276.3411	292.8465	296.5487	306.8110
317.0349	322.0614	332.2305	339.8371	349.0440	359.5692
370.2148	391.1238	408.4855	428.1017	437.4802	449.5507
471.6916	482.0664	483.6573	488.9002	503.4787	510.6056
518.1107	523.3089	528.3365	539.2208	546.0006	553.0285
562.0511	567.3969	571.3680	572.7876	585.6496	603.0910
608.3651	626.5127	633.1224	673.1001	681.7462	696.7917
746.5298	751.3919	759.4398	769.6374	777.4651	785.6295
806.3934	807.8621	821.8466	878.8048	885.8953	890.0265
896.8113	902.6440	914.7466	918.6738	924.6000	941.7776
958.1652	967.0328	973.6732	976.0794	978.8238	985.3750
992.8060	997.9513	1003.8686	1010.4239	1012.9515	1023.2694
1033.8827	1036.6790	1037.1972	1039.4024	1046.0162	1048.9970
1049.8854	1050.1919	1060.3724	1061.4405	1062.3056	1065.7373
1067.2791	1085.9374	1101.5626	1131.8506	1178.5810	1179.2875
1181.8097	1186.8599	1198.3266	1200.8164	1232.0772	1246.9018
1261.6972	1278.8287	1279.5805	1284.1052	1304.7574	1310.5251
1313.3188	1321.7938	1327.0080	1340.7044	1345.8197	1354.0168
1356.5979	1369.7759	1374.4211	1397.0916	1404.8880	1408.6819
1413.7283	1414.9011	1418.7764	1421.4888	1425.4952	1436.2128
1442.8984	1448.8716	1453.7060	1457.3397	1470.3760	1470.8868
1472.5018	1473.3452	1476.6955	1479.5942	1480.3105	1481.9883
1484.9089	1489.7923	1491.2217	1495.0732	1496.9454	1498.7434

1500.5392	1505.6088	1506.4485	1511.3967	1515.9031	1517.0773
1522.4109	1528.6303	1534.3478	1538.1497	1615.9517	1620.4801
1630.3971	1631.3600	1647.4646	1657.9337	1662.0268	3037.0750
3037.9904	3041.5221	3052.3573	3052.6737	3052.9624	3062.0862
3063.7583	3072.0542	3089.8174	3100.6234	3105.8699	3107.3136
3107.8072	3108.1691	3108.6056	3115.6156	3133.1910	3138.2410
3143.0588	3154.2475	3155.7661	3158.2150	3158.8716	3159.7521
3177.3953	3183.3351	3193.5983	3199.0066	3203.4741	3206.2505
3207.2941	3208.2600	3214.6828	3225.0066	3233.4662	3789.9558

[^{HS}Mn^{III}(L^{2})]^{0} *S*=2, Isomer 1

17.2891	19.9290	31.7210	32.4164	35.1855	39.5812
44.8975	52.4879	59.6220	68.8617	80.8836	89.0324
107.0478	122.5975	126.9280	139.2357	142.0424	147.2061
152.4303	161.6735	169.7939	181.4163	183.9808	195.1925
200.4185	205.8232	211.2194	219.8727	224.7452	227.7589
235.0681	245.8375	255.9524	263.5729	272.3979	287.1771
287.6695	305.4073	316.8173	322.1902	327.3102	345.9449
355.7430	360.2183	363.8136	374.3039	411.4240	425.4402
435.8477	456.5288	467.8642	486.2597	498.6223	505.8209
508.6305	520.9134	523.6549	532.3073	548.9064	551.8852
555.7846	567.4650	574.8226	584.3613	585.6705	586.8321
588.9458	604.1804	623.3427	628.1545	637.6651	667.3319
683.7124	705.8070	739.9638	750.1570	762.7850	776.5661
783.6399	795.9458	809.8295	817.9023	833.0730	838.3284
876.7099	881.2820	882.4583	887.1556	902.3207	908.6472
910.8537	916.2852	923.3128	952.5849	965.9926	969.2914
974.1699	976.6940	977.2082	985.0392	1002.0849	1006.2610
1011.2253	1021.4803	1036.1337	1037.8478	1038.2114	1042.8685
1052.0518	1060.4320	1060.7767	1061.1688	1061.8627	1062.0224
1063.0867	1064.3065	1064.7643	1074.1640	1086.6085	1127.6639
1158.8730	1183.1065	1184.3988	1188.7041	1189.4894	1191.0933
1198.9754	1248.8113	1254.3012	1269.4427	1270.5510	1281.8807
1286.7659	1290.8326	1296.5266	1299.5602	1300.3616	1305.4662
1330.2474	1336.2025	1336.6781	1346.0922	1351.8592	1354.3458
1357.8423	1392.4312	1398.9836	1402.9711	1419.4755	1419.8638
1420.8849	1422.9490	1424.5043	1425.0451	1452.8189	1453.6970
1455.3722	1460.9340	1479.3816	1482.1938	1482.7819	1482.8737
1483.4374	1486.3687	1487.0497	1489.2797	1489.8376	1490.5745
1490.6512	1498.0477	1500.1489	1506.1455	1507.7050	1508.9417
1511.4087	1512.4422	1514.7061	1517.2890	1520.3136	1533.4924
1614.2469	1619.6167	1620.6167	1638.9958	1649.2344	1658.8448
1660.2070	1661.3213	3031.1458	3031.4673	3034.1057	3035.5375
3038.6807	3040.2960	3040.6999	3041.3577	3058.2411	3061.5563
3082.4036	3085.4286	3086.6474	3091.2715	3094.7539	3095.8619
3098.4226	3099.8408	3114.6098	3117.1307	3117.8772	3119.6890
3122.5873	3125.1426	3126.4079	3136.1288	3156.9678	3158.2728
3159.0801	3159.5523	3163.1694	3165.5423	3176.4717	3198.1170
3207.5268	3215.8444	3223.0747			

[^{HS}Mn^{III}(L^{2})]^{0} *S*=2, Isomer 2

18.4648	19.8284	33.4256	36.5357	37.4713	39.9346
48.6223	53.1270	56.2592	71.9662	83.0861	96.4056
108.8271	121.9785	132.9193	137.2222	145.0363	149.4275
152.2230	169.7531	174.4612	181.7011	187.3523	192.4284
197.0609	208.7528	220.0430	223.0981	229.5808	240.6914
246.3267	253.8697	261.6119	263.7337	269.0012	286.2719
297.6624	305.5835	309.8399	323.7597	336.8889	344.7790
357.9028	366.2965	367.9372	377.3204	419.1736	429.1243
435.9079	445.1575	457.9793	490.4219	496.7453	507.1467
508.4590	520.7081	526.6318	535.4096	543.7446	550.1752
554.5735	563.1554	576.8179	584.6224	586.0582	586.9361
588.7110	606.6900	615.4058	625.4506	636.1922	684.2377
687.4220	695.3817	737.3141	750.4674	762.3285	769.2964
778.3049	785.6477	811.0230	825.9837	832.0409	835.5153
877.7147	878.6465	880.9503	885.4196	902.6647	908.3317
909.3726	919.4328	934.1571	961.9375	966.3656	969.6265
970.4941	976.2062	981.2424	987.5474	1003.4753	1005.1150
1012.5696	1025.1533	1036.0022	1037.9295	1038.5798	1049.2739
1049.7740	1059.5528	1059.7648	1060.7480	1062.0601	1062.1827
1062.3327	1063.6942	1072.0427	1076.3353	1087.7959	1126.2491
1161.6762	1181.4537	1185.4229	1186.9308	1187.9907	1189.4941
1196.2145	1244.5206	1251.3028	1269.2529	1271.4849	1281.5004
1282.9240	1291.3051	1296.8501	1298.5886	1302.3419	1310.4620
1331.0216	1333.3564	1341.0564	1347.8779	1350.7079	1354.6183
1358.2015	1364.4158	1396.4299	1419.3454	1420.6534	1422.1705
1422.7743	1423.9473	1425.2129	1427.7968	1453.1574	1453.4409
1455.0040	1462.8868	1479.4380	1479.9198	1481.6229	1483.8778
1485.6291	1487.0202	1489.2684	1489.8823	1491.1034	1492.3501
1496.5652	1498.2645	1506.4311	1509.0133	1509.6839	1510.4948

1511.5177	1513.5215	1516.7075	1517.3546	1520.8908	1532.6732
1611.9023	1619.7947	1620.9554	1638.4603	1649.9660	1658.9091
1659.5540	1660.7449	3028.2061	3031.0184	3031.0828	3031.4263
3037.6193	3038.8091	3039.4717	3041.6507	3043.0982	3050.9629
3082.2064	3087.3771	3088.0831	3090.2399	3092.9482	3093.2690
3095.7451	3099.9217	3101.6328	3116.7309	3118.7638	3119.4531
3121.6014	3124.5487	3125.8723	3142.6318	3155.6515	3158.3053
3159.3076	3159.3618	3166.1449	3167.2890	3184.1548	3197.4512
3206.4308	3214.4054	3221.5069			

[^{LS}Mn^{III}(L^{2})]^{0} *S*=1

11.3350	27.3000	32.3487	33.8985	34.8320	40.8095
44.1114	45.6070	54.7394	75.3769	81.8973	90.9440
99.9138	112.8631	134.8564	139.0054	146.7706	147.6295
156.0884	174.7112	187.4176	189.0315	189.6684	198.8805
205.1102	215.9205	222.4270	230.5083	236.9487	244.9422
256.4418	265.5318	273.0705	280.9143	286.4566	294.5369
303.8934	311.4748	313.7970	320.7333	330.3179	354.3964
359.0240	369.0414	375.0166	381.2148	424.8535	431.1074
440.0761	447.4897	468.1094	489.8431	496.3642	505.9952
509.5792	518.8170	528.3087	538.4106	546.6683	550.2337
555.3882	569.5254	578.0699	585.0138	586.6148	588.1821
592.2389	608.8737	613.1759	632.5458	651.2995	686.0417
686.4664	698.9996	737.7232	751.4355	760.7151	773.6731
775.8131	785.6445	811.2223	824.7294	831.7715	840.2172
877.3867	877.7917	880.4947	885.0409	901.4974	907.8875
909.1833	911.0193	936.5341	961.2755	964.8526	966.7662
970.0727	974.8498	982.9611	989.4920	1004.4819	1007.5412
1012.8428	1025.9199	1035.8015	1036.9010	1038.7060	1045.7990
1049.5555	1054.8209	1060.0638	1060.8647	1061.6297	1062.1779
1062.4617	1063.6029	1066.2718	1074.0231	1078.4599	1120.9739
1159.1938	1178.0308	1185.9730	1188.8167	1189.2162	1190.9640
1199.8443	1240.7987	1247.7533	1268.8384	1272.2478	1282.1471
1286.3853	1291.3944	1297.4679	1298.8336	1306.3024	1313.6145
1328.8638	1331.0414	1345.3044	1349.9542	1351.2046	1357.4624
1361.1760	1367.0121	1392.1954	1416.9472	1421.8671	1422.1604
1422.8015	1424.2584	1427.0006	1429.3472	1453.0860	1453.4820
1455.6098	1459.9127	1474.4503	1481.3391	1483.0543	1483.7085
1484.0236	1489.1992	1489.2553	1490.5262	1491.2356	1492.1148
1492.2984	1497.3904	1503.3055	1505.3445	1507.3026	1510.5449
1511.3653	1512.1092	1515.9611	1517.0314	1522.2238	1532.6207
1608.6768	1620.9073	1622.1536	1644.5074	1649.6659	1659.0814
1659.9792	1662.0636	3028.7530	3031.1863	3031.3479	3032.5621
3037.8033	3042.3153	3043.6666	3044.9772	3059.1630	3070.1125
3079.3300	3084.4636	3087.7271	3087.7559	3087.8375	3091.7859
3096.0873	3099.9698	3114.5695	3118.3695	3119.0242	3119.4540
3125.3515	3125.6840	3127.3266	3152.5248	3155.0645	3159.4730
3159.8674	3164.0309	3164.6187	3167.2255	3200.0710	3208.0335
3208.9622	3216.8545	3223.6104			

[^{HS}Mn^{III}(L^{2})]$^{+}$ *S*=3/2, Isomer 1

15.2707	27.6326	31.5109	35.4190	37.9722	42.9877
51.3625	53.4555	63.7792	67.4787	82.3468	92.1938
111.0346	116.6624	120.9708	122.9391	131.6975	137.8289
145.6311	160.6292	170.8220	176.9971	182.0007	190.8938
195.8207	211.0596	214.0067	218.7821	224.6868	230.2302
238.7419	242.1084	255.9583	265.7440	269.8634	289.7331
293.6264	301.7619	314.6235	327.9102	343.4559	352.7772
356.3752	362.4355	372.0877	377.7273	401.3781	417.3947
428.2490	456.5442	463.9917	477.2021	485.1535	494.3704
513.0443	514.7730	523.7428	527.5026	543.9989	548.6028
560.4273	560.6530	572.4031	579.0092	583.7369	585.3262
591.0826	605.3659	616.5623	635.2463	640.2297	661.3894
680.6240	700.0130	743.4211	750.6601	759.7544	771.4245
783.8417	793.8161	806.6244	814.6077	821.0173	842.7236
881.3176	883.8986	888.6701	896.2039	901.2577	911.2885
914.0356	923.5415	934.4983	952.6688	958.8065	970.7188
974.9760	976.7064	976.8863	985.7942	1002.4197	1005.9454
1008.9187	1033.7733	1034.5904	1037.6539	1038.9335	1039.3935
1044.5672	1050.8389	1052.2293	1059.8664	1061.0805	1063.1125
1063.4231	1063.8612	1065.5928	1075.1860	1089.5635	1124.0191
1157.7093	1178.6822	1182.5985	1182.6428	1189.5465	1194.8109
1199.3770	1246.1273	1252.8795	1269.6203	1271.5719	1275.7102
1283.9114	1293.2873	1301.2000	1301.9070	1309.1975	1321.9328
1329.0195	1331.7547	1341.1796	1344.2131	1349.2600	1353.9303
1389.4711	1396.5904	1406.8788	1408.1235	1416.4905	1421.4980
1422.1167	1424.8860	1425.5212	1431.3208	1451.4220	1453.5938
1457.6598	1469.0468	1470.7669	1475.0508	1478.7997	1481.2982
1481.5016	1482.5548	1485.3387	1486.4535	1488.6771	1489.7891
1490.2226	1495.3246	1498.2627	1500.3852	1505.9504	1509.4791

1510.8138	1512.8766	1515.8357	1521.9894	1528.2343	1532.3997
1548.1666	1621.7493	1624.8444	1639.1524	1645.7746	1649.6908
1655.5134	1659.8401	3036.5559	3038.9779	3039.7623	3041.0990
3042.9115	3050.8079	3052.2153	3059.6362	3063.6604	3066.2236
3091.0209	3092.6633	3094.3632	3095.2710	3096.5640	3098.8417
3108.3617	3118.6541	3120.3237	3122.9732	3126.0469	3128.4658
3132.1301	3142.4476	3152.3700	3153.1279	3165.7390	3168.9739
3170.5511	3174.7822	3178.1272	3193.3326	3201.6746	3203.2397
3211.8851	3220.6141	3228.3355			

$[^{HS}Mn^{III}(L^2)]^+$ *S*=3/2, Isomer 2

13.0812	29.1292	36.0060	38.2574	43.0148	48.2850
50.9552	53.3057	64.6355	76.5139	87.9234	93.6757
106.4849	113.9840	125.6586	126.6945	130.5331	134.6098
150.8096	168.1510	172.2009	179.1798	183.5772	187.4267
195.0099	203.8407	210.7186	217.8522	226.2971	233.8754
239.8771	253.9243	260.6160	266.1061	267.2810	285.2345
294.7024	302.9487	305.6454	308.9060	339.5006	348.5595
356.1517	359.1735	375.8881	385.6229	413.2131	431.0107
435.5115	440.1136	456.1056	476.8030	482.4924	496.4470
509.4305	511.5923	523.0113	529.3361	542.8989	546.3055
552.2073	557.5765	571.3518	577.7990	583.4593	585.5800
587.6660	604.6637	617.8810	625.0209	633.0186	672.4357
685.8403	693.4881	736.4459	750.7746	758.9578	766.7106
775.2744	786.4805	800.1340	820.0324	833.1253	838.4664
881.3117	883.5729	887.8312	895.9076	902.7703	912.5704
914.0947	929.1853	933.4003	960.9460	962.4602	969.3255
971.1018	975.5385	982.0250	987.3586	1002.4794	1005.9747
1010.1862	1024.8468	1034.2049	1037.5301	1039.3307	1040.5995
1048.9822	1051.5541	1053.3653	1059.7285	1060.2088	1061.5177
1062.5389	1063.5150	1070.7829	1076.7223	1088.2883	1123.0049
1162.5001	1178.3389	1182.0876	1185.0536	1188.2176	1188.8705
1197.8105	1239.6389	1247.5102	1269.6834	1272.0259	1279.6552
1286.2033	1286.8591	1297.9317	1299.7529	1312.3294	1316.6726
1328.7048	1339.1188	1340.4412	1343.6118	1344.5961	1355.7934
1360.4616	1388.1592	1409.7975	1415.8413	1421.0252	1422.2321
1423.4880	1425.7796	1427.9102	1429.6668	1451.2666	1453.0494
1457.3924	1471.6918	1471.8655	1474.9081	1476.6408	1480.5285
1482.0508	1484.3377	1486.0265	1487.3905	1491.3486	1491.7808
1492.3819	1493.6725	1499.9952	1503.8084	1507.4520	1508.8897
1511.1125	1511.7894	1513.9562	1517.2101	1520.7356	1527.4946
1531.4097	1620.3737	1621.7362	1639.3792	1640.4842	1649.5668
1653.9251	1656.3552	3035.4856	3035.9581	3042.2479	3042.7120
3044.2100	3044.8355	3048.8813	3051.2187	3052.9574	3056.3168
3095.2450	3095.2907	3095.2922	3097.5529	3097.6400	3106.4906
3106.9480	3108.8190	3111.7941	3125.3508	3125.9891	3131.4858
3132.4586	3148.1112	3152.7472	3153.2382	3168.6183	3169.0907
3175.1065	3175.3935	3187.1769	3189.6442	3199.3706	3203.1057
3211.1829	3218.7122	3226.1377			

$[^{HS}Mn^{III}(L^2)]^+$ *S*=5/2, Isomer 1

14.4380	30.7642	34.8666	37.7907	42.6222	46.8353
51.0074	54.2977	68.7584	72.1763	79.8204	99.0098
108.6559	118.0303	119.7176	133.1155	139.3912	146.0523
150.7721	154.8142	171.3915	178.6342	181.6190	184.4619
192.4261	194.0171	211.3024	215.9796	222.7771	228.8710
236.7636	240.9387	253.8982	264.3587	270.2788	290.3859
294.5414	302.3438	313.3881	320.2609	327.1200	348.7325
352.7286	357.3210	361.9785	372.3315	403.4786	415.9668
430.8358	455.4501	464.7677	478.7505	488.3232	494.8713
510.7338	515.3536	523.9973	524.7371	542.7004	548.6812
558.6116	560.0281	571.0230	577.5221	584.0704	587.2523
589.9587	602.4614	615.3456	634.1299	637.2462	661.4262
678.2227	700.3891	740.8164	750.2457	759.1103	770.6183
782.4218	791.6682	803.8412	812.1941	818.0366	843.4374
881.0638	885.3486	888.7887	897.3277	901.1469	911.2215
914.4895	922.6596	931.6488	953.1323	958.1663	969.5528
973.9518	975.5237	976.6371	985.6113	1003.4590	1006.5198
1008.3573	1026.7277	1034.3209	1037.9378	1038.8680	1039.3071
1042.1652	1051.1645	1053.0308	1060.0685	1061.4468	1062.7078
1063.4727	1063.7019	1064.3404	1073.9006	1087.3755	1120.7987
1155.7240	1179.2749	1180.2245	1183.7745	1188.3228	1191.8834
1195.8089	1243.2507	1248.8751	1264.9070	1272.5425	1272.9962
1282.6671	1289.8576	1291.6593	1298.1816	1307.2463	1319.6930
1322.7965	1330.2355	1339.4777	1341.2642	1347.2567	1354.7307
1382.7801	1391.6662	1395.2081	1408.5891	1417.4662	1421.6651
1422.0698	1425.4827	1425.6231	1428.8098	1451.8553	1454.3270
1458.3687	1464.3456	1473.5489	1475.2305	1478.8216	1480.6625
1481.8862	1483.5984	1484.5462	1485.5296	1489.0450	1489.4486
1489.9483	1494.5956	1496.5236	1498.7423	1503.1334	1509.8753

1510.9727	1513.5083	1515.6016	1520.4691	1524.6118	1529.7125
1532.3658	1621.2154	1625.0961	1637.9054	1645.4846	1649.1132
1656.1302	1660.2251	3037.1595	3039.5256	3039.7296	3040.1954
3043.1066	3050.1749	3052.1266	3054.0043	3060.0412	3070.4041
3090.9410	3091.5190	3092.5672	3094.3627	3096.8441	3098.7650
3107.7296	3116.2268	3123.7446	3124.3164	3126.5836	3128.5264
3131.9405	3144.0374	3153.4584	3153.9770	3165.9975	3168.5857
3170.6736	3176.4394	3181.9292	3196.7536	3202.2125	3204.1661
3212.8016	3220.8522	3227.3935			

$[^{HS}Mn^{III}(L^2)]^+$ *S*=5/2, Isomer 2

13.9676	26.0731	31.1391	34.6761	37.2637	42.6136
45.7947	50.5884	53.5980	75.9835	87.9678	94.6908
106.3927	114.7235	127.5186	129.7505	131.5895	134.2921
149.3509	168.3614	171.6519	179.1391	183.8552	186.4623
194.5181	202.1578	209.0543	216.6049	224.7360	233.4465
245.8093	251.4910	259.2084	265.3309	267.1119	283.1748
295.2995	301.8522	306.6946	312.1567	330.8188	347.6036
357.1724	359.7221	373.2497	375.4460	407.0479	430.8064
435.4857	439.1471	454.2173	476.9368	483.7609	497.0669
510.2983	512.4002	523.0246	528.9672	543.9628	547.6284
552.6753	559.0416	569.6989	577.4399	583.1704	585.4721
587.4576	606.9815	617.0704	628.4436	635.6974	670.3115
686.0570	692.9766	736.4093	750.5512	758.6881	766.9508
775.5903	786.4514	798.6488	817.4052	833.9127	840.6446
881.3352	882.9126	887.8423	895.6631	902.0766	912.6936
914.0848	927.9407	933.6198	959.4509	961.1542	969.0076
971.2016	975.6630	981.9131	987.5099	1002.5901	1004.1252
1010.2287	1026.4283	1033.7126	1037.2425	1039.5106	1039.5708
1048.5032	1050.1459	1051.3041	1059.7943	1060.2717	1062.3084
1062.6456	1063.5413	1070.3217	1074.7009	1085.8459	1122.1156
1158.9069	1176.1921	1180.9937	1185.2999	1188.5183	1188.7702
1197.3692	1241.3567	1246.2425	1267.2361	1271.7503	1279.0186
1285.6916	1287.8744	1297.6939	1298.3955	1311.6442	1314.7268
1330.5588	1338.1598	1340.8798	1344.2498	1345.4881	1355.3644
1363.3834	1388.3762	1409.6647	1414.6633	1420.8526	1422.2494
1423.5312	1426.3152	1428.5316	1429.9606	1451.5377	1453.1570
1456.0666	1469.8264	1471.2730	1475.0948	1477.2764	1481.3029
1482.3371	1484.9539	1486.2788	1487.8279	1490.9812	1491.7017
1493.2738	1498.4461	1499.1378	1505.0933	1508.0923	1508.1945
1511.2324	1511.8712	1512.7553	1515.6446	1520.4290	1528.0839
1530.9595	1621.3670	1623.8591	1639.3241	1642.0792	1649.4926
1655.4240	1658.1193	3035.5673	3036.2040	3039.1830	3040.5186
3044.6243	3044.8083	3052.3201	3053.0089	3056.2072	3065.3779
3094.8701	3094.9417	3095.0840	3097.4004	3097.7803	3107.4259
3107.8211	3110.0217	3117.1636	3125.0136	3125.6788	3131.7183
3132.8138	3148.2428	3153.1339	3153.3337	3168.2884	3169.0974
3174.8329	3175.2464	3188.6205	3188.9176	3200.6607	3202.8986
3210.1396	3217.4509	3225.5622			

$[^{HS}Mn^{III}(L^2)]^{2+}$ *S*=1, Isomer 1

6.5153	22.0422	25.6704	35.3287	38.7835	42.8569
51.4821	57.4979	59.5104	72.8294	77.0882	88.2780
101.2841	112.8351	120.7068	125.6652	134.6083	137.8518
143.7252	161.6275	163.7401	169.2450	179.5697	186.7014
194.5275	203.4405	211.0664	213.2364	222.7137	227.9853
231.7410	236.7790	244.2942	259.7016	270.7704	280.4652
286.9900	302.8426	313.9471	323.4333	333.6760	341.4809
351.2016	358.1672	364.5107	368.1672	400.8506	405.3706
415.2728	455.7741	461.3779	475.3547	486.1814	490.3217
493.4123	509.3943	515.3246	517.7824	530.1182	545.6525
547.8740	556.0046	566.7569	570.9513	576.0308	586.8758
587.8003	598.9142	613.7479	616.8560	634.0374	659.6295
669.9368	695.6153	739.4161	747.6639	756.7307	765.8996
781.8777	791.6277	800.3092	809.8368	813.9773	821.6154
883.8659	891.8293	894.5994	898.8002	899.8944	913.3994
919.8644	928.6616	932.7454	944.1672	957.9055	969.1837
972.2911	975.3289	976.3915	983.5710	1002.6020	1006.1282
1012.7205	1020.3176	1033.4779	1034.9289	1036.1087	1037.0117
1041.0751	1048.5789	1050.1617	1051.2646	1054.8762	1059.2068
1061.8003	1063.9216	1064.1521	1070.3330	1086.1966	1119.4311
1156.2179	1179.1782	1179.5259	1180.7837	1181.6601	1192.9889
1199.7019	1241.9411	1251.3504	1266.2258	1274.5632	1275.2560
1291.4925	1293.8366	1297.7248	1310.6461	1314.4251	1317.9263
1324.9828	1341.7995	1342.8836	1345.0898	1348.2419	1382.5634
1386.6965	1396.2751	1404.6154	1404.8813	1413.6717	1416.9426
1423.0073	1424.5733	1426.4038	1426.7913	1449.4484	1456.1284
1456.8429	1464.8259	1469.4192	1470.8516	1472.2345	1473.0678
1476.2463	1476.4507	1477.9185	1483.6906	1484.8088	1488.8500
1490.1255	1493.8222	1496.5432	1498.2102	1499.3744	1506.0613

1507.6410	1510.2755	1512.5422	1518.6607	1524.4477	1530.4656
1531.3644	1534.6370	1614.6954	1638.5973	1647.2925	1647.5393
1653.2690	1654.8428	3039.8838	3041.0845	3044.3249	3049.0667
3053.5880	3054.5951	3058.2665	3068.0596	3068.3940	3083.8988
3092.9619	3093.3628	3101.1930	3104.5340	3109.0719	3111.0196
3112.7923	3120.7174	3134.5413	3140.1037	3140.4515	3150.5423
3157.6143	3157.7036	3159.4418	3159.5767	3178.2135	3188.0979
3188.9872	3197.2420	3202.6420	3208.4778	3208.5428	3208.6400
3215.6249	3223.0814	3230.1626			

$[^{HS}Mn^{III}(L^2)]^{2+}$ *S*=1, Isomer 2

21.7719	27.2301	37.9815	39.4706	45.7315	49.1233
50.3007	67.1331	67.9866	70.5963	74.4269	96.7012
103.4436	107.5387	117.6976	127.6160	132.8283	136.1174
148.8124	158.9902	173.0206	178.2127	183.9374	188.8632
193.5479	197.1534	211.1867	216.8906	220.1747	232.0104
248.3992	260.5899	263.5273	266.1787	271.8484	284.5392
297.6754	302.8590	310.8439	316.0927	331.8695	340.6679
351.5214	361.6228	375.2041	377.4246	403.1952	414.7735
428.4010	434.4002	450.1314	472.7432	483.4676	486.5161
487.1709	508.3414	510.8756	520.2308	523.2970	533.9388
546.1244	550.6712	567.9180	570.6633	573.4171	582.1636
583.7391	596.4221	601.7304	618.4831	629.0709	672.3914
678.6203	686.1075	735.5799	749.4335	756.4436	764.7663
772.9949	787.0558	800.4633	811.2733	816.9027	822.2178
884.0027	889.5380	897.0128	897.9870	906.0752	912.0971
918.6534	928.8444	933.1878	957.5266	962.7283	967.2091
971.5498	976.0878	981.0354	983.8340	1003.4630	1006.5459
1015.4977	1020.9887	1032.4055	1034.9523	1037.7767	1039.1939
1043.6594	1050.2478	1050.7263	1052.2583	1056.0041	1057.0522
1059.2914	1063.6637	1068.3875	1074.3698	1085.6615	1121.3325
1159.6390	1174.3142	1177.7507	1178.9023	1181.7308	1190.5122
1199.0170	1246.6249	1249.0499	1254.5516	1271.3878	1272.8039
1287.7842	1299.7379	1300.3455	1306.2030	1316.3096	1319.1699
1328.6698	1342.7434	1344.6239	1347.5732	1356.1936	1369.5370
1388.4658	1398.8362	1406.5465	1406.8231	1414.5772	1419.3642
1421.1396	1423.2382	1430.3124	1435.0622	1442.7497	1451.7129
1454.5557	1466.4098	1469.0218	1472.2606	1472.5605	1473.0485
1473.2943	1475.7511	1479.5874	1482.9368	1487.9375	1488.8284
1492.0447	1492.6752	1496.5967	1501.0350	1502.5058	1504.5261
1509.6550	1510.2509	1513.0361	1516.7136	1518.4712	1528.4152
1528.8523	1530.9039	1590.0904	1628.6480	1639.8693	1643.2680
1648.0991	1651.1155	3038.8118	3041.8197	3042.0318	3053.0646
3053.6694	3055.5029	3055.5813	3062.5755	3064.7010	3073.3975
3094.4854	3097.6094	3103.9693	3105.1629	3108.0987	3109.2427
3111.3190	3118.9103	3131.2331	3137.3874	3145.9528	3151.0634
3157.3285	3157.3934	3157.6148	3157.8304	3185.5393	3185.7582
3192.2596	3196.1562	3196.7128	3204.2547	3207.9299	3208.8149
3215.7509	3223.2929	3230.6729			

$[^{HS}Mn^{III}(L^2)]^{2+}$ *S*=3, Isomer 1

16.2417	29.1455	32.5139	37.6795	45.2359	47.7161
48.6551	52.1769	67.7027	81.2059	92.0098	98.9111
112.3002	120.3874	130.0911	135.3167	138.0687	144.0535
150.8627	156.8509	165.4290	169.0063	180.5204	187.9909
191.0661	202.3787	207.6236	214.0305	221.8341	227.2781
232.1028	238.5398	253.5053	266.7151	273.5008	292.0119
297.9453	301.7943	319.0838	329.8122	335.5424	344.4197
360.2754	362.6407	369.9084	389.8665	405.5158	411.9605
424.6516	454.5073	460.5114	474.5552	488.5176	489.5411
495.4126	511.8117	517.3314	517.9615	531.5363	548.1551
551.0349	557.4597	567.0612	572.0152	576.0233	586.5234
589.2039	602.8459	616.6443	620.2662	634.6538	658.8654
669.5664	696.4734	742.2334	750.2411	757.2335	768.2099
784.4305	794.6120	801.0423	808.8281	811.5894	828.4334
885.9447	892.1338	896.2328	901.2225	902.4911	916.4782
923.4893	929.6415	932.7550	945.6971	956.8764	970.5709
972.7989	974.3455	976.7949	983.9686	1003.4529	1007.5866
1013.9418	1026.5108	1034.8378	1035.9491	1036.8692	1038.9342
1043.1518	1049.8609	1050.1380	1051.2664	1055.3952	1061.3511
1061.9004	1064.0345	1066.2811	1072.9404	1088.1665	1119.6329
1159.9947	1177.9468	1178.5015	1180.9449	1181.9621	1192.7258
1199.0206	1244.6779	1248.2359	1261.3984	1271.6960	1279.2429
1288.7163	1299.9905	1305.5121	1311.7098	1317.6653	1322.0345
1323.7143	1341.5015	1341.9530	1345.2319	1348.5181	1380.5861
1395.8120	1400.4851	1405.0925	1405.6916	1414.4209	1416.4846
1421.0420	1424.7562	1425.3703	1429.4090	1448.2759	1453.4442
1455.6179	1468.8999	1469.8814	1470.9324	1471.1308	1472.2270
1475.0866	1475.6438	1476.8759	1483.4309	1483.9721	1488.6749
1490.5387	1493.2096	1495.7791	1497.0734	1503.4607	1507.2363
1509.5765	1509.9764	1511.3818	1516.7450	1529.7102	1530.7858
1533.6616	1606.7867	1619.4637	1637.8438	1646.0611	1647.4167
1651.7124	1654.6705	3039.1309	3040.9611	3043.6985	3047.9879
3052.1815	3053.1170	3061.1478	3066.8368	3070.6375	3079.4600
3092.6831	3093.2973	3100.6956	3103.1181	3107.7007	3108.4113
3111.9990	3121.4778	3133.8162	3138.0144	3140.5652	3153.8586
3156.5409	3158.2910	3158.3971	3159.2722	3178.1259	3186.4369
3189.3732	3196.5731	3200.4521	3207.7876	3209.3875	3210.0404
3216.9957	3224.5439	3231.0870			

$[^{HS}Mn^{III}(L^2)]^{2+}$ *S*=3, Isomer 2

15.1781	29.8838	39.3339	40.3733	44.5614	50.4958
55.8389	61.4773	63.2494	73.3434	82.2198	95.0630
98.1358	106.2203	123.0878	129.8825	133.0023	140.8708
149.9165	164.9971	171.1468	173.1504	178.5738	181.3743
190.1637	197.9387	205.4875	212.7403	216.4897	232.2453
238.9035	254.3899	262.4818	267.8769	279.8566	289.8178
293.8984	299.5296	307.6572	315.1666	323.5307	340.7036
347.5315	355.6206	362.8667	375.1101	399.4506	411.8117
434.6626	438.6460	448.6041	473.3068	481.6710	485.7335
488.1650	504.7280	512.8640	521.3488	527.6980	541.2977
548.6186	553.5894	566.0385	569.2972	572.6765	582.2342
584.4928	599.2843	607.1918	619.8557	628.8724	668.5978
676.1202	684.0647	733.2379	748.3199	756.0066	765.8017
771.4775	786.9788	798.6530	806.0127	815.4511	826.1792
882.3668	888.2994	895.6440	900.3283	902.2421	914.0765
922.1405	926.5895	934.1188	956.1488	959.0387	965.0533
971.0232	976.9509	980.8128	985.0460	1004.3353	1005.0679
1015.8678	1018.0322	1029.7590	1034.1240	1034.8181	1035.2480
1042.2274	1047.8651	1050.3898	1050.7731	1053.1606	1058.9674
1061.8727	1062.2264	1068.6104	1069.4706	1083.0070	1119.2159
1153.9059	1174.7385	1175.4461	1177.2862	1183.5839	1187.9213
1197.6001	1245.6173	1249.2459	1263.8919	1267.8261	1271.5154
1286.8099	1297.6558	1299.2440	1310.9627	1314.4412	1319.2578
1330.9623	1340.7536	1341.0375	1345.3886	1355.1363	1366.9238
1388.4259	1401.5543	1405.8287	1410.9404	1413.7610	1420.8477
1423.3608	1427.3938	1429.8260	1432.5762	1448.9962	1450.5293
1451.8968	1466.8849	1468.7109	1469.6548	1471.6262	1472.2806
1473.2382	1474.4259	1478.6210	1487.9686	1489.6266	1492.3390
1493.4013	1493.7814	1496.7723	1498.8485	1505.0810	1508.0450
1508.5564	1512.6670	1513.1272	1515.5529	1519.2249	1529.7325
1530.6615	1534.0486	1615.5332	1639.7045	1647.6703	1647.8194
1649.9047	1657.7286	3035.2754	3037.9833	3042.2849	3050.7571
3052.7822	3053.9151	3057.9260	3062.2844	3065.1922	3078.8442
3096.6108	3097.0527	3103.3781	3104.5846	3108.0997	3108.6113
3108.8134	3119.7094	3133.9719	3134.5727	3141.6625	3151.9135
3157.1043	3158.1654	3159.7958	3160.6163	3180.6414	3188.5244
3190.6708	3192.6767	3203.3004	3207.1100	3207.5222	3210.4235
3213.3316	3220.6698	3229.1704			

Table B6. Energetics for all optimized structures. Energies are in Hartree, coupling constant J is in cm^{-1}.

Species	S^2	E(sol) 6-31G(d,p)	E(sol) 6-311+G(d,p)	G_{corr} 6-31G(d,p)	G(sol)	J
$[^{HS}Mn^{III}(L^1)(CH_3OH)]^0$ S=2	6.06	-2879.455014	-2879.923775	0.561075	-2879.362700	-
$[^{LS}Mn^{III}(L^1)(CH_3OH)]^0$ S=1	2.02	-2879.441113	-2879.910207	0.565973	-2879.344234	-
$[^{HS}Mn^{III}(L^1)(CH_3OH)]^+$ S=3/2	4.78	-2879.270648	-2879.730538	0.561932	-2879.168606	–154
$[Mn^{IV}(L^1)(CH_3OH)]^+$ S=3/2	3.82	-2879.277296	-2879.733024	0.568829	-2879.164195	-
$[^{HS}Mn^{III}(L^1)(CH_3OH)]^+$ S=5/2	8.84	-2879.267185	-2879.727694	0.558832	-2879.168862	-
$[^{HS}Mn^{III}(L^1)(CH_3OH)]^{2+}$ S=1	3.90	-2879.072052	-2879.524129	0.565731	-2878.958398	–310
$[^{HS}Mn^{III}(L^1)(CH_3OH)]^{2+}$ S=3	12.17	-2879.059247	-2879.512424	0.561623	-2878.950801	-
$[^{HS}Mn^{III}(L^2)]^0$ S=2, Isomer 1	6.05	-2804.214938	-2804.656154	0.563796	-2804.092358	-
$[^{HS}Mn^{III}(L^2)]^0$ S=2, Isomer 2	6.05	-2804.215057	-2804.656437	0.564745	-2804.091692	-
$[^{LS}Mn^{III}(L^2)]^0$ S=1	2.26	-2804.178296	-2804.621514	0.565626	-2804.055888	-
$[^{HS}Mn^{III}(L^2)]^+$ S=3/2, Isomer 1	4.79	-2804.032027	-2804.464697	0.564892	-2803.899805	–84
$[^{HS}Mn^{III}(L^2)]^+$ S=3/2, Isomer 2	4.80	-2804.031785	-2804.464757	0.565196	-2803.899561	–79
$[^{HS}Mn^{III}(L^2)]^+$ S=5/2, Isomer 1	8.82	-2804.030311	-2804.463153	0.564531	-2803.898622	-
$[^{HS}Mn^{III}(L^2)]^+$ S=5/2, Isomer 2	8.84	-2804.029951	-2804.463300	0.563908	-2803.899392	-
$[^{HS}Mn^{III}(L^2)]^{2+}$ S=1, Isomer 1	4.03	-2803.825411	-2804.250566	0.562924	-2803.687642	–106
$[^{HS}Mn^{III}(L^2)]^{2+}$ S=1, Isomer 2	4.07	-2803.822777	-2804.248523	0.565508	-2803.683015	–156
$[^{HS}Mn^{III}(L^2)]^{2+}$ S=3, Isomer 1	12.13	-2803.820741	-2804.246651	0.565357	-2803.681294	-
$[^{HS}Mn^{III}(L^2)]^{2+}$ S=3, Isomer 2	12.16	-2803.816046	-2804.242754	0.564375	-2803.678379	-

$$E(sol) = E(SCF) + \Delta G_{solv} \qquad \text{(Equation B1)}$$

$$G(sol) = E(sol) + G_{corr} \qquad \text{(Equation B2)}$$

E(SCF) is the electronic energy, ΔG_{solv} is the solvation free energy, and G_{corr} is the thermal free energy corrections (0 K → 298 K) for a given species. Tabulated G(sol) values combine the triple-zeta E(sol) with the double-zeta free energy corrections G_{corr}. Coupling constants for the broken symmetry wavefunctions[1,2] were computed using equation 3.

$$J = -(E^{HS} - E^{BS}) / (\langle S^2 \rangle^{HS} - \langle S^2 \rangle^{BS}) \qquad \text{(Equation B3)}$$

REFERENCES

1. Lewis, N. S.; Nocera, D. G., Powering the Planet: chemical challenges in solar energy utilization. *Proc. Natl. Acad. Sci. U. S. A.* **2006,** *103* (43), 15729-35.
2. OECD, *Energy: The Next Fifty Years*. OECD Publishing.
3. Landsberg, H. H., Policy Elements of US Resource Supply Problems. *Resources Policy* **1974,** *1* (2), 104-114.
4. Thoi, V. S.; Karunadasa, H. I.; Surendranath, Y.; Long, J. R.; Chang, C. J., Electrochemical Generation of Hydrogen from Acetic acid using a Molecular Molybdenum–oxo catalyst. *Energy & Environ. Sci.* **2012,** *5* (7), 7762.
5. Du, P.; Knowles, K.; Eisenberg, R., A Homogeneous System for the Photogeneration of Hydrogen from Water Based on a Platinum(II) Terpyridyl Acetylide Chromophore and a Molecular Cobalt Catalyst. *J. Am. Chem. Soc.* **2008,** *130* (38), 12576-12577.
6. Cady, C. W.; Crabtree, R. H.; Brudvig, G. W., Functional Models for the Oxygen-Evolving Complex of Photosystem II. *Coord. Chem. Rev.* **2008,** *252* (3-4), 444-455.
7. Cady, C. W.; Shinopoulos, K. E.; Crabtree, R. H.; Brudvig, G. W., [(H_2O)(terpy)Mn(mu-O)$_2$Mn(terpy)(OH_2)](NO3)3 (terpy = 2,2':6,2"-terpyridine) and its Relevance to the Oxygen-Evolving Complex of Photosystem II Examined through pH Dependent Cyclic Voltammetry. *Dalton Trans.* **2010,** *39* (16), 3985-9.
8. Pal, R.; Negre, C. F.; Vogt, L.; Pokhrel, R.; Ertem, M. Z.; Brudvig, G. W.; Batista, V. S., S0-State Model of the Oxygen-Evolving Complex of Photosystem II. *Biochemistry* **2013,** *52* (44), 7703-6.
9. Walter, M. G.; Warren, E. L.; McKone, J. R.; Boettcher, S. W.; Mi, Q.; Santori, E. A.; Lewis, N. S., Solar Water Splitting Cells. *Chem. Rev.* **2010,** *110* (11), 6446-6473.

10. Kaveevivitchai, N.; Kohler, L.; Zong, R.; El Ojaimi, M.; Mehta, N.; Thummel, R. P., A Ru(II) Bis-terpyridine-like Complex that Catalyzes Water Oxidation: The Influence of Steric Strain. *Inorg. Chem.***2013,** *52* (18), 10615-10622.

11. Liu, F.; Concepcion, J. J.; Jurss, J. W.; Cardolaccia, T.; Templeton, J. L.; Meyer, T. J., Mechanisms of Water Oxidation from the Blue Dimer to Photosystem II. *Inorg. Chem.* **2008,** *47* (6), 1727-1752.

12. Wanniarachchi, D. C.; Heeg, M. J.; Verani, C. N., Effect of Substituents on the Water Oxidation Activity of [RuII(terpy)(phen)Cl]+ Procatalysts. *Inorg. Chem.* **2014,** *53* (7), 3311-3319.

13. Cline, E. D.; Adamson, S. E.; Bernhard, S., Homogeneous Catalytic System for Photoinduced Hydrogen Production Utilizing Iridium and Rhodium Complexes. *Inorg. Chem.* **2008,** *47* (22), 10378-10388.

14. Connolly, P.; Espenson, J. H., Cobalt-catalyzed Evolution of Molecular Hydrogen. *Inorg. Chem.* **1986,** *25* (16), 2684-2688.

15. Baffert, C.; Artero, V.; Fontecave, M., Cobaloximes as Functional Models for Hydrogenases. 2. Proton Electroreduction Catalyzed by Difluoroborylbis(Dimethylglyoximato)Cobalt(II) Complexes in Organic Media. *Inorg. Chem.* **2007,** *46* (5), 1817-24.

16. Hu, X.; Brunschwig, B. S.; Peters, J. C., Electrocatalytic Hydrogen Evolution at Low Overpotentials by Cobalt Macrocyclic Glyoxime and Tetraimine Complexes. *J. Am. Chem. Soc.* **2007,** *129* (29), 8988-8998.

17. Jacques, P. A.; Artero, V.; Pecaut, J.; Fontecave, M., Cobalt and Nickel Diimine-Dioxime Complexes as Molecular Electrocatalysts for Hydrogen Evolution with Low Overvoltages. *Proc. Natl. Acad. Sci. U. S. A.* **2009,** *106* (49), 20627-32.

18. Bigi, J. P.; Hanna, T. E.; Harman, W. H.; Chang, A.; Chang, C. J., Electrocatalytic Reduction of Protons to Hydrogen by a Water-compatible Cobalt Polypyridyl Platform. *Chem. Commun.* **2010,** *46* (6), 958-60.

19. Caramori, S.; Husson, J.; Beley, M.; Bignozzi, C. A.; Argazzi, R.; Gros, P. C., Combination of Cobalt and Iron Polypyridine Complexes for Improving the Charge Separation and Collection in Ru(Terpyridine)(2)-Sensitised Solar Cells. *Chemistry* **2010,** *16* (8), 2611-8.

20. Losse, S.; Vos, J. G.; Rau, S., Catalytic Hydrogen Production at Cobalt Centres. *Coord. Chem. Rev.* **2010,** *254* (21-22), 2492-2504.

21. Wasylenko, D. J.; Ganesamoorthy, C.; Borau-Garcia, J.; Berlinguette, C. P., Electrochemical evidence for catalytic water oxidation mediated by a high-valent cobalt complex. *Chem. Commun.* **2011,** *47* (14), 4249-51.

22. Zhang, M.; Zhang, M. T.; Hou, C.; Ke, Z. F.; Lu, T. B., Homogeneous electrocatalytic water oxidation at neutral pH by a robust macrocyclic nickel(II) complex. *Angew. Chem. Int. Ed.* **2014,** *53* (48), 13042-8.

23. Zhang, P.; Wang, M.; Yang, Y.; Zheng, D.; Han, K.; Sun, L., Highly efficient molecular nickel catalysts for electrochemical hydrogen production from neutral water. *Chem. Commun.* **2014,** *50* (91), 14153-6.

24. Martin, D. J.; McCarthy, B. D.; Donley, C. L.; Dempsey, J. L., Electrochemical hydrogenation of a homogeneous nickel complex to form a surface adsorbed hydrogen-evolving species. *Chem. Commun.* **2015,** *51* (25), 5290-5293.

25. Tatematsu, R.; Inomata, T.; Ozawa, T.; Masuda, H., Electrocatalytic Hydrogen Production by a Nickel(II) Complex with a Phosphinopyridyl Ligand. *Angew. Chem. Int. Ed.* **2016,** *55* (17), 5247-50.

26. Zhang, M. T.; Chen, Z.; Kang, P.; Meyer, T. J., Electrocatalytic water oxidation with a copper(II) polypeptide complex. *J. Am. Chem. Soc.* **2013,** *135* (6), 2048-51.

27. Gerlach, D. L.; Bhagan, S.; Cruce, A. A.; Burks, D. B.; Nieto, I.; Truong, H. T.; Kelley, S. P.; Herbst-Gervasoni, C. J.; Jernigan, K. L.; Bowman, M. K.; Pan, S.; Zeller, M.; Papish, E. T., Studies of the pathways open to copper water oxidation catalysts containing proximal hydroxy groups during basic electrocatalysis. *Inorg. Chem.* **2014,** *53* (24), 12689-98.

28. Fillol, J. L.; Codola, Z.; Garcia-Bosch, I.; Gomez, L.; Pla, J. J.; Costas, M., Efficient water oxidation catalysts based on readily available iron coordination complexes. *Nature Chem.* **2011,** *3* (10), 807-13.

29. Hong, D.; Mandal, S.; Yamada, Y.; Lee, Y. M.; Nam, W.; Llobet, A.; Fukuzumi, S., Water oxidation catalysis with nonheme iron complexes under acidic and basic conditions: homogeneous or heterogeneous? *Inorg. Chem.* **2013,** *52* (16), 9522-31.

30. Acuna-Pares, F.; Codola, Z.; Costas, M.; Luis, J. M.; Lloret-Fillol, J., Unraveling the mechanism of water oxidation catalyzed by nonheme iron complexes. *Chemistry* **2014,** *20* (19), 5696-707.

31. Artero, V.; Chavarot-Kerlidou, M.; Fontecave, M., Splitting Water with Cobalt. *Angew. Chem. Int. Ed.* **2011,** *50* (32), 7238-7266.

32. Cook, T. R.; Dogutan, D. K.; Reece, S. Y.; Surendranath, Y.; Teets, T. S.; Nocera, D. G., Solar Energy Supply and Storage for the Legacy and Nonlegacy Worlds. *Chem. Rev.* **2010,** *110* (11), 6474-6502.

33. Britt, R. D.; Campbell, K. A.; Peloquin, J. M.; Gilchrist, M. L.; Aznar, C. P.; Dicus, M. M.; Robblee, J.; Messinger, J., Recent pulsed EPR studies of the photosystem II oxygen-evolving complex: implications as to water oxidation mechanisms. *Biochim Biophys Acta* **2004,** *1655* (1-3), 158-71.

34. Messinger, J., Evaluation of different mechanistic proposals for water oxidation in photosynthesis on the basis of Mn4OxCa structures for the catalytic site and spectroscopic data. *PCCP* **2004,** *6* (20), 4764.

35. Zong, R.; Thummel, R. P., A New Family of Ru Complexes for Water Oxidation. *J. Am. Chem. Soc.* **2005,** *127* (37), 12802-12803.

36. Meelich, K.; Zaleski, C. M.; Pecoraro, V. L., Using small molecule complexes to elucidate features of photosynthetic water oxidation. *Phil. Trans. Soc. B, Biological sciences* **2008,** *363* (1494), 1271-9; discussion 1279-81.

37. Mullins, C. S.; Pecoraro, V. L., Reflections on Small Molecule Manganese Models that Seek to Mimic Photosynthetic Water Oxidation Chemistry. *Coord. Chem. Rev.* **2008,** *252* (3-4), 416-443.

38. Concepcion, J. J.; Jurss, J. W.; Norris, M. R.; Chen, Z.; Templeton, J. L.; Meyer, T. J., Catalytic water oxidation by single-site ruthenium catalysts. *Inorg. Chem.* **2010,** *49* (4), 1277-9.

39. Wang, L. P.; Wu, Q.; Van Voorhis, T., Acid-base mechanism for ruthenium water oxidation catalysts. *Inorg. Chem.* **2010,** *49* (10), 4543-53.

40. Wasylenko, D. J.; Ganesamoorthy, C.; Koivisto, B. D.; Berlinguette, C. P., Examination of Water Oxidation by Catalysts Containing Cofacial Metal Sites. *Eur. J. Inorg. Chem.* **2010,** *2010* (20), 3135-3142.

41. Wasylenko, D. J.; Ganesamoorthy, C.; Koivisto, B. D.; Henderson, M. A.; Berlinguette, C. P., Insight into water oxidation by mononuclear polypyridyl Ru catalysts. *Inorg. Chem.* **2010,** *49* (5), 2202-9.

42. Yamazaki, H.; Shouji, A.; Kajita, M.; Yagi, M., Electrocatalytic and photocatalytic water oxidation to dioxygen based on metal complexes. *Coord. Chem. Rev.* **2010,** *254* (21-22), 2483-2491.

43. Rutherford, A. W.; Boussac, A., Biochemistry. Water photolysis in biology. *Science* **2004,** *303* (5665), 1782-4.

44. Rappaport, F.; Guergova-Kuras, M.; Nixon, P. J.; Diner, B. A.; Lavergne, J., Kinetics and Pathways of Charge Recombination in Photosystem II. *Biochemistry* **2002,** *41* (26), 8518-8527.

45. Parent, A. R.; Crabtree, R. H.; Brudvig, G. W., Comparison of primary oxidants for water-oxidation catalysis. *Chem. Soc. Rev.* **2013,** *42* (6), 2247-52.

46. Solis, B. H.; Hammes-Schiffer, S., Theoretical analysis of mechanistic pathways for hydrogen evolution catalyzed by cobaloximes. *Inorg. Chem.* **2011,** *50* (21), 11252-62.

47. Marinescu, S. C.; Winkler, J. R.; Gray, H. B., Molecular mechanisms of cobalt-catalyzed hydrogen evolution. *Proc. Natl. Acad. Sci. U. S. A.* **2012,** *109* (38), 15127-31.

48. Mandal, S.; Shikano, S.; Yamada, Y.; Lee, Y. M.; Nam, W.; Llobet, A.; Fukuzumi, S., Protonation equilibrium and hydrogen production by a dinuclear cobalt-hydride complex reduced by cobaltocene with trifluoroacetic acid. *J. Am. Chem. Soc.* **2013,** *135* (41), 15294-7.

49. Roberts, J. A. S.; Bullock, R. M., Direct Determination of Equilibrium Potentials for Hydrogen Oxidation/Production by Open Circuit Potential Measurements in Acetonitrile. *Inorg. Chem.* **2013,** *52* (7), 3823-3835.

50. Razavet, M.; Artero, V.; Fontecave, M., Proton Electroreduction Catalyzed by Cobaloximes: Functional Models for Hydrogenases. *Inorg. Chem.* **2005,** *44* (13), 4786-4795.

51. Wiedner, E. S.; Bullock, R. M., Electrochemical Detection of Transient Cobalt Hydride Intermediates of Electrocatalytic Hydrogen Production. *J. Am. Chem. Soc.* **2016,** *138* (26), 8309-8318.

52. Costentin, C.; Dridi, H.; Savéant, J.-M., Molecular Catalysis of H2 Evolution: Diagnosing Heterolytic versus Homolytic Pathways. *J. Am. Chem. Soc.* **2014,** *136* (39), 13727-13734.

53. Hu, X.; Cossairt, B. M.; Brunschwig, B. S.; Lewis, N. S.; Peters, J. C., Electrocatalytic hydrogen evolution by cobalt difluoroboryl-diglyoximate complexes. *Chem. Commun.* **2005,** (37), 4723-4725.

54. Basu, D.; Mazumder, S.; Niklas, J.; Baydoun, H.; Wanniarachchi, D.; Shi, X.; Staples, R. J.; Poluektov, O.; Schlegel, H. B.; Verani, C. N., Evaluation of the coordination preferences and catalytic pathways of heteroaxial cobalt oximes towards hydrogen generation. *Chem. Sci.* **2016,** *7* (5), 3264-3278.

55. Lei, H.; Fang, H.; Han, Y.; Lai, W.; Fu, X.; Cao, R., Reactivity and Mechanism Studies of Hydrogen Evolution Catalyzed by Copper Corroles. *ACS Catal.* **2015,** *5* (9), 5145-5153.

56. Zee, D. Z.; Chantarojsiri, T.; Long, J. R.; Chang, C. J., Metal–Polypyridyl Catalysts for Electro- and Photochemical Reduction of Water to Hydrogen. *Acc. Chem. Res.* **2015,** *48* (7), 2027-2036.

57. Lehn, J., Chemical storage of light energy. Catalytic generation of hydrogen by visible light or sunlight. Irradiation of neutral aqueous solutions. *Nouveau Journal de Chimie* **1977,** *1* (6), 449-451.

58. Du, P.; Knowles, K.; Eisenberg, R., A homogeneous system for the photogeneration of hydrogen from water based on a platinum(II) terpyridyl acetylide chromophore and a molecular cobalt catalyst. *J. Am. Chem. Soc.* **2008,** *130* (38), 12576-7.

59. Chen, L.; Wang, M.; Gloaguen, F.; Zheng, D.; Zhang, P.; Sun, L., Tetranuclear iron complexes bearing benzenetetrathiolate bridges as four-electron transformation templates and their electrocatalytic properties for proton reduction. *Inorg. Chem.* **2013,** *52* (4), 1798-806.

60. Simmons, T. R.; Artero, V., Catalytic hydrogen oxidation: dawn of a new iron age. *Angew. Chem. Int. Ed.* **2013,** *52* (24), 6143-5.

61. Han, Z.; McNamara, W. R.; Eum, M. S.; Holland, P. L.; Eisenberg, R., A nickel thiolate catalyst for the long-lived photocatalytic production of hydrogen in a noble-metal-free system. *Angew. Chem. Int. Ed.* **2012,** *51* (7), 1667-70.

62. Smith, R. D.; Prevot, M. S.; Fagan, R. D.; Trudel, S.; Berlinguette, C. P., Water oxidation catalysis: electrocatalytic response to metal stoichiometry in amorphous metal oxide films containing iron, cobalt, and nickel. *J. Am. Chem. Soc.* **2013,** *135* (31), 11580-6.

63. Smith, R. D.; Berlinguette, C. P., Accounting for the Dynamic Oxidative Behavior of Nickel Anodes. *J. Am. Chem. Soc.* **2016,** *138* (5), 1561-7.

64. Zarkadoulas, A.; Field, M. J.; Papatriantafyllopoulou, C.; Fize, J.; Artero, V.; Mitsopoulou, C. A., Experimental and Theoretical Insight into Electrocatalytic Hydrogen Evolution with Nickel Bis(aryldithiolene) Complexes as Catalysts. *Inorg. Chem.* **2016,** *55* (2), 432-44.

65. Cobo, S.; Heidkamp, J.; Jacques, P. A.; Fize, J.; Fourmond, V.; Guetaz, L.; Jousselme, B.; Ivanova, V.; Dau, H.; Palacin, S.; Fontecave, M.; Artero, V., A Janus cobalt-based catalytic material for electro-splitting of water. *Nat. Mater.* **2012,** *11* (9), 802-7.

66. Eckenhoff, W. T.; McNamara, W. R.; Du, P.; Eisenberg, R., Cobalt complexes as artificial hydrogenases for the reductive side of water splitting. *Biochimica et Biophysica Acta (BBA) - Bioenergetics* **2013,** *1827* (8), 958-973.

67. King, A. E.; Surendranath, Y.; Piro, N. A.; Bigi, J. P.; Long, J. R.; Chang, C. J., A mechanistic study of proton reduction catalyzed by a pentapyridine cobalt complex: evidence for involvement of an anation-based pathway. *Chem. Sci.* **2013,** *4* (4), 1578.

68. Schrauzer, G. N.; Holland, R. J., Hydridocobaloximes. *J. Am. Chem. Soc.* **1971,** *93* (6), 1505-1506.

69. Baffert, C.; Artero, V.; Fontecave, M., Cobaloximes as Functional Models for Hydrogenases. 2. Proton Electroreduction Catalyzed by Difluoroborylbis(dimethylglyoximato)cobalt(II) Complexes in Organic Media. *Inorg. Chem.* **2007,** *46* (5), 1817-1824.

70. Bigi, J. P.; Hanna, T. E.; Harman, W. H.; Chang, A.; Chang, C. J., Electrocatalytic reduction of protons to hydrogen by a water-compatible cobalt polypyridyl platform. *Chem. Commun.* **2010,** *46* (6), 958-960.

71. Vennampalli, M.; Liang, G.; Katta, L.; Webster, C. E.; Zhao, X., Electronic Effects on a Mononuclear Co Complex with a Pentadentate Ligand for Catalytic H2 Evolution. *Inorg. Chem.* **2014,** *53* (19), 10094-10100.

72. Lewandowska-Andralojc, A.; Baine, T.; Zhao, X.; Muckerman, J. T.; Fujita, E.; Polyansky, D. E., Mechanistic Studies of Hydrogen Evolution in Aqueous Solution Catalyzed by a Tertpyridine–Amine Cobalt Complex. *Inorg. Chem.* **2015,** *54* (9), 4310-4321.

73. Basu, D.; Mazumder, S.; Shi, X.; Baydoun, H.; Niklas, J.; Poluektov, O.; Schlegel, H. B.; Verani, C. N., Ligand transformations and efficient proton/water reduction with cobalt catalysts based on pentadentate pyridine-rich environments. *Angew. Chem. Int. Ed.* **2015,** *54* (7), 2105-10.

74. Szymczak, N. K.; Berben, L. A.; Peters, J. C., Redox rich dicobalt macrocycles as templates for multi-electron transformations. *Chem. Commun.* **2009,** (44), 6729-6731.

75. Valdez, C. N.; Dempsey, J. L.; Brunschwig, B. S.; Winkler, J. R.; Gray, H. B., Catalytic hydrogen evolution from a covalently linked dicobaloxime. *Proc. Natl. Acad. Sci. U. S. A.* **2012,** *109* (39), 15589-93.

76. Valdez, C. N.; Dempsey, J. L.; Brunschwig, B. S.; Winkler, J. R.; Gray, H. B., Catalytic hydrogen evolution from a covalently linked dicobaloxime. *Proc. Natl. Acad. Sci. U. S. A.* **2012,** *109* (39), 15589-15593.

77. Kal, S.; Filatov, A. S.; Dinolfo, P. H., Electrocatalytic proton reduction by a dicobalt tetrakis-Schiff base macrocycle in nonaqueous electrolyte. *Inorg. Chem.* **2014,** *53* (14), 7137-45.

78. Gao, Y.; Crabtree, R. H.; Brudvig, G. W., Water oxidation catalyzed by the tetranuclear Mn complex [Mn(IV)4O5(terpy)4(H2O)2](ClO4)6. *Inorg. Chem.* **2012,** *51* (7), 4043-50.

79. Kurahashi, T.; Kikuchi, A.; Shiro, Y.; Hada, M.; Fujii, H., Unique Properties and Reactivity of High-Valent Manganese−Oxo versus Manganese−Hydroxo in the Salen Platform. *Inorg. Chem.* **2010,** *49* (14), 6664-6672.

80. Lassalle-Kaiser, B.; Hureau, C.; Pantazis, D. A.; Pushkar, Y.; Guillot, R.; Yachandra, V. K.; Yano, J.; Neese, F.; Anxolabéhère-Mallart, E., Activation of a water molecule using a mononuclear Mn complex: from Mn-aquo, to Mn-hydroxo, to Mn-oxyl via charge compensation. *Energy & Environ. Sci.* **2010,** *3* (7), 924-938.

81. Wasylenko, D. J.; Palmer, R. D.; Schott, E.; Berlinguette, C. P., Interrogation of electrocatalytic water oxidation mediated by a cobalt complex. *Chem. Commun.* **2012,** *48* (15), 2107-9.

82. Cooper, S. R.; Calvin, M., Mixed valence interactions in di-.mu.-oxo bridged manganese complexes. *J. Am. Chem. Soc.* **1977,** *99* (20), 6623-6630.

83. Gersten, S. W.; Samuels, G. J.; Meyer, T. J., Catalytic oxidation of water by an oxo-bridged ruthenium dimer. *J. Am. Chem. Soc.* **1982,** *104* (14), 4029-4030.

84. Llobet, A.; Doppelt, P.; Meyer, T. J., Redox properties of aqua complexes of ruthenium(II) containing the tridentate ligands 2,2':6',2"-terpyridine and tris(1-pyrazolyl)methane. *Inorg. Chem.* **1988,** *27* (3), 514-520.

85. Zhang, G.; Zong, R.; Tseng, H.-W.; Thummel, R. P., Ru(II) Complexes of Tetradentate Ligands Related to 2,9-Di(pyrid-2‘-yl)-1,10-phenanthroline. *Inorg. Chem.* **2008,** *47* (3), 990-998.

86. Tseng, H.-W.; Zong, R.; Muckerman, J. T.; Thummel, R., Mononuclear Ruthenium(II) Complexes That Catalyze Water Oxidation. *Inorg. Chem.* **2008,** *47* (24), 11763-11773.

87. Greenwood, N. N.; Earnshaw, A., *Chemistry of the elements*. 1st ed.; Pergamon Press: Oxford ; New York, 1984; p xxi, 1542 p.

88. Limburg, J.; Brudvig, G. W.; Crabtree, R. H., O2 Evolution and Permanganate Formation from High-Valent Manganese Complexes. *J. Am. Chem. Soc.* **1997,** *119* (11), 2761-2762.

89. Collomb, M.-N.; Deronzier, A., Electro- and Photoinduced Formation and Transformation of Oxido-Bridged Multinuclear Mn Complexes. *Eur. J. Inorg. Chem.* **2009,** *2009* (14), 2025-2046.

90. Karlsson, E. A.; Lee, B.-L.; Åkermark, T.; Johnston, E. V.; Kärkäs, M. D.; Sun, J.; Hansson, Ö.; Bäckvall, J.-E.; Åkermark, B., Photosensitized Water Oxidation by Use of a Bioinspired Manganese Catalyst. *Angew. Chem. Int. Ed.* **2011,** *50* (49), 11715-11718.

91. Hammarström, L.; Styring, S., Coupled electron transfers in artificial photosynthesis. *Phil. Trans. Soc. B: Bio.Sci.* **2008,** *363* (1494), 1283-1291.

92. Anderlund, M. F.; Zheng, J.; Ghiladi, M.; Kritikos, M.; Rivière, E.; Sun, L.; Girerd, J.-J.; Åkermark, B., A new, dinuclear high spin manganese(III) complex with bridging phenoxy and methoxy groups. Structure and magnetic properties. *Inorg. Chem. Commun.* **2006,** *9* (12), 1195-1198.

93. Anderlund, M. F.; Högblom, J.; Shi, W.; Huang, P.; Eriksson, L.; Weihe, H.; Styring, S.; Åkermark, B.; Lomoth, R.; Magnuson, A., Redox Chemistry of a Dimanganese(II,III) Complex with an Unsymmetric Ligand: Water Binding, Deprotonation and Accumulative Light-Induced Oxidation. *Eur. J. Inorg. Chem.* **2006,** *2006* (24), 5033-5047.

94. Anderlund, M. F.; Zheng, J.; Ghiladi, M.; Kritikos, M.; Rivière, E.; Sun, L.; Girerd, J.-J.; Åkermark, B., A new, dinuclear high spin manganese(III) complex with bridging phenoxy and methoxy groups. Structure and magnetic properties. *Inorg. Chem. Commun.* **2006,** *9* (12), 1195-1198.

95. Borgström, M.; Shaikh, N.; Johansson, O.; Anderlund, M. F.; Styring, S.; Åkermark, B.; Magnuson, A.; Hammarström, L., Light Induced Manganese Oxidation and Long-Lived

Charge Separation in a Mn2II,II−RuII(bpy)3−Acceptor Triad. *J. Am. Chem. Soc.* **2005,** *127* (49), 17504-17515.

96. Burdinski, D.; Bothe, E.; Wieghardt, K., Synthesis and Characterization of Tris(bipyridyl)ruthenium(II)-Modified Mono-, Di-, and Trinuclear Manganese Complexes as Electron-Transfer Models for Photosystem II. *Inorg. Chem.* **1999,** *39* (1), 105-116.

97. Kurahashi, T.; Hada, M.; Fujii, H., Critical Role of External Axial Ligands in Chirality Amplification of trans-Cyclohexane-1,2-diamine in Salen Complexes. *J. Am. Chem. Soc.* **2009,** *131* (34), 12394-12405.

98. Kurahashi, T.; Fujii, H., One-Electron Oxidation of Electronically Diverse Manganese(III) and Nickel(II) Salen Complexes: Transition from Localized to Delocalized Mixed-Valence Ligand Radicals. *J. Am. Chem. Soc.* **2011,** *133* (21), 8307-8316.

99. Schmitt, H.; Lomoth, R.; Magnuson, A.; Park, J.; Fryxelius, J.; Kritikos, M.; Mårtensson, J.; Hammarström, L.; Sun, L.; Åkermark, B., Synthesis, Redox Properties, and EPR Spectroscopy of Manganese(III) Complexes of the Ligand N,N-Bis(2-hydroxybenzyl)-N′-2-hydroxybenzylidene-1,2-diaminoethane: Formation of Mononuclear, Dinuclear, and Even Higher Nuclearity Complexes. *Chem. Eur. J.* **2002,** *8* (16), 3757-3768.

100. Kurahashi, T.; Kikuchi, A.; Tosha, T.; Shiro, Y.; Kitagawa, T.; Fujii, H., Transient Intermediates from Mn(salen) with Sterically Hindered Mesityl Groups: Interconversion between MnIV-Phenolate and MnIII-Phenoxyl Radicals as an Origin for Unique Reactivity. *Inorg. Chem.* **2008,** *47* (5), 1674-1686.

101. Colpas, G. J.; Hamstra, B. J.; Kampf, J. W.; Pecoraro, V. L., The Preparation of VO3+ and VO2+ Complexes Using Hydrolytically Stable, Asymmetric Ligands Derived from Schiff Base Precursors. *Inorg. Chem.* **1994,** *33* (21), 4669-4675.

102. Hong, D.; Jung, J.; Park, J.; Yamada, Y.; Suenobu, T.; Lee, Y.-M.; Nam, W.; Fukuzumi, S., Water-soluble mononuclear cobalt complexes with organic ligands acting as precatalysts for efficient photocatalytic water oxidation. *Energy & Environ. Sci.* **2012,** *5* (6), 7606-7616.

103. Rigsby, M. L.; Mandal, S.; Nam, W.; Spencer, L. C.; Llobet, A.; Stahl, S. S., Cobalt analogs of Ru-based water oxidation catalysts: overcoming thermodynamic instability and kinetic lability to achieve electrocatalytic O2 evolution. *Chem. Sci.* **2012,** *3* (10), 3058.

104. Stuart, B., Infrared Spectroscopy. In *Kirk-Othmer Encyclopedia of Chemical Technology*, John Wiley & Sons, Inc.: 2000.

105. Kebarle, P.; Verkerk, U. H., On the Mechanism of Electrospray Ionization Mass Spectrometry (ESIMS). In *Electrospray and MALDI Mass Spectrometry*, John Wiley & Sons, Inc.: 2010; pp 1-48.

106. Weil, J. A.; Bolton, J. R., Basic Principles of Paramagnetic Resonance. In *Electron Paramagnetic Resonance*, John Wiley & Sons, Inc.: 2006; pp 1-35.

107. Stoll, S.; Schweiger, A., EasySpin, a comprehensive software package for spectral simulation and analysis in EPR. *J Magn Reson* **2006,** *178* (1), 42-55.

108. Bruker Single Crystal X-ray Diffraction. https://www.bruker.com/products/x-ray-diffraction-and-elemental-analysis/single-crystal-x-ray-diffraction.html.

109.<Product_Sheet_31_APEX_II_CCD_Detector_DOC-S86EXS031_V2_en_low.pdf>.

110. <APEX2 User Manual.pdf>.

111. Bourhis, L. J.; Dolomanov, O. V.; Gildea, R. J.; Howard, J. A.; Puschmann, H., The anatomy of a comprehensive constrained, restrained refinement program for the modern

computing environment - Olex2 dissected. *Acta Crystallogr A Found Adv* **2015,** *71* (Pt 1), 59-75.

112. Sheldrick, G., A short history of SHELX. *Acta Crystallogr. A* **2008,** *64* (1), 112-122.

113. <07_solving_phase_problem_mir_sir_lecture7.pdf>.

114. Bard, A. J.; Faulkner, L. R., *Electrochemical methods : fundamentals and applications*. Wiley: New York, 1980; p xviii, 718 p.

115. Basu, D.; Allard, M. M.; Xavier, F. R.; Heeg, M. J.; Schlegel, H. B.; Verani, C. N., Modulation of electronic and redox properties in phenolate-rich cobalt(III) complexes and their implications for catalytic proton reduction. *Dalton Trans.* **2015,** *44* (7), 3454-66.

116. Milner, G. W. C.; Phillips, G., *Coulometry in analytical chemistry*. 1st ed.; Pergamon Press: Oxford, New York, 1967; p x, 207 p.

117. Verani, C. N.; Kpogo, K.; Mazumder, S.; Wang, D.; Schlegel, H. B.; Fiedler, A., Bimetallic Cooperativity in Proton Reduction with an Amido-bridged Cobalt Catalyst. *Chem. Eur. J.* **2017**.

118. Zhou, W.; Apkarian, R.; Wang, Z. L.; Joy, D., Fundamentals of Scanning Electron Microscopy (SEM). In *Scanning Microscopy for Nanotechnology: Techniques and Applications*, Zhou, W.; Wang, Z. L., Eds. Springer New York: New York, NY, 2007; pp 1-40.

119. Vernon-Parry, K. D., Scanning electron microscopy: an introduction. *III-Vs Review* **2000,** *13* (4), 40-44.

120. McCarthy, J. J.; McMillan, D. J., Application of X-ray Optics to Energy-Dispersive Spectroscopy. *Microsc Microanal* **1998,** *4* (6), 632-639.

121. Williams, T. J., Scanning electron microscopy and x-ray microanalysis, 3rd edition. By Joseph Goldstein, Dale Newbury, David Joy, Charles Lyman, Patrick Echlin, Eric Lifshin, Linda Sawyer, Joseph Michael Kluwer Academic Publishers, New York (2003) ISBN 0306472929; hardback; 688; $75.00. *Scanning* **2005,** *27* (4), 215-216.

122. Calais, J.-L., Density-functional theory of atoms and molecules. R.G. Parr and W. Yang, Oxford University Press, New York, Oxford, 1989. IX + 333 pp. *Intl. J. Quantum Chem.* **1993,** *47* (1), 101-101.

123. M. J. Frisch, G. W. T., H. B. Schlegel, G. E. Scuseria, M. A. Robb, J. R. Cheeseman, G. Scalmani, V. Barone, B. Mennucci, G. A. Petersson, H. Nakatsuji, M. Caricato, X. Li, H. P. Hratchian, A. F. Izmaylov, J. Bloino, G. Zheng, J. L. Sonnenberg, W. Liang, M. Hada, M. Ehara, K. Toyota, R. Fukuda, J. Hasegawa, M. Ishida, T. Nakajima, Y. Honda, O. Kitao, H. Nakai, T. Vreven, J. A. Montgomery, Jr., J. E. Peralta, F. Ogliaro, M. Bearpark, J. J. Heyd, E. Brothers, K. N. Kudin, V. N. Staroverov, T. Keith, R. Kobayashi, J. Normand, K. Raghavachari, A. Rendell, J. C. Burant, S. S. Iyengar, J. Tomasi, M. Cossi, N. Rega, J. M. Millam, M. Klene, J. E. Knox, J. B. Cross, V. Bakken, C. Adamo, J. Jaramillo, R. Gomperts, R. E. Stratmann, O. Yazyev, A. J. Austin, R. Cammi, C. Pomelli, J. W. Ochterski, R. L. Martin, K. Morokuma, V. G. Zakrzewski, G. A. Voth, P. Salvador, J. J. Dannenberg, S. Dapprich, P. V. Parandekar, N. J. Mayhall, A. D. Daniels, O. Farkas, J. B. Foresman, J. V. Ortiz, J. Cioslowski, and D. J. Fox, , Gaussian Development Version, Revision H.31. Gaussian, Inc: Wallingford, CT, 2010.

124. Becke, A. D., Density-functional exchange-energy approximation with correct asymptotic behavior. *Phys. Rev. A.* **1988,** *38* (6), 3098-3100.

125. Becke, A. D., Density-functional exchange-energy approximation with correct asymptotic behavior. *Phys. Rev. A Gen. Phys.* **1988,** *38* (6), 3098-3100.

126. Pople, P. C. H. a. J. A., *Theoretica Chimica Act.* **1973,** *28*, 213-222.

127. M. M. Francl, W. J. P., W. J. Hehre, J. S. Binkley, M. S. Gordon, D. J. DeFrees and J. A. Pople *J. Chem. Phys.* **1982,** *77*, 3654-3665.

128. M. Dolg, U. W., H. Stoll and H. Preuss *J. Chem. Phys.* **1987,** *86*, 866-872.

129. Wilson, A. D.; Newell, R. H.; McNevin, M. J.; Muckerman, J. T.; Rakowski DuBois, M.; DuBois, D. L., Hydrogen oxidation and production using nickel-based molecular catalysts with positioned proton relays. *J. Am. Chem. Soc.* **2006,** *128* (1), 358-66.

130. Kankanamalage, P. H. A.; Mazumder, S.; Tiwari, V.; Kpogo, K. K.; Bernhard Schlegel, H.; Verani, C. N., Efficient electro/photocatalytic water reduction using a [NiII(N2Py3)]2+ complex. *Chem. Commun.* **2016**.

131. Solis, B. H.; Hammes-Schiffer, S., Substituent effects on cobalt diglyoxime catalysts for hydrogen evolution. *J. Am. Chem. Soc.* **2011,** *133* (47), 19036-9.

132. Muckerman, J. T.; Fujita, E., Theoretical studies of the mechanism of catalytic hydrogen production by a cobaloxime. *Chem. Commun.* **2011,** *47* (46), 12456-8.

133. Solis, B. H.; Yu, Y.; Hammes-Schiffer, S., Effects of ligand modification and protonation on metal oxime hydrogen evolution electrocatalysts. *Inorg. Chem.* **2013,** *52* (12), 6994-9.

134. Concepcion, J. J.; Jurss, J. W.; Templeton, J. L.; Meyer, T. J., One Site is Enough. Catalytic Water Oxidation by [Ru(tpy)(bpm)(OH2)]2+ and [Ru(tpy)(bpz)(OH2)]2+. *J. Am. Chem. Soc.* **2008,** *130* (49), 16462-16463.

135. Concepcion, J. J.; Jurss, J. W.; Brennaman, M. K.; Hoertz, P. G.; Patrocinio, A. O. T.; Murakami Iha, N. Y.; Templeton, J. L.; Meyer, T. J., Making Oxygen with Ruthenium Complexes. *Acc. Chem. Res.* **2009,** *42* (12), 1954-1965.

136. Wasylenko, D. J.; Ganesamoorthy, C.; Henderson, M. A.; Koivisto, B. D.; Osthoff, H. D.; Berlinguette, C. P., Electronic modification of the [Ru(II)(tpy)(bpy)(OH(2))](2+) scaffold: effects on catalytic water oxidation. *J. Am. Chem. Soc.* **2010,** *132* (45), 16094-106.

137. Wang, L.-P.; Wu, Q.; Van Voorhis, T., Acid−Base Mechanism for Ruthenium Water Oxidation Catalysts. *Inorg. Chem.* **2010,** *49* (10), 4543-4553.

138. Tong, L.; Duan, L.; Xu, Y.; Privalov, T.; Sun , L., Structural Modifications of Mononuclear Ruthenium Complexes: A Combined Experimental and Theoretical Study on the Kinetics of Ruthenium-Catalyzed Water Oxidation. *Angew. Chem. Int. Ed.* **2011,** *50* (2), 445-449.

139. England, J.; Britovsek, G. J. P.; Rabadia, N.; White, A. J. P., Ligand Topology Variations and the Importance of Ligand Field Strength in Non-Heme Iron Catalyzed Oxidations of Alkanes. *Inorg. Chem.* **2007,** *46* (9), 3752-3767.

140. Bruker Corporation. Datamonitor.: New York, NY. http://proxy.lib.wayne.edu/login?url=http://search.ebscohost.com/direct.asp?db=bth&jid=BDE4&scope=site.

141. Becke, A. D., Density-functional exchange-energy approximation with correct asymptotic behavior. *Phys. Rev. A.* **1988,** *38* (6), 3098.

142. Perdew, J. P., Density-functional approximation for the correlation energy of the inhomogeneous electron gas. *Physical Review B* **1986,** *33* (12), 8822.

143. Frisch, M. J.; Trucks, G. W.; Schlegel, H. B.; Scuseria, G. E.; Robb, M. A.; Cheeseman, J. R.; Scalmani, G.; Barone, V.; Petersson, G. A.; Nakatsuji, H.; Li, X.; Caricato, M.;

Marenich, A.; Bloino, J.; Janesko, B. G.; Gomperts, R.; Mennucci, B.; Hratchian, H. P.; Ortiz, J. V.; Izmaylov, A. F.; Sonnenberg, J. L.; Williams-Young, D.; Ding, F.; Lipparini, F.; Egidi, F.; Goings, J.; Peng, B.; Petrone, A.; Henderson, T.; Ranasinghe, D.; Zakrzewski, V. G.; Gao, J.; Rega, N.; Zheng, G.; Liang, W.; Hada, M.; Ehara, M.; Toyota, K.; Fukuda, R.; Hasegawa, J.; Ishida, M.; Nakajima, T.; Honda, Y.; Kitao, O.; Nakai, H.; Vreven, T.; Throssell, K.; Montgomery, J. A.; Jr.; Peralta, J. E.; Ogliaro, F.; Bearpark, M.; Heyd, J. J.; Brothers, E.; Kudin, K. N.; Staroverov, V. N.; Keith, T.; Kobayashi, R.; Normand, J.; Raghavachari, K.; Rendell, A.; Burant, J. C.; Iyengar, S. S.; Tomasi, J.; Cossi, M.; Millam, J. M.; Klene, M.; Adamo, C.; Cammi, R.; Ochterski, J. W.; Martin, R. L.; Morokuma, K.; Farkas, O.; Foresman, J. B.; Fox, D. J., Gaussian 09, revision E01. **2016**.

144. Andrae, D.; Häußermann, U.; Dolg, M.; Stoll, H.; Preuß, H., Energy-adjusted ab initio pseudopotentials for the second and third row transition elements. *Theoretica chimica acta* **1990,** *77* (2), 123-141.

145. Dolg, M.; Wedig, U.; Stoll, H.; Preuss, H., Energy-adjusted abinitio pseudopotentials for the first row transition elements. *J. Chem. Phys.* **1987,** *86* (2), 866-872.

146. Ditchfield, R.; Hehre, W. J.; Pople, J. A., Self-consistent molecular-orbital methods. IX. An extended Gaussian-type basis for molecular-orbital studies of organic molecules. *J. Chem. Phys.* **1971,** *54* (2), 724-728.

147. Francl, M. M.; Pietro, W. J.; Hehre, W. J.; Binkley, J. S.; Gordon, M. S.; DeFrees, D. J.; Pople, J. A., Self-Consistent Molecular Orbital Methods. XXIII. A Polarization-Type Basis Set for Second-Row Elements. *J. Chem. Phys.* **1982,** *77* (7), 3654-3665.

148. Hariharan, P. C.; Pople, J. A., The Influence of Polarization Functions on Molecular Orbital Hydrogenation Energies. *Theoretica chimica acta* **1973,** *28* (3), 213-222.

149. Hehre, W. J.; Ditchfield, R.; Pople, J. A., Self-Consistent Molecular Orbital Methods. XII. Further Extensions of Gaussian-Type Basis Sets for Use in Molecular Orbital Studies of Organic Molecules. *J. Chem. Phys.* **1972,** *56* (5), 2257-2261.

150. Clark, T.; Chandrasekhar, J.; Spitznagel, G. W.; Schleyer, P. V. R., Efficient diffuse function-augmented basis sets for anion calculations. III. The 3-21+G basis set for first-row elements, Li-F. *J. Computational Chemistry* **1983,** *4* (3), 294-301.

151. Marenich, A. V.; Cramer, C. J.; Truhlar, D. G., Universal Solvation Model Based on Solute Electron Density and on a Continuum Model of the Solvent Defined by the Bulk Dielectric Constant and Atomic Surface Tensions. *J. Phys. Chem. B* **2009,** *113* (18), 6378-6396.

152. Dennington, R.; Keith, T.; Millam, J., GaussView, version 5. *Semichem Inc., Shawnee Mission, KS* **2009**.

153. Tong, L.; Zong, R.; Thummel, R. P., Visible light-driven hydrogen evolution from water catalyzed by a molecular cobalt complex. *J. Am. Chem. Soc.* **2014,** *136* (13), 4881-4.

154. <Ortep3.pdf>.

155. Wang, H. Y.; Mijangos, E.; Ott, S.; Thapper, A., Water oxidation catalyzed by a dinuclear cobalt-polypyridine complex. *Angew. Chem. Int. Ed.* **2014,** *53* (52), 14499-502.

156. Song, X.; Wen, H.; Ma, C.; Chen, H.; Chen, C., Hydrogen photogeneration catalyzed by a cobalt complex of a pentadentate aminopyridine-based ligand. *New J. Chem.* **2015,** *39* (3), 1734-1741.

157. Queyriaux, N.; Jane, R. T.; Massin, J.; Artero, V.; Chavarot-Kerlidou, M., Recent developments in hydrogen evolving molecular cobalt(II)–polypyridyl catalysts. *Coord. Chem. Rev.* **2015**.

158. Stubbert, B. D.; Peters, J. C.; Gray, H. B., Rapid water reduction to H2 catalyzed by a cobalt bis(iminopyridine) complex. *J. Am. Chem. Soc.* **2011,** *133* (45), 18070-3.

159. Knijnenburg, Q.; Hetterscheid, D.; Kooistra, T. M.; Budzelaar, Peter H. M., The Electronic Structure of (Diiminopyridine)cobalt(I) Complexes. *Eur. J. Inorg. Chem.* **2004,** *2004* (6), 1204-1211.

160. Zhang, P.; Wang, M.; Gloaguen, F.; Chen, L.; Quentel, F.; Sun, L., Electrocatalytic hydrogen evolution from neutral water by molecular cobalt tripyridine-diamine complexes. *Chem. Commun.* **2013,** *49* (82), 9455-7.

161. Di Giovanni, C.; Gimbert-Surinach, C.; Nippe, M.; Benet-Buchholz, J.; Long, J. R.; Sala, X.; Llobet, A., Dinuclear Cobalt Complexes with a Decadentate Ligand Scaffold: Hydrogen Evolution and Oxygen Reduction Catalysis. *Chemistry* **2016,** *22* (1), 361-9.

162. Fukuzumi, S.; Mandal, S.; Mase, K.; Ohkubo, K.; Park, H.; Benet-Buchholz, J.; Nam, W.; Llobet, A., Catalytic four-electron reduction of O2 via rate-determining proton-coupled electron transfer to a dinuclear cobalt-mu-1,2-peroxo complex. *J. Am. Chem. Soc.* **2012,** *134* (24), 9906-9.

163. Nelson, J. H.; Nathan, L. C.; Ragsdale, R. O., Complexes of aromatic amine oxides. 4-Substituted quinoline 1-oxide complexes of cobalt(II) and nickel(II) perchlorates. *Inorg. Chem.* **1968,** *7* (9), 1840-1845.

164. Tong, L.; Kopecky, A.; Zong, R.; Gagnon, K. J.; Ahlquist, M. S.; Thummel, R. P., Light-Driven Proton Reduction in Aqueous Medium Catalyzed by a Family of Cobalt Complexes with Tetradentate Polypyridine-Type Ligands. *Inorg. Chem.* **2015,** *54* (16), 7873-84.

165. Sun, Y.; Bigi, J. P.; Piro, N. A.; Tang, M. L.; Long, J. R.; Chang, C. J., Molecular cobalt pentapyridine catalysts for generating hydrogen from water. *J. Am. Chem. Soc.* **2011,** *133* (24), 9212-5.

166. Singh, W. M.; Baine, T.; Kudo, S.; Tian, S.; Ma, X. A.; Zhou, H.; DeYonker, N. J.; Pham, T. C.; Bollinger, J. C.; Baker, D. L.; Yan, B.; Webster, C. E.; Zhao, X., Electrocatalytic and photocatalytic hydrogen production in aqueous solution by a molecular cobalt complex. *Angew. Chem. Int. Ed.* **2012,** *51* (24), 5941-4.

167. Wasylenko, D. J.; Palmer, R. D.; Schott, E.; Berlinguette, C. P., Interrogation of electrocatalytic water oxidation mediated by a cobalt complex. *Chem. Commun.* **2012,** *48* (15), 2107-2109.

168. Karkas, M. D.; Akermark, B., Water oxidation using earth-abundant transition metal catalysts: opportunities and challenges. *Dalton Trans.* **2016,** *45* (37), 14421-14461.

169. Zhao, Y.; Lin, J.; Liu, Y.; Ma, B.; Ding, Y.; Chen, M., Efficient light-driven water oxidation catalyzed by a mononuclear cobalt(iii) complex. *Chem. Commun.* **2015,** *51* (97), 17309-17312.

170. Das, B.; Orthaber, A.; Ott, S.; Thapper, A., Water oxidation catalysed by a mononuclear CoII polypyridine complex; possible reaction intermediates and the role of the chloride ligand. *Chem. Commun.* **2015,** *51* (66), 13074-13077.

171. Lei, H.; Han, A.; Li, F.; Zhang, M.; Han, Y.; Du, P.; Lai, W.; Cao, R., Electrochemical, spectroscopic and theoretical studies of a simple bifunctional cobalt corrole catalyst for oxygen evolution and hydrogen production. *PCCP* **2014,** *16* (5), 1883-1893.

172. Crandell, D. W.; Ghosh, S.; Berlinguette, C. P.; Baik, M. H., How a [Co(IV) a bond and a half O](2+) fragment oxidizes water: involvement of a biradicaloid [Co(II)-(O)](2+) species in forming the O-O bond. *ChemSusChem* **2015,** *8* (5), 844-52.

173. Dogutan, D. K.; McGuire, R., Jr.; Nocera, D. G., Electocatalytic water oxidation by cobalt(III) hangman beta-octafluoro corroles. *J. Am. Chem. Soc.* **2011,** *133* (24), 9178-80.

174. Schilling, M.; Patzke, G. R.; Hutter, J.; Luber, S., Computational Investigation and Design of Cobalt Aqua Complexes for Homogeneous Water Oxidation. *J. Phys. Chem. C* **2016,** *120* (15), 7966-7975.

175. Nguyen, A. I.; Ziegler, M. S.; Oña-Burgos, P.; Sturzbecher-Hohne, M.; Kim, W.; Bellone, D. E.; Tilley, T. D., Mechanistic Investigations of Water Oxidation by a Molecular Cobalt Oxide Analogue: Evidence for a Highly Oxidized Intermediate and Exclusive Terminal Oxo Participation. *J. Am. Chem. Soc.* **2015,** *137* (40), 12865-12872.

176. Brunschwig, B. S.; Chou, M. H.; Creutz, C.; Ghosh, P.; Sutin, N., Mechanisms of water oxidation to oxygen: cobalt(IV) as an intermediate in the aquocobalt(II)-catalyzed reaction. *J. Am. Chem. Soc.* **1983,** *105* (14), 4832-4833.

177. Gerken, J. B.; McAlpin, J. G.; Chen, J. Y. C.; Rigsby, M. L.; Casey, W. H.; Britt, R. D.; Stahl, S. S., Electrochemical Water Oxidation with Cobalt-Based Electrocatalysts from pH 0–14: The Thermodynamic Basis for Catalyst Structure, Stability, and Activity. *J. Am. Chem. Soc.* **2011,** *133* (36), 14431-14442.

178. Wasylenko, D. J.; Palmer, R. D.; Berlinguette, C. P., Homogeneous water oxidation catalysts containing a single metal site. *Chem. Commun.* **2013,** *49* (3), 218-227.

179. Lo, W. K. C.; Castillo, C. E.; Gueret, R.; Fortage, J.; Rebarz, M.; Sliwa, M.; Thomas, F.; McAdam, C. J.; Jameson, G. B.; McMorran, D. A.; Crowley, J. D.; Collomb, M.-N.;

Blackman, A. G., Synthesis, Characterization, and Photocatalytic H2-Evolving Activity of a Family of [Co(N4Py)(X)]n+ Complexes in Aqueous Solution. *Inorg. Chem.* **2016,** *55* (9), 4564-4581.

180. Kankanamalage, P. H. A.; Mazumder, S.; Tiwari, V.; Kpogo, K. K.; Bernhard Schlegel, H.; Verani, C. N., Efficient electro/photocatalytic water reduction using a [NiII(N2Py3)]2+ complex. *Chem. Commun.* **2016,** *52* (91), 13357-13360.

181. Xie, J.; Zhou, Q.; Li, C.; Wang, W.; Hou, Y.; Zhang, B.; Wang, X., An unexpected role of the monodentate ligand in photocatalytic hydrogen production of the pentadentate ligand-based cobalt complexes. *Chem. Commun.* **2014,** *50* (49), 6520-6522.

182. Han, Z.; McNamara, W. R.; Eum, M.-S.; Holland, P. L.; Eisenberg, R., A Nickel Thiolate Catalyst for the Long-Lived Photocatalytic Production of Hydrogen in a Noble-Metal-Free System. *Angew. Chem. Int. Ed.* **2012,** *51* (7), 1667-1670.

183. Varma, S.; Castillo, C. E.; Stoll, T.; Fortage, J.; Blackman, A. G.; Molton, F.; Deronzier, A.; Collomb, M.-N., Efficient photocatalytic hydrogen production in water using a cobalt(iii) tetraaza-macrocyclic catalyst: electrochemical generation of the low-valent Co(I) species and its reactivity toward proton reduction. *PCCP* **2013,** *15* (40), 17544-17552.

184. Turner, J. A., Sustainable Hydrogen Production. *Science* **2004,** *305* (5686), 972-974.

185. Rountree, E. S.; Martin, D. J.; McCarthy, B. D.; Dempsey, J. L., Linear Free Energy Relationships in the Hydrogen Evolution Reaction: Kinetic Analysis of a Cobaloxime Catalyst. *ACS Catal.* **2016,** *6* (5), 3326-3335.

186. Pilkington, N. H.; Robson, R., Complexes of binucleating ligands. III. Novel complexes of a macrocyclic binucleating ligand. *Australian Journal of Chemistry* **1970,** *23* (11), 2225-2236.

187. Ōkawa, H.; Furutachi, H.; Fenton, D. E., Heterodinuclear metal complexes of phenol-based compartmental macrocycles. *Coord. Chem. Rev.* **1998,** *174* (1), 51-75.

188. Laga, S. M.; Blakemore, J. D.; Henling, L. M.; Brunschwig, B. S.; Gray, H. B., Catalysis of Proton Reduction by a [BO4]-Bridged Dicobalt Glyoxime. *Inorg. Chem.* **2014,** *53* (24), 12668-12670.

189. Di Giovanni, C.; Gimbert-Suriñach, C.; Nippe, M.; Benet-Buchholz, J.; Long, J. R.; Sala, X.; Llobet, A., Dinuclear Cobalt Complexes with a Decadentate Ligand Scaffold: Hydrogen Evolution and Oxygen Reduction Catalysis. *Chem. Eur. J.* **2016,** *22* (1), 361-369.

190. Basu, D.; Mazumder, S.; Shi, X.; Staples, R. J.; Schlegel, H. B.; Verani, C. N., Distinct Proton and Water Reduction Behavior with a Cobalt(III) Electrocatalyst Based on Pentadentate Oximes. *Angew. Chem. Int. Ed.* **2015,** *54* (24), 7139-43.

191. Wang, D.; Lindeman, S. V.; Fiedler, A. T., Bimetallic Complexes Supported by a Redox-Active Ligand with Fused Pincer-Type Coordination Sites. *Inorg. Chem.* **2015,** *54* (17), 8744-54.

192. Perdew, J. P.; Wang, Y., Accurate and simple analytic representation of the electron-gas correlation energy. *Phys. Rev. B* **1992,** *45* (23), 13244-13249.

193. A. V. Marenich, C. J. C., D. G. Truhlar, , *J. Phys. Chem. B* **2009,** *113*, 6378-6396.

194. Neese, F. J., *Phys. Chem. Solids* **2004,** *65*, 781-785.

195. R. Dennington, T. K., J. Millam, Version 5 ed ed.; Semichem Inc: Shawnee Mission, KS, 2009.

196. C. P. Kelly, C. J. C. a. D. G. T., *J. Phys. Chem. B.* **2006,** *110*, 16066-16081.

197. Fourmond, V.; Jacques, P. A.; Fontecave, M.; Artero, V., H2 evolution and molecular electrocatalysts: determination of overpotentials and effect of homoconjugation. *Inorg. Chem.* **2010,** *49* (22), 10338-47.

198. de Bruin, B.; Bill, E.; Bothe, E.; Weyhermüller, T.; Wieghardt, K., Molecular and Electronic Structures of Bis(pyridine-2,6-diimine)metal Complexes [ML2](PF6)n (n = 0, 1, 2, 3; M = Mn, Fe, Co, Ni, Cu, Zn). *Inorg. Chem.* **2000,** *39* (13), 2936-2947.

199. When referenced to the experimental acid, protonation of Co(I)-Co(I) B will be slightly uphill by 2.6 kcal/mol. Similarly, protonation and release of H2 from C will be downhill by 19.2 kcal/mol., When referenced to the experimental acid, acetic acid (pKa = 22.3), protonation of Co(I)-Co(I) B will be slightly uphill by 2.6 kcal/mol. Similarly, protonation and release of H2 from C will be downhill by 19.2 kcal/mol.

200. Hurst, J. K.; Roemeling, M. D.; Lymar, S. V., Mechanistic Insight into Peroxydisulfate Reactivity: Oxidation of the cis,cis-[Ru(bpy)2(OH2)]2O(4+) "Blue Dimer". *J. Phys. Chem. B* **2015,** *119* (24), 7749-60.

201. Karlsson, E. A.; Lee, B.-L.; Åkermark, T.; Johnston, E. V.; Kärkäs, M. D.; Sun, J.; Hansson, Ö.; Bäckvall, J.-E.; Åkermark, B., Photosensitized Water Oxidation by Use of a Bioinspired Manganese Catalyst. *Angew. Chem. Int. Ed.* **2011,** *50* (49), 11715-11718.

202. Gagliardi, C. J.; Wang, L.; Dongare, P.; Brennaman, M. K.; Papanikolas, J. M.; Meyer, T. J.; Thompson, D. W., Direct observation of light-driven, concerted electron–proton transfer. *Proc. Natl. Acad. Sci. U. S. A.* **2016,** *113* (40), 11106-11109.

203. Xu, Y.; Eilers, G.; Borgström, M.; Pan, J.; Abrahamsson, M.; Magnuson, A.; Lomoth, R.; Bergquist, J.; Polívka, T.; Sun, L.; Sundström, V.; Styring, S.; Hammarström, L.; Åkermark, B., Synthesis and Characterization of Dinuclear Ruthenium Complexes Covalently Linked to RuII Tris-bipyridine: An Approach to Mimics of the Donor Side of Photosystem II. *Chem. Eur. J.* **2005,** *11* (24), 7305-7314.

204. Kurahashi, T.; Kikuchi, A.; Tosha, T.; Shiro, Y.; Kitagawa, T.; Fujii, H., Transient Intermediates from Mn(salen) with Sterically Hindered Mesityl Groups: Interconversion between MnIV-Phenolate and MnIII-Phenoxyl Radicals as an Origin for Unique Reactivity. *Inorg. Chem.* **2008,** *47* (5), 1674-1686.

205. Lassalle-Kaiser, B.; Hureau, C.; Pantazis, D. A.; Pushkar, Y.; Guillot, R.; Yachandra, V. K.; Yano, J.; Neese, F.; Anxolabehere-Mallart, E., Activation of a water molecule using a mononuclear Mn complex: from Mn-aquo, to Mn-hydroxo, to Mn-oxyl via charge compensation. *Energy & Environ. Sci.* **2010,** *3* (7), 924-938.

206. Tezgerevska, T.; Alley, K. G.; Boskovic, C., Valence tautomerism in metal complexes: Stimulated and reversible intramolecular electron transfer between metal centers and organic ligands. *Coord. Chem. Rev.* **2014,** *268*, 23-40.

207. Lanznaster, M.; Hratchian, H. P.; Heeg, M. J.; Hryhorczuk, L. M.; McGarvey, B. R.; Schlegel, H. B.; Verani, C. N., Structural and electronic behavior of unprecedented five-coordinate iron(III) and gallium(III) complexes with a new phenol-rich electroactive ligand. *Inorg. Chem.* **2006,** *45* (3), 955-7.

208. Allard, M. M.; Sonk, J. A.; Heeg, M. J.; McGarvey, B. R.; Schlegel, H. B.; Verani, C. N., Bioinspired five-coordinate iron(III) complexes for stabilization of phenoxyl radicals. *Angew. Chem. Int. Ed.* **2012,** *51* (13), 3178-82.

209. Lanznaster, M.; Heeg, M. J.; Yee, G. T.; McGarvey, B. R.; Verani, C. N., Design of Molecular Scaffolds Based on Unusual Geometries for Magnetic Modulation of Spin-Diverse Complexes with Selective Redox Response. *Inorg. Chem.* **2007,** *46* 72-78.

210. Allard, M. M.; Xavier, F. R.; Heeg, M. J.; Schlegel, H. B.; Verani, C. N., Sequential Phenolate Oxidations in Octahedral Cobalt(III) Complexes with [N2O3] Ligands. *Eur. J. Inorg. Chem.* **2012,** *2012* (29), 4622-4631.

211. Lesh, F. D.; Shanmugam, R.; Allard, M. M.; Lanznaster, M.; Heeg, M. J.; Rodgers, M. T.; Shearer, J. M.; Verani, C. N., A Modular Approach to Redox-Active Multimetallic Hydrophobes of Discoid Topology. *Inorg. Chem.* 7226-7228.

212. <Bruker SMART X2S User Manual.pdf>.

213. Vosko, S. H.; Wilk, L.; Nusair, M., Accurate spin-dependent electron liquid correlation energies for local spin density calculations: a critical analysis. *Canadian Journal of Physics* **1980,** *58* (8), 1200-1211.

214. Stephens, P. J.; Devlin, F. J.; Chabalowski, C. F.; Frisch, M. J., Ab Initio Calculation of Vibrational Absorption and Circular Dichroism Spectra Using Density Functional Force Fields. *J. Phys. Chem.* **1994,** *98* (45), 11623-11627.

215. Scalmani, G.; Frisch, M. J.; Mennucci, B.; Tomasi, J.; Cammi, R.; Barone, V., Geometries and properties of excited states in the gas phase and in solution: Theory and application of a time-dependent density functional theory polarizable continuum model. *J. Chem. Phys.* **2006,** *124* (9), 094107.

216. Johnson Carroll K, "ORTEP: A FORTRAN Thermal-Ellipsoid Plot Program for Crystal Structure Illustrations". Oak Ridge, T., Oak Ridge National Laboratory., Ed. 1965.

217. Dutta, A.; Biswas, S.; Dolai, M.; Shaw, B. K.; Mondal, A.; Saha, S. K.; Ali, M., Mononuclear manganese(iii) complexes of bidentate NO donor Schiff base ligands: synthesis, structural characterization, magnetic and catecholase studies. *RSC Advances* **2015,** *5* (30), 23855-23864.

218. Li, Q.-B.; Han, Y.-J.; Zhao, G.-Q.; Xue, L.-W., Synthesis, Crystal Structures and Catalytic Oxidation of Manganese(III) Complexes Derived from Salen-Type Schiff Base N,N'-Bis(5-nitrosalicylidene)ethane-1,2-diamine. *Acta Chimica Slovenica* **2017,** *64* (2), 500-505.

219. Addison, A. W.; Rao, T. N.; Reedijk, J.; van Rijn, J.; Verschoor, G. C., Synthesis, structure, and spectroscopic properties of copper(II) compounds containing nitrogen-sulphur donor ligands; the crystal and molecular structure of aqua[1,7-bis(N-methylbenzimidazol-2[prime or minute]-yl)-2,6-dithiaheptane]copper(II) perchlorate. *Dalton Trans.* **1984,** (7), 1349-1356.

220. <v17n8a09.pdf>.

221. Herrero, C.; Hughes, J. L.; Quaranta, A.; Cox, N.; Rutherford, A. W.; Leibl, W.; Aukauloo, A., Intramolecular light induced activation of a Salen-Mn(III) complex by a ruthenium photosensitizer. *Chem. Commun.* **2010,** *46* (40), 7605-7.

222. Ghachtouli, S. E.; Guillot, R.; Dorlet, P.; Anxolabehere-Mallart, E.; Aukauloo, A., Influence of second sphere hydrogen bonding interaction on a manganese(ii)-aquo complex. *Dalton Trans.* **2012,** *41* (6), 1675-1677.

223. Gandolfi, C.; Cotting, T.; Martinho, P. N.; Sereda, O.; Neels, A.; Morgan, G. G.; Albrecht, M., Synthesis and self-assembly of spin-labile and redox-active manganese(III) complexes. *Dalton Trans.* **2011,** *40* (9), 1855-65.

224. Evangelio, E.; Ruiz-Molina, D., Valence Tautomerism: More actors than just electroactive ligands and metal ions. *Comptes Rendus Chimie* **2008,** *11* (10), 1137-1154.

225. Ruiz-Molina, D.; Veciana, J.; Wurst, K.; Hendrickson, D. N.; Rovira, C., Redox-Tunable Valence Tautomerism in a Cobalt Schiff Base Complex. *Inorg. Chem.* **2000,** *39* (3), 617-619.

226. Sedo, J.; Saiz-Poseu, J.; Busque, F.; Ruiz-Molina, D., Catechol-based biomimetic functional materials. *Adv. Mater.* **2013,** *25* (5), 653-701.

227. Shimazaki, Y.; Stack, T. D. P.; Storr, T., Detailed Evaluation of the Geometric and Electronic Structures of One-electron Oxidized Group 10 (Ni, Pd, and Pt) Metal(II)-(Disalicylidene)diamine Complexes. *Inorg. Chem.* **2009,** *48* (17), 8383-8392.

228. Franks, M.; Gadzhieva, A.; Ghandhi, L.; Murrell, D.; Blake, A. J.; Davies, E. S.; Lewis, W.; Moro, F.; McMaster, J.; Schröder, M., Five Coordinate M(II)-Diphenolate [M = Zn(II), Ni(II), and Cu(II)] Schiff Base Complexes Exhibiting Metal- and Ligand-Based Redox Chemistry. *Inorg. Chem.* **2013,** *52* (2), 660-670.

229. Ghorai, S.; Sarmah, A.; Roy, R. K.; Tiwari, A.; Mukherjee, C., Effect of Geometrical Distortion on the Electronic Structure: Synthesis and Characterization of Monoradical-Coordinated Mononuclear Cu(II) Complexes. *Inorg. Chem.* **2016,** *55* (4), 1370-1380.

230. Houmam, A., Electron Transfer Initiated Reactions: Bond Formation and Bond Dissociation. *Chem. Rev.* **2008,** *108* (7), 2180-2237.

231. Lee, W.-T.; Muñoz, S. B.; Dickie, D. A.; Smith, J. M., Ligand Modification Transforms a Catalase Mimic into a Water Oxidation Catalyst. *Angew. Chem. Int. Ed.* **2014,** *53* (37), 9856-9859.

232. Han, Z.; Horak, K. T.; Lee, H. B.; Agapie, T., Tetranuclear Manganese Models of the OEC Displaying Hydrogen Bonding Interactions: Application to Electrocatalytic Water Oxidation to Hydrogen Peroxide. *J. Am. Chem. Soc.* **2017,** *139* (27), 9108-9111.

233. Kpogo, K. K.; Mazumder, S.; Wang, D.; Schlegel, H. B.; Fiedler, A. T.; Verani, C. N., Bimetallic Cooperativity in Proton Reduction with an Amido-Bridged Cobalt Catalyst. *Chem. Eur. J.* **2017,** *23* (39), 9272-9279.

ABSTRACT

EVALUATION OF EARTH-ABUNDANT MONOMETALLIC AND BIMETALLIC COMPLEXES FOR CATALYTIC WATER SPLITTING

by

KENNETH KWAME KPOGO

December 2017

Advisor: Dr. Cláudio N. Verani

Major: Major (Inorganic Chemistry)

Degree: Doctor of Philosophy

The development of affordable water-splitting catalysts from Earth-abundant transition metal ions such as Co and Mn is of immense scientific interest. Aiming to develop an efficient water-splitting catalyst, a Co(II) complex featuring an asymmetric, pentadentate quinolyl-bispyridine ligand with a phenylenediamine backbone was synthesized and characterized by spectroscopic, spectrometric, and X-ray analysis. The Co ion was selected because of its ability to undergo redox conversions from $3d^5$ Co^{IV} through $3d^8$ Co^{I} thereby making it a suitable catalyst that can withstand harsh structural, and electronic changes during catalysis.

The electrocatalytic water reduction activity of the catalyst at neutral pH, gave a turnover frequency (TOF) of 970 moles of H_2/h at an overpotential of 0.65 V. Sustained catalytic water reduction over 18 hours gave a TON of 12,100 and (%FE) of 97% suggesting a stable catalyst. Post-catalytic analysis of a grafoil electrode using SEM, EDS, and UV-visible spectroscopy shows no evidence of catalyst degradation or transformation into other species thus confirming the molecular nature of the catalyst. $\mathbf{[Co^{II}(L^{Qpy})H_2O]ClO_4}$ is active towards water oxidation as well, operating with a %FE of 91% during catalysis in a 0.1 M borate buffer (pH 8.0), and giving a TON

of 97, at an applied potential of 1.50 $V_{Ag/AgCl}$. By using a series of experimental methods as well as DFT techniques, I isolated and characterized the catalytic oxidized intermediates for **$[Co^{II}(L^{Qpy})H_2O]ClO_4$**, and proposed a 'water nucleophilic-attack' (WNA) mechanism of water oxidation where, the highly electrophilic $3d^5$ [$^{HS}Co^{IV}$=O] intermediate is attacked by a nucleophilic water molecule thus forming the essential O-O bond and releasing dioxygen. The photocatalytic activity in the presence of $[Ru(bpy)_3]^{2+}$ and ascorbic acid in acetate buffer (pH 4) shows a TON of 295 and TOF of 50 moles of O_2/h.

Monometallic cobalt complexes have been shown to efficiently catalyze water reduction and therefore, enhanced activity is expected from binuclear analogs of these monometallic catalysts. Close proximity between two Co centers could trigger cooperativity either by facilitating homolytic pathways or by enabling electron transfer between the metallic centers, thus avoiding formation of a Co^{III}–H^- species. We hypothesize that cooperativity will be dependent on (i) the distance between the Co centers, (ii) the relative topology of the coordination environments, and (iii) the degree of orientation and overlap between redox-active orbitals. I analyzed the catalytic potential of the bimetallic complex **$[Co^{II}_2(L^{1'})(bpy)_2]Cl_4$**, by means of electrochemical, spectroscopic, and computational methods and observed that it efficiently reduces H^+ to H_2 in acetonitrile in the presence of 100 equiv of acetic acid with a TON of 18 and %FE of 94 after 3 h at –1.6 $V_{Ag/AgCl}$. This observation allows us to propose that this bimetallic cooperativity is associated with distance, angle, and orbital alignment of the two Co centers, as promoted by the unique Co-N_{amido}-Co environment offered by $L^{1'}$.

Experimental results reveal that the parent [$Co^{II}Co^{II}$] complex undergoes two successive metal-based $1e^-$ reductions to generate the catalytically active species [$Co^{I}Co^{I}$], and DFT calculations suggest that addition of a proton to one Co^{I} triggers a cooperative $1e^-$ transfer by each

of these Co^{I} centers. This $2e^{-}$ transfer is an alternative route to generate a more reactive $[Co^{II}(Co^{II}–H^{-})]$ hydride avoiding the $Co^{III}–H^{-}$ required in monometallic species. This $[Co^{II}(Co^{II}–H^{-})]$ species then accepts another H^{+} in order to release H_2.

The manganese ion, with its broad range of oxidation states and considerable Earth-abundance, is an appropriate choice for the study of electron transfer processes involved in catalytic water oxidation as it has been used as an efficient electron donor in PS II. It has been proposed that incorporation of phenolate moieties into manganese species could lead to catalytic activity as well. I synthesized two manganese complexes, the hexacoordinate $[Mn^{III}L^{1}CH_3OH]$ and the pentacoordinate $[Mn^{III}L^{2}]$, with a pentadentate tris-phenolate ligands H_3L^{1} and H_3L^{2} respectively. Detailed results from the structural, spectroscopic, and electrochemical evaluation of the two Mn complexes suggest that whilst both complexes show ligand-based oxidations favoring formation of a $[Mn^{III}$/phenoxyl] species, the hexacoordinate analog could form a $[Mn^{IV}$/phenolate] species. This is specifically due to the low energy difference between the frontier orbitals (<5 kcal/mol) of the Mn center, and the redox-active phenolate ligands. This low energy barrier allows electronic interaction between the Mn ion, and the phenolate ligand, causing valence tautomerism through electron transfer.

We therefore tested the hexacoordinate $[Mn^{III}L^{1}CH_3OH]$ for water oxidation catalysis and observed an overpotential of 0.77 V and TON of 53 in three hours with the catalyst operating at a %FE of 85. This study is particularly useful because it provides a basis for ligand design that favors either a radical or a high-valent metal pathway for catalytic water oxidation.

AUTOBIOGRAPHICAL STATEMENT

EDUCATION

Ph.D. Degree (Inorganic Chemistry): Wayne State University, Detroit, MI (2012 – 2017)

M.Sc. Degree (Inorganic): East Tennessee State University (ETSU), Johnson City, TN (2012)

B.Sc. in Chemistry (Honors thesis): University of Cape Coast (UCC), Cape Coast, Ghana (2005)

PROFESSIONAL SOCIETY MEMBERSHIPS

American Chemical Society – ACS (2013 – Present)

AWARDS AND PROFESSIONAL MEMBERSHIP

- Wayne State University Summer Dissertation Fellowship–2017
- Mary G. Wood Award for Excellence in Research and Service – Wayne State University (2017)
- Graduate Thesis/Dissertation Scholarship – Wayne State University (2017)
- Thomas C. Rumble Graduate Fellowship – Wayne State University (2016 – 2017)
- Best Poster Presentation Award – Wayne State Graduate and Postdoc Research Symposium (2017)
- Graduate Thesis/Dissertation Scholarship – East Tennessee State University (2012)
- Best Oral Presentation – (Graduate Science Division) Appalachian Student Research Conference (2012)

PUBLICATIONS.

- **Kpogo, K. K.,** and Verani, C.N., "Efficient Electro/photocatalytic Water Splitting using a $[Co^{II}(L^{Qpy})]^{+}$ Complex" **2017,** *manuscript in preparation.*
- **Kpogo, K. K**., Wang, D., Mazumder, S., Schlegel, H.B., Fiedler, A., and Verani, C.N., *Chem. Eur. J.* **2017** *23*, 9272.
- Kankanamalage, P. H. A., Mazumder, S., Tiwari, V., **Kpogo, K. K.**, Schlegel, H. B. and Verani, C. N., *Chem. Commun.* **2016,** *52*, 13357-13360.
- Gonawala, S., Leopoldino, V. R., **Kpogo, K. K.,** and Verani, C. N., *Chem. Commun.* **2016,** *52*, 11155-11158.
- Wickramasinghe, L. D., Mazumder, S., **Kpogo, K. K.,** Staples, R. J., Schlegel, H.B., and Verani, C.N., *Chem. Eur. J.* **2016,** *22*, 10786-10790.
- Verani, C. N., Shanmugam, R., Xavier, F. R., Allard, M. M., **Kpogo, K. K**., *Dalton Trans.* **2013,** *42* (43), 15296-306

PRESENTATIONS/CONFERENCES

1. **Kpogo, K. K**., Wang, D., Mazumder, S., Schlegel, H.B., Verani, C.N., and Fiedler, A., 48th Central Regional Meeting (ACS), June 6-10, 2017, Dearborn, MI, USA (poster presentation)
2. **Kpogo, K. K.,** Wang, D., Mazumder, S., Schlegel, H.B., Verani, C.N., and Fiedler, A., Ohio Inorganic Weekend, November 4-5, 2016, University of Akron, Akron, OH, USA (oral presentation)
3. **Kpogo, K. K.,** Basu, D., Verani, C. N., Ohio Inorganic Weekend, November 13-14, 2015, Bowling Green State University, Bowling Green, OH, USA (poster presentation)
4. **Kpogo, K. K.,** Verani, C. N., 246th ACS National Meeting, September 8-12, 2013 Indianapolis, IN (oral presentation)
5. **Kpogo, K. K.,** Verani, C. N., 20th International Symposium on the Photophysics and Photochemistry of Coordination Compounds, July 7-11, 2013, Traverse city, Michigan, USA
6. **Kpogo, K. K.** Eagle, C. T. **Best Science Oral Presentation**, Appalachian Student Research Conference April 12-13, **2012**, Johnson City, Tennessee, USA (oral presentation)